Modeling Assessments of Climate

Engineering

Dissertation zur Erlangung des Doktorgrades
der Mathematsch-Naturwissenshaftlichen Falkutät
der Christian-Albrechts-Universität zu Kiel

vorgelgt von

Yuming Feng

Kiel, Dezember 2016

Referent: Prof. Dr. Andreas Oschlies

Korreferent #1: Prof. Dr. Martin Visbeck

Tag der mündlich Prüfung: 2017-02-15

Summary

Climate Engineering (CE), defined as the deliberate intervention in the Earth's climate system in large scale to alleviate global warming, has been discussed as an important option to counter climate change challenges. In this thesis, I conducted five assessments on some specific CE technologies using the University of Victoria Earth System Climate Model (UVic_ESCM). Each individual assessment investigated the climate responses when particular CE technologies were applied under high CO_2 emission scenarios from year 2020 to 2099. The main aim of those assessments is to improve the understanding of CE technologies regarding their global warming offset efficacy, environmental side effects, simulation uncertainties, and extended usages potentially.

Artificial Ocean Alkalinization (AOA), which could remove carbon dioxide from atmosphere by artificially dissolving alkaline minerals (e.g. lime and olivine), was the focus for the first two assessments. In the first assessment, implementing lime-based AOA in Barrier Reef, Caribbean Sea and South China Sea, was tested effective for protecting local coral habitat from ocean acidification threats. However a rapid rebound to the acidified conditions of the experimental regions was observed if AOA was stopped. The second assessment studied the climate responses when olivine-based AOA was implemented along the ice-free coastal waters. Decreasing olivine grain diameter from 1000 to 10 μm could provide a higher overall CO_2 sequestration efficiency despite the fact that grinding smaller olivine grains could emit more CO_2. If some aragonite Ω upper limits were taken to prevent excessive alkalinization from harming the

marine ecosystems, AOA in coastal waters could still reduce atmospheric CO_2 by 89.4~595.56

GtC cumulatively by year 2100.

In the third assessment, sulphate aerosol injection-based SRM, and direct air capture-based CDR, were evaluated under different equilibrium climate sensitivities (ECSs) as well as CE intensities separately. Under the same CE intensities, SRM and CDR induced global-mean surface temperature reductions from respective control run levels in year 2099, were larger if ECS was set higher. While under higher ECS, more SRM and CDR were required than the case under lower ECS, if they were employed for stopping >1.5 °C global warming from the preindustrial in 21st century. For the studied cases, the climate feedback caused cooling were 14%~52% and 45%~86% in magnitude to that from direct SRM and CDR radiative perturbations. Preliminary results from the forth assessment found that to prevent global warming and ocean acidification concurrently, combining lime-based AOA with sulphate aerosol injection-based SRM had some economic advances compared to implementing it alone, but the marginal costs for this approach would increase dramatically due to the nonlinearity interactions generated within those combined schemes.

The last assessment was a comprehensive study that compares the climate mitigation effectiveness and side effects of Afforestation, Artificial Ocean Upwelling, Ocean Iron Fertilization, AOA, and SRM. As a summary, the results showed those CE technologies were either not effective enough for mitigating the global warming obviously, or potentially having some severe environmental side effects.

iv

Zusammenfassung

Climate Engineering (CE) wird als eine gezielte großskalige Intervention ins Erd- und Klimasystem definiert, um die globale Erwärmung und die damit verbundenen Klimaauswirkungen zu verringern. Es wird schon als wichtige Alternative zur Bewältigung der Klimaveränderung gesehen. In dieser Arbeit habe ich mit dem University of Victoria Earth System Climate Model (UVic_ESCM) fünf Evaluierungen zu einigen vorhandenen CE-Technologien durchgeführt. Jede einzelne Evaluierung untersucht die Reaktion des Klimas, wenn eine oder mehrere CE-Technologien unter besonderen CO_2-Emissionsszenarien von 2020 bis 2099 eingesetzt wurden. Das Hauptziel dieser Evaluierungen ist, das Verständnis für die Effektivität der Reduzierung der globalen Erwärmung, umweltbedingte Nebenwirkungen, Simulationsunsicherheiten und potenzielle Anwendungen der spezifischen CE-Technologien zu verbessern.

Artificial Ocean Alkalinization (AOA) war der Schwerpunkt der ersten beiden Evaluierungen, was das CO_2 aus der Atmosphäre durch künstliche Auflösung von alkalischen Mineralien (z. B. Calciumoxid und Olivin) entfernen könnte. In der ersten Evaluierung wurde nachgewiesen, dass die Umsetzung der zeitbasierten AOA in Great Barrier Reef, Caribbean Sea and South China Sea ein wirksamer Ansatz ist, den lokalen Korallenlebensraum vor den Bedrohungen der Ozeanversauerung schützen zu können. Allerdings existiert ein schneller Rückgang zu den angesäuerten Bedingungen der Zielregionen, wenn die Anwendung der AOA beendet wird. Die zweite Evaluierung schätzte das erzielte Klimaschutzpotenzial, als olivinbasierte AOA entlang

v

der eisfreien Küstengewässer angewandt wurde. Es gab eine rasch erhöhte Klimaschutzeffizienz,

wenn kleinere Olivinkörner sogar unter Berücksichtigung des Mahlprozesses verwendet wurden,

der mit der CO_2-Kompensation in Zusammenhang steht. Im Allgemeinen hatte AOA in den

Küstengewässern Klimaschutzpotenziale, obwohl die Aragonit-Ω-Obergrenze genommen wurde,

um übermäßige Alkalisierung zu vermeiden, die die Meeresökosysteme schädigen könnte.

Die dritte und die vierte Evaluierung untersuchten zwei verschiedene CE-Technologien. In der

dritten Evaluierung werden auf der Einspritzung der Sulfatsaerosol-basierten SRM und auf der

Basis von direkter Erfassung der Luft stehenden CDR unter verschiedenen Gleichgewichts-

Klimasensitivitäten (equilibrium climate sensitivities, ECS) und Ingenieurintensitäten analysiert.

Der Stand der Temperatursenkung der globalen Oberfläche, der durch ausgewerteter CE-

Technologie verursacht war und mit der Referenz verglichen wurde, war umso größer, je größer

ECS war. In diesem Fall wurden jedoch mehr SRM und CDR benötigt, um die globale

Erwärmung auf nicht mehr als 1.5 ° C im 21. Jahrhundert effektiv zu beschränken. Erste

Ergebnisse aus der vierten Evaluierung zeigten, um die gleichen Klimaschutzziele – das

gleichzeitige Vorkommen der globalen Erwärmung und Ozeanversauerung zu vermeiden - zu

erreichen, hat die Kombination von calciumoxidbasiertem AOA mit auf der Einspritzung der

Sulfatsaerosol basierten SRM einen wirtschaftlichen Vorteil als einzelne Umsetzung, aber die

negativen Externalitäten wie Niederschlagsanomalien könnten bleiben.

Die letzte Evaluierung war eine Synthese-Studie, die die Wirksamkeit der Effekte des

Klimaschutzes und Nebenwirkungen von Aufforstung, künstlichem Ozeanauftrieb,

Ozeaneisendüngung, Ozeanalkalinisierung und Solar Radiation Management (SRM) vergleicht.

Jedoch zeigten die Ergebnisse, dass die CE-Technologien entweder nicht wirksam genug waren,

um die globale Erwärmung zu reduzieren, oder potenziell einige starke Nebenwirkungen hatten.

Contents

1. Introduction

1.1. Climate Engineering Concepts

Climate change is considered one of the biggest threats to mankind in the 21st century. The Intergovernmental Panel on Climate Change (IPCC 2014) shows that the global average temperature has a linear trend of warming with 0.85 °C (IPCC-WG1 2013) since 1880 to 2012. The unequivocal concept of climate change is associated with impacts such as sea level rise, ocean acidification, oceanic oxygen decrease and extreme weather conditions, etc. The climate change caused by anthropogenic green house gas (GHG) emissions begins to result in severe consequences, for both human society and biodiversity (Figure 1-1).

For the future, numerical climate models have demonstrated a continued surface temperature increase (Figure 1-1) if GHG emissions keep on. The temperature will exceed 1.5 °C by 2100 under medium and high emission pressure (IPCC-WG1 2013). Continued climate change will amplify the current risks for urban and natural ecosystems, and some of the associated impacts, such as ocean acidification, can still last for several centuries after surface temperature stabilization. Therefore measures such as climate adaptation and mitigation, are required to prevent the above-mentioned pervasive consequences from happening (IPCC-WG2 2014).

(a) Risks from climate change...

(b) ...depend on cumulative CO₂ emissions

(c) ...which in turn depend on annual GHG emissions over the next decades
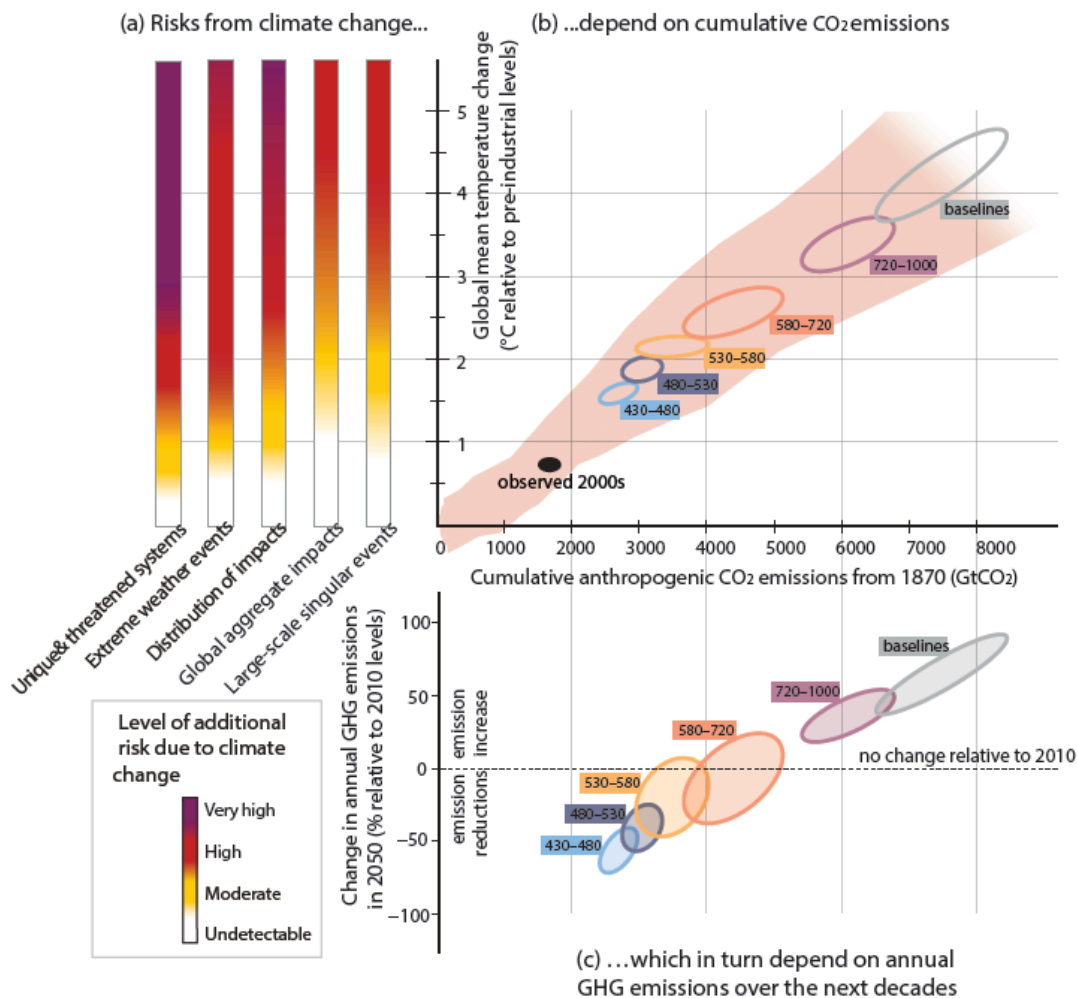
Figure 1-1. The environmental risks from climate change and their relationship to global-mean surface temperature change (referenced to preindustrial level) (a), cumulative anthropogenic CO_2 emissions (counted from year 1870) (b) and global GHG emission changes between year 2050 to 2010 (c). The results are based on Coupled Model Intercomparison Project Phase 5 (CMIP5) simulations (pink plume in Panel (b)) and on a simple climate model for the baselines and five mitigation scenarios (colored ellipses). This figure is achieved and modified from IPCC-WG1 (2013).

Climate adaptation is the process of adjustment to avoid the direct harmful climate impacts, while climate mitigation refers to technologies that can reduce or prevent GHG emissions. Climate adaption is considered essential, but it has limited effectiveness if the rate of climate change is high. Climate mitigation measures can ideally reduce emissions close to zero, and therefore diminish the climate change

13

risks. An example of such climate mitigation technology is the carbon capture and storage (CCS). CCS captures waste carbon dioxide from large point sources (e.g. industrial sectors) and deposits it in geological formations resulting in overall CO_2 emission declines. However to massively reduce anthropogenic CO_2 concentrations in 21st century via climate mitigation technologies alone, humanity will require intensive global industrial reformations (Figure 1-2). This large-scaled reformation can be very difficult to fully commit to due to the industrial inertia and short time window left to avert harmful climate change impacts.
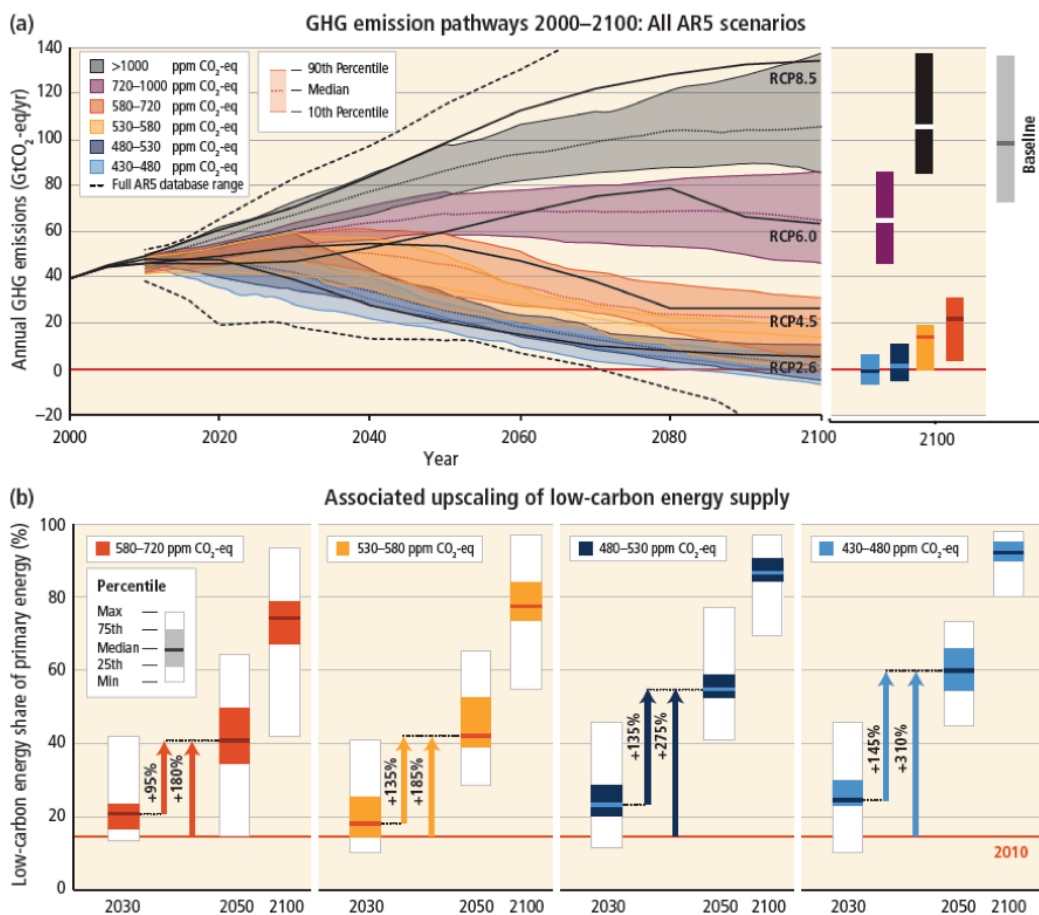
Figure 1-2. Atmospheric GHG emissions (as CO_2 equivalent) under different future GHG scenarios (a) and associated scale-up requirements for low-carbon energy sources for year 2030, 2050 and 2100, compared to the level in 2010 (b). Figure is from IPCC-WG2 (2014).

14

Besides climate adaptation and mitigation, a potential alternative to deal with climate change is climate engineering (CE, also named *geoengineering*). CE is the process that is designed to deliberately alter the climate system on a large scale for alleviating climate change impacts. In specific, most CE technologies can be categorized into either "Solar Radiation Management" (SRM) branch, which aims to reduce incoming solar radiation, or "Carbon Dioxide Removal" (CDR) branch, which operates by enriching terrestrial and oceanic carbon reservoirs (Figure 1-3). This categorization is not given according to a CE technology's climate affects. Whether a CE technology should be considered as SRM or CDR, depends on if it primarily deals with the cause or the consequence of anthropogenic climate change. If the primary aim of a CE technology is to mitigate the continuously increased atmospheric CO_2, i.e. the cause of climate change, this CE technology usually belongs to CDR branch. In contrast, if a CE technology in the first place aims to offset the increase of surface temperature, i.e. the consequence of climate change, via solar insolation reduction, this technology is usually considered SRM.

Though CE is brought up apart from climate mitigation in previous paragraphs, it has some overlaps with climate mitigation. Since CDR can decrease the atmospheric CO_2, it is a particular climate mitigation technology by definition. Albeit several CDR technologies such as Reforestation (RFO) have been included in some mitigation scenarios (e.g. Representative Concentration Pathway 2.6), most CE methods (mainly SRM methods) have not yet been involved. In the CE research community, "geoengineering" in early studies is widely used to describe SRM technologies. In some particular contexts, climate mitigation refers to any effort that

can decrease the global warming rate other than the atmospheric CO_2 elevation. Upon this definition, SRM, which has weak intervention to carbon cycle, can also be regarded as climate mitigation technology. To avoid those terminological complexities, "climate mitigation" used in this chapter is defined as the measures to decrease atmospheric CO_2 concentrations.

1.2. Climate Engineering History

Since the industrial revolution, the first idea to modify the weather and climate for serving humanity came from American Meteorologist *James Pollard Espy*, who introduced a method of setting fires to generate precipitation on command in year 1841. In the middle of the 20st century, the Soviet and the United States government both established their institutes to study "cloud seeding" to alter the weather. During the Vietnam War, the US air force deployed cloud seeding operations as a hostile weather manipulation for the first time. Learning from the history of Vietnam War, the United Nations general assembly later approved the Environmental Modification Convention (EMC) that was ratified by 76 countries for banning the wartime and other hostile use of modifying weather and climate. In 1974, Russian scientist *Mikhail Budyko* brought up the idea of burning sulfur and sending these aerosols in the stratosphere to reverse global warming. Following his proposal the concept of "Solar Radiation Management" is gradually formed and became one of the two major study branches of CE (Keith 2000). During the cold war, the concerns of nuclear war eventually formed the theory of "nuclear winter". In nuclear warfare scenarios, the firestorms caused by massive nuclear bomb explosions could generate a huge aerosol/dust shield to reflect solar radiation for years and

reverse anthropogenic global warming effects (Robock 1984). The catastrophic consequence of nuclear winter was compared to Cretaceous-Paleogene (K-Pg) extinction event. One popular hypothesis for this event suggests this extinction is due to the Earth cooling effect caused by planetary albedo enhancement from massive volcanism and firestorm during the Chicxulub Asteroid impact (Pope *et al.* 1998). In 1991, Mount Pinatubo erupted and threw millions of tons of volcanic ashes into the atmosphere and reduced the global-mean surface temperature by 0.5 °C in the following two years (McCormick *et al.* 1995). This natural phenomenon is often considered as an analogue to implementing SRM. In 2006, Nobel Prizer *Paul Crutzen* advocated for promoting SRM related research (Crutzen 2006), which triggered a new bloom for SRM study till nowadays.

The earliest work on CDR was traced back to the 1970s in the US Department of Energy. After 1970s, the idea of planting tress to remove CO_2 from atmosphere began to occur. In 1977, *Marchetti* proposed to scrub CO_2 from smoke stacks and inject the stream into Mediterranean outflow water as a prototype to capture CO_2 from both atmosphere (CDR) and industrial exhaust (CCS). In 1992, the First International Conference on Carbon Dioxide Removal (ICCDR-1) was held in Amsterdam, representing the first major gathering of researchers in the field of CO_2 capture, disposal and utilization (Blok *et al.* 1992). Thereafter the CDR branch was gradually established.

After 2010, due to the urgency of dealing with climate change and the potential CE, several strategic projects designed to study CE were initiated in UK (Royal Society 2009, Pidgeon *et al.* 2013), USA (NAS 2015), Germany (Rickels *et al.*

17

2011) and China (Cao *et al.* 2015). In 2011, an IPCC expert meeting on climate engineering was held in Lima, Peru (Edenhofer *et al.* 2011). In 2014, IPCC in its fifth assessment began to discuss CE options (IPCC-WG1 2013).
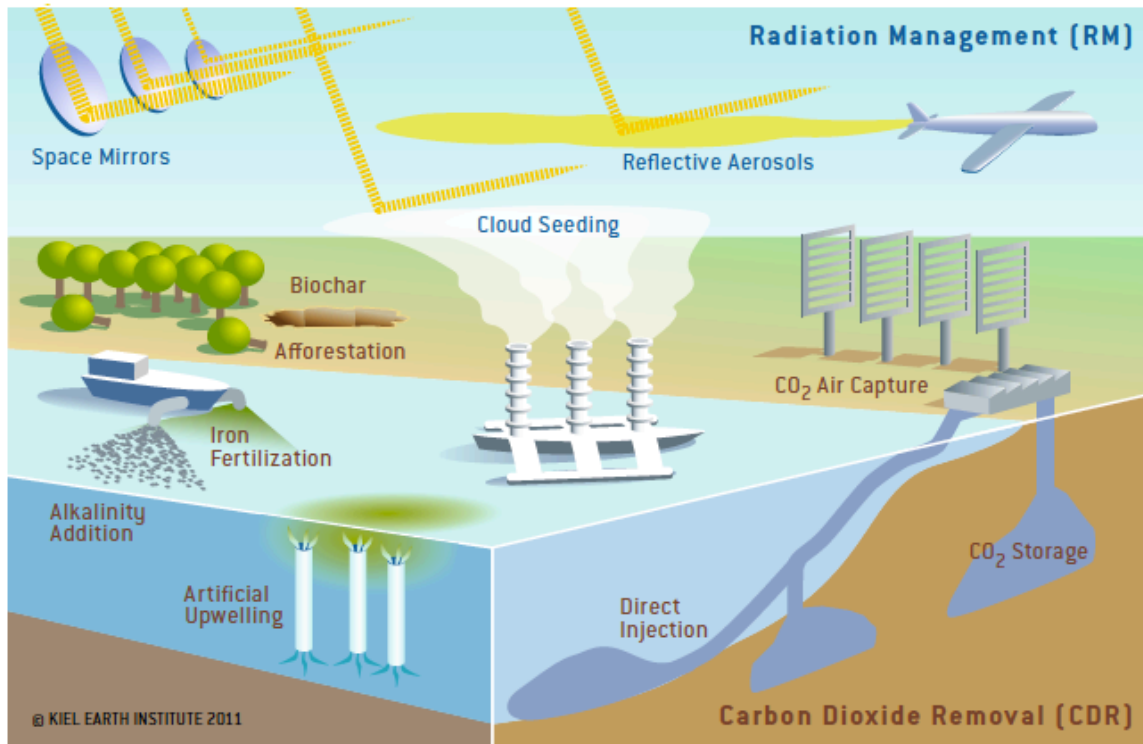
Figure 1-3. Illustration for commonly discussed CE technologies. Figure Source: Rickels *et al.* (2011).

Due to the complexity and uncertainties of climate system as well as CE technologies, implementing CE in present world, is expensive and will likely lead to some environmental side effects. Therefore scientists tend to use climate models to study CE technologies upon their environmental and social-economical impacts. The past several years have witnessed a great improvement in our understanding of CE. In following paragraphs I will examine some of the most discussed CE technologies in specific and give a brief literature review of the relevant studies.

1.2. Solar Radiation Management

1.2.1. Stratospheric Aerosol Injection

SRM has been suggested as a policy response to avert some of the most severe impacts of anthropogenic global warming (Crutzen 2006). Stratospheric aerosol injection (SAI), the most frequently discussed method of SRM, involves injection of sulfur dioxide (SO2) into the tropical stratosphere to raise the planetary albedo. It reduces insolation in an attempt to offset some fraction of anthropogenic warming. The meridional circulation of the stratosphere is mainly governed by vast regions of upwelling in the tropics and large-scale sinking in the extratropics. SO_2 injections into the tropical stratosphere will mix well globally within weeks through this Brewer-Dobson circulation, resulting with a relatively homogeneous stratosphere (Bala *et al.* 2003).

Climate models with comprehensive atmosphere dynamics and chemistry can simulate a stratospheric aerosol layer in several ways, including by direct injection of sulfates into the stratosphere or a prescribed aerosol layer (Kravitz *et al.* 2011). However, many modeling groups choose to simply dim the sun by changing the solar constant in a climate model. This simpler design is often used because solar dimming may be easier to implement than SAI in coding aspects. In many cases, it allows modelers to study the effects of reduced insolation even if the model is incapable to simulate complex dynamical changes induced by SAI. One large difference between SAI simulations and solar dimming simulations is the perturbation over the circulation near the Southern Ocean. Stratospheric heating triggered by SAI is not seen in solar dimming simulations. SAI simulations induce a

19

large equator to pole temperature gradient in the stratosphere, strengthening the Jetstream and high-latitude surface winds. This anomalous wind stress applied to the ocean allows for greater mixing in the Southern Ocean, and subsequently promotes warm advection of water toward the Antarctic ice-sheets (McCusker *et al.* 2015). In addition, solar dimming cannot be used to simulate the changes in atmospheric chemistry triggered by SAI. Those different model designs are summarized Geoengineering Model Intercomparison Project (GeoMIP) (Kravitz *et al.* 2011), in which solar dimming design is presented in the G1 (solar dimming deployed to compensate instantaneous 4xCO_2 increase) and G2 (solar dimming deployed to compensate 1% yr^{-1} CO_2 increase) Groups while SAI is set in G3 (SAI deployed to compensate CO_2 forcing following RCP 4.5 scenario) and G4 (SAI deployed in constant rates per year) Groups. Therefore, while solar dimming is often a good approximation of an SAI engineered climate, the difference may become significant when discussing particular elements of the climate response to SAI.

A major concern associated with SAI is the perturbation over global hydrological cycles. Globally, the precipitation under SAI is reduced compared to the case without it (Tilmes *et al.* 2013). According to an SAI model comparison study (Kravitz *et al.* 2013a), global precipitation is reduced by around 4.5% once radiative forcing rebounds to preindustrial level by SAI under quadrupled CO_2 condition using solar dimming approach. Kleidon *et al.* (2015) found that much of the global-scale change in the hydrologic cycle can be robustly predicted by the response of the thermodynamically constrained surface energy balance to altered radiative forcing. Bala *et al.* (2008) found that SAI could not offset temperature elevation and

hydrological perturbation under climate change at once, because insolation change by SAI can directly perturb both the surface latent and sensible heat flux. Kravitz *et al.* (2013b) figured out the SAI runs have a smaller magnitude of land sensible but larger latent heat flux adjustments than the control run, which implies a greater reduction of evaporation and less land temperature increase induced by SAI.

SAI can also perturb the cloud and associated thermal dynamics in atmosphere. Besides the mentioned perturbation on circulation over Southern Ocean, English *et al.* (2012) found simulated SAI in tropical atmosphere will result a significant perturbation to tropospheric aerosols with enhanced sulfate burden particularly in upper layer and near poles. There is also evidence indicating that SAI will change the pattern of extreme weathers in global patterns and frequencies (Curry *et al.* 2014). When SAI is terminated abruptly while atmospheric CO_2 level is still high, the global-mean precipitation rate is increased (Matthews and Caldeira 2007), while mitigated global-mean temperature (Jones *et al.* 2013) will rebound to unmitigated level in less than several years.

SAI can also affect the global biogeochemical cycles. Studies (Tilmes *et al.* 2008, Tilmes *et al.* 2012 and Heckendorn *et al.* 2011) found sulphate aerosols can accelerate the hydroxyl catalyzed ozone destruction and caused a rapid depletion even though future halogen concentration will be much reduced. Carbon changes are often observed in SRM engineered future. Matthews and Caldeira (2007) using a climate model with fully coupled carbon cycle found SAI could enhance the terrestrial and ocean carbon uptake compared with the control run. Some other

research also confirmed that land carbon sinks will be enhanced through increasing diffuse solar radiation (Mercado *et al.* 2009, Xia *et al.* 2016).

While many studies show that SRM would be effective in reducing global-mean temperature, there are likely disparate regional impacts. Yu *et al.* (2015) and Jones *et al.* (2010) looked into the temperature and precipitation compensation inequalities under SAI and found those inequalities vary greatly from one region to another. Ricke *et al.* (2011) found that when SAI is used in an attempt to reduce the rate of increase in surface air temperature, the effectiveness of the SAI in stabilizing regional climates decreases if climate sensitivity is higher.

Some studies investigated the socioeconomic impacts induced by SAI. SAI itself has been long considered inexpensive (Barrett 2008). McClellan *et al.* (2012) concluded that the engineering price to implement SAI to effectively mitigate climate change is less than 8 billion USD per year. However, Klepper and Rickels (2012) pointed out that price and external effects are not yet sufficiently accounted for, and that the question of dynamic efficiency is still unresolved.

More recently, some scientists began to focus on improving the implementation strategies to enhance SAI's efficiency to reduce global warming to avoid harmful environmental side effects and to diminish the involved uncertainties. Keith and MacMartin (2015) pointed that the environmental impacts of SAI are largely depending on the implementation scenario, and the negative externality is not SAI's inherent feature. MacMartin *et al.* (2014) suggested only implementing SAI for constraining the rate of global-mean temperature change instead of atmospheric CO_2 forcing change. It will lead to a finite deployment period depending on

emission pathway. Apart from SO_2, other aerosol options such as magnetic or electrostatic torques, solid aerosols, were brought up for improving scatter efficiency and decreasing ozone loss, though they were not proven as feasible as sulfur aerosols (Keith 2010, Weisenstein *et al.* 2015). MacMartin *et al.* (2012) optimized the latitudinal and seasonal distribution of SAI in order to improve the fidelity with which SAI can better offset anthropogenic climate change. Wigley (2006) proposed to combine CO_2 reduction and SAI technologies together to reduce mitigation costs and prevent severe climate impacts before massive emission reductions can be undertaken. Though reflecting incoming solar radiation was intuitively more urgent in polar regions due to "polar amplification", Caldeira and Wood (2008) found at high latitudes (polar regions), there is less sunlight deflected per unit albedo change but climate system feedbacks operate more powerfully. They concluded the SAI effectiveness was insensitive to latitude.

Some scientists also tried to undertake experiments for testing SAI. Izrael *et al.* (2009) studied the field tests of radiation transmission with different aerosol particles. Dykema *et al.* (2014) proposed to use small-scale in-situ experimentation under well-regulated circumstances. Keith *et al.* (2014) examined the possible platforms to conduct a field SAI test and summarized a portfolio over this topic.

1.2.2. Cloud Whitening

SAI is considered as a CE strategy to modify the incoming solar radiation in long term and global scale, while cloud whitening (CW) can be sued to modify solar radiation within a shorter time period and more regional scopes. CW works by injecting the aerosols over marine regions into the low atmosphere to first enhance

the cloud condense nuclei (CCN) concentration, subsequently to boost stratocumulus clouds, and ultimately to block the sunlight through both the clouds formation (i.e. the "Twomey Effect") and the aerosol particles (Latham 2002). This proposal is explained in detail through Salter *et al.* (2008) regarding its mechanisms and hardware platforms. But unlike SAI using sulphate, the proposed aerosol particles for CW are the sea salt particles (sea spray), which are usually larger and heavier. Also, the altitude of aerosol injection for CW is within marine troposphere instead of stratosphere for SAI.

Numerical models in recent years were used to evaluate the potential of CW when it is implemented in planetary scale to offset climate change, and in regional scale to modify local climate. Unlike SAI which is designed to inject aerosols in tropical stratosphere, CW is simulated in marine areas where cloud droplet number concentration (CDNC) is susceptible to increase (Rasch *et al.* 2009), and has a higher fraction of low-level cloud with little overlaying high-level cloud (Jones *et al.* 2009). Globally, North Pacific, South Pacific and South Atlantic are the most feasible areas for CW. Some study (Partanen *et al.* 2012) found beside the aerosol indirect effects by forming cloud, the aerosol particles reflection contributes 29% of the CW induced cooling effects. Alterskjær *et al.* (2012) combined model (Norwegian Earth System Model) results with cloud observations from MODIS (Moderate Resolution Imaging Spectroradiometer), and confirmed stratocumulus regions off the west continents coasts are most susceptible for CW implementation. Kravitz *et al.* (2013c) concluded that the CW induced effective radiative forcing compensation is largely confined to the latitudes in which injection occurs. The results showed increased land-sea

temperature contrast, arctic warming, and large shifts in annual-mean precipitation patterns.

Besides being used as a specific CE technology to mitigate climate change, CW has been recently proposed to prevent hurricanes (Latham *et al.* 2012) and coral bleaching (Latham *et al.* 2013) as it cools down the sea surface temperature. Those examples have demonstrated that some CE technologies might be used in weather modification and biodiversity conservation.

1.3. Carbon Dioxide Removal

1.3.1. CO_2 Direct Air Capture

The most direct forward approach to sequestrate atmospheric CO_2 is through direct air capture (DAC). DAC includes two main processes: capturing the atmospheric CO_2, and immobilizing CO_2 into geological structures (Keith *et al.* 2006).

The immobilization process of DAC, e.g. depositing captured CO_2 into geological formations, is similar to CCS, but there is substantial difference between DAC and CCS in capturing atmospheric CO_2. For CCS technologies, the secret of absorbing CO_2 is the carbon dioxide scrubber at energy intensive sectors such as electricity industry and power plants. Amine, (e.g. momoethanolamine) (Rochelle 2009), basic oxides/hydroxides (CaO and NaOH), active carbon and ion-exchange membrane can all be used to absorb the CO_2 disposal from above sectors. While for DAC, chemical vents for capturing carbon dioxide, repeatedly described as 'artificial trees' with alkaline solids/solution filled scrubbers, are set in open fields to uptake CO_2 from the air.

Since CO_2 concentration is very low in atmosphere, the efficiency for DAC is predicted low (IPCC-WG1 2013). Consequently the economic costs will become a major constrain for DAC's commercialization. House *et al.* (2011) has demonstrated that air capture processes would be significantly more expensive than mitigation technologies aimed at decarbonizing the electricity sector. In environmental science aspects, DAC cannot be considered a reversed process completely, because the oceanic pH and oxygen decrease caused by climate change cannot be completely fixed by implementing DAC (Mathesius *et al.* 2015) in next several centuries.

1.3.2. Artificial Ocean Alkalinization

Artificial Ocean Alkalinization (AOA) adds alkaline minerals, such as lime (CaO and its hydrate form)(Kheshgi 1995), olivine ($[Mg^{+2},Fe^{+2}]_2SiO_4$) (Schuiling and Krijgsman 2006, Köhler *et al.* 2010) and limestone ($CaCO_3$) (Rau and Caldeira 1999) into the ocean, rivers, lakes and land surface (Moosdorf *et al.* 2014). Equations (1-1)(1-2) and (1-3) indicate the bulk chemical reactions when alkaline minerals dissolve in water:

$$Ca(OH)_2 + 2CO_2 \rightarrow Ca^{2+} + 2HCO_3^- \tag{1-1}$$

$$Mg_2SiO_4 + 4CO_2 + 4H_2O \rightarrow 2Mg^{2+} + 4HCO_3^- + H_4SiO_4 \tag{1-2}$$

$$CaCO_3 + CO_2 + H_2O \rightarrow Ca^{2+} + 2HCO_3^- \tag{1-3}$$
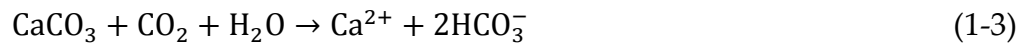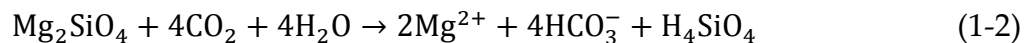
Being represented in the context of AOA "enhanced weathering", chemical reactions (1-1) and (1-2) can occur the natural environment spontaneously while reaction (1-3) only happens when local oceanic calcium carbonate is undersatruated.

26

In nature, weathering processes, namely hydrolysis of silicates and dissolution of carbonate, are slow feedbacks transforming airborne CO_2 into dissolved inorganic carbon (DIC), which ultimately enters the ocean, mostly via riverine transport. Natural weathering can increase ocean total alkalinity (TA), however, on timescales of tens of thousands to millions of years (Kump *et al.* 2000). When lime and ground olivine deployed at ocean surface, they can react rapidly with oceanic dissolved CO_2 and transform acidic soluble CO_2 into bicarbonate. Through this process AOA may provide considerable climate mitigation potential by increasing oceanic carbon uptake.

To achieve the goal of dramatically removing atmospheric CO_2, how to prepare and add such large amount of alkaline minerals into the ocean is the first task to be solved. As commonly acknowledged that limestone cannot spontaneously dissolve in natural waters, some studies suggest to dump limestone into upwelling regions where local DIC is particularly high (Harvey 2008). Some early research (Kheshgi 1995) proposed to construct limestone-based AOA facilities on the coast to produce lime through calcination, and to use CCS technology to capture emitted CO_2 during the whole process. To enhance the CDR efficiency, Rau *et al.* (2001) proposed to use limestone particles to react with CO_2-rich effluent gas stream in water solution/spray. This solution from above step could ultimately be discharged to the ocean. Rau (2008) also proposed a new technique by dissolving limestone in electrochemical chambers while producing H_2 gas to compensate the electricity input. Ilyina *et al.* (2013a) used an Earth system model to simulate dumping quick lime in global ocean in long-term run over several thousand years, and found AOA can

effectively mitigate ocean acidification and therefore decrease atmospheric CO_2. Renforth *et al.* (2013) recalculated mitigation efficiency of ocean liming, and found every tonne of sequestered CO_2 requires between 1.4 and 1.7 ton of limestone to be crushed, calcined, and distributed.

The dissolution of olivine however is highly predominated by its grain size, ambient water temperature and pH. As for the grain size, Hangx and Spiers (2009) found increasing olivine grain size from 10 um to 1000 um could prolong the complete dissolution duration from 23 years to 2300 years. In their study, they also confirmed that cold water and high water pH (larger than 9) could strongly inhibit olivine dissolution. To enhance the olivine dissolution rate with less energy input, House *et al.* (2007) introduced a process via electrochemical chambers, in which olivine dissolves in high NaCl solutions. Köhler *et al.* (2013) used an Earth system coupled with silicate cycle to examine the CDR potential of adding olivine into open ocean. They found adding olivine could trigger plankton bloom due to the iron and silicon fertilization. However large olivine particles can sink below ocean mixing layer quickly, leaving olivine-AOA in large grain size inefficient to decrease atmospheric CO_2 in a short period of time. Several studies proposed to implement olivine on the coastlines (Schuiling and Krijgsman 2006, Hangx and Spiers 2009) because high dynamical mixing of tides and waves can greatly enhance olivine dissolution efficiency. But those proposals have not been comprehensively tested within the Earth system models.

1.3.3. Enhanced Biological Production

Atmospheric CO_2 reduction can also be achieved by enhanced biological production from both land and ocean

1.3.3.1. Afforestation

Forest turns absorbed CO_2 into forest biomass, dead organic matter and soil biomass. Deforestation has caused CO_2 emitted into the atmosphere and loss of biodiversity (IPCC-WG1 2013). A reversed approach, "Afforestation" (AF; Sometimes "Reforestation" is used for planting more "native" species where deforestation has occurred) of fast-growing trees on non-forested land, has been applied/exerted as a CDR method.

However, forest can also be carbon source when trees burn or decay after aging or insect attack caused death. Replacing landscape of sands with dark-colored forests can also enhance the radiation absorption via albedo-feedback effect (Bernier *et al.* 2011). Planting large number of trees will strongly modify the local hydrological cycle and heat fluxes, and perturb the climate. Research found afforestation in low latitude is likely to cause a net cooling effect whereas AF in high latitude with snow cover can cause net warming effect (Bala *et al.* 2007, Bathiany *et al.* 2010, Boysen *et al.* 2014).

1.3.3.2. Blue Carbon Enhancement

"Blue carbon" refers to the carbon that is stored by oceans and coastal ecosystems, including mangroves, salt marshes, sea grasses and algae. In contrast to forest "green carbon", the blue carbon has a much higher carbon sequestration rate and stores more carbon mass per equivalent area. By far sea grass (Zhang *et al.* 2012)

and mangrove (Greiner *et al.* 2013) restoration projects have been launched to increase blue carbon. But among those blue carbon species, microalgae, which is abundant in both coastal open ocean marine ecosystems, is considered the marine engine to produce aquatic biomass and serves as the first level in marine food chain. Those microalgae including cyanobacteria, diatom, dinoflagellate and cocollithophore and green algae, are also the main participants in the ocean biological pump. The microalgae that generate calcium or silicon carbonate accounts for the largest fraction of direct carbon sequestration in the ocean. Half of the carbon-rich biomass generated by microalgae is consumed by grazers, and around 20-30% organic and mineralized carbons will sediment below the thermocline. This marine biological pump is an important component in global carbon cycle, and some significant perturbation in this process can also affect the global climate system substantially, e.g. Azolla Event in middle Eocene epoch (Pearson and Palmer 2000).

Above-mentioned phytoplankton usually requires light, appropriate temperature and abundant nutrients (nitrogen, iron and phosphorus) to maintain their bioactivity. Those nutrients are important elements for the cells and complex molecules of phytoplankton. Most nutrients that can be taken by phytoplankton are in the form of inorganic compounds such as nitrate, ammonia and phosphate. In open ocean surface, the limited and insufficient nutrients remain a major constrain for phytoplankton growth. Therefore supplying the limiting nutrients for phytoplankton are predicted an effective measure to enhance the biological carbon sequestration.

Nutrient addition: Many studies have proposed to manually add nutrients, e.g. phosphorus (Lenton and Vaughan 2009) and nitrogen (Jones 1996) into the ocean to enhance biomass. Silicon is an important nutrient for diatoms, therefore silicon addition can potentially lead to diatom blooms (Allen *et al.* 2005). The most often discussed nutrient addition strategy is however Ocean Iron Fertilization (OIF). Approximately 20% of the global ocean is considered as "high-nutrient, low-chlorophyll" (conservatively the "nutrient" does not include bioavailable iron, despite that in nutriology iron is also nutrient) zones where iron is believed the reason for low phytoplankton growth rate and productivity. Watson *et al.* (2000) studied the effect of OIF in southern ocean from glacial times, and confirmed that moderate CO_2 reduction via OIF is possible.

To further test the effectiveness of OIF, several projects have been commenced in the past few years. In "European Iron Fertilization Experiment (EIFEX)" (Smetacek *et al.* 2012), scientists observed massive diatom blooms after four weeks in a mesocosm experiment in Atlantic Circumpolar Current, and the detritus formed after phytoplankton mortality sank into the deep ocean successfully. Another experiment "the Croszet Natural Iron Bloom and Export Experiment (CROZEX)", found that compared with natural iron influx from currents, artificial iron addition is not efficient due to the rapid dilution of the iron compound into the water (Pollard *et al.* 2009). "Indian and German Iron Fertilization Experiment (LOHAFEX)" commenced in year 2009 also confirmed small potential of OIF for biological bloom because silicon was limited for phytoplankton growth in the region where LOHAFEX was undertaken. Since silicon concentration was low for 65% of the

southern ocean, the potential of OIF as a means to sequester anthropogenic CO_2 should be much smaller than believed so far (~1 GtC per year). Besides, OIF might regulate the halocarbons-based on change of phytoplankton activities under OIF (Wingenter *et al.* 2004). It is generally accepted that, OIF can only mitigate less than 100 ppm atmospheric CO_2 within 100 years even under very idealized scenario.

Artificial upwelling: Upwelling is a phenomenon that involves motion of denser, cooler, and usually nutrient-rich water towards the ocean surface. It can boost the biological pump through enhanced surface primary production, and subsequently draws down atmosphere CO_2. Inspired by this feature, researchers proposed to use artificial upwelling (AU), as a CE strategy to mitigate CO_2 increase (Lovelock and Rapley 2007). AU is generated by device that can use ocean wave energy or ocean thermal energy to pump water to the surface. To evaluate its practical efficacy, some AU prototypes have been tested in Japan (Mizumukai *et al.* 2008), Norway (McClimans *et al.* 2010), the US (Liu and Jin 1995) and China (Pan *et al.* 2015). Those proposed AU prototypes with a self-pumping system could bring the water below the thermocline upward adiabatically, and enhance primary production remarkably. The main negative side of AU is that the regions to deploy AU are limited (IPCC-WG1 2013) and AU can cause downwelling in remote areas (Yool *et al.* 2009, Lenton and Vaughan 2009). Simulated surface temperatures and atmospheric CO_2 concentrations will rise quickly if AU is stopped, and reach even higher levels than the conditions that AU is not engaged (Oschlies and Pahlow *et al.* 2010).

1.4. Research Motivations and Thesis Outline

In year 2015 at Paris, a new agreement within United Nations Framework Convention on Climate Change (UNFCC) was negotiated by representatives of 195 countries to deal with climate change. Paris Agreement set a goal on "holding the increase in the global average temperature to well below 2 °C above preindustrial level, and pursuing efforts to limit the temperature increase to 1.5 °C above pre-industrial levels". Since CE is designed to mitigate the climate change and reduce global warming risks, the scientific understanding on CE's effectiveness, side effects and uncertainties appears crucial on determining whether CE should be seriously considered as an option for achieving the 2 and 1.5 °C mitigation goals.

Employing an Earth system climate model, this thesis will evaluate some of the proposed CE methods in the perspective of climate science with complementary comments about their engineering and economical feasibilities (Figure 1-4). Since there are relatively fewer modeling studies on AOA, I conducted two separate studies on this CE technology at first. For the first time in climate modeling society, I explored the potential of lime-based AOA's in protecting tropical coral reef from ocean acidification (Research #1), and investigated the climate responses to adding olivine minerals along coastal waters (Research #2). To better understand how CE model results are affected by the uncertainties within climate feedbacks, I conducted a modeling intercomparison study for SAI and DAC under different equilibrium climate sensitivities (ECSs) and CE implementation intensities, the relevant contents from which are summarized in "Research #3". Previous CE studies have made many assessments for sole implementation of a specific CE technology, "Research #4",

however attempts to understand how future climate involves if SAI and AOA are implemented in some combined schemes. At last, "Research #5" commenced a comprehensive evaluation on five CE technologies, and analyzed their potential for stopping the global warm risks and possible environmental side effects.
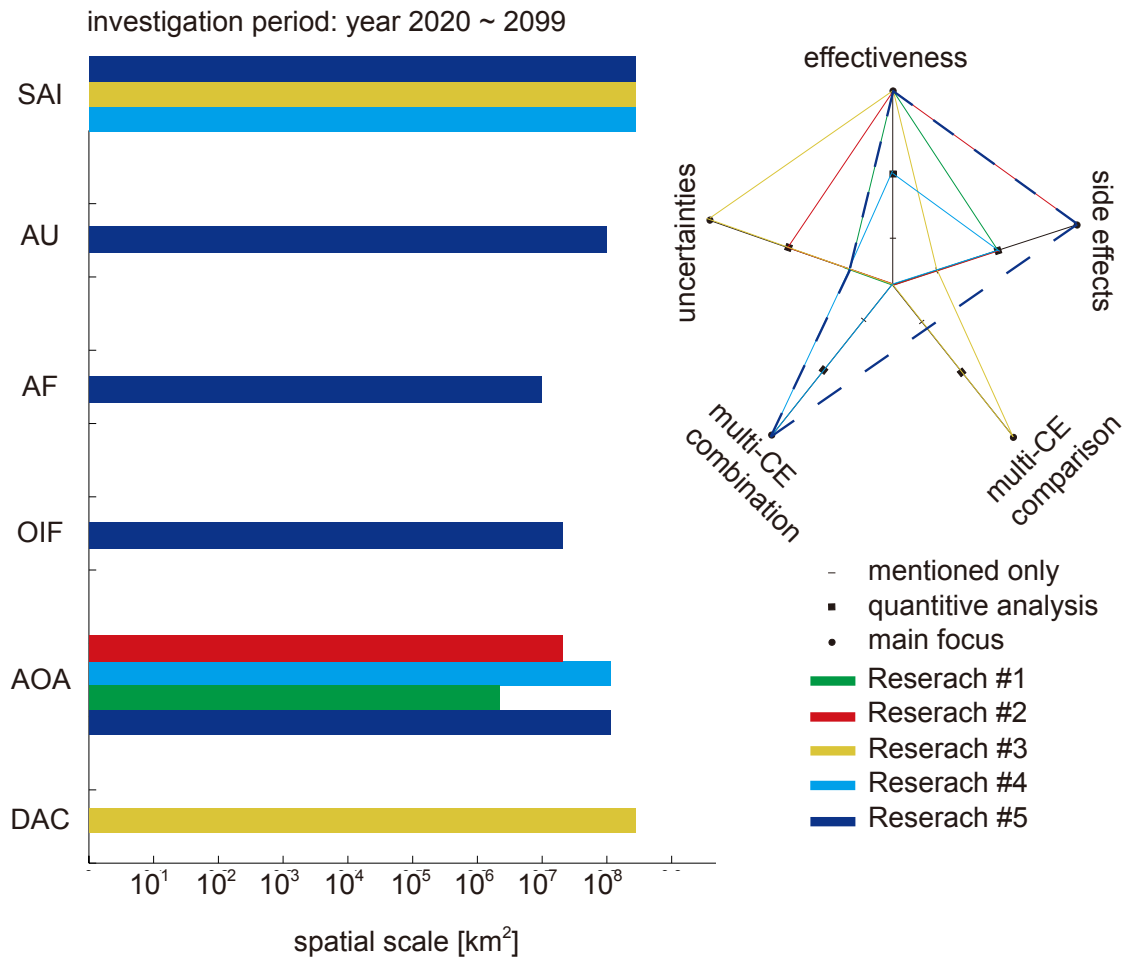
Figure 1-4. The studied CE technologies in this thesis are Sulphate Aerosol Injection (SAI), Artificial Upwelling (AU), Afforestration (AF), Ocean Iron Fertilization (OIF), Artificial Ocean Alkalinization (AOA) and CO$_2$ Direct Air Capture (DAC). In the radar diagram to the right side, individual research with related manuscript written as first author, is marked in solid curves (#1, #2, #3, #4), and in dashed curve curve (#5) as second author.

1.5. Publications and Author Contributions

Research #1

(E.) Y. Feng (冯玉铭), D. P. Keller, W. Koeve and A. Oschlies (2016): **Could artificial ocean alkalinization protect tropical coral ecosystems from ocean acidification**?

Environmental Research Letters, **11** (7) [highlighted by journal]

Contributions:

Idea and experimental design: D. P. Keller and Y. Feng

Model simulations: Y. Feng

Data analysis: Y. Feng, D. P. Keller, W. Koeve and A. Oschlies

Manuscript preparation: Y. Feng with inputs and comments from D. P. Keller, W. Koeve and A. Oschlies

----

Research #2

(E.) Y. Feng, W. Koeve, D. P. Keller and A. Oschlies (to be submitted): **Model-based assessment of the potential of coastal ocean alkalinization** *Environmental Research Letters*,

Contributions:

Idea and experimental design: Idea is raised by A. Oschlies, W. Koeve and D. P. Keller, experiment and algorithm designs are undertaken by Y. Feng

Modeling simulations: Y. Feng

Data analysis: Y. Feng

35

Manuscript preparation: Y. Feng with inputs and comments from W. Koeve, D. P. Keller and A. Oschlies

----

Research #3

(E.) Y. Feng, D. P. Keller and A. Oschlies (prepared manuscript): **Cooling effects from climate feedbacks in climate engineering implementations** *Journal of Climate (targeted)*

Contributions:

Idea and experimental design: Y. Feng and A. Oschlies

Modeling simulations: Y. Feng

Data analysis: Y. Feng

Manuscript preparation: Y. Feng with inputs and comments from D. P. Keller

----

Research #4

(E.) Y. Feng (prepared manuscript): **Modeling assessment of combined SRM/AOA scheme** *Climatic Change (targeted)*

Contributions:

Idea and experimental design: Y. Feng

Modeling simulations: Y. Feng

Data analysis: Y. Feng

Manuscript preparation: Y. Feng

Research #5

D. P. Keller, (E.) Y. Feng, and A. Oschlies (2014): **Potential climate engineering effectiveness and side-effects during a high carbon dioxide emission scenario**?

Nature Communications, doi:10.1038

Contributions:

Idea and experimental design: Idea is raised by D. P. Keller, experiment and code designs are undertaken by D. P. Keller and Y. Feng

Modeling simulations: D. P. Keller

Data analysis: D. P. Keller

Manuscript preparation: D. P. Keller with comments from A. Oschlies and Y. Feng

2. Research #1

Could artificial ocean alkalinization protect tropical coral ecosystems from ocean acidification?

Ellias Y. Feng (冯玉铭)[1,2], David P. Keller[1], Wolfgang Koeve[1] and Andreas Oschlies[1,2].

[1] GEOMAR Helmholtz Centre for Ocean Research Kiel

[2] University of Kiel

[1] E-mail: yfeng@geomar.de

Abstract: *Artificial ocean alkalinization (AOA) is investigated as a method to mitigate local ocean acidification and protect tropical coral ecosystems during a 21st century high CO2 emission scenario. Employing an Earth system model of intermediate complexity, our implementation of AOA in the Great Barrier Reef, Caribbean Sea and South China Sea regions, shows that alkalinization has the potential to counteract expected 21st century local acidification in regard to both oceanic surface aragonite saturation Ω and surface pCO2. Beyond preventing local acidification, regional AOA, however, results in locally elevated aragonite oversaturation and pCO2 decline. A notable consequence of stopping regional AOA is a rapid shift back to the acidified conditions of the target regions. We conclude that artificial ocean alkalinization may be a method that could help to keep regional coral ecosystems within saturation states and pCO2 values close to present-day values even in a high-emission scenario and thereby might "buy some time" against the ocean acidification threat, even though regional AOA does not significantly mitigate the warming threat.*

2.1. Introduction

Anthropogenic CO_2 invades the ocean and thereby perturbs ocean chemistry, this phenomenon is also known as "ocean acidification" (e.g. Caldeira and Wickett 2003, Feely *et al.* 2004). If CO_2 emissions continue to increase and the ocean continues to become more acidic these changes will further affect the ambient saturation state of aragonite (described by aragonite Ω). Since calcification, which is a crucial skeleton building process for most stony corals, is considered to be highly sensitive to ambient aragonite Ω, coral calcification is likely to become inhibited in the future (Gattuso *et al.* 1998, Langdon and Atkinson 2005). Stony coral reefs sustain the most diverse ecosystems in the tropical oceans, and the coral-supported tropical fish (Munday *et al.* 2014), coralline algae (McCoy and Ragazzola 2014), echinoderms (Dupont *et al.* 2010), molluscs (Gazeau *et al.* 2007), crustaceans (Whiteley 2011), and corals themselves (Kleypas *et al.* 1999a, Hoegh-Guldberg *et al.* 2007, Cao and Caldeira 2008, Crook *et al.* 2011, Meissner *et al.* 2012a) are expected to face difficulties in adapting to future ocean conditions in coming decades because of both ocean acidification itself and the loss of the reef structure. A potential loss of coral reefs and their ecosystems may also have a direct impact on coastal resources and services (Brander *et al.* 2009). Besides the threat from ocean acidification coral reefs face a number of other significant threats such as coral bleaching, which is triggered by persistent heat stress and is thought to be one of the most serious climate change related threats (Hoegh-Guldberg 1999, Cooper *et al.* 2008, De'ath *et al.* 2009, Frieler *et al.* 2012, Caldeira 2013).

Since efforts to mitigate global warming and ocean acidification by reducing emissions have, up to now, been unsuccessful in terms of a significant reduction in the growth of atmospheric CO_2 concentrations, there has been growing interest in climate engineering (CE) to mitigate or prevent various consequences of anthropogenic climate change (Crutzen 2006, Schuiling and Krijgsman 2006, Oschlies *et al.* 2010). For example, several modelling studies have examined "Artificial Ocean Alkalinization (AOA)" which modifies ocean alkalinity. These studies simulated the use of alkalizing agents such as olivine (a $Mg-Fe-SiO_4$ mineral) (Köhler *et al.* 2010, 2013, Hartmann *et al.* 2013), calcium carbonate (Caldeira and Rau 2000, Harvey 2008), or calcium hydroxide (Ilyina *et al.* 2013a, Keller *et al.* 2014) to elevate the ocean's alkalinity to increase CO_2 uptake and mitigating ocean acidification. While these simulations suggested that AOA could potentially be used to mitigate global warming and ocean acidification to some degree, some studies also suggested that deploying AOA at a global scale may face prohibitive logistical and economical constraints and could possibly cause undesired side effects (Renforth *et al.* 2013, Keller *et al.* 2014).

In this paper we use Earth system model simulations of regional AOA to investigate the potential of AOA to protect specific stony coral reef regions against ocean acidification. We also investigate possible environmental side effects of AOA and possible regional differences in effectiveness or undesired side effects. The model simulations show AOA could mitigate ocean acidification in our investigated coral reef regions, albeit at substantial economic costs and with the termination risk of a rapid return to acidified conditions after the stop of local AOA.

2.2. Method

We simulated calcium hydroxide (Ca(OH)2)-based AOA in the Great Barrier Reef (GB, 9.0°S~27.0°S, 140.4°E~154.8°E, an area of 1.7 x 106 km^2), the Caribbean Sea (CS, 10.8°N~27°N, 68.4°W~93.6°W, an area of 3.9 x 106 km^2) and the South China Sea (SC, 0°N~23.4°N, 104.4°E~129.6°E, an area of 5.2 x 10^6 km^2) (Figure 2-1) using the University of Victoria Earth System Climate Model (UVic) version 2.9. These areas contain some of the world's most abundant coral reefs (http://www.reefbase.org/) and are large enough to be addressed by the UVic model. From the data obtained from ReefBase (http://www.reefbase.org/), we found that from a total of 10,048 coral reef locations, 3323 are located in the Great Barrier Reef box, 601 in the Caribbean Sea box, and 2060 in the South China Sea box. Altogether 5984 reef points are included in our three regions, which is more than half of the global coral reef locations collected from ReefBase.

The UVic model consists of an energy-moisture balance atmospheric component, a 3D primitive-equation oceanic component that includes a sea-ice sub-component, and a terrestrial component (Weaver *et al.* 2001, Meissner *et al.* 2003). Wind velocities are prescribed from NCAR/NCEP monthly climatological data. Accordingly, UVic does not feature decadal ocean-atmosphere oscillations, like ENSO. The model has a spatial resolution of 3.6°×1.8° with 19 vertical layers in the ocean. The global carbon cycle is simulated with air-sea gas exchange of CO_2 and marine inorganic carbonate chemistry following the Ocean Carbon-Cycle Model Intercomparison Project Protocols (Orr *et al.* 1999). The inorganic carbon cycle is coupled to a marine ecosystem model that includes phytoplankton, zooplankton,

detritus, the nutrients nitrate and phosphate, and oxygen (Keller *et al.* 2012). The model has been evaluated in several model intercomparison projects (Eby *et al.* 2013, Zickfeld *et al.* 2013, Weaver *et al.* 2012), and shows a reasonable response to anthropogenic CO_2 forcing that is well within the range of other models. In order to illustrate that our model is robust in reproducing general ocean circulation and chemistry, we validate our model against GLODAP (Global Ocean Data Analysis Data Project) v1.1 data for ocean total alkalinity and oceanic dissolved inorganic carbon (Key *et al.* 2004) (Figure A1 and A2 in Appendix A), SOCAT (Surface Ocean CO_2 Atlas) data (Bakker *et al.* 2014, Landschützer *et al.* 2014) for sea surface pCO_2 (Figure A3), and WOA (World Ocean Atlas) 2013 data for sea surface temperature (Figure A4). The validation illustrates that UVic can generally reproduce the global patterns of surface ocean alkalinity and dissolved inorganic carbon as well as sea surface pCO_2. UVic's performance in reconstructing sea surface temperature (SST) is also generally good, especially in regions where AOA is implemented in our study with less than a 0.8 ℃ model-data misfit. Overall, the model-data differences displayed by the UVic model are well within the range data-error bonds from CMIP5 model simulations (Wang *et al.* 2014, Ilyina *et al.* 2013b, Jungclaus *et al.* 2013).

The model was spun-up for 10,000 years under pre-industrial atmospheric and astronomical boundary conditions. From year 1800 to 2005 the model was forced with historical fossil fuel and land-use carbon emissions. Then, from the year 2006 onwards the Representative Carbon Pathway 8.5 (RCP 8.5) anthropogenic CO_2 emission scenario forcing was used (Meinshausen *et al.* 2011). CO_2 is the only greenhouse gas taken into account. Continental ice sheets, volcanic forcing, and

astronomical boundary conditions were held constant to facilitate the experimental

set-up and analysis.
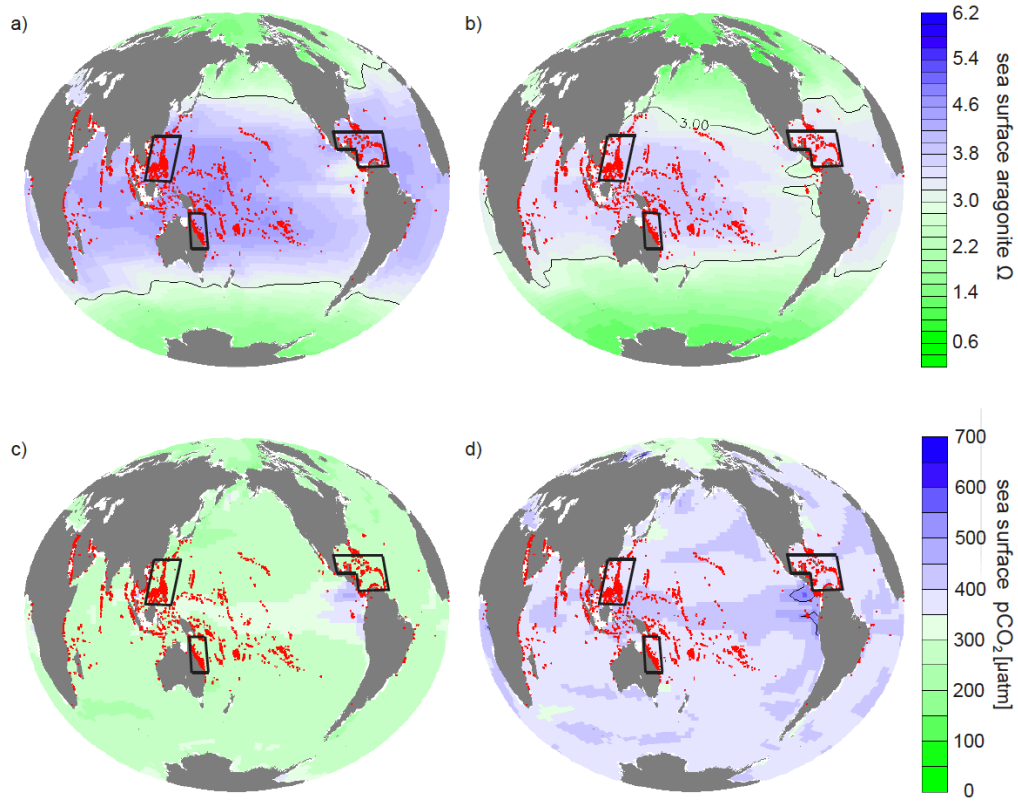
Figure 2-1. Annual-mean surface aragonite Ω and pCO₂ simulated by the UVic model control run without regional artificial ocean alkalinization (AOA) for preindustrial (a, c) and 2020 (b, d). AOA experimental regions are marked by black boxes. Coral Reef locations are marked in cyan.

Ca(OH)₂-based AOA is simulated in an idealized manner by increasing

surface alkalinity (Keller *et al.* 2014). The rationale behind this method is that

dissolving one mole of Ca(OH)₂ in seawater increases total alkalinity by 2 moles

(Ilyina *et al.* 2013a). We simulate Ca(OH)₂-based AOA by homogeneously and

continuously adding alkalinity to the upper 50m of the targeted regions. In the

following, we therefore use the term "lime addition" to refer to our simulated

Ca(OH)₂ addition. Directly simulating individual reefs or corals is beyond our

43

current model's capacity and we therefore focus on AOA-induced impacts on regional and global marine chemistry. Also, we ignore the impact of increasing water temperature on corals, which will accompany elevated levels of atmospheric CO_2 and would likely also have a detrimental impact on coral reefs.

We use a fixed threshold aragonite Ω to describe suitable stony coral habitats since most of today's coral reefs are found in waters with ambient seawater aragonite Ω above a critical value (Kleypas *et al.* 1999b, Meissner *et al.* 2012a, 2012b, Ricke *et al.* 2013). However, this approach involves some uncertainties (Kleypas *et al.* 1999b, Guinotte *et al.* 2003) due to the neglect of seasonal and diurnal Ω fluctuations, species variety, and species ability to adapt. Critical coral habitat threshold values of ambient aragonite Ω ranging from $\Omega = 3$ (Meissner *et al.* 2012b), $\Omega = 3.3$ (Meissner *et al.* 2012a), to $\Omega = 3.5$ (Ricke *et al.* 2013) have been used in recent climate change studies, acknowledging that these represent regional mean values and that local reef-scale carbonate chemistry may display large diurnal fluctuations also in healthy reefs. Ignoring sea surface temperature as a regulator of coral reef habitats may be a further simplification (Couce *et al.* 2013). We follow these earlier studies and, in this paper, use an aragonite Ω threshold of 3 to determine whether or not seawater chemistry with a region is suitable for stony corals.

A healthy coral ecosystem usually includes a multitude of both calcifying and non-calcifying organisms. Aragonite Ω is commonly used to evaluate the impact of ocean acidification on marine calcifying organisms. Nevertheless, ocean acidification can also affect non-calcifying organisms, e.g. by reducing their metabolic rates (Rosa and Seibel 2008) or damaging their larval and juvenile stages (Frommel *et al.* 2011).

Concerning non-calcifying organisms, often pCO_2 is employed as a metric to evaluate impacts of ocean acidification. We therefore also consider how seawater pCO_2 will develop under increasing atmospheric pCO_2 and continuous AOA. Without AOA, annual-mean surface seawater pCO_2 will follow atmospheric pCO_2 with some small time lag (e.g. Bates 2007). A meta-study of resistance of different marine taxa to elevated pCO_2 (Wittmann and Pörtner 2013) found that 50% of the species of corals, echinoderms, molluscs, fishes and crustaceans are negatively affected if seawater pCO_2 reaches high levels (between 632 to 1,003 µatm) with many species, except for crustaceans, also being significantly affected by pCO_2 levels between 500-650 µatm. Among the studied species, 57 % of echinoderms and 50 % of molluscs were negatively affected by the lowest levels of experimental pCO_2 manipulations. Since the loss of even one species, such as a keystone species, could potentially be detrimental for reef health, we chose a relatively low threshold of 500 µatm pCO_2 (as an annual average) to determine whether or not conditions were suitable for maintaining a healthy reef habitat. Moreover, by choosing a lower threshold we can better account for any variability in pCO_2 that may not be well simulated by our model. However, we must acknowledge that there are considerable uncertainties concerning such a threshold. Furthermore, these thresholds can be modulated by other environmental factors (Manzello 2015) and may not be absolutely applicable in every reef location. To avoid unnecessary complexity, the thresholds for both pCO_2 and Ω are considered here in terms of regional and annual averages.

Four sets of model simulations were carried out (Table 1-1), beginning at the start of the year 2020 and ending at the end of the year 2099 of the RCP 8.5 emission scenario. Ensemble A is the control run (no AOA). In Ensemble B constant amounts of lime (from 1 to 10 Gt yr^{-1} with 1 Gt yr^{-1} increments) were added homogenously to each region. In Ensemble C we sought a solution where a linear increase of AOA over time ensured that our thresholds were met with a minimum lime addition, with the chosen rate of increase guided by the results from Ensemble B. Runs of Ensemble D are identical to those of Ensemble C, except for the fact that we stop AOA at the beginning of the year 2070 and continue the run without AOA until the end of the year 2099. This is to study the impact of a planned or unplanned stop of AOA.

Table 1-1. Description of simulated Artificial Ocean Alkalinization (AOA) experiments during RCP 8.5 CO2 emissions scenario forcing

| Experimental Ensemble	AOA starts in year	AOA ends in year	Lime addition (Gt yr-1)	Number of runs†
A (control)	-	-	0	1
B (constant addition)	2020	2099	1, 2, 3, 4, 5, 6, 7, 8, 9, and 10	10
C (optimal)	2050* or 2048**	2099	Linear increase with time	60
D (optimal/termination)	2050* or 2048**	2070	Linear increase with time	60

† in each region respectively
* Great Barrier Reef; ** Caribbean Sea and South China Sea

2.3. Results

In the control run, regionally averaged surface aragonite Ω drops below 3 in the Great Barrier Reef (GB) after year 2057, in the Caribbean Sea (CS) after year 2049, and in the South China Sea (SC) after year 2057 (Figure 2-2). The mean pCO$_2$

threshold of 500 µatm is crossed in the GB at year 2050, in the CS at year 2048, and in the SC at year 2048. With constant AOA (Ensemble B) the thresholds are crossed at a later date or not at all, depending on the intensity of AOA. After an initial increase of Ω and decrease of pCO_2, respectively, the surface aragonite Ω declines and pCO_2 increases almost linearly with time as ocean acidification intensifies because of the increasing invasion of atmospheric CO_2. The minimum amount of lime that is needed to prevent regionally averaged surface aragonite Ω from dropping below 3 before the end of year 2099 in these constant AOA simulations is 1.1 (GB), 1.9 (CS), and 1.5 Gt yr^{-1} (SC), respectively. In order to prevent regional annual-mean surface pCO_2 from exceeding 500 µatm, the minimum amount of lime that is needed is always significantly larger, i.e. 2.5 (GB), 4.9 (CS), and 5.7 Gt yr^{-1} (SC), respectively. These results indicate that meeting the pCO_2 threshold in our setup always requires a higher alkalinity addition than it does to meet the aragonite saturation threshold, thus in our particular case of combined pCO_2 and Ω thresholds, only the pCO_2 threshold needs to be considered.
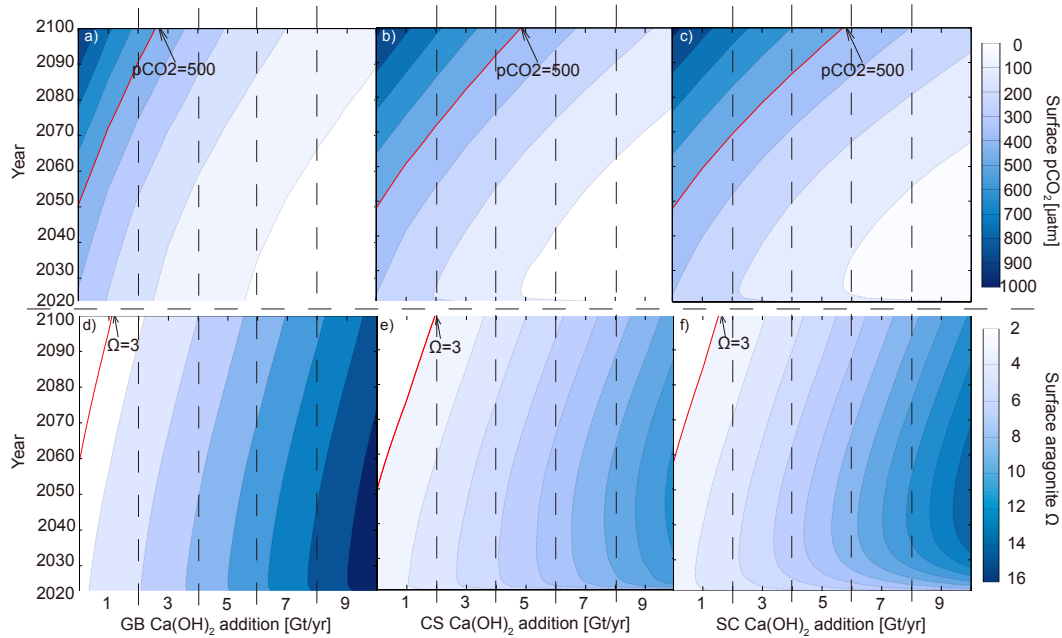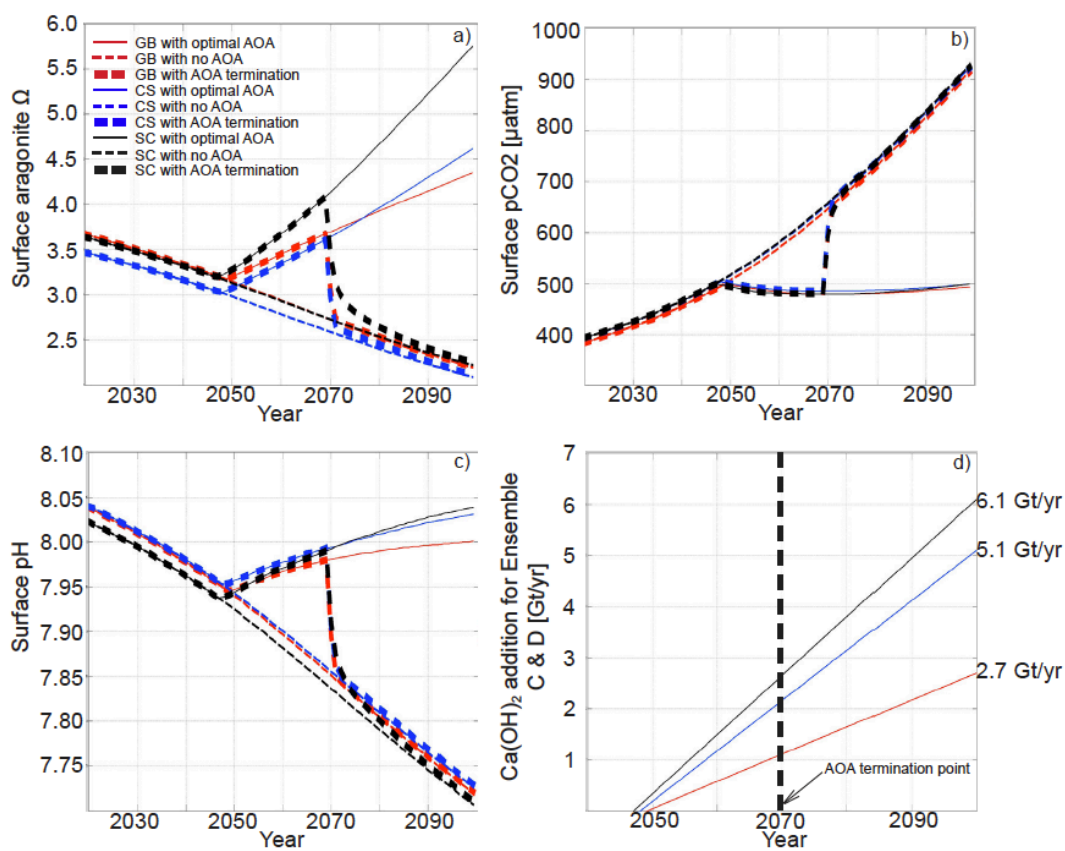
Figure 2-2. Regionally-averaged surface aragonite Ω and surface pCO₂ that occur in the Great Barrier Reef (a, d), Caribbean Sea (b, e), and the South China Sea (c,f) regions for the Ensemble A and B simulations as a function of time. Thresholds are highlighted by red isoclines.

Ensemble C includes a total of 60 model runs for each region that were initiated with output from the control run years 2050 (GB) and 2048 (CS and SC), respectively, which are the time points just before our chosen threshold values for surface pCO₂ was crossed in the respective experimental regions. Thereafter, simulated lime additions increase linearly from 0 Gt yr⁻¹ to a maximum addition in year 2099, which ranges from 2 to 7 Gt yr⁻¹ depending on the region (not shown; see Figure 2-3(d) for the "optimal" example). Of the 3 x 60 runs composing Ensemble C, our specific interest was in the runs ending at 2.7 (GB), 5.1 (CS) and 6.1 (SC) Gt lime per year (year 2100) since these "optimal" runs require the least time integrated amount of AOA to prevent our chosen thresholds from being crossed (Figure 2-3(b)). In year 2099 of these runs we find surface aragonite Ω =4.3, 4.6, and 5.7 and surface

pH=7.99, 8.03, and 8.04 in the GB, CS, and SC, respectively (Figure 2-3(a)). That is, in order to prevent local seawater pCO_2 from increasing above our chosen threshold, one would have to accept a considerable increase in seawater Ω compared to the situation in 2020. In the year 2099, the region-averaged alkalinity additions are 42.6 mol m^{-2} yr^{-1} (GB), 34.9 mol m^{-2} yr^{-1} (CS) and 31.2 m^{-2} yr^{-1} (SC). This regional AOA leads to an additional global oceanic carbon uptake of ~15.36, 32.54, and 35.41 Gt C for the GB, CS, and SC runs by the end of the year 2099, respectively.

Terminating regional AOA (Ensemble D) has a strong and rapid impact on surface aragonite Ω, seawater pCO_2 and pH in the respective regions (Figure 2-3). After termination the AOA related regional changes disappear on an annual timescale and quickly converge back to conditions very close to those of the control run.

Figure 2-3. Comparison between the Great Barrier Reef, Caribbean Sea, and South China Sea regionally averaged annual surface aragonite Ω (a), seawater pCO₂ (b), and sea surface pH (c) values during the control (Ensemble A) and the "optimal" AOA simulations (single optimized simulation from Ensembles C and D). Note that AOA ends in the year 2070 in the Ensemble D simulations. The amount of lime needed for the "optimal" AOA implementation in year 2100 is labeled in (d).

Regional AOA also has effects on global ocean biogeochemistry (Figures 2-4 and 2-5). Within a few decades, AOA in the CS affects surface Ω and seawater pCO₂ in much of the western North Atlantic. On the timescales considered, AOA in the GB region appears to be the most locally confined in our runs, but nevertheless affects the coastal waters of Papua New Guinea and Indonesia. Overall, however, remote effects are moderate compared with local impacts. Compared with the control run, the optimal runs (Ensemble C) have annual regional surface pCO₂ partial pressures

50

that are ~300 to 800 μatm lower and an aragonite Ω that is of ~2.5 to 10 times higher in AOA regions compared to the control run without AOA. At the same time, both the globally averaged increase in surface Ω and the decrease in pCO_2 are moderately small (Figure A5 in Appendix A).   Thus, in our optimal AOA simulations, atmospheric CO_2 is drawn down by the end of 2099, relative to the control run, by about 7 ppm for GB run, 15 ppm for CS run and 16 ppm for SC.
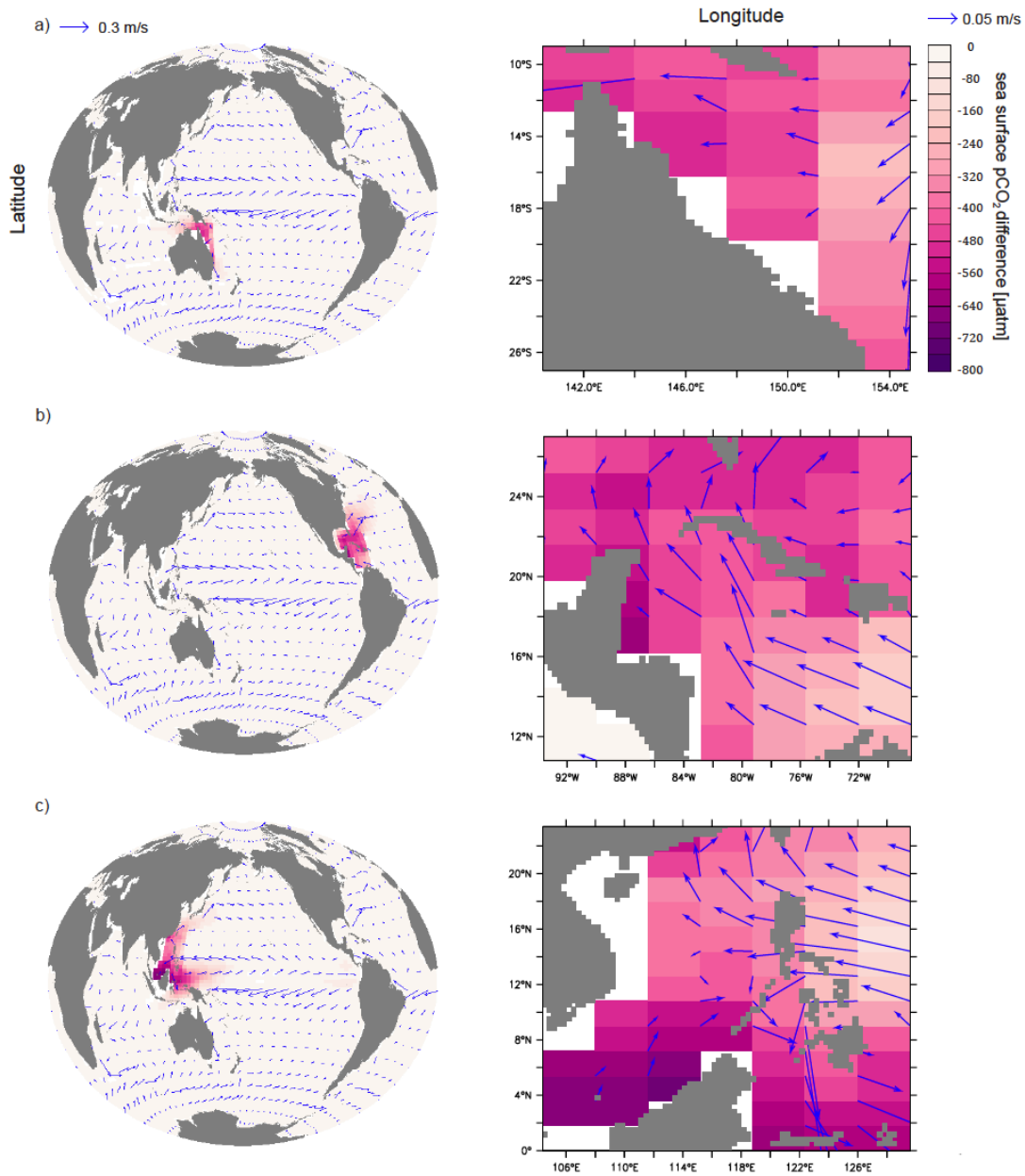
Figure 2-4. Simulated year 2099 surface pCO₂ differences between the optimal runs (Ensemble C) and the control run for the Great Barrier Reef (a), Caribbean Sea (b), and South China Sea (c) Each is shown with respect to the global impact (left) and the impact over the respective region where AOA is applied (right). Annual-mean surface current velocities are marked as blue arrows.

Figure 2-5. Simulated year 2099 surface aragonite Ω differences between the optimal runs (Ensemble C) and the control run for the Great Barrier Reef (a), Caribbean Sea (b), and South China Sea (c). Each is shown with respect to the global impact (left) and the impact over the respective region where AOA is applied (right). Annual-mean surface current velocities are marked as blue arrows.
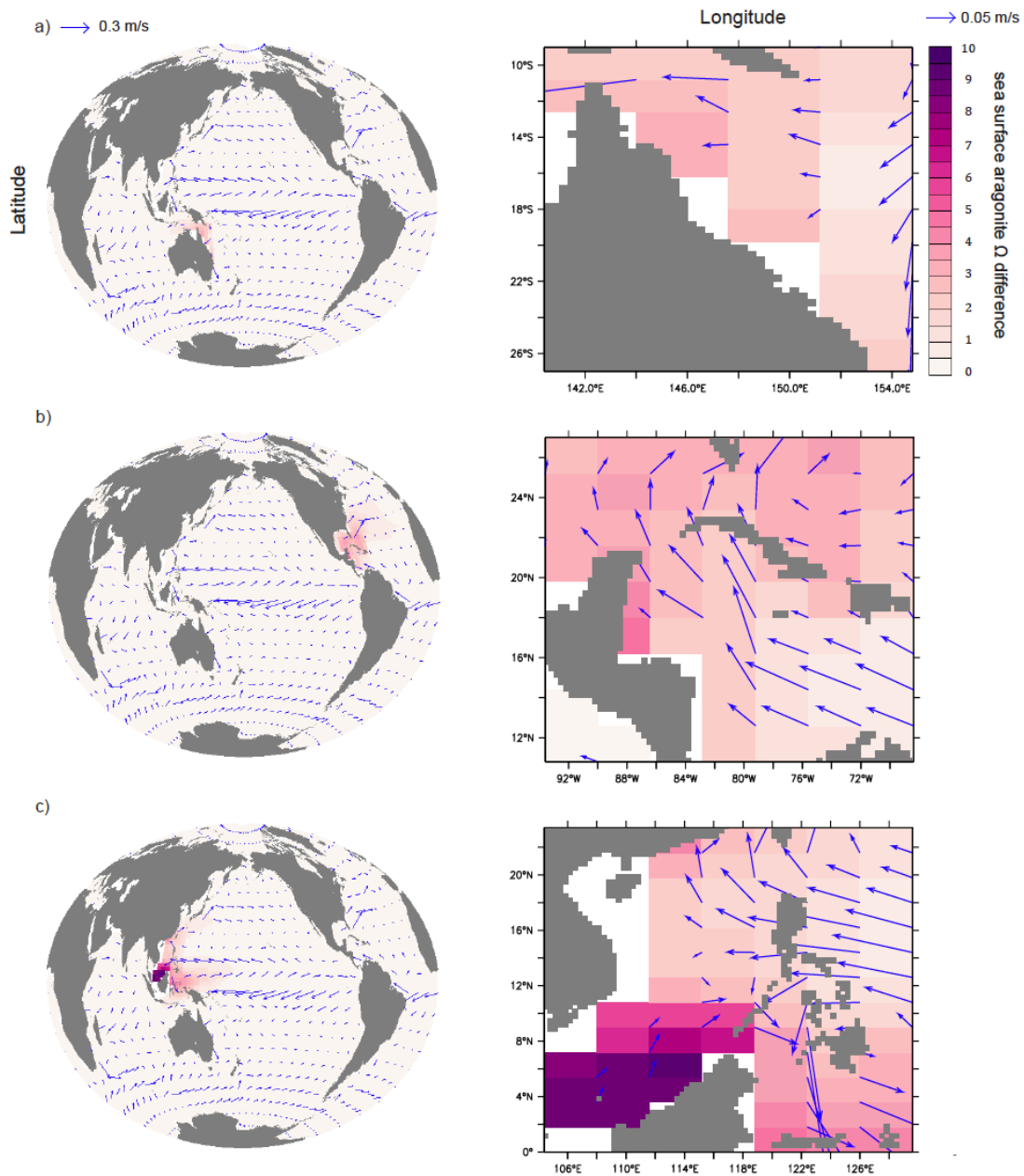
2.4. Discussion

From a marine biogeochemical perspective, our results indicate that regional AOA could potentially be an effective means to mitigate regional ocean acidification.

53

In our AOA simulations (Ensemble B, C and D) the increase of surface seawater pCO_2 levels, as well as the reduction of local pH and aragonite saturation states are all mitigated or even reversed in the targeted regions (Figure 2-2, 2-3 and 2-4). However, increasing surface ocean alkalinity also induces an additional uptake of CO_2. For the optimal runs (Ensemble C), AOA modifies the oceanic DIC system (Figure A6) leading to an increase in both carbonate and bicarbonate ions. The increase of Ω and the carbonate ion concentration beyond current or preindustrial levels in Figure 2-3(a) may have unforeseen consequences in the real ocean as elevated supersaturation may have biological impacts (Cripps *et al.* 2013) or even cause the spontaneous abiotic precipitation of $CaCO_3$. Like the biotically induced precipitation of $CaCO_3$, this process would directly lead to an increase of pCO_2, i.e. constituting a negative feedback to intentional alkalinization. If spontaneous $CaCO_3$ precipitation due to elevated total alkalinity happens, this would be detrimental as coral reefs are known to be sensitive to high levels of turbidity (Broecker and Takahashi 1966, Roy and Smith 1971). Previous research by Renforth *et al.* (2013) suggest to use an optimum lime particle size of 80~100 since such particles can be fully dissolved in a typical surface ocean with a depth less than 100 meters. For most tropical stony coral ecosystems, which are generally within 100 meters of the surface, the direct addition of such particulate lime could affect water column transparency and may even result in particles settling directly onto organisms. To minimize this side effect, lime could be dissolved in seawater before adding it.

In addition to CO_2-system changes, AOA, if done with lime, will add calcium to the system. In our optimum simulations (Ensemble C), the surface calcium

concentration could be elevated by up to 0.16, 0.26, and 0.34 mmol/kg for the GB, CS, and SC respectively (Figure A7). Natural calcium behaves conservatively in the ocean and for a salinity of 35 the calcium concentration is about 10.27 mmol/kg (Pilson 2013). The amount of calcium added during alkalinization is hence less than 4% of the background calcium concentration.

How well do our simulations reflect the real environmental conditions that coral reef ecosystems might experience during a high CO_2 climate scenario (control run) and AOA deployment? An estimate of potential impacts of model errors in simulated carbonate chemistry (Table A1) suggests uncertainties in the calculated regionally averaged alkalinity requirements of less than 10%. This result indicates that the seawater chemistry simulated by UVic is acceptable for such an initial study of potential AOA. Three limitations of our study, however, remain: First, the current model's coarse resolution does not resolve small-scale physical processes like boundary currents, local upwelling and temperature variability around reef archipelagos or in shallow lagoons (Meissner *et al.* 2012a). Studies with higher resolution models would be necessary to assess these local aspects. Second, most reported massive coral bleaching incidents are associated with El-Niño years (Aronson *et al.* 2002), which are not resolved in our UVic model simulations driven by climatological winds. The observed ENSO-associated variability in our studied regions is relatively weak, as revealed by an analysis of historical SST and air-sea delta-pCO_2 records (Appendix Figure A14 and A15). However, it is not well known how ENSO variability will develop in the future (Collins *et al.* 2010)(Guilyardi *et al.* 2009) and thus its impact on our study region will remain another uncertainty. Third,

local calcification, dissolution, photosynthesis and respiration within coral reefs affect local ocean chemistry and are not in detail included in our model. For example, over a diel cycle the aragonite saturation state may vary considerably, as has been observed at a coral reef off Okinawa, Japan where Ω ranged from 1.08 to 7.77 (Ohde and Hossain 2004). Similarly, seawater pCO_2 has been observed to vary between 420 µatm to 596 µatm during a 24 hour period (Dufault *et al.* 2012). These large variations are due to day-night fluctuations in carbon uptake and metabolism within coral reefs (Comeau *et al.* 2012), which our model cannot simulate. Because the ocean's uptake of anthropogenic CO_2 is associated with a decrease in the ocean's buffering capacity, natural fluctuations of the carbonate system on seasonal and diurnal scales are expected to increase (Riebesell *et al.* 2009, Melzner *et al.* 2012). Lacking the small-scale variability in general, our simulations may underestimate the stress that might go along with even stronger fluctuations in the future. However, since AOA would increase the regional ocean buffering capacity, it could dampen future carbonate system fluctuations otherwise expected in a high CO_2 emission world.

Our results also reveal different regional sensitivities of the AOA deployments. To stay within our chosen mitigation guardrails (seawater $pCO_2 < 500$ µatm, $\Omega > 3$ in the regional and annual-means) during the 21st century the GB requires the smallest amount of total lime input while the SC requires the largest. These differences are largely due to the size difference of our studied regions. In the year 2099, the regional mean alkalinity additions are 42.6 mol m^{-2} yr^{-1} (GB), 34.9 mol m^{-2} yr^{-1} (CS) and 31.2 m^{-2} yr^{-1} (SC). These differences can be explained by a combination of local hydrography and biogeochemistry. For example, the local

surface alkalinity decline during the first year after AOA termination in Ensemble D, i.e. between the beginning and end of year 2070 is largest in CS (80 mmol m^{-3}), intermediate for GB (70 mmol m^{-3}) and smallest for SC (61 mmol m^{-3}). Figure 2-3(b) reveals that even though surface pCO$_2$ is almost identical in the three areas, the evolution of surface aragonite saturation levels during AOA differs among the regions (Figure 2-3(a)). For the same pCO$_2$ levels, aragonite Ω in the SC increases more rapidly than in the CS and GB. This variation in carbonate chemistry also leads to regionally different sensitivities to ocean acidification, which determines the initiation and duration of AOA in Ensemble C.

The effectiveness of AOA can be described by the ratio between oceanic inventory changes of DIC referenced to the control run and added total lime by the end of year 2099. The optimal runs of Ensemble C show an effectiveness of 1.4 for GB, 1.5 for CS and 1.4 for SC, close to the value of 1.4 that we calculated based on data from Keller *et al.* (2014). Compared to previous estimates of AOA effectiveness that are above 1.6 (Renforth *et al.* 2013), our slightly lower values can be explained by the downward transport of added alkalinity on time scales shorter than the air-sea equilibration time of CO$_2$ (Figure A8). This loss of alkalinity from the surface layer leads, in our model, to a lower effectiveness than predicted by theory and adds another element of uncertainty to predicting how AOA would work if actually deployed.

General surface ocean acidification can be detected in the runs of ensemble C until the year when AOA is initiated (Figure A9). Thereafter total alkalinity accumulates until year 2099 with regional TA reaching concentrations about 200 ~

500 mmol/m^3 higher than the initial values. Comparisons between this study and other AOA studies that included regional applications, such as Ilyina *et al.* (2013a), are difficult because those studies were designed to investigate AOA as a means for global CO_2 mitigation, and thus even when AOA was applied regionally it was in still relatively large areas that have a high potential for increasing the uptake of atmospheric CO_2. An implementation of AOA on a regional scale of less than 10 geographical degrees across for only a short time of less than 100 years, has only a limited impact on atmospheric CO_2, while a global implementation of AOA (Keller *et al.* 2014), in particular when applied for centuries to millennia (Ilyina *et al.* 2013a), can significantly impact atmospheric CO_2 and the global carbon cycle. In contrast to results of the global AOA studies, only a relatively low carbon sequestration and storage potential, with less than 20 ppm atmospheric CO_2 reduction, is achieved in our regional AOA simulations. In Keller *et al.* (2014) a global implementation of lime-based AOA is deployed from year 2020 to year 2100 leads to an atmospheric CO_2 decrease about 166 ppm, while Ilyina *et al.* (2013a) observe a CO_2 drawdown of up to 450 ppm in their global and "Atlantic+Pacific" AOA implementation scenarios. Our results imply that from the regions we selected, regional and decadal- to centennial-scale AOA would not be an appropriate means for significant climate remediation.

Differences between regional and global AOA also affect the local seawater chemistry after a termination of AOA. If regional AOA is terminated abruptly, regional seawater pCO_2, aragonite Ω and pH rapidly return to the levels found in the control run (Figure 2-3) on an annual timescale. This is different from the findings of large-scale AOA simulations where such a termination effect is not observed (Ilyina

et al. 2013a, Keller *et al.* 2014). In the case of regional AOA, lime and the dissolution products are dispersed rapidly and diluted by seawater from outside the deployment area. Such a rapid change in regional ocean chemistry, which is faster than in any climate change scenario, could potentially put substantial stress on regional ecosystems. Thus, if regional AOA was done without reducing atmospheric CO_2, the process of adding lime would potentially have to continue for very long times or be phased out carefully to avoid risks to coral reef ecosystems.

A practical consideration is how much our optimal AOA applications would cost. For CaO-based AOA ($Ca(OH)_2$ is hydrated CaO) cost estimates provided by Renforth *et al.* (2013) indicate that every ton of CO_2 taken up by the ocean as a result of AOA costs approximately \$72-159 (USD). These estimates include the extraction, calcination, hydration, and surface ocean dispersion costs associated with AOA and are likely higher than AOA in our study would be since the transportation costs were based on covering the entire global ocean. In our optimal simulation, the cumulative amount of atmospheric CO_2 that is sequestered by AOA in the year 2099 is 56.32 Gt CO_2 in the GB, 119.28 Gt CO_2 in the CS and 129.84 Gt CO_2 in the SC. Based on Renforth *et al.* (2013), AOA would cost around USD 51-112 billion for the GB per year (if we assume an even sharing of costs over the 80 year periods of our AOA simulations), USD 107-237 billion for the CS per year, and USD 117-258 billion for the SC per year. Among all three studied regions, GB has the largest number of coral reef locations and the AOA costs for it are the lowest from our study. The Gross Domestic Product (GDP) for Australia in the year 2014 was USD 1.45 trillion. According to our model results, Australia could keep the GB region from crossing our chosen

59

guardrails by spending 3.5% ~ 7.7% of its GDP for coral reef protection. Admittedly, this is a huge investment compared with the estimated benefits (5~7 billion USD per year) related to coral reefs (GBRMPA (2013)).

Ocean acidification is only one of the stressors that corals reefs face in the future. Our study has not addressed other problems such as overfishing (Loh *et al.* 2015) or thermal stress (Goreau and Hayes 1994). Coral reef bleaching, caused by thermal stress, is one of the most lethal and enduring threats to coral reefs. For example, in the Great Barrier Reef, between 11 to 83% of coral colonies were affected by large-scale bleaching due to unusually high temperatures during 1998, an El-Niño year, with the mortality rate varying between 1% and 16% (Marshall and Baird 2000). The GB coral coverage declined by around 50% between 1985 to 2012, with 10% of the total loss attributed to coral bleaching (De'ath *et al.* 2012). In the Caribbean Sea (CS), thermal stress in the year 2005 exceeded observed levels in the previous 20 years causing over 80% of corals to bleach and resulting in a 40% population loss (Eakin *et al.* 2010). In the South China Sea (SC), massive coral bleaching in 1997 and 1998 affected 40% of coral colonies, but many of them recovered within a year (Waheed *et al.* 2015). Model simulations have suggested that coral bleaching incidents will increase with global warming, and the threat will become more severe in the future if CO_2 emissions remain high and significant warming occurs (Frieler *et al.* 2012, Caldeira 2013). According to Teneva *et al.* (2012)'s model simulations, our three study areas are in coral bleaching hot spots (Goreau and Hayes 1994) with a middle to high likelihood of experiencing bleaching. Donner (2009) predicted that the 10 years' mean SST during 2090 to 2099 in our studied regions are 3.2°C (SC),

3.3°C (GB) and 3.4°C (CS) higher than those during 1980 to 2000 under a business-as-usual high CO_2 emission scenario. Given such predictions, the question arises as to whether or not regional AOA would be sufficient if CO_2 emissions remain high, e.g., warming might harm coral reefs long before acidification becomes a significant threat. There have been proposals to use cloud brightening (Latham *et al.* 2013) to cool down surface temperatures to prevent coral bleaching and it is possible that other solar radiation management (SRM) methods may be envisaged in a similar manner. If SRM were seriously considered for this purpose when atmospheric CO_2 levels are high, AOA would be worth considering as well.

2.5. Conclusions

Our results show that with simulated AOA, regional surface aragonite Ω and pCO_2 could be prevented from crossing the acidification thresholds that we set (pCO_2 < 500 μatm, Ω > 3). In this respect, marine biota could benefit from AOA. To successfully protect corals and associated marine biota from OA within all three regions examined in our study, one would need to deploy about 356 Gt lime over next 80 years, with estimated implementation costs between 275 and 607 billion US dollars annually. This can possibly "buy sometime" before ocean acidification induces physiological stress and ecological shifts. We have also shown that the carbon sequestration potential of regional AOA is small, with regional differences in its effectiveness and sensitivities. Due to rapid exchange with untreated waters from outside the regions, a termination effect would have to be taken into account should deployment of regional AOA be considered in reality. This research shows that AOA has the potential to mitigate regional ocean acidification for the purpose of protecting

61

tropical coral reef ecosystems. Details about environmental side effects will have to be explored with higher resolution models and dedicated lab and possibly field experiments. From a climate change perspective the best solution would obviously be to stop emitting CO_2 and thereby prevent warming and ocean acidification from occurring and affecting coral reef ecosystems in the first place. Since this is unlikely to happen in the near future, it is worth investigating climate engineering methods such as AOA, since they might be able to provide an alternative or complementary means of protection.

Acknowledgments

3. Research #2

Model-based Assessment of the Potential of Coastal Ocean Alkalinization

Ellias Y. Feng[1,2], Wolfgang Koeve[1], David P. Keller[1], and Andreas Oschlies[1,2].

[1] **GEOMAR Helmholtz Centre for Ocean Research Kiel**

[2] **University of Kiel**
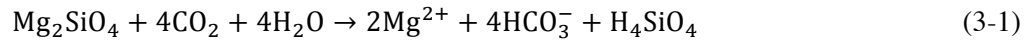
[1] **E-mail: yfeng@geomar.de**

Abstract: *Coastal Ocean Alkalinization (COA) as a carbon dioxide removal (CDR) strategy is investigated with an Earth system model. As alkalinity source we assume olivine with dissolution rates controlled by olivine grain size, ambient seawater temperature and pH. Simulated COA is implemented along ice-free coasts and the CDR potential and possible environmental side-effects are estimated for various deployment scenarios. Our results indicate that for large enough olivine production, implementing COA alone has some potential to mitigate the expected 21st century CO2 increase as well as ocean acidification. As olivine grain size increases from 10 μm to 1000 μm, the net CO2 sequestration potential decreases rapidly even when accounting for the CO2 offset associated with grinding. However, ambitious CDR through COA would increase coastal aragonite Ω to levels well beyond those typically experienced by marine biota until now. When local aragonite saturation levels of 3.4, 5.6 and 9 are taken as the thresholds to prevent excessive alkalinization, COA could potentially reduce atmospheric CO2 by 7.42~13.53, 10.04~28.96 and 17.63~49.63 Pmol cumulatively by year 2100.*

3.1. Introduction

Emissions of the greenhouse gas CO_2 have led, and continue to lead, to elevated atmospheric CO_2 concentrations causing global warming and associated environmental change with possibly severe consequences over the next decades (IPCC 2014). To reduce the risk of dangerous climate change, multiple adaptation and mitigation strategies are being implemented and even climate engineering ideas are being discussed. Among the measures under consideration, the artificial increase of ocean alkalinity (Kheshgi 1995), e.g. Artificial Ocean Alkalinization (AOA), has been proposed as a potential carbon dioxide removal (CDR) strategy and means of mitigating ocean acidification (Feng *et al.* 2016). As a climate engineering proposal, AOA would be implemented by adding naturally occurring abundant alkaline minerals, such as olivine ($[Mg^{+2},Fe^{+2}]_2SiO_4$) (Schuiling and Krijgsman 2006, Köhler *et al.* 2010), or limestone ($CaCO_3$) (Rau and Caldeira 1999) to the ocean to alter its carbonate chemistry and ultimately remove CO_2 from the atmosphere. Upon dissolution in the surface waters, olivine reacts with oceanic dissolved CO_2 and transforms it into bicarbonate and silicic acid, thereby increasing oceanic CO_2 uptake (Equation (3-1)). Limestone (calcium carbonate), however, can dissolve only within limited areas with very high oceanic dissolved inorganic carbon (DIC) concentrations (Harvey 2008). To overcome this dissolution barrier, some studies suggest reacting refined (ground) limestone with CO_2-rich effluent gas streams in a water solution/spray, prior to adding the reaction products to the ocean (Equation (3-2)) (Rau *et al.* 2001 and Rau 2008). Alternatively, Renforth *et al.* (2013) suggest that lime or quick lime ($Ca(OH)_2$), produced via calcination, could be added directly to the

ocean where it would quickly dissolve. Compared with olivine, the preparation process required for using limestone for AOA appears more complex and essentially involves the production and release of additional CO_2 that would have to be captured and stored (Kheshgi 1995).

$$Mg_2SiO_4 + 4CO_2 + 4H_2O \rightarrow 2Mg^{2+} + 4HCO_3^- + H_4SiO_4 \qquad (3\text{-}1)$$

$$CaCO_3 + CO_2 + H_2O \rightarrow Ca^{2+} + 2HCO_3^- \qquad (3\text{-}2)$$

Due to the engineering challenges of limestone-based AOA, we focus here on exploring the CDR potential and associated environmental impacts of olivine-based AOA (Equation (3-1)). Olivine dissolution occurs naturally on timescales of thousands to millions of years during the process known as weathering (Kump *et al.* 2000). Hence, AOA has also sometimes been referred to as "enhanced weathering". Recent theoretical and modelling studies of olivine-based AOA in the open ocean (Köhler *et al.* 2013) and on coastal beaches (Hangx and Spiers 2009) have suggested that the CDR potential of AOA varies considerably with the specific implementation strategies. Concerning open ocean implementations, unless ground into sufficiently small particles, olivine grains will likely sink through the surface mixed layer prior to completed dissolution (Köhler *et al.* 2013) and, hence, not efficiently increase ocean carbon uptake and storage. Since grinding is energy (and cost) intensive, grinding olivine would greatly decrease the net efficiency in terms of CO_2 sequestration (Hangx and Spiers 2009, Köhler *et al.* 2013). Additionally, cargo ships would likely have to be utilized for distributing olivine in the open ocean, thereby, further increasing energy consumption and likely CO_2 emissions. Concerning AOA on

65

coastal beaches (Schuiling and Krijgsman 2006), previous studies (Wogelius and Walther 1991, Pokrovsky and Schott 2000) have shown that the olivine dissolution rate will decline as ambient pH increases. Accordingly, the potential for dissolving olivine may be limited because of the local pH elevation induced by olivine dissolution itself (Hartmann *et al.* 2013).

Given these limitations on implementing AOA in the open ocean and on coastal beaches, we consider here the climate mitigation potential and environmental side-effects of implementing AOA in "coastal seas", which includes oceanic continental shelves shallower than approximately 200 meters; referred to hereafter as Coastal Ocean Alkalinization (COA). For conceptual simplicity, we consider these coastal waters well mixed from surface to sea bed on an annual basis, driven, e.g., by tidally and wind-induced turbulence. Thus, even if deposited at the coastal sea bed, olivine particles would essentially remain in contact with the atmosphere and COA may therefore have a higher potential for olivine to increase ocean carbon uptake and storage than open-ocean AOA. While not taken into account in our assessment here, we note that COA would probably be less cost and energy intensive than open-ocean AOA (Hangx and Spiers 2009, Köhler *et al.* 2013). COA might also be a strategy to mitigate regional coastal acidification (e.g. Feng *et al.* 2016).

In this study, we conduct several numerical experiments using an Earth system model of intermediate complexity to investigate COA by simulating the addition of olivine to coastal waters. We focus on the CO_2 sequestration potential as well as biogeochemical effects of different COA implementations, aiming to provide

information that can be used to assess whether or not COA could be seriously considered as a potential CDR method.

3.2. Method

3.2.1. Model Description

Simulations are conducted with the University of Victoria Earth System Climate Model (version 2.9) (Weaver *et al.* 2001, Eby *et al.* 2013), which is an Earth system model of intermediate complexity. The model components include a three-dimensional general circulation model of the ocean (Pacanowski 1996) that includes biogeochemistry (Keller *et al.* 2012), a terrestrial model (Meissner *et al.* 2003), a simple one-layer atmospheric energy-moisture balance model-based on Fanning and Weaver (1996) and a dynamic-thermodynamic sea-ice model (Bitz and Liscomb 1999). All components have a common horizontal resolution of 3.6° longitude x 1.8° latitude. The oceanic component has 19 vertical levels with thicknesses ranging from 50 m near the surface to 500 m in the deep ocean. Formulations of the air-sea gas exchange and seawater carbonate chemistry are based on the OCMIP abiotic protocol (Orr *et al.* 1999). Simulated sea surface temperature (SST) and oceanic pCO_2 have been verified against World Ocean Atlas (WOA, Locarnini *et al.* 2013) and Surface Ocean CO_2 Atlas (SOCAT, Landschützer *et al.* 2014) data (see Appendix A). The verification showed that UVic can simulate sea surface pCO_2 within the range of observations, but that UVic also generates a slightly cooler Atlantic and warmer eastern continental boundaries, which is a common bias also in CMIP5 models (Wang *et al.* 2014).

3.2.2. COA Simulation Design

Simulated COA is implemented in ocean grid cells that are adjacent to the land-sea boundary between 58.5°N~59.4°S ($3.11×10^7$ km^2, i.e. 8.6% of the global ocean surface area). Collectively, we refer to these model grid cells as "coastal sea" regions in this study. These coastal seas are roughly consistent with the national Exclusive Economic Zones (EEZ), i.e. waters extending seaward to a distance of 200 nautical miles (approximately 370 km) from the coastline. In our implementation of COA, for simplicity we assume that the waters in these coastal areas are well mixed annually. This ignores that some coastal regions, e.g., the eastern Pacific off South America, are characterized by deep trenches. We further assume that all undissolved olivine grains stay in the coastal deployment site, i.e., they are not transported out of the region by currents. We also do not consider the unintentional addition of nutrients, such as Si or Fe, or other contaminates that may be contained in olivine rocks (Köhler *et al.* 2013)(Hauck *et al.* 2016).

Since the theoretical dissolution of one mole of olivine in seawater is equivalent to adding 4 moles of alkalinity, we technically simulate olivine addition in our model, after accounting for the dissolution process, by increasing the surface alkalinity in this ratio in the respective model grid cells, thus avoiding the complication of adding a new model tracer for olivine. We thus quantify and present olivine addition and dissolution, in terms of "alkalinity units", which is four times the respective molar value of olivine.

We assume added olivine in year i is U_i Gt, and the dissolution rate for those added olivine at different year t is $\chi_i(t)$ (unit: % yr^{-1}). Since added olivine U_i will

continuously dissolve in the following years, in the beginning of year j ($j \geq i$), the undissolved fraction of added olivine U_i can be written as U_{r_ij}:

$$U_{r\_ij} = U_i \cdot (1 - \int_{i-1}^{j-1} \chi_i \, dt) \tag{3-3a}$$

And the dissolved fraction of U_{r_ij} in the end of year j can be written as U_{d_ij}

$$U_{d\_ij} = U_{r\_ij} \int_{j-1}^{j} \chi_i \, dt \tag{3-3b}$$

We put U_{d_ij} into determinant D ($i \times j$). The sum of elements along each j column is the annually dissolved olivine in year j, while the sum of elements along the i row is the cumulative dissolved olivine added in year i:

$$D = \begin{pmatrix} U_1 \cdot (1 - \int_0^0 \chi_1 \, dt) \cdot \int_0^1 \chi_1 \, dt & \cdots & U_1 \cdot (1 - \int_0^{j-1} \chi_1 \, dt) \cdot \int_{j-1}^{j} \chi_1 \, dt \\ \vdots & \ddots & \vdots \\ 0 & \cdots & U_i \cdot (1 - \int_{i-1}^{j-1} \chi_i \, dt) \cdot \int_{j-1}^{j} \chi_i \, dt \end{pmatrix} \tag{3-3c}$$

The explicit form of χ_i is described by Equations (3-4) to (3-7).

$$\chi(t) = \min \left[\frac{d}{dt} \sqrt{\frac{t}{f_{size} \times f_T \times f_{pH} \times 0.023}}, 100 \right] \tag{3-4}$$

$$f_{size} = \frac{d_{size}}{100\mu m} \tag{3-5}$$

$$f_T = \begin{cases} e^{-0.1 \times (T-25)}, T > 15\,°C \\ \dfrac{6}{\cosh^2(\frac{T+2}{17.5})}, T \leq 15\,°C \end{cases} \tag{3-6}$$

$$f_{pH} = \frac{1}{1.623 \times 10^{(3-0.54 \times pH)} + 0.9394} \tag{3-7}$$

Equation (3-4) (3-5) and (3-6) are adopted and modified from Köhler *et al.* (2013) to represent how ambient water temperature, pH and olivine grain size affect the instantaneous dissolution rate for individual olivine particle. For the temperature dependency of dissolution in Equation (3-6), a splitting point exists at 15 °C. The

parameterization of f_{pH} from Equation (3-7) is based on experimental work from Wogelius and Walther (1991). The pH response is normalized with respect to a mean ocean pH of 8.2. At pH larger than 9, recent studies on olivine solubility disagree and have found that under different experimental conditions the olivine dissolution rate can vary by two orders of magnitude (Wogelius and Walther 1991, Pokrovsky and Schott 2000, Golubev *et al.* 2005). This implies a large uncertainty for olivine dissolution when the ambient pH is higher than 9.

3.2.3. COA Experimental Design

The model is spun-up for 10,000 years with a prescribed pre-industrial atmospheric CO_2 concentration. It is then run for another 200 years without prescribing CO_2, before it is forced with historical CO_2 emissions from 1765 until the year 2005. Thereafter, the RCP 8.5 high CO_2 emissions scenario (Meinshausen *et al.* 2011) is imposed until the year 2099. We ignore greenhouse gas forcing other than CO_2 as well as land use changes. All COA simulations begin in the year 2020 and continue to be forced with the RCP 8.5 emission scenario.

The COA experiments are divided into 2 groups (Table 3-1). The first group, i.e., "constant supply group", has two subgroups. The first is the "continuous constant supply subgroup" that simulates a constant olivine addition of 30 Gt yr^{-1} with assumed spherical particles of different sizes. Diameters of olivine particles in the different simulations are assumed infinitesimally small (*OlivInf_con*), 0.1 μm (*Oliv0.1_con*), 1 μm (*Oliv1_con*), 10 μm (*Oliv10_con*), 100 μm (*Oliv100_con*) and 1000 μm (*Oliv1000_con*), respectively. For these model runs, we purposefully prescribed an olivine supply rate of 30 Gt yr^{-1} much exceeding current olivine mining

production (~70 Mt yr^{-1}; Fortey 2000) based on following reasons: First, olivine is abundant in low-silica mafic and ultramafic igneous rocks and is widespread in large massifs at the Earth's surface (Schuiling and Krijgsman 2006). Bide *et al.* (2014) estimate that more than 90 teratones of olivine minerals are available globally. Second, An olivine supply rate similar to the current annual mining production would predictably only have a minor impact on CO_2 sequestration and ocean biogeochemistry, while an input of 30 Gt yr^{-1} will generate a much higher signal-to-noise ratio for many model variables. Yet, an olivine input of 30 Gt yr^{-1}, e.g. ~ a density of 1kg m^{-2} yr^{-1} over the coastal regions used in our study, is a moderate supply rate compared to supply rates applied in earlier AOA studies (e.g. 5 kg m^{-2} yr^{-1}, Taylor *et al.* 2015). In experiments where the olivine grain diameter is set as "infinitesimal", we assume that olivine grains instantaneously dissolve, without limitations related to ambient pH, temperature or grain size. This provides an upper estimate for olivine dissolution rate and may also be used to assess possible effects of adding alkalinity from other sources (e.g. limestone-based). The second subgroup (*OlivInf_con_t*, *Oliv0.1_con_t*, *Oliv1_con_t*, *Oliv10_con_t*, *Oliv100_con_t* and *Oliv1000_con_t*) is carried out with the same general model set-up from year 2020 to 2070, but COA is terminated in year 2070 to investigate the response to a planned or unplanned COA stop.

Table 3-1. Experimental design and model results

Model run	Grain size (µm)	CO_2 drawdown (ppm) [*]	Coastal aragonite Ω [†]	Cumulative olivine dissolution (Pmol Alk) [§]	Cumulative olivine input (Pmol Alk) [§]
OlivInf_con	1/∞	-214	5.14	62	62
Oliv0.1_con	0.1	-213	5.14	62	62
Oliv1_con	1	-200	5.04	58	62
Oliv10_con	10	-144	4.17	40	62
Oliv100_con	100	-68	2.81	19	62
Oliv1000_con	1000	-25	2.14	7	62
OlivInf_con_t	1/∞	-130	2.31	39	39
Oliv0.1_con_t	0.1	-130	2.31	39	39
Oliv1_con_t	1	-130	2.39	38	39
Oliv10_con_t	10	-101	2.50	29	39
Oliv100_con_t	100	-50	2.21	14	39
Oliv1000_con_t	1000	-19	1.96	5	39
OlivInf_Omega3.4	1/∞	-123	3.41	34	34
Oliv10_Omega3.4	10	-104	3.34	28	51
Oliv100_Omega3.4	100	-75	2.99	20	80
Oliv1000_Omega3.4	1000	-39	2.44	11	111
OlivInf_Omega5.6	1/∞	-246	5.46	73	73
Oliv10_Omega5.6	10	-208	5.28	59	97
Oliv100_Omega5.6	100	-139	4.36	39	138
Oliv1000_Omega5.6	1000	-56	2.85	15	150
OlivInf_Omega9	1/∞	-384	8.87	125	125
Oliv10_Omega9	10	-337	8.78	104	166
Oliv100_Omega9	100	-238	7.19	69	243
Oliv1000_Omega9	1000	-100	3.85	27	271

[*] **Annual-mean atmospheric CO_2 differences relative to the control run *RCP8.5* in year 2099 (944.4 ppm).**
[†] **Annual-mean sea surface aragonite Ω in year 2099 of coastal grid boxes where COA has been implemented. The value in the control run, *RCP8.5,* is 1.80. (The mean is computed as area weighted arithmetic mean.). For reference the global-mean sea surface aragonite Ω for *RCP8.5* run is 1.60.**
[§] **Integrations are undertaken from year 2020 to year 2099. The olivine molar mass is assumed to be 153.31 g mol^{-1}. Values from columns "cumulative olivine dissolution" and "cumulative olivine input" are presented in alkalinty units (Pmol Alk).**

The second group of model runs is the "Ω threshold group". It consists of another 12 COA simulations and is designed to investigate a COA implementation with local thresholds-based on surface aragonite Ω. Ω-based thresholds are introduced because previous research has suggested that excessive alkalinity additions could perturb ocean biogeochemistry and cause undesirable side effects,

e.g., respiratory alkalosis and hyperkalaemia of crustaceans (Cripps *et al.* 2013). There is also a relatively poorly constrained upper limit on the amount of olivine that can be added, after which spontaneous, abiotic calcium carbonate or phosphate precipitation may occur (De Rooij *et al.* 1984, Marion *et al.* 2009). To this end, we "optimize" the simulated olivine addition, again in individual model experiment for different olivine grain sizes, by setting local upper bounds of aragonite Ω: namely Ω of 3.4 (*OlivInf_Omega3.4, Oliv10_Omega3.4, Oliv100_Omega3.4, Oliv1000_Omega3.4*), 5.6 (*OlivInf_Omega5.6, Oliv10_Omega5.6, Oliv100_Omega5.6, Oliv1000_Omega5.6*), and 9 (*OlivInf_Omega9, Oliv10_Omega9, Oliv100_Omega9, Oliv1000_Omega9*). In these experiments we relate the global olivine addition targets to be in proportional molar ratios (molar ratio 0.6, 1.0 and 1.8 for Ω threshold of 3.4, 5.6 and 9 runs) to annual anthropogenic CO_2 emissions following the approach of a previous study (Ilyina *et al.* 2013a). Locally, however, olivine addition is only simulated as long as the local aragonite Ω is below the respective aragonite Ω threshold in that COA grid box.

The choices of 3.4 and 5.6 for aragonite Ω are based on the criteria proposed from planetary boundaries (Rockström *et al.* 2009) and the Last Glacial Maximum (LGM) record respectively. The planetary boundaries define several environmental tolerance thresholds to maintain a habitable Earth. Among those lines, aragonite Ω of 3.4 is defined as the "preindustrial level" that can maintain a sustainable marine ecosystems in terms of ocean geochemistry. This "preindustrial level" can be taken as a plausible target for climate/ocean acidification mitigation. The other one, Ω of 5.6, is based on a study by Gattuso *et al.* (1998) quantifying the CO_2 chemistry in tropical oceans at glacial times. The rationale behind this choice is that some marine species,

i.e. coral reefs, have maintained a stable calcification rate over last glacial-interglacial cycle. Therefore this representative value from LGM can provide a reasonable higher tolerance for marine biota. Although some studies have found that high pH can limit the growth of phototrophic organisms as a result of decreasing external hydrogen concentrations (Hansen *et al.* 2007) (Nielsen *et al.* 2007), setting a precise Ω threshold to characterize the general physiological tolerance against very high COA implementation is however difficult. Hence, we choose Ω = 9 as an arbitrary threshold at the high end of what could be viewed as reasonably safe Ω levels.

Finally, a control run (*RCP8.5*), without any COA implementation, is undertaken for comparison and reference usage. Three additional sensitivity runs following the protocol for run *Oliv100_con* but excluding the olivine dissolution dependencies on oceanic pH alone (*Oliv_noph*), oceanic temperature alone (*Oliv_nosst*) as well as on both pH and temperature (*Oliv_no*) are used to examine how above ambient variables can affect the dissolution process (see Appendix Table B1 and Figure B1 for the sensitivity tests).

3.3. Results

For the control run (*RCP8.5*), simulated atmospheric CO_2 reaches 944.4 ppm at end of the 21st century. The North Pacific and North Atlantic display the largest SST increases of about +4 ℃ between year 2020 and 2099. Global and coastal mean surface ocean aragonite Ω drop to 1.60 and 1.80 at the end of the century, respectively. The largest decline in aragonite Ω by up to 1.65 relative to year 2020 is simulated for the tropical oceans (Figure B2).

Aggregated results of the COA runs are listed in Table 3-1. The cumulative olivine input for "continuous constant supply subgroup" runs causes 62 Pmol of alkalinity increment in year 2099. Only *OlivInf_con* and *Oliv0.1_con* runs exhibit complete olivine dissolution, i.e., dissolution equals input. For the other four model runs in this subgroup, the amount of annually dissolved olivine gradually increases throughout the simulation (Figure 3-1(a)) due to the continuous addition of olivine and the ongoing dissolution of accumulated left-over undissolved olivine from previous years, and as an inverse function of olivine grain size. By the year 2099, the accumulated amount of dissolved olivine for *Oliv1_con, Oliv10_con, Oliv100_con and Oliv1000_con* is 94%, 65%, 31%, and 11% (termed the "olivine dissolution ratio") of the respective inputs. This result shows that less than half of the added olivine has dissolved by the year 2099 if the grain diameter is larger than 10 μm. Overall, the olivine dissolution ratios from our experiments are close to the analytical solutions given by Hangx and Spiers (2009). As the olivine grain diameter increases from infinitesimal to 1000 μm, the atmospheric CO_2 reduction relative to the control run decreases from 214 to 25 ppm in the year 2099 (Figure 3-1(b)) and the coastal-mean aragonite Ω (pH) in COA-implemented regions decreases from 5.14 (8.13) to 2.14 (7.76) (Figure 3-1(c) and B3). Due to COA implementation, the oceanic carbon uptake from coastal sea increases to 4.2 GtC yr^{-1} (0.35 Pmol yr^{-1}) in 2099, meanwhile the global oceanic carbon uptake reaches 13.2 GtC yr^{-1} (1.1 Pmol yr^{-1})(Figure B3).
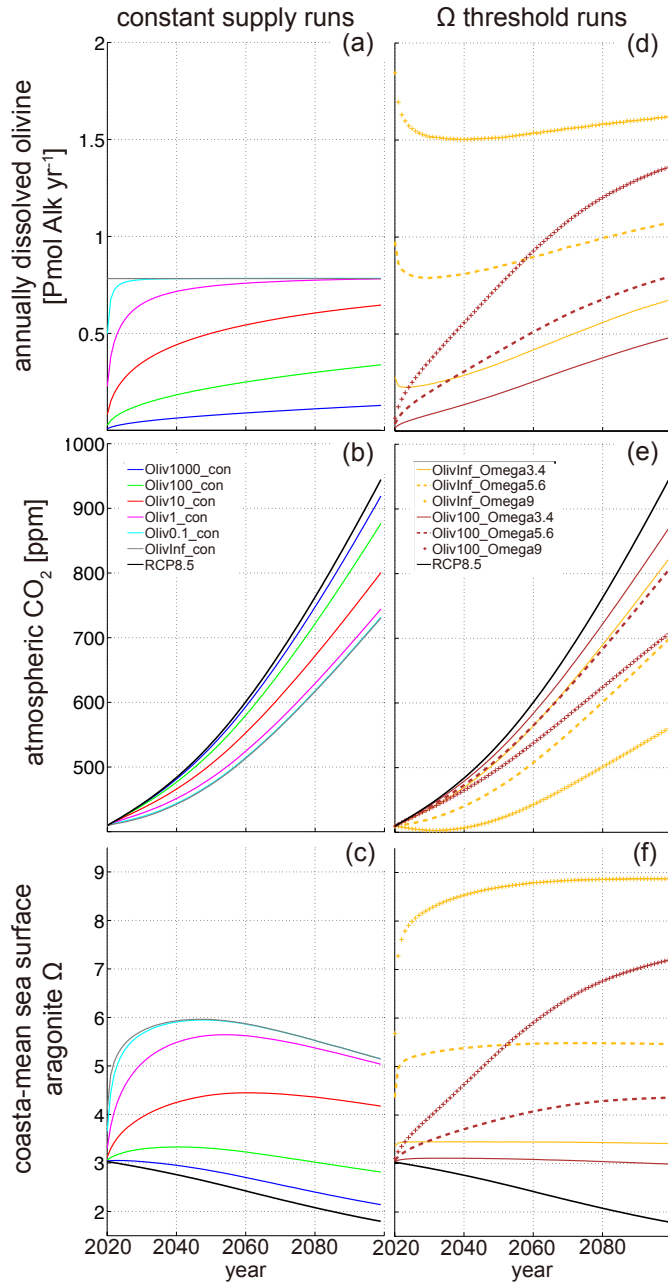
Figure 3-1. Time series of annually dissolved olivine (a, d), global-mean atmospheric CO₂ concentration (b, e), and coastal-mean sea surface aragonite Ω in COA regions (c, f). Simulations for continuous constant supply are shown in the left column, simulations with local Ω thresholds are shown in the right column. "*RCP8.5*" denotes the RCP 8.5 control run without COA.

Runs from "discontinuous constant supply subgroup" show a rapid drop in

the amount of annually dissolved olivine after year 2070 compared with those runs

without such stop. The drop is more "abrupt" when the grain size is smaller (Figure B4(a)), while in experiments with larger grain sizes undissolved olivine deposited before 2070 buffers this decrease. As expected, atmospheric CO_2 increases faster after year 2070 in model runs with COA termination compared to runs without (Figure B4(b)). Except for the run *OlivInf_con_t*, the coastal-mean aragonite Ω decreases rapidly after the termination of COA, but the rate of decline is smaller in experiments with larger olivine grain sizes (Figure B4(c)).

In the "Ω threshold group" model runs, the atmospheric CO_2 from *OlivInf_Omega3.4, OlivInf_Omega5.6 and OlivInf_Omega9* is reduced by 123, 246 and 384 ppm relative to the control run in year 2099 (Table 3-1, Figure 3-1(e)), and the respective coastal-mean aragonite Ω stays right below the respective Ω thresholds (Figure 3-1(f)). Assuming an upper limit of $\Omega = 9$, we find a reduction of 384 ppm to be the upper limit of atmospheric CO_2 reduction by COA with approximately 125 Pmol olivine (in alkalinity units) being added cumulatively. COA runs from this group with larger grain sizes show much smaller aragonite Ω increases and CO_2 reductions (Figure 3-1(e), 3-1(f), B4(e) and B4(f)). In addition, less than 63% of the added olivine dissolves in the ocean before year 2099 if the olivine grain size is larger than 10 μm. This percentage decreases by a factor of 5 to 6 when grain size approaches 1000 μm (Table 3-2).

Table 3-2. [*] **Grinding process corrected CO₂ sequestration potential**

Model run	COA efficiency (%)[+]	Olivine dissolution ratio (%)	Grinding offset (%)[§]	Cumulative CO₂ sequestration (GtC) [^]		
				P_0	ΔP	P
OlivInf_con	67.62	100	-	-	-	-
Oliv0.1_con	67.74	100	-	-	-	-
Oliv1_con	68.23	93.55	-	-	-	-
Oliv10_con	69.38	64.51	17.4	333	-90	243
Oliv100_con	69.84	30.65	1.34	159	-7	152
Oliv1000_con	71.53	11.29	0.49	60	-3	57
OlivInf_con_t	65.95	100	-	-	-	-
Oliv0.1_con_t	66.13	100	-	-	-	-
Oliv1_con_t	67.02	97.44	-	-	-	-
Oliv10_con_t	68.33	74.36	17.4	238	-56	182
Oliv100_con_t	69.13	35.90	1.34	116	-4	112
Oliv1000_con_t	71.31	12.82	0.49	43	-2	41
OlivInf_Omega3.4	69.82	100	-	-	-	-
Oliv10_Omega3.4	70.76	54.90	17.4	238	-75	162
Oliv100_Omega3.4	70.95	25.00	1.34	170	-9	161
Oliv1000_Omega3.4	71.01	9.91	0.49	94	-5	89
OlivInf_Omega5.6	67.25	100	-	-	-	-
Oliv10_Omega5.6	68.76	60.82	17.4	487	-139	347
Oliv100_Omega5.6	70.02	28.26	1.34	328	-15	312
Oliv1000_Omega5.6	70.38	10.00	0.49	127	-6	120
OlivInf_Omega9	63.39	100	-	-	-	-
Oliv10_Omega9	65.56	62.65	17.4	818	-227	591
Oliv100_Omega9	68.01	28.40	1.34	563	-27	537
Oliv1000_Omega9	68.67	9.96	0.49	222	-11	212

[*] **Data is obtained from model outputs. See Appendix B for detailed calculation and analysis**

[+] **COA efficiency is defined as the amount of sequestrated CO₂ for one unit added alkalinty.**

[§] **Values are from Hangx and Spiers 2009, refering to the ratio of emitted CO₂ during the grinding process versus total CO₂ sequestration.**

[^] **Values are given as cumulative CO₂ sequestration by year 2099. P_0 is the one derived from model output directly. P is corrected value considering grinding offset, and ΔP is the variance between the two.**

We use the results of model run *Oliv100_Omega3.4* to show in more detail how COA affects ocean biogeochemistry (A general analysis for the global olivine dissolution distribution for all model runs is given in Figure B7). From a global perspective, Figure 3-2(a) shows how olivine dissolution varies spatially within our defined coastal grid boxes. Compared to the control run, significant aragonite Ω and

pH elevation occurs in coastal ocean grid boxes (Figure 3-2(b) and B5) particularly in tropical ocean coastal grid boxes. However, surface ocean aragonite increases also in the open ocean, e.g., by up to 0.5 Ω units in the tropical Atlantic. Though we control olivine addition to avoid crossing the aragonite Ω-threshold of 3.4 locally, some tropical coastal grid boxes have an annual-mean aragonite Ω that is higher than 3.4 even though olivine addition stopped upon reaching the threshold, presumably due to dissolution of accumulated previously deposited undissolved olivine (Figure 3-2(c) and B6). The biggest COA-induced CO_2 uptake, relative to the control run, is located at middle to high latitude coasts, and there is also COA-induced CO_2 flux from the open ocean far from where olivine was added back to the atmosphere due to the COA-induced decrease in atmospheric CO_2 partial pressure (Figure 3-2(d)).
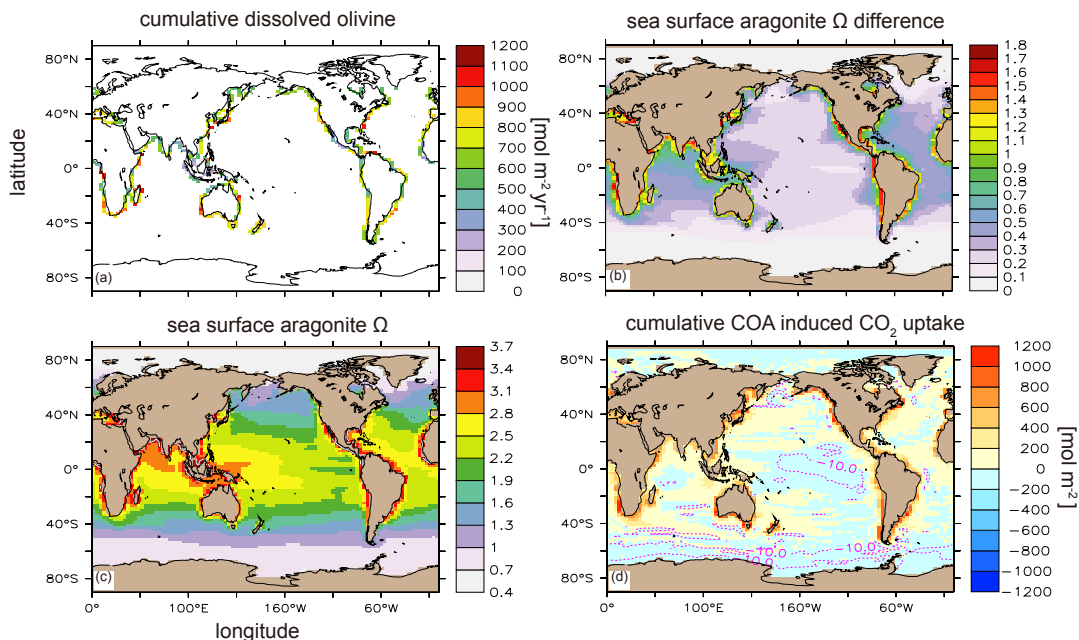
Figure 3-2. For simulation *Oliv100_Omega3.4* in year 2099, the global distribution of cumulative dissolved olivine in year 2099 of coastal ocean alkalinisation simulation assuming 100 μm olivine grains and with sea surface aragonite Ω threshold of 3.4 (a), sea surface aragonite Ω difference relative to the control run (b), sea surface aragonite Ω (c) and COA induced cumulative CO_2 uptake (d).

3.4. Discussions

Observational evidence as well as model projections has indicated that coastal regions are among the areas most vulnerable to global change, especially concerning ocean eutrophication and acidification. In the tropical oceans, coral ecosystems are threatened by ocean acidification in addition to warming (Hoegh-Guldberg *et al.* 2007). If COA was applied at the scale illustrated in the study and olivine was ground to allow enough dissolution, COA could effectively protect coastal regions from acidification. However, there are also potential side effects to be considered. The addition of olivine, which contains silicon and iron, may act as a fertilizer and could cause or increase coastal eutrophication (Blain *et al.* 2007, Hauck *et al.* 2016). Particulate olivine grains also have specific optical properties related to the green colour of the crystals. Adding olivine to seawater (or beaches) could thus change the water transparency, light spectrum and sea surface albedo. Optical perturbations may also arise from spontaneous calcium carbonate precipitation (Broecker and Takahashi 1966), which might be triggered by COA-induced increase in calcium carbonate saturation levels and possible changes in the magnesium to calcium ratio (Reddy and Wang 1980, Bischoff 1968, Berner 1975, Mekmene *et al.* 2009). Besides calcium carbonate precipitation, some studies suggest that calcium phosphate may precipitate when the pH is increased above a critical level (Rooij *et al.* 1984，Song *et al.* 2002). Yet, phosphate precipitation induced by olivine addition to seawater has not been verified under natural conditions. Undissolved olivine grains would likely exert mechanical stress on benthic environments. In summary,

elaborately designed experiments downscaling to micro-scale physical chemistry are needed (Hartmann *et al.* 2013) to better understand these processes.

According to our model experiments and analysis, the choice of a local upper limit for aragonite saturation level limits the potential of COA (in addition to logistical limitations not considered in this study). In the following, we discuss the relationship between the coastal-mean aragonite Ω and the atmospheric CO_2 levels at year 2099 for each individual model run (Figure 3-3). We find that in our business-as-usual scenario (RCP 8.5) a trade-off exists between maintaining relatively low saturation levels and removing CO_2 from the atmosphere via COA. According to the results from *OlivInf_Omega3.4* run, if we want to prevent coastal-mean aragonite from exceeding 3.4, on average at least 16.5 Gt olivine needs to be mined, processed, and added to coastal seas every year. This is also the amount required to prevent local surface aragonite Ω from dropping below 3.4. For this example, atmospheric CO_2 levels can be reduced by 123 ppm compared to the control run by the end of year 2099. The recent Paris Climate Agreement sets the target of limiting the global warming to 1.5 °C to significantly reduce risks and impacts of climate change. To reach the above target, atmospheric CO_2 levels of a business-as-usual emission scenario would have to be reduced by approximately 400 ~ 450 ppm (Rogelj *et al.* 2016). Except for the runs *OlivInf_Omega9* and *Oliv10_Omega9*, COA induced CO_2 uptake in our study cannot alone achieve a CO_2 reduction consistent with the 1.5 °C target in a high-emission scenario. Moreover, coastal-mean aragonite Ω close to 9 reached in these two runs in year 2099, may prove unfavourable for many marine biota.
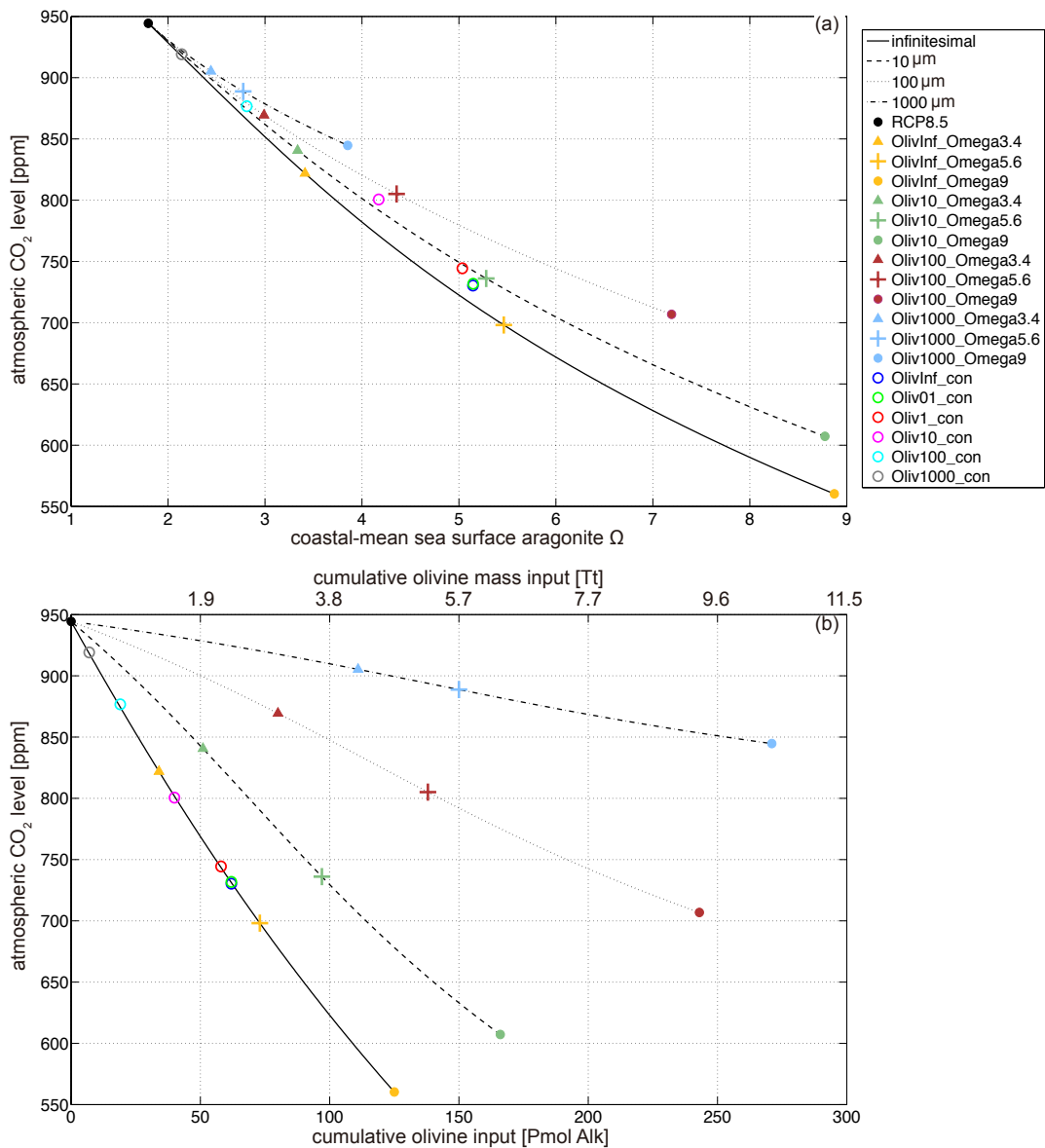
Figure 3-3. Relationship between simulated atmospheric CO_2 and coastal-mean aragonite Ω from COA implemented regions in the year 2099 (upper panel), and between atmospheric CO_2 and cumulative olivine input (lower panel, molar units at bottom x axis, mass units at top x axis.). CO_2 emissions associated with COA preparation and operation processes, i.e. mining, grinding and transport are neglected.

The above analysis is based on idealized simulations where COA associated CO_2-costs of mining, grinding, and transport processes are not considered. To gain any significant mitigation effect through COA, olivine mining would have to be expanded by more than two orders of magnitude, and likely other alkaline minerals

(e.g. lime) have to be considered for COA usage as well. Though CO_2 emissions from mining and transport are minor (Hangx and Spiers 2009, Moosdorf *et al.* 2014), grinding olivine minerals into small particles is energy intensive and can significantly reduce the overall efficiency of COA. Grinding one ton olivine into grains that are smaller than 10 μm is estimated to cost more than 60 kg CO_2, which is extremely expensive for any practical use (Hangx and Spiers 2009). Hence, in the following analysis we only compare model runs with grain sizes larger than 10 μm to evaluate the CO_2 sequestration offset due to grinding. From our calculations we find that the CO_2-costs of grinding reduces the overall CO_2 sequestration potential for each model run we analysed (Table 3-2). In general, around 23% to 32% of the sequestrated CO_2 have to be cancelled out for the 10 μm runs if grinding caused CO_2 is considered. For 100 μm and 1000 μm runs the respective values are 3% to 5% despite 100 μm run generating lower CO_2 emissions during grinding. This is because within 80 years the olivine dissolution rate for 1000 μm runs are basically much slower than 100 μm runs, leading to a lower realised CDR potential. Besides, 10 μm (100 μm) runs all have higher amounts of CO_2 sequestration than the 100 μm (1000 μm) grain-size runs in their respective groups even if the grinding process is accounted for. This suggests that small olivine grains (>10 μm) could still have advantages in terms of COA induced CO_2 removal.

3.5. Conclusions

For the first time, olivine-based Coastal Ocean Alkalinization (COA) is simulated in a fully coupled Earth system model with explicit parameterization of the olivine dissolution process. We evaluated the CDR potential as well as

environmental side effects for both olivine additions within coastal sea grid boxes in business-as-usual high CO_2 emission scenario.

If current olivine production can be enhanced by more than two orders of magnitude, olivine-based COA may have a considerable CDR potential through enhanced oceanic CO_2 uptake during the next 80 years. It may further help to mitigate coastal ocean acidification. Apart from the minor CO_2-emissions during mining and transport indicated from previous studies, around 3~32% of the sequestrated CO_2 has to be cancelled out due to the olivine grinding process. We find that low latitude coasts have the highest potential to mitigate aragonite Ω decline and subsequently may help to protect tropical coral reefs from the threat of ocean acidification. However, applying COA as a single means to achieve ambitious climate goals such as the Paris 1.5° C atmospheric temperature target, might cause extremely high alkalinity (aragonite Ω) levels in coastal waters and hence, lead to a series of undesired side effects such as calcium carbonate/phosphate precipitation, a seawater optical anomaly, biological perturbations, etc. The process uncertainties identified in our study should be assessed in the future through both high-resolution modeling and dedicated lab and possibly small-scale field experiments.

Acknowledgements

4. Research #3

Cooling effects from climate feedbacks in climate engineering implementations

Ellias Y. Feng[1,2], David P. Keller[1], and Andreas Oschlies[1,2].

[1] GEOMAR Helmholtz Centre for Ocean Research Kiel

[2] University of Kiel

[1] E-mail: yfeng@geomar.de

Abstract: *Sulphate aerosol injection (SAI)-based SRM and direction air capture (DAC)-based CDR, have been investigated within an Earth system model of intermediate complexity. Referenced to our control runs reached global-mean surface temperature level driven by high CO2 emission scenario, the temperature reductions caused by our evaluated technologies become larger if the equilibrium climate sensitivity (ECS) is predicted higher for the same CE intensity. However under high ECSs, more SRM and CDR are needed if they are used to reach <1.5-degree warming target in the 21st century. When CE is implemented, the cooling effects caused by climate feedbacks, are 14%~52% and 45%~86% in magnitude of cooling from the direct CE raidative perturbations for SRM and CDR runs respectively, implying a significant influence from climate feedback uncertainties for asserting the CE climate mitigation efficacies.*

4.1. Introduction

Climate engineering (CE) is gaining growing attention from scientists and policy makers (Lenton and Vaughan 2009) (Keith 2000)(IPCC 2014). Unlike the measures to reduce anthropogenic GHG emissions, CE aims to offset and mitigate climate change by deliberately intervening the climate system. CE technologies that focus on reducing incoming solar radiation are usually named Solar Radiation Management (SRM) (Crutzen 2006)(Latham *et al.* 2013). The other branch that can reduce the level of atmospheric CO_2 are usually named Carbon Dioxide Removal (CDR)(Kheshgi 1995) (Cao and Caldeira 2010) (Blain *et al.* 2007).

It has been widely acknowledged that large-scale implementations of CE technologies might cause some environmental side effects such as ozone depletion and anomalies in global biogeochemical cycles (Tilmes *et al.* 2008) (Keller *et al.* 2014). Assessing the uncertainties of CE technologies is therefore essential prior to CE large-scale experimentations or eventually deployments (Kravitz *et al.* 2011)(Keller *et al.* 2014) (Ilyina *et al.* 2013a). So far, many modeling studies have focused on assessing the potential effectiveness and environmental side effects of specific CE technologies. For example, the CO_2 direct air capture (DAC) technology, which is supposed to sequester airborne CO_2 molecules through chemical absorption and permanently store the CO_2 in geological reservoirs, was evaluated in an Earth system model of intermediate complexity (EMIC) to study its impact on ocean acidification (Mathesius *et al.* 2015). Stratospheric Aerosol Injection (SAI), which can create a global cooling effect through injecting aerosols into stratosphere (Keith 2010), was

investigated in another EMIC model to learn its impact on global hydrological and carbon cycle (Matthews and Caldeira 2007). Besides these evaluations by individual climate model, Kravitz *et al.* (2011) conducted a modeling intercomparison following some particular SRM implementation scenarios. Recently, Keller *et al.* (2014) used one EMIC model to comparatively evaluate multiple CE technologies for their effectiveness and side effects. Despite the fact that these modeling studies have helped to better understand how CE can affect the Earth climate, the degree of uncertainties of CE model simulations in general still remains high (Royal Society 2009, IPCC-WG1 2013).

The difference of specific model's numerical structure as well as parameterizations for important climate feedbacks can lead to large varieties in modeling results. Over long term, the rate of global warming under a given anthropogenic carbon forcing, is affected by physical feedbacks associated with water vapor, lapse rate, albedo and clouds (IPCC 2014). Besides the uncertainties in those physical feedbacks, climate change can also affect the natural carbon reservoirs and consequently cause climate-carbon feedbacks to regulate atmospheric CO_2. Previous studies (Cox *et al.* 2000)(Friedlingstein *et al.* 2006) have demonstrated additional CO_2 increase caused by global warming mainly due to terrestrial carbon loss.

However, both physical and climate-carbon feedbacks contain many complex processes and the uncertainties therein are usually not easy to resolve directly. Instead, scientists can use the Equilibrium Climate Sensitivity (ECS) to effectively address climate affects caused by those feedback uncertainties. ECS is defined as the

equilibrium global-mean surface atmospheric temperature (SAT) change relative to the preindustrial period, when atmospheric CO_2 concentration is doubled from preindustrial level. Based on analysis from paleo-climate data, model simulations and historical records, the predicted ECS has more than a 66% probability of being between 2.0 K and 4.5 K (IPCC 2014). A higher ECS prediction indicates a stronger temperature response when a same small radiative perturbation in feedbacks occurs. In climate modeling studies, the analysis for climate-carbon feedbacks, combined with estimates of physical feedbacks, determines the compatibility of modeling prediction for future climate change (IPCC 2014).

Should SAI and DAC be implemented, the net cooling effects will come from (i) CE direct radiation perturbation and, (ii) radiative forcing anomalies caused by (i) induced climate feedbacks. Matthews and Caldeira (2007) found a doubled ECS does not affect SAI's effectiveness in terms of reduced solar forcing, but the temperature decrease due to SAI is larger under high ECS prediction. They also found compared to control runs, implementing SAI can cause the carbon sink to grow strong, with reduction in atmospheric CO_2 contributing to the cooling. Predictably extracting a fraction of CO_2 from atmosphere will decrease the temperature and cause some back flux from land and ocean carbon. Upon a same amount of sequestrated CO_2, the ultimate atmospheric carbon concentration and global temperature reduction could be different if ECS is varied. So far there is no detailed analysis on how much in magnitude the climate feedbacks can offset or enhance the CE direct cooling effects. This study is therefore dedicated to investigate how future climate will involve in context of varied CE engineering intensities as well as varied ECSs.

4.2. Model and Simulations

The University of Victoria Earth System Climate Model (UVic) version 2.9 is the model used in this study. This model consists of an energy-moisture balance atmospheric component, a 3D primitive-equation oceanic component that includes a sea-ice sub-component, and a terrestrial component (Weaver *et al.* 2001, Eby *et al.* 2013). It has a spatial resolution of 3.6°×1.8° with 19 vertical layers in the ocean. The global carbon cycle is simulated with the air-sea gas exchange of CO_2 and marine inorganic carbonate chemistry following the Ocean Carbon-Cycle Model Intercomparison Project protocols (Orr *et al.* 1999). The inorganic carbon cycle is also coupled to a marine ecosystem model that includes phytoplankton, zooplankton, detritus, the nutrients nitrate and phosphate, and oxygen to make it a suitable tool for marine biogeochemical simulations (Keller *et al.* 2012). The terrestrial carbon of UVic model is based on Hadley Center model TRIFFID (Meissner *et al.* 2003). The UVic model has been evaluated in several model intercomparisons (Eby *et al.* 2013, Zickfeld *et al.* 2013, Weaver *et al.* 2012), and shows a reasonable response to anthropogenic CO_2 forcing which is well within the range of other models. Recently UVic has been employed to conduct CE simulations (Keller *et al.* 2014, Matthews and Caldeira 2007). In the following sections, since SAI and DAC are the only discussed and can be representative cases for other SRM and CDR technologies within this study, we use "SRM" and "CDR" to refer to SAI-based SRM and DAC-based CDR for terminological convenience.

In this research, we first spin the model up for 10,000 years under preindustrial conditions. It is then run for another 200 years without prescribing CO_2,

before being forced with historical CO_2 emissions until the year 2005. Thereafter, the RCP 8.5 high CO_2 emission forcing scenario (Meinshausen *et al.* 2011) is used until the year 2099 under different ECSs. We categorize all model runs into three groups: Control Group, SRM Group and CDR Group. In the Control Group, three model runs are conducted with ECSs of 2.0 K, 3.2 K and 4.5 K separately in parallel till the year 2099 without applying any CE technology. We change UVic's ECS to 2.0, 3.2 (UVic's default value) and 4.5 K by altering outgoing longwave radiation parameters following the example of Ross *et al.* (2012). Above modifications on ECS are only valid from year 2000 to guarantee that the simulations are the same prior to this time point. However, since instantaneous altered outgoing longwave radiation will cause perturbations to the radiation budget, and lead to some climatological fluctuations in the first several year (Ross *et al.* 2012), we allow the model to adjust to the new ECSs from the years 2000 to 2019 before implementing CE in the year 2020. To ensure the climatic variables excluding ECS are approximately the same in year 2020, we parameterize the global-mean surface atmospheric temperature (SAT) for all model runs so that it can converge to the same level (14.2 °C) in the year 2020:

$$L_{out}^*(t) = L_{out}(t) + p(T(t) - T_0) \tag{4-1}$$

In above equation, "$L_{out}(t)$" and "$L_{out}^*(t)$" are the unmodified and modified outgoing longwave radiation in year "t". "T_0" is the global-mean SAT in °C in year 2020. This value is diagnosed from a prior model run with UVic parameterizations in default (Appendix Figure C2 and C3). "$T(t)$" is global-mean SAT in year "t". "p (W m^{-2} °C^{-1} or W m^{-2} K^{-1})", which is determined from a set of prior model simulations

(Appendix C). In our study when p is set 0.734, 0 and -0.342 respectively, the model's ECS is adjusted to 2.0, 3.2 and 4.5 K.

In SRM Group, the model runs are similar to those in Control Group regarding the basic set-up and ECS choices, except that SRM technology is applied by reducing the solar constant S_c^0 in a scaling factor "$(1 - \sigma) \cdot X$":

$$S_c = S_c^0 \cdot (1 - \sigma) \cdot X \tag{4-2}$$

$$\sigma = \frac{F \cdot \ln \left(\frac{\varphi CO_2}{\chi CO_2} \right)}{\frac{S_c^0}{4} \cdot (1 - \alpha_p)} \tag{4-3}$$

In each SRM operating year, S_c is the modified solar constant. σ is obtained from anthropogenic carbon forcing as shown in Equation (4-3), and "X" in Equation (4-2) indicates the SRM engineering intensity. "F" is the atmospheric CO_2 radiative forcing constant 5.35 W m^{-2}, while φCO_2 is the atmospheric CO_2 concentration in SRM operating year, and χCO_2 is the preindustrial atmospheric CO_2 concentration (280 ppm). α_p equaling 0.3 is the global-mean planetary albedo. The reduced solar insolation energy is approximately equivalent to the CO_2 radiation change from the preindustrial if X is set 1.

Since the atmospheric CO_2 is well mixed in UVic model, we use reduced CO_2 emission as an analogue to simulate capturing atmospheric CO_2. Similar to SRM Group, we use a factor "Y" to refer to the CDR engineering intensities. When "Y" is set "1", 20 GtC CO_2 will be removed from the atmosphere annually from year 2020 to 2099. There are five SRM and CDR intensities in respected groups by setting "X (Y)" to "0.2", "0.4", "0.6", "0.8" and "1"(Figure C1 in Appendix) in a row. Since each SRM (CDR) run under one specific SRM (CDR) intensity needs to be evaluated for 3

different ECSs, altogether we have conducted 33 model runs including the three control runs.

4.3. Results

4.4.1. Results with Single CE Intensity

We first look into the global-mean model output of the control runs and CE runs under the maximum intensities. In the control runs with three different ECSs, the global-mean surface atmospheric temperature (SAT) have increased by 1.85 (ECS=2.0 K), 2.75 (ECS=3.2 K) and 3.50 °C (ECS=4.5 K) from year 2020 to 2099 (Figure 4-1(a)). Within the same period, atmospheric CO_2 has increased from 411 to 932.2 (ECS=2.0K), 968.6 (ECS=3.2 K) and 999.8 ppm (ECS=4.5 K), while the sea surface mean pH has decreased by 0.31 (ECS=3.2 K), 0.33 (ECS=3.2 K) and 0.34 (ECS=3.2 K). Global-mean precipitation has slightly declined by 0.041 (ECS=2.0 K), 0.026 (ECS=3.2 K) and 0.015 mm d^{-1} (ECS=4.5 K). In SRM and CDR Groups, cooling effect has obviously occurred, concurrently atmospheric CO_2 is reduced, and the ocean is less acidified (Figure 4-1(c)) when compared to the control runs. For the SRM runs, global-mean SAT decreases until it is close to preindustrial level. By year 2099 the global-mean SAT for the SRM runs stabilizes at 13.5 (ECS =2.0 K), 13.3 (ECS =3.2 K) and 13.1 °C (ECS = 4.5 K). While for CDR runs, global-mean SAT first declines and later slightly increases in response to gradually increased CO_2 emissions. The global-mean SAT reaches 14.4 (ECS=2.0 K), 14.5 (ECS=3.2 K), and 14.6 °C (ECS=4.5 K) by year 2099. Compared to the control runs with the same ECS, atmospheric CO_2 is lower with CE applied, and reaches around 800 ppm for SRM runs and 445 ppm for CDR runs by year 2099. Global-mean sea surface pH has decreased to 8.0 for CDR

runs and 7.8 for SRM runs. In addition, SRM and CDR have different impact on global precipitation. Compared to control runs, global-mean precipitation has decreased around 0.14 (ECS=2.0 K), 0.16 (ECS=3.2 K) and 0.17 mm d^{-1} (ECS=4.5 K) for SRM runs, while increased by 0.046 (ECS=2.0 K), 0.034 (ECS=3.2 K) and 0.026 mm d^{-1} (ECS=4.5 K) for CDR runs (Figure 4-1(d)).
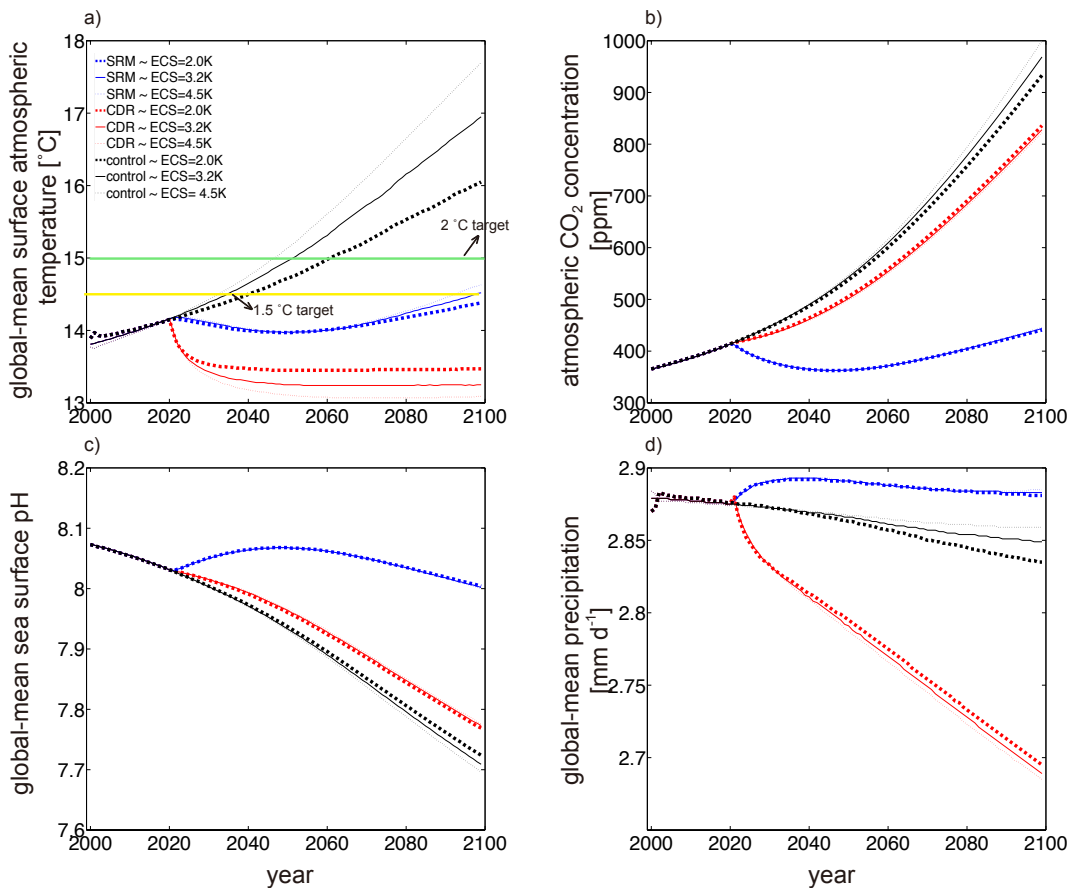
Figure 4-1. Time series of the global-mean surface atmosphere temperature (SAT) (a), atmospheric CO$_2$ concentration (b), global-mean sea surface pH (c), and global-mean precipitation (d) for the control (black), SRM (red) and CDR (blue) runs. The intensities of CE runs are set "1". Runs with ECSs equaling 2.0 K, 3.2 K and 4.5 K are plotted with bold dashed, solid and light dashed lines. 1.5 and 2 °C global warming referenced to preindustrial level are highlighted in yellow and green in Panel (a)

For the control runs in the year 2099, atmospheric CO$_2$ is close to the same level despite of the different choices of ECS, but global-mean SAT difference can be as much as 1 °C under different ECSs. We find that global-mean SAT difference

between control and CE runs in year 2099 is largest for runs with ECS=4.5 K and smallest with ECS=2.0 K. According to Equation (4-1), less (more) outgoing longwave radiation is transmitted back to space under high (low) ECSs. Though this adjustment does not modify atmospheric carbon directly, temperature induced changes in air-sea and air-land carbon fluxes can trigger responded change to global atmospheric CO_2 and ocean pH (Table 4-1, Figure 4-1(c)). For global-mean precipitation, previous studies find the precipitation (evaporation) will decrease on land if atmospheric CO_2 continues to increase due to evapotranspiration feedbacks (Lammertsma *et al.* 2011)(de Boer *et al.* 2011). The precipitation (evaporation) over sea however will likely increase when sea surface temperature tends to get warmer following Clasius-Claperone relationship. Similar to the results from Matthews and Caldeira (2007), SRM technology in our study strongly cools the planet and cause less carbon lost to atmosphere, which leads to much decreased oceanic precipitation and moderately increased terrestrial precipitation (Table 4-1) when compared to the control runs. In contrast, the cooling caused by CDR is mainly through atmospheric CO_2 decline. This leads to more precipitation over land due to stronger evapotranspiration, and less precipitation over the sea cooling due to the cooling compared to the control runs (Table 4-1).

Table 4-1. Terrestrial and oceanic annual-mean precipitation and carbon stocks in the year 2099 under ECSs of 2.0, 3.2 and 4.5 K for the control ("Ctrl" row) and CE simulations ("SRM" and "CDR" rows). Absolute values are given for control runs and relative changes are given for CE runs under intensity 1.0

ECS	Model runs	Precipitation over land [mm d⁻¹]	Precipitation over ocean [mm d⁻¹]	Land carbon [GtC]	Ocean carbon [GtC]
	Ctrl	1.866	3.254	2253	37765
2.0 K	SRM	-0.07	-0.17	210	-4
	CDR	0.204	-0.022	-250	-274
	Ctrl	1.868	3.274	2176	37767
3.2 K	SRM	-0.076	-0.197	303	-5
	CDR	0.203	-0.039	-180	-275
	Ctrl	1.867	3.288	2108	37769
4.5 K	SRM	-0.078	-0.215	383	-6
	CDR	0.205	-0.051	-118	-276

4.4.2. Introduction of Diagnostic Metric

Before approaching how ECS can affect model output under multiple CE intensities, we introduce a new diagnostic metric for further investigations. In a changing climate, illustrated here from year 2020 to 2099, the effect of changing CO_2 forcing on global-mean SAT can be written as

$$\Delta T = \lambda \, \Delta F \qquad\qquad (4\text{-}4)$$

where ΔT is the global-mean SAT change referenced to preindustrial (unit: K), ΔF is the longwave carbon forcing change (unit: W m⁻²) relative to that of the preindustrial average. λ, as a linear approach factor, is the climate sensitivity (unit: K m² W⁻¹) to CO_2 forcing change. Note that longwave carbon forcing change ΔF can also be presented as the CO_2 change, ΔA, following Myhre *et al.* (1998):

$$dF = 5.35 \, \ln(A/A_0) \qquad\qquad (4\text{-}5)$$

where dF is the differential of carbon forcing, A is the atmospheric CO_2 concentration and A_0 is that of reference. Combining Equation (4-4) and (4-5) we can also have

$$\Delta T = k \, \Delta A \tag{4-6}$$

where k in Equation (4-6) is climate sensitivity to CO_2 in K ppm^{-1} (Friedlingstein *et al.* 2006). If CE is applied, the variables in Equation (4-4) and (4-6) can be expanded to become:

$$\Delta T = \Delta T_0 + \Delta T' \tag{4-7}$$

$$\lambda = \lambda' + \lambda_0 \tag{4-8}$$

$$\Delta F = \Delta F' + \Delta F_0 \tag{4-9}$$

$$k = k' + k_0 \tag{4-10}$$

$$\Delta A = \Delta A' + \Delta A_0 \tag{4-11}$$

where in Equation (4-7) to (4-11), ΔT_0, λ_0, ΔF_0, k_0 and ΔA_0 is the change of global-mean SAT, climate sensitivity to CO_2 forcing, longwave radiative carbon forcing, climate sensitivity to CO_2, and atmospheric CO_2 relative to the preindustrial level without the implementation of CE. The new variables $\Delta T'$, λ', $\Delta F'$, k' and $\Delta A'$ are the climate engineering induced anomalies (Table 4-2). These cannot be directly calculated by the model and must be derived. To describe the CE perturbation under different ECSs and CE intensities, we explore the quantitive relationship between λ' and $\Delta F'$ (k' and $\Delta A'$) by rewriting Equation (4-4) to (4-11) as:

$$\Delta F' = \frac{\Delta T}{\frac{\Delta T_0}{\Delta F_0} + \lambda'} - \Delta F_0 \tag{4-12}$$

$$\Delta A' = \frac{\Delta T}{\frac{\Delta T_0}{\Delta A_0} + k'} - \Delta A_0 \tag{4-13}$$

The CE perturbation in the year 2099 under different ECSs and CE intensities is illustrated in Figure 4-2 which shows the CE climate sensitivity to CO_2 forcing change anomaly, λ', plotted against the CE longwave radiative forcing anomaly, $\Delta F'$,

and the CE climate sensitivity to CO_2 concentration change anomaly, k', plotted against the CE induced changed in CO_2, $\Delta A'$. Enhancing the CE intensity increases the perturbation of both the climate sensitivity and the global carbon cycle. For SRM runs, λ', $\Delta F'$, k' and $\Delta A'$ are negative regardless of the ECSs and CE intensities, with a higher perturbation at higher ECSs. This result indicates that implementing SRM can reduce the atmospheric CO_2 level as well as climate sensitivity to CO_2 change. CDR perturbation of λ', $\Delta F'$, k', $\Delta A'$ are slightly different. The relevant results show that sequestrating atmospheric CO_2 leads to a reduction of atmospheric CO_2 ($\Delta F'$ and $\Delta A'$), but it also increases in the climate sensitivity to CO_2 (k'). Interestingly, the CE climate sensitivity anomaly to CO_2 forcing (λ') for CDR runs is positive under low ECS but negative under high ECS. Note λ' equals $\frac{\Delta T}{5.35 log \frac{\Delta A}{280}} - \frac{\Delta T_0}{5.35 log \frac{\Delta A_0}{280}}$. If ECS is varied from 2.0 to 4.5 K, $\frac{\Delta T}{5.35 log \frac{\Delta A}{280}}$ changes little while $\frac{\Delta T_0}{5.35 log \frac{\Delta A_0}{280}}$ increase significantly, causing λ' to change from positive to negative.

Table 4-2. Used variables and the descriptions

Variable	Description	Unit
ΔT	Global-mean SAT change referenced to preindustrial level	K
ΔT_0	Global-mean SAT change referenced to preindustrial level for control run	K
$\Delta T'$	CE induced global-mean SAT anomaly compared to control run	K
ΔF	longwave carbon forcing change referenced to preindustrial level	W m^{-2}
ΔF_0	longwave carbon forcing change referenced to preindustrial level for control run	W m^{-2}
$\Delta F'$	CE induced longwave carbon forcing anomaly compared to control run	W m^{-2}
$\overline{\Delta F'}$	Averaged CE induced longwave carbon forcing anomaly compared to control run from year 2020 to 2099	W m^{-2}
A	Global atmospheric CO_2 concentration	ppm
A_0	Referenced Global atmospheric CO_2 concentration	ppm
ΔA	Global atmospheric CO_2 concentration change referenced to preindustrial level	ppm
ΔA_0	Global atmospheric CO_2 concentration change referenced to preindustrial level for control run	ppm
$\Delta A'$	CE induced global atmospheric CO_2 concentration anomaly compared to control run	ppm
λ	Climate sensitivity to carbon forcing change	K m^2 W^{-1}
λ_0	Climate sensitivity to carbon forcing change for control run	K m^2 W^{-1}
λ'	CE induced climate sensitivity anomaly to carbon forcing change compared to control run	K m^2 W^{-1}
$\bar{\lambda}'$	Averaged CE induced climate sensitivity anomaly to carbon forcing change compared to control run from year 2020 to 2099	K m^2 W^{-1}
k	Climate sensitivity to CO_2 concentration change	K ppm^{-1}
k_0	Climate sensitivity to CO_2 concentration change for control run	K ppm^{-1}
k'	CE induced climate sensitivity anomaly to CO_2 concentration change compared to control run	K ppm^{-1}
$\Delta T_{SRM}^{d},$	Direct effects term for SRM	K
$\Delta T_{SRM}^{f},$	Feedback effects term for SRM	K
$\Delta T_{CDR}^{d},$	Direct effects term for CDR	K
$\Delta T_{CDR}^{f},$	Feedback effects term for CDR	K

4.4.2. Results with Multiple CE Intensities

One use of introducing above diagnostic metric is to assess CE's the ability to alter the global-mean temperature when both CE intensity and ECS are changed. The variables in Figure 4-2 are all from the output in year 2099. If we plot the isoclines of 1.5 °C global warming from preindustrial in Figure 4-2 (zoomed-in view in Figure C4), then it is possible to see how much SRM and CDR are requested to avoid a global warming higher than that. In Figure 4-2(a), points A1 (B1), A2 (B2), A3 refer to the smallest SRM (CDR) intensity/input needed to prevent the 1.5 °C target from being crossed under ECS of 2.0, 3.2 and 4.5 K. Through interpolations we find that the exact CE intensities for those points are 0.55 (A1, ~ 2.3 W m^{-2}), 0.59 (A2, ~ 2.49 W m^{-2}), 0.62 (A3, ~ 2.61 W m^{-2}), 0.85 (B1, ~14.5 GtC yr^{-1}) and 0.78 (B2, ~18.5 GtC yr^{-1}). This result indicates that under higher ECSs, more SRM and CDR are needed to prevent the 1.5 °C warming threshold from being crossed than that under lower ECSs.
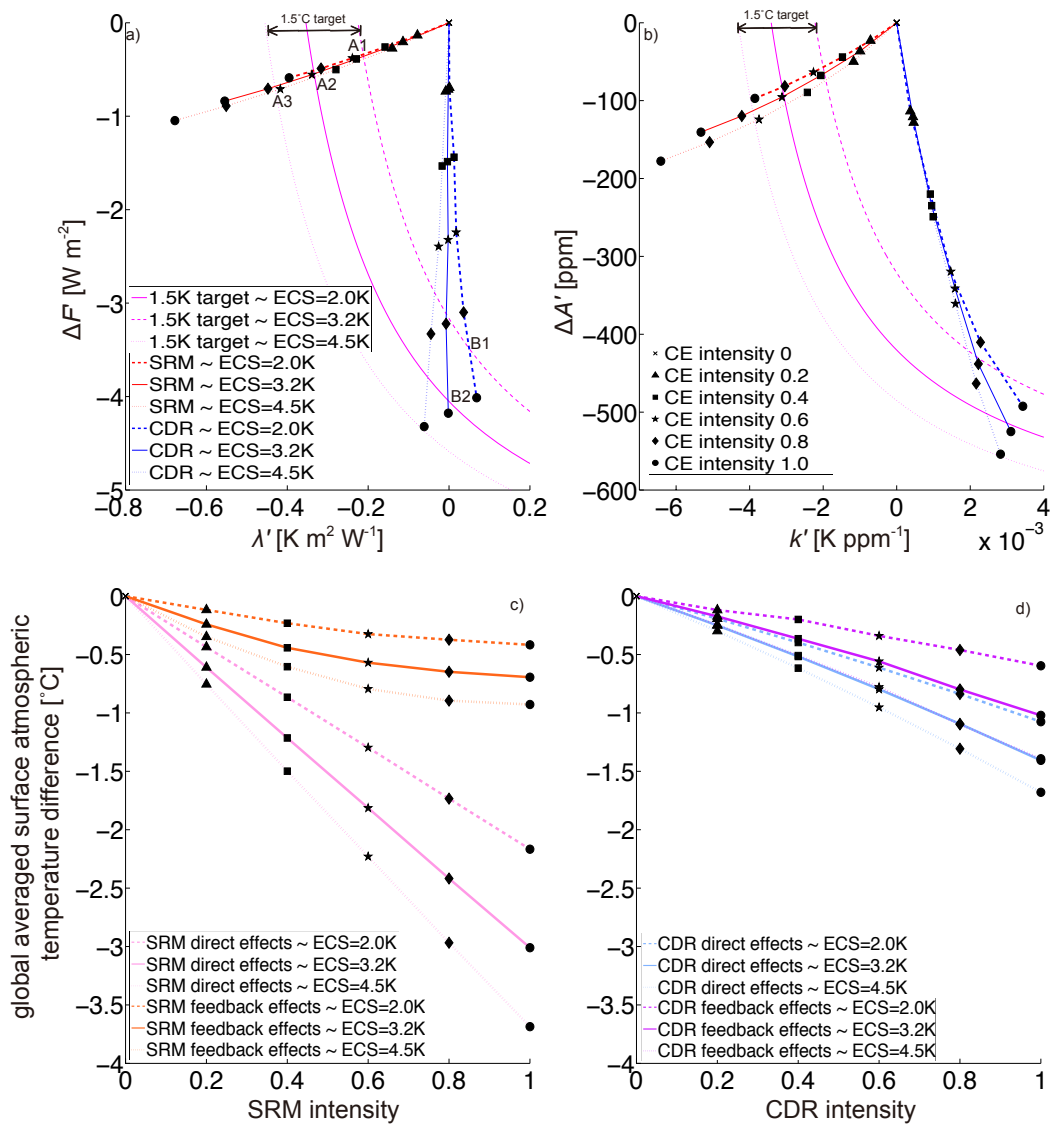
Figure 4-2. In year 2099, CE perturbation plotted as the CE induced climate sensitivity to CO₂ forcing change anomaly versus the CE induced longwave radiative forcing anomaly (a) and the CE induced climate sensitivity to CO₂ concentration anomaly versus the CE induced atmospheric CO₂ anomaly (b). Zoomed-in views of (a)(b) can be found in Figure C4. Global-mean 1.5 °C warming from preindustrial level is highlighted in pink isoclines. Plots with ECS of 2.0, 3.2 and 4.5 K are showed in solid, bold dashed and light dashed curves. Crossing points (e.g. A1, A2, A3, etc.) are marked when CE curves have crossed with the 1.5 °C mitigation target isoclines under the same ECSs. Panel (c) and (d) show the global-mean surface temperature difference between CE runs and control runs in year 2099, with their respective cools contributions from direct effects and feedback effects.

4.4.3. CE Perturbation on Climate Feedbacks

Another important use of above diagnostic metric is to estimate the relative cooling contributions from (i) CE direct radiation perturbation and (ii) radiative forcing anomalies caused by (i) induced feedbacks. Similar to the derivation of climate sensitivity in Equation (4-4), the SRM induced temperature anomaly through direct shortwave reduction in first order approximation, ΔT_{SRM}^d, is defined as

$$\Delta T_{SRM}^d = \bar{\lambda}' \, \Delta F_0 \qquad (4\text{-}14)$$

$\bar{\lambda}'$ is SRM induced climate sensitivity anomaly compared to control run in average from year 2020 to 2099 (Table 4-2). As a result, ΔT_{SRM}^d is the SRM caused cooling if the global atmospheric CO_2 is unchanged from control run. In addition, the temperature anomaly caused by uncertainties in climate feedbacks ΔT_{SRM}^f, is defined as

$$\Delta T_{SRM}^f = \Delta T' - \Delta T_{SRM}^D \qquad (4\text{-}15)$$

where $\Delta T'$ is still CE induced global-mean SAT anomaly compared to control run. For the CDR runs, the induced temperature anomaly that occurs due to the removal of CO_2, similar to ΔT_{SRM}^d, is defined as ΔT_{CDR}^d

$$\Delta T_{CDR}^d = \lambda_0 \overline{\Delta F'} \qquad (4\text{-}16)$$

where $\Delta F'$ is the averaged CDR induced longwave radiative carbon forcing anomaly to control run from year 2020 to 2099 (Table 4-2). ΔT_{CDR}^d indicates the CDR caused cooling effect if the physical feedbacks are unchanged from control run. In following, the temperature anomaly that is involved from feedbacks (e.g. sea ice albedo change) is defined as ΔT_{CDR}^f

$$\Delta T_{CDR}^f = \Delta T' - \Delta T_{CDR}^d \qquad (4\text{-}17)$$

101

For convenience, in following paragraphs we name ΔT_{SRM}^d (ΔT_{CDR}^d) as SRM (CDR) direct effects terms while ΔT_{SRM}^f and ΔT_{CDR}^f are named feedback effects terms (Table 4-2).

In Figure 4-2(c)(d), ΔT_{SRM}^d, ΔT_{SRM}^f, ΔT_{CDR}^d and ΔT_{CDR}^f are plotted under different ECSs and intensities. When ECS is increased from low to high, magnitudes of ΔT_{SRM}^d, ΔT_{SRM}^f, ΔT_{CDR}^d and ΔT_{CDR}^f all become larger. The feedback effects terms for SRM and CDR are always smaller in magnitude than their direct effects terms under the same CE intensity and ECS. For SRM runs, as SRM intensity increases, magnitude of ΔT_{SRM}^d increases almost in constant rate. But the slope for such change gradually becomes smooth. This result implies that the strength of climate-carbon feedback can be inhibited if the temperature drops down too much. Mechanisms e.g. the ocean buffer and the temperature sensitivity for metabolisms (e.g. Q10 relationship) can be explanations for this phenomenon. In SRM runs, the temperature cooling generated from direct effects are approximately 2~7 times larger than that from feedback effects. Instead, magnitudes of ΔT_{CDR}^d and ΔT_{CDR}^f increase linearly when CE intensity increases. For CDR runs, the cooling contribution from feedback effects are approximately 45% ~ 86% of the direct effects.

4.4. Discussion

Using idealized SAI and DAC as representative SRM and CDR technologies, our research first show how future climate would involve if SRM and CDR is implemented under different ECSs and CE engineering intensities. We found within our chosen range for ECS, SRM and CDR are more effective considering the larger temperature reductions from the control run levels if ECS is predicted high for the

102

same CE intensity. However in a high-ECS world, more CE will be needed than that under low ECS to reach the 1.5 °C warming target, which will likely lead to more CE implementation costs. It appears to us whether should human utilize CE to mitigate climate change risks will depend on the trade-offs between the environmental as well as social-economic loss from failing the 1.5 °C target, and the comprehensive costs to implement CE continuously.

The cooling effects generated from climate feedbacks when SRM (CDR) is implemented, is approximately 14%~ 52% (45% ~ 86%) of SRM (CDR) direct cooling effect depending on the choice of ECS and CE intensity. Therefore to better restrain the uncertainties in CE simulations, it is necessary to further evaluate the feedback strength and relevant climatic changes when CE is applied. Considering the big impacts of such feedback uncertainties can have, we suggest some intercomparsion and CE perturbation studies to be commenced.

Acknowledgement

5. Research #4

Modeling assessment for combined SRM and AOA implementation schemes

Ellias Y. Feng[1, 2]

[1] **GEOMAR Helmholtz Centre for Ocean Research Kiel**

[2] **University of Kiel**

[1] **E-mail: yfeng@geomar.de**

Abstract: *The concurrent administration of two climate engineering (CE) technologies, stratospheric solar radiation management (SRM), as simulated by a solar constant reduction, and artificial ocean alkalinization (AOA), are tested in an Earth climate system model in several intensity combinations. Under Representative Concentration Pathway 8.5, the business as usual high global emission scenario, combined implementation of SRM and AOA can effectively prevent a global-mean temperature increase of more than 2°C and simultaneously stop the 2.75 global-mean ocean surface aragonite Ω threshold from being crossed. An annual-mean solar insolation reduction of 5.6 W m-2 for SRM, combined with an annual CO_2 sequestration of 39.7 GtCO2 for AOA, is the cheapest of the combined and single-method CE implementation schemes in both minimizing the global-mean temperature increase and limiting the decline in global-mean sea surface Ω. Since the interactions between SRM and CDR interventions are nonlinear, the efficiency of reducing global warming will gradually diminish. As the intensity of SRM and AOA increases in combined schemes, the marginal costs for CE implementation will dramatically increase.*

5.1. Introduction

Solar radiation management (SRM) and carbon dioxide removal (CDR) are two separate categories of climate engineering (CE) techniques designed to avoid the

negative consequences of anthropogenic global warming. The most discussed SRM approach involves injection of sulfur dioxide (SO_2) into the tropical stratosphere, thereby reducing incoming solar radiation and cooling the planet. CDR techniques seek to remove carbon from the atmosphere. Artificial ocean alkalinization (AOA) is a CDR technique that can increase the ocean carbon sink. This is accomplished by adding alkaline minerals such as lime and olivine to the ocean.

SRM by sulfate aerosol injection (SAI) into the stratosphere is effective in reducing gradually increased global-mean temperature (Kravitz *et al.* 2011) and is an analogue of volcanism. However, injecting sulfur into the stratosphere may trigger ozone depletion (Pope *et al.* 2012)(Tilmes *et al.* 2008) and weaken the global hydrological cycle (Tilmes *et al.* 2013). The abrupt termination of SAI would result in a rapid global temperature rebound to what the temperature would if SAI was never implemented, with severe consequences for society and nature (Matthews and Caldeira 2007). In addition, SAI's effectiveness in limiting ocean acidification is low (Williamson and Turley 2012). The economic costs of injecting aerosols into the stratosphere are on the order of 1-3 billion per year per W m^{-2} of insolation reflected by the stratospheric aerosol layer (McClellan and Sisco 2010), which is much lower than climate mitigation costs. Therefore cost would very likely not be a limiting factor in the decision to implement SAI (Barrett 2008, McClellan and Sisco 2010).

Meanwhile, AOA shows a great potential for reducing the atmospheric CO_2 concentration if implemented on a global scale (Ilyina *et al.* 2013a). In contrast to SAI, AOA can counter balance ocean acidification. The impacts of AOA on Earth's ocean and atmosphere will persist after AOA is stopped. However, unlike SAI,

implementation of AOA could be expensive. Renforth *et al.* (2013) simulated

placement of lime as an AOA agent and showed that 1.4 to 1.7 tons of limestone is

required to capture one ton of CO_2 from the atmosphere. In their estimation the

ultimate cost to sequester one ton of CO_2 throughout the entire process is 72 ~ 159

USD. Since SAI is the most frequently discussed SRM technology and no other SRM

technologies will be studied in this research, we use "SRM" in following paragraphs

to represent SAI.

Previous research has demonstrated that implementing SRM or AOA alone,

cannot reduce the global temperature increase without causing other environmental

side effects (Keller *et al.* 2014). However, if SRM is applied with climate mitigation

efforts, the risk of SRM induced side effects and the economic cost for climate

mitigation can both be reduced (Wigley 2006). In this study, I will explore the

combined effects when SRM and AOA are applied simultaneously under high CO_2

emission scenario during 21st century, and investigate whether the high engineering

costs can be reduced if SRM is implemented within AOA scenarios.

5.2. Methods

I use the University of Victoria Earth System Climate Model (UVic) version

2.9 for this study. This model consists of an energy-moisture balance atmospheric

component, a 3D primitive-equation oceanic component that includes a sea-ice sub-

component, and a terrestrial component (Weaver *et al.* 2001). It has a spatial

resolution of 3.6°×1.8° with 19 vertical layers in the ocean. The global carbon cycle is

simulated with the air-sea gas exchange of CO_2 and marine inorganic carbonate

chemistry following the Ocean Carbon-Cycle Model Intercomparison Project

protocols (Orr *et al.* 1999). The inorganic carbon cycle is also coupled to a marine ecosystem model that includes phytoplankton, zooplankton, detritus, the nutrients nitrate and phosphate, and oxygen making it a suitable tool for marine biogeochemical simulations (Weaver *et al.* 2001, Keller *et al.* 2012). The UVic model has been evaluated in several model intercomparisons (Eby *et al.* 2013, Zickfeld *et al.* 2013, Weaver *et al.* 2012), and shows a reasonable response to anthropogenic CO_2 forcing which is well within the range of other models. Previously UVic model has been employed for both SRM and AOA simulations (Matthews and Caldeira 2007)(Feng *et al.* 2016), thus UVic model is an appropriate tool to undertake simulations for combined SRM/AOA schemes.

A spin-up has been taken for 4000 years at first. Then we use combined historical green house gases (GHG) record and representative carbon pathway (RCP) 8.5 scenarios to drive the anthropogenic climate change from industrial revolution to year 2019. From year 2020 to 2099, I conducted two control runs without applying any CE technologies under RCP 8.5 and 4.5 emission scenarios separately (runs named *"RCP8.5"* and *"RCP 4.5"* respectively). In the same period with control runs, SRM combined with AOA are applied continuously under RCP 8.5 emission scenario for CE experimental runs. When designing those experimental runs, I introduce "SRM/AOA intensity" to characterize the different SRM/AOA combinations. In detail, I use reduced solar constant to simulate SRM (Matthews and Caldeira 2007), and if the reduced solar constant in each SRM operating year is identical to the radiative forcing difference between two control runs, the SRM intensity is set "1.0". The SRM runs with reduced solar constants scaled respectively by a factor of 0.75, 0.5,

107

0.25 and 0 of that under intensity "1.0", are assigned with intensity "0.75", "0.5", "0.25" and "0.0". AOA is simulated by increasing the total alkalinity of surface waters between 70° N and 60° S. In this approach, alkalinity increment by two mole is regarded as one mole $Ca(OH)_2$ addition in ocean surface (Ilyina *et al.* 2013a), which converts CO_2 into bicarbonate in seawater:

$$Ca(OH)_2 + 2CO_2 \rightarrow Ca^{2+} + 2HCO_3^- \qquad\qquad (5\text{-}1)$$

Similar to SRM, I assign intensity "1.0" to model runs with AOA applied, when the amount of globally added $Ca(OH)_2$ (alkalinity unit) is identical to anthropogenic CO_2 emissions in each AOA operating year. The other AOA intensities, "0.75", "0.5", "0.25", and "0.0", indicate the added $Ca(OH)_2$ is in factor of 0.75, 0.5, 0.25 and 0 to the amount given in intensity "1.0" (Figure D1 in Appendix D). I combine five SRM and five AOA intensities and generate 25 model runs with different SRM/AOA combinations. For convenience in following paragraphs, I name model run under SRM intensity "x" and AOA intensity "y" as "*SRM_AOA_x_y*".

5.3. Results

For model run with both SRM and AOA being set off in high emission scenario ("*RCP_8.5*" run), global-mean SAT has approximately increased by 3 °C from year 2020 to year 2099. Whereas model runs with SRM or AOA applied, e.g., "*SRM_AOA_1.0_0.0*" and "*SRM_AOA_0.0_1.0*", the global-mean SAT have only increased by 1.5 and 1.4 °C within the same period (Figure 5-1). For the run "*SRM_AOA_1.0_1.0*", the global-mean SAT has increased only by 0.8 °C compared to year 2020. Without implementing SRM or AOA, global-mean sea surface aragonite Ω decreases from 2.8 in year 2020 to 1.6 in year 2099, implying a gradually acidified

ocean. In *SRM_AOA_0.0_1.0*, global-mean sea surface aragonite Ω has been brought up to 4.6 in 2099, but *SRM_AOA_1.0_0.0* run has no obvious affects on the global-mean sea surface aragonite level, implying that SRM alone with this intensity has little potential to mitigate ocean acidification globally (Figure 5-1).
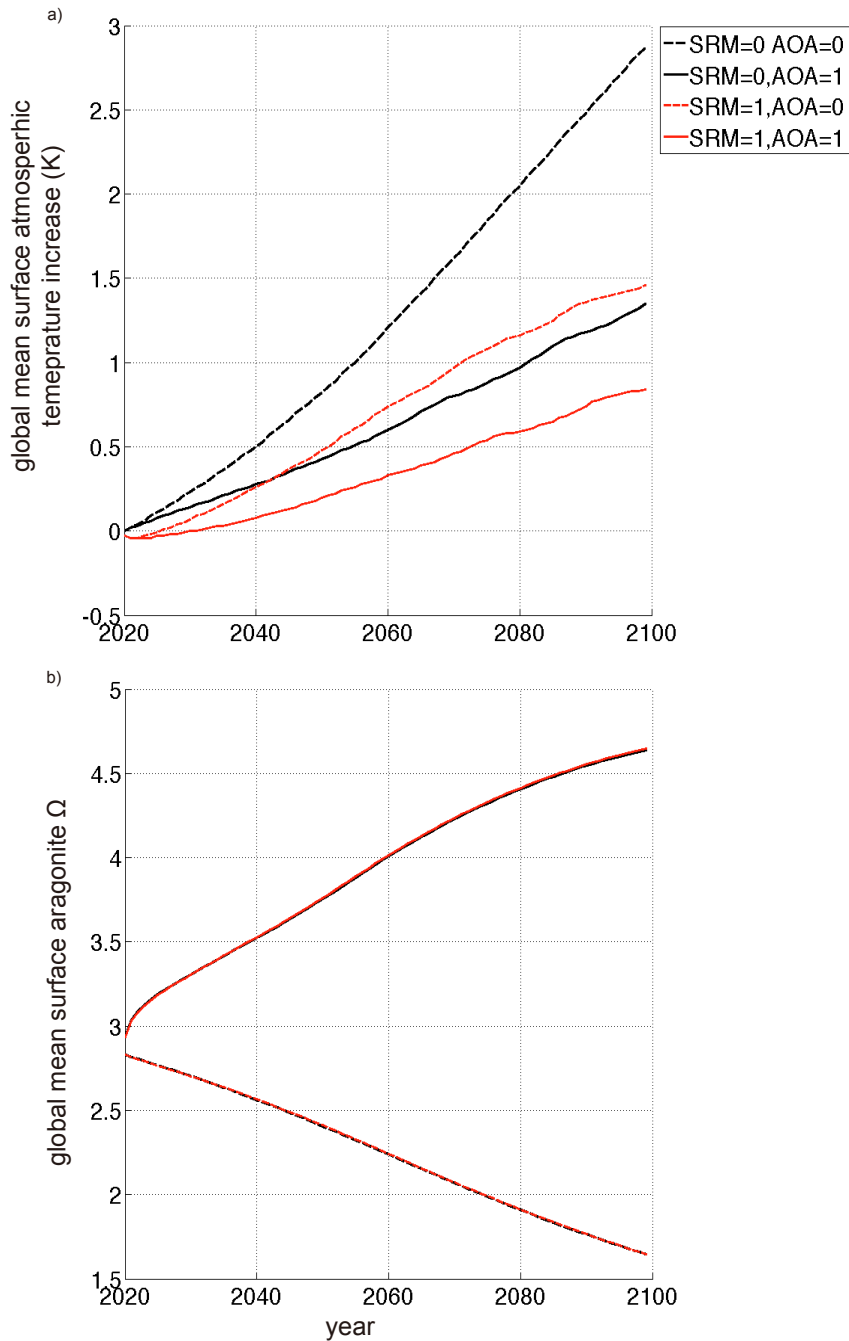
Figure 5-1. Time series of global-mean surface atmospheric temperature elevation referenced to year 2020 (a) and global-mean sea surface aragonite Ω (b) for

RCP_8.5 **control run (in black dashed), "SRM_AOA_0.0_1.0" run (in black solid), "SRM_AOA_1.0_0.0" run (in red dashed) and "SRM_AOA_1.0_1.0" run (in red solid).**

I used polynomial regression to parameterize the global-mean SAT change from year 2020 to 2099, and global-mean surface aragonite Ω in year 2099, against the climate engineering intensities (Table 5-1). For CE runs, increasing SRM (AOA) intensity for every 0.25 unit, global-mean SAT elevation will approximately decrease by 0.3 °C (Figure 5-2(a)). For combined SRM/AOA, the global-mean SAT change from year 2020 to 2099, increases in a gradually reduced rate when SRM and AOA intensity increase simultaneously (Figure 5-2(c)). When SRM and AOA intensities are both set "1.0", the nonlinearity effects caused by combining SRM/AOA can offset 15.1% global-mean SAT decrease. Since this nonlinearity is quadratic (Table 5-1), the offset in temperature drawdown can dramatically increase when SRM and AOA intensities become higher. Therefore the global cooling effect of combined SRM/AOA is not a linear summation of SRM and AOA solely induced temperature decline, especially when SRM and AOA intensities are both high. When one assumes that the marginal loss of genuine externality of a CE technology increases along the increasing scale of the CE practice as shown in our study, the combined option will lead to a higher marginal cost due to the nonlinearity effect. However since SRM cannot affect surface aragonite Ω obviously, above nonlinearity is not seen in surface aragonite Ω output from combined SRM/AOA schemes (Table 5-1, Figure 5-2(d)).

Table 5-1. Regressions for global-mean surface atmospheric temperature (SAT) elevation from year 2020 to 2099 and global-mean sea surface aragonite Ω against CE engineering intensities. Polynomial-fit parameterization are shown in format of "A=aX+bY+cXY+d" in which SRM and AOA intensities are given as "X", "Y". The regressive coefficients "a", "b", "c", "d" and correlation coefficients are listed in columns 2~6

Regressed variable (A)	SRM-coefficient (a)	AOA-coefficient (b)	Interaction coefficient (c)	Constant term (d)	Correlation coefficient
Global-mean SAT change (SRM sole)	-1.408	0	0	2.858	0.9996
Global-mean surface aragonite Ω (SRM sole)	-0.001	0	0	1.647	0.5000
Global-mean SAT change (AOA sole)	0	-1.532	0	2.894	0.9989
Global-mean surface aragonite Ω (AOA alone)	0	2.996	0	1.482	0.9837
Global-mean SAT change (SRM&AOA combined)	-1.381	-1.517	0.894	2.879	0.9964
Global-mean surface aragonite Ω (SRM&AOA combined)	-0.001	2.996	0.007	1.482	0.9838
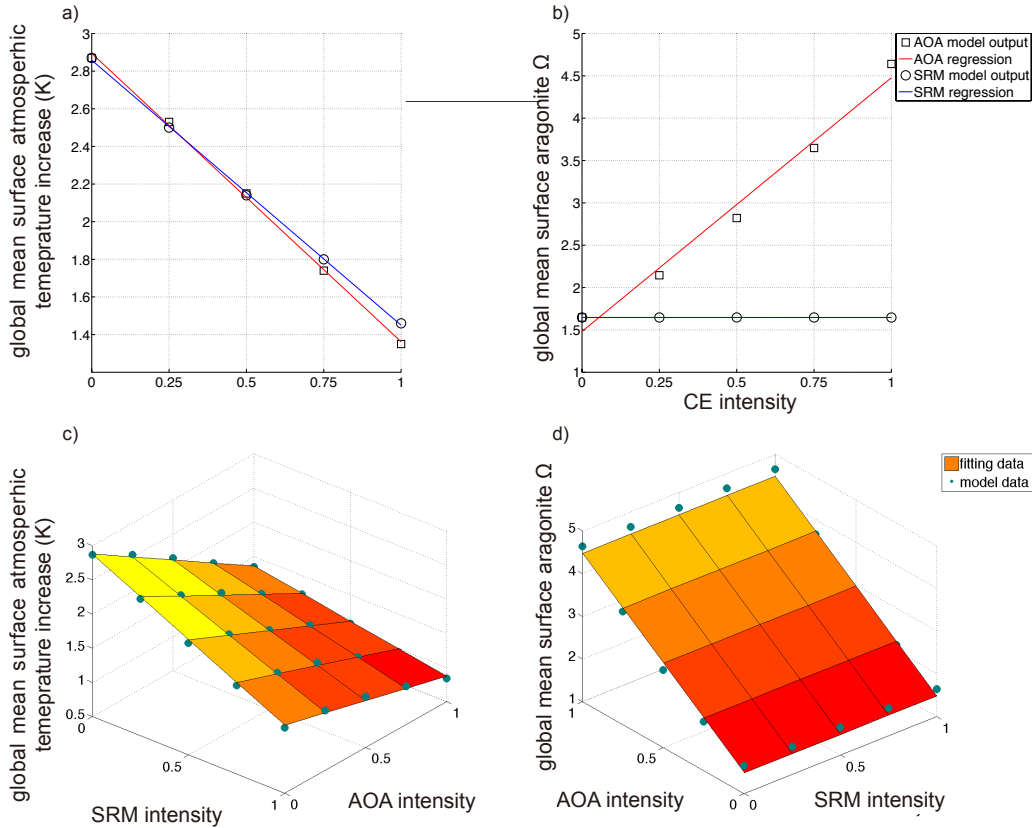
Figure 5-2. In year 2099, global-mean surface atmospheric temperature (SAT) difference referenced to year 2020 (a) and global-mean sea surface aragonite Ω (b) for sole SRM and AOA implementation with different CE intensities. The same two variables from combined schemes with different CE intensities (c)(d), in which model output is regressed according to functions in Table 5-1.

5.4. Discussion

I assume the engineering unit cost for CE is "*u*" USD per W m^{-2} for SRM, and "*v*" USD per ton captured CO_2 for AOA. According to my definitions, AOA intensity "1.0" is equivalent to capturing 82.77 Gt CO_2 per year while SRM intensity "1.0" refers to 6.58 W m^{-2} per year in average. McClellan *et al.* (2012) concludes that 1 Mt of sulfur per year can provide 1 W m^{-2} solar flux reduction with cost around 1~3 billion USD, therefore the annually engineering cost for SRM with intensity "1.0" is around 6.58~19.74 billion USD in average. In contrast, the cost for AOA with intensity "1.0" is estimated around 5959~13160 billion USD based on Renforth *et al.* (2013). Since the

temperature decrease from *SRM_AOA_0.0_1.0* is very close to that from *SRM_AOA_1.0_0.0* (Figure 5-1), AOA will cost approximately two to three orders of magnitude higher than SAI for the same temperature drawdown.

Paris Agreement confirmed to use 2 °C target, i.e. the global-mean SAT increase of 2 °C at end of 21st century referenced to preindustrial level, as the political goal for climate mitigation to avoid severe climate change impacts. In addition, planetary boundary (Rockström *et al.* 2009), in which several environmental safe guardrails have been proposed from different climate dimensions, has demonstrated that sea surface aragonite Ω of 2.75 can be used as the lower threshold for marine ecology. I applied above two thresholds into my model output from year 2099. Through interpolation I acquired the SRM/AOA combinations that can prevent above two thresholds from being crossed (Figure 5-3). In those combinations, the intensity of SRM can be given as low as "0.0", concurrently the AOA intensity has to be no lower than "0.97". This combination will cost approximately 5780.2 ~12765 USD per year. In the contrast, the minimal AOA intensity can reach "0.48", and in response the SRM intensity has to be no lower than "0.85". The engineering cost for this combination, i.e. around 2865.9 ~ 6333.6 USD per year, is only half in price of the previous one.

Above estimation is based on early studies arguing that SRM is economically cheap. Nevertheless this idea is challenged recently if more determinants such as price or external effects are taken into account (Klepper and Rickels 2012) (Goes *et al.* 2011). In previous paragraphs I also did not consider the possible environmental costs for other side effects that combined SRM/AOA scheme might bring. In addition,

113

I simulated another test run (named "*SRM_AOA_opt*" run) with SRM in intensity "0.85" (5.6 W m^{-2} in annual average) and AOA in intensity "0.48" (39.7 GtCO$_2$ captured per year), to illustrate what other environmental /external effects could be like.

In comparison between the output from year 2099 and year 2020 for *SRM_AOA_opt*, I found implementing combined SRM/AOA has decreased the Atlantic Meridinal Overturning Circulation (AMOC) strength by 15%, net primary production on land by 28%, precipitation over land by 9%, but increased oceanic precipitation by 7%. In year 2099 compared with control run *RCP_8.5*, the AMOC and precipitation over land from *SRM_AOA_opt* are 8% and 3.1% higher, while the net primary production on land and precipitation over ocean are 4.6% and 1.5% lower. In general, *SRM_AOA_opt* have slightly mitigated the climate impacts by high CO$_2$ emissions other than temperature increase and ocean acidification. However, combined SRM/CDR is incapable to get rid of some involved externality beyond what the model can present. In detail, SRM has been known with the negative externality in terms of (i) alternation of climate pattern, especially precipitation pattern (Trenberth and Dai 2007, Robock *et al.* 2008); (ii) the increase of acid rain (Rasch *et al.* 2008); (iii) further depletion of ozone layer so that it would expose human to higher risk of skin cancers (Harris *et al.* 1997, Baldwin *et al.* 2003, Shaw and Shepherd 2008, Tilmes *et al.* 2008). AOA also demands extra mining practice on land (Royal Society 2009, Schäfer *et al.* 2015), which will potentially lead to local environmental pollution in-situ. Moreover, it is uncertain and therefore not excludible whether it has negative impacts on the marine ecosystem, though its first-

order impact is to counteract ocean acidification, which is regarded as benign (Royal Society 2009). The negative externality involved from combined CE schemes may still remain significant due to the environmental side effects beyond this study's concern.
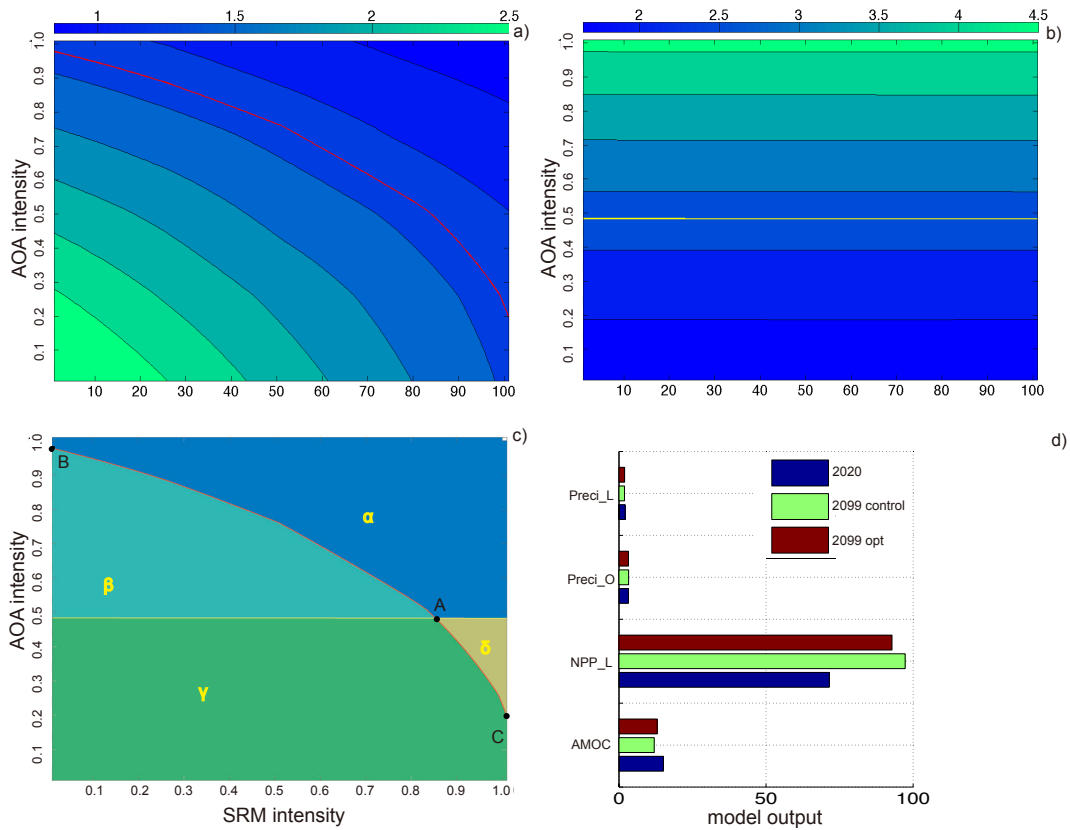
Figure 5-3. **In year 2099, contour plots of global-mean surface atmospheric temperature (SAT) elevation referenced to preindustrial level and global-mean sea surface aragonite Ω for all CE combinations (a)(b). Panel (c) is an overlay of (a) and (b) with 2 °C global-mean SAT elevation threshold isocline (in red) and 2.75 aragonite Ω threshold isocline (in yellow). Among the four divided areas by threshold isoclines, area "α" refers to the combinations crossing neither temperature nor Ω threshold, β refers to the combinations crossing only temperature threshold, δ refers to the combinations crossing only Ω threshold, and γ refers to the combinations crossing both temperature and Ω thresholds. Strength of Atlantic Meridional Overturning Circulation ("AMOC", unit: Sv s^{-1}), net primary production in land ("NPP_L", unit: GtC yr^{-1}), mean precipitation in land ("precip_L", unit: mm d^{-1}) and mean precipitation in ocean ("precip_O", unit: mm d^{-1}) of model run "*SRM_AOA_opt*" in year 2099 and 2020 as well as control run (*RCP_8.5*) in year 2099 are compared in Panel (d)**

5.5. Conclusion

This study investigated new CE scenarios with combined SRM/AOA implementation in the 21st century through an Earth climate system model. If sulphate aerosols injection-based SRM and lime-based AOA are used to avoid global 2°C warming (referenced to preindustrial level) and global-mean aragonite Ω dropping blow 2.75 simultaneously by year 2100, the implementation cost can be minimized to 2865.9 ~ 6333.6 billion USD per year by combining SRM and AOA, which is half in price of using AOA alone. The marginal loss of genuine externality has been seen to gradually increase when CE intensity increases due to the internal nonlinearity generated from combining SRM and AOA together. I conclude, combined SRM/AOA is attractive in regard of reducing engineering cost, but marginal cost to deploy those technologies will dramatically increase when the implementation scale is enlarged.

6. Research #5

Potential climate engineering effectiveness and side effects during a high CO₂-emission scenario

David P. Keller[1], Ellias Y. Feng[1,2], and Andreas Oschlies[1,2]

[1] GEOMAR Helmholtz Centre for Ocean Research Kiel

[2] University of Kiel

[1] E-mail: dkeller@geomar.de

Abstract: *The realization that mitigation efforts to reduce CO2 emissions have, until now, been relatively ineffective has led to an increasing interest in climate engineering as a possible means of preventing the potentially catastrophic consequences of climate change. While many studies have addressed the potential effectiveness of individual methods there have been few attempts to compare them. Here we use an Earth system model to compare the effectiveness and side effects of afforestation, artificial ocean upwelling, ocean iron fertilization, ocean alkalinization, and solar radiation management during a high CO2-emissions scenario. We find that even when applied continuously and at scales as large as currently deemed possible, all methods are, individually, either relatively ineffective with limited (<8%) warming reductions, or they have potentially severe side effects and cannot be stopped without causing rapid climate change. Our simulations suggest that the potential for these types of climate engineering to make up for failed mitigation may be very limited.*

6.1. Introduction

The realization that despite all mitigation efforts to reduce CO_2 emissions, atmospheric CO_2 concentrations are still rapidly increasing and closely follow the IPCC's high emission scenario (Peters *et al.* 2013), has led to an increasing interest in climate engineering as a potential means of preventing the potentially unacceptable consequences of global warming (Crutzen 2006, Vaughan and Lenton 2011). Evaluating the potential effectiveness and risks of different climate engineering methods prior to any large-scale field experiments is an important first step in informing scientists and society if, and how, further research or physical experimentation should be done (Boyd 2008). Besides informing about potential opportunities and risks, theoretical research has also proven to be a useful way to learn about the climate system. While there is a growing body of literature on individual methods, comparisons among different studies are difficult to make when the studies have been conducted with different models and climate change scenarios (Vaughan and Lenton 2011). A previous comparison of the radiative forcing potential of different climate engineering methods (Lenton and Vaughan 2009) addressed the question of how efficient the methods are at preventing global warming. However, the analytical methodology that was used did not allow for the quantification of side effects and the possible feedbacks in the climate system that may cause a method to be more or less effective than predicted. Earth system models can be used to better evaluate the effectiveness, side effects, and climate feedbacks of different climate engineering methods in a comprehensive way, but have not yet been used to compare different climate engineering methods.

The objective of this paper is to compare and assess the potential effectiveness, in terms of intended climate remediation, as well as the unintended physical and biogeochemical side effects of several climate engineering methods during transient Earth system simulations with a high CO_2 emissions representative concentration pathway (RCP 8.5) scenario (Meinshausen *et al.* 2011) (Figure 6-1). We employ the University of Victoria Earth system model (UVic) (Eby 2009, Keller *et al.* 2012), a model of intermediate complexity (EMIC), and investigate various climate engineering methods of different character in terms of deployment medium, spatial and temporal scales, as well as ethical, legal, and cultural aspects. These methods are large-scale afforestation (AF), ocean iron fertilization (OIF), artificial ocean upwelling (OU), ocean alkalinization (OA), and solar radiation management (SRM). For simplicity, our approach for many of the methods is idealized to simulate the effects that deploying a method would have, without introducing unnecessary complexity. Moreover, we also evaluate the methods in a manner that essentially investigates near maximum potential effects (i.e., large to global scale deployments with an intensity as large as currently deemed feasible – see Methods). The economic, legal, political, and technological feasibility of the methods are not considered here, nor are ethical aspects. Instead we focus solely on the potential atmospheric CO_2 reductions, climate impacts, and the physical and biogeochemical side effects of each method. We find that even when applied continuously at scales as large as currently deemed possible, all methods are, individually, either relatively ineffective with limited warming reductions, or they have potentially severe side effects and cannot be stopped without causing rapid climate change. Our simulations suggest that the

119

potential for these types of climate engineering to make up for failed mitigation may

be very limited.
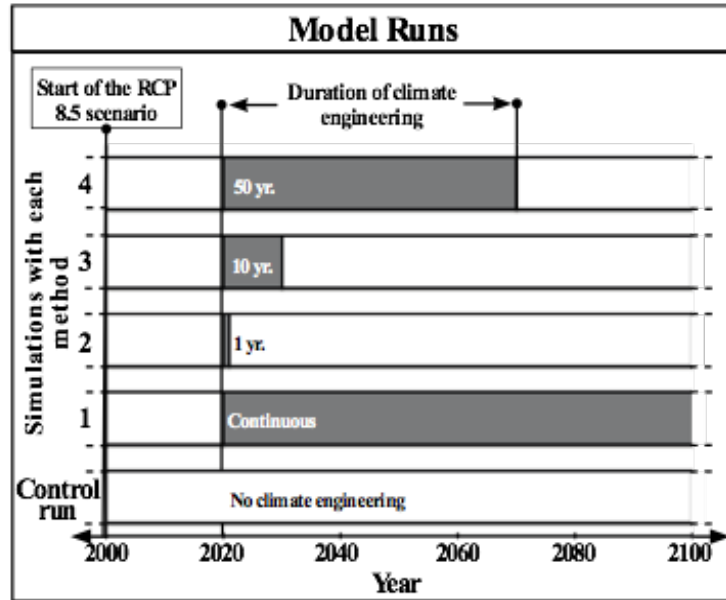
Figure 6-1. Description of the climate engineering methods and the model runs.

6.2. Results

6.2.1. Model Trends during the RCP 8.5 Climate Change Scenario

The UVic model has recently been evaluated in several model

intercomparison exercises (Eby *et al.* 2013, Zickfeld *et al.* 2013, Weaver *et al.* 2012) and

generally has a similar response to CO_2 emission forcing as other models. Here we

will briefly mention how the results of our RCP 8.5 scenario control run compare

with other models. We will also point out the trends that differ from other models

since these (possible) biases need to be taken into consideration when evaluating the

model's response to climate engineering. For surface air temperature simulations the

RCP 8.5 model simulation has a global-mean warming of 2.8 °C by the year 2100

relative to a 1986–2005 reference period, which is within the ranges of an EMIC

intercomparison (1.6–4.1 °C) (Zickfeld *et al.* 2013) and the CMIP5 models (2.5–5.0 °C)

(Knutti and Sedlacek 2013). Atlantic Meridional Overturning Circulation decreases by 38% in our simulations, which are near the mean (40%) and within the range (36%-44%) of 26 other models (mostly CMIP5 models) (Weaver *et al.* 2012). For ocean biogeochemistry a CMIP5 model intercomparison study has not yet been published so instead we have made comparisons to the Community Earth System Model (CESM1 [BGC]) RCP 8.5 scenario results (Moore *et al.* 2013). By the year 2100 export production has decreased by 11% in our simulations and 13% in the CESM1 simulations. Net primary production decreases by 5.8 % in our simulations and 5.7 % in the CESM1 simulation. Mean ocean oxygen decreases by 7 μM in our simulations and 10 μM in the CESM1 simulations. However, for the volume of the oxygen minimum zones, our results are in contrast to CESM1, since our simulations show a decrease in the size of the oxygen minimum zones (OMZs)(Figure E3 and E4) and theirs show an increase of 24 %. Since most Earth system models have problems simulating oxygen distributions and the volume of OMZs it is difficult to determine which trend is correct (Moore *et al.* 2013, Oschlies *et al.* 2008, Duteil and Oschlies 2011), although observations suggest that OMZs have been expanding in recent decades (Stramma *et al.* 2008). Evaluating terrestrial carbon uptake or loss is difficult since there are large differences (i.e., uncertainty) in total carbon uptake between the CMIP5 models (ranging from -0.97 to 2.27 Pg C yr^{-1} during 2006 to 2100) with some models predicting that the terrestrial biosphere will become a net source of carbon and other predicting that it will become a larger sink (Ahlstroem *et al.* 2012). In our simulations the terrestrial biosphere becomes a larger sink with a terrestrial carbon pool of 2247 Pg C at the year 2100, which is 15 Pg C larger than the highest value

reported for the CMIP5 models (Ahlstroem *et al.* 2012). For soil moisture our model indicates that globally soil moisture will decrease in June, July, and August and increase in December, January, and February (DJF). The first result is largely consistent with CMIP5 model results (Dirmeyer *et al.* 2013). However, the majority of CMIP5 models indicate that while a large proportion of the globe will have higher soil moisture in DJF an even larger proportion will have drier conditions (Dirmeyer *et al.* 2013), which is inconsistent with our results. For precipitation our model does not show a global increase of 1-3 % K^{-1} as warming occurs, which is inconsistent with most models (Liu and Allan 2013, Allan *et al.* 2014, Went *et al.* 2007). Instead global precipitation in the model decreases by 0.3% K^{-1}. This inconsistency occurs despite an increase in atmospheric water vapor of 7.4% K^{-1}, which is consistent with other models, observations, and in line with the Clausius-Claperyron equation (Liu & Allan 2013, Allan *et al.* 2014, Went *et al.* 2007). The decrease in global precipitation is entirely due to a decrease in terrestrial precipitation of 3.41% K^{-1} since precipitation and evaporation over the ocean increase by ~1.26% K^{-1}, which is in good agreement with other models (Figure E5). The decrease in terrestrial precipitation is related to the simulated sensitivity of evapotranspiration to increasing CO_2 (i.e., the physiological response of plant stomata to CO_2 fertilization and its effect on water vapour loss), which results in a reduction in terrestrial evaporation of 8% K^{-1}. While this strong decrease in evapotranspiration is inconsistent with the general trend of other models (despite significant differences and uncertainty among them (Fyfe *et al.* 2013)), recent research (Keenan *et al.* 2013) has suggested that existing theory and the

13 most commonly used terrestrial biosphere models underestimate forest water-use efficiency when CO_2 increases.

6.2.2. Effects of Climate Engineering on Temperature and CO_2

When climate engineering is deployed continuously from the year 2020 onward, atmospheric CO_2 is reduced in all of the simulations (Figure 6-2(a), Table 6-1). However, these reductions are small compared to expected business-as-usual anthropogenic emissions and atmospheric CO_2 continues to increase rapidly and still reaches more than twice current levels by the end of the century in all simulations. Those methods that have been proposed to reduce atmospheric CO_2 as a means of preventing warming, i.e., carbon dioxide reduction (CDR) methods (Figure 6-1), are thus, as expected from other studies (Vaughan and Lenton 2011, Lenton and Vaughan 2009, Köhler *et al.* 2013, Aumont and Bopp 2006, Oschlies and Koeve *et al.* 2010, Oschlies and Pahlow *et al.* 2010), unable to prevent a 2.7 to 3.9° C mean temperature increase (temperature increases by 3.8° C with no climate engineering) in our model simulations under the RCP 8.5 emission scenario by the year 2100 (Table 6-1, Figure 6-2(c); 6-3(a), (c), (e), (g)). Indeed, the albedo change caused by simulated AF (Table 6-2) actually results in more warming (see text below for details) than if no climate engineering was implemented. Solar radiation management is the only method in our simulations that is potentially able to restore the temperature to a near pre-industrial value within the 21st century (Table 6-1, Figure 6-2(c) and 6-3(i)) and to prevent many warming-related Earth system changes from occurring. However, as already known from other studies employing different scenarios

123

(Matthews and Caldeira 2007, Broken *et al.* 2009), a persistent reduction of warming requires that SRM is applied continuously.
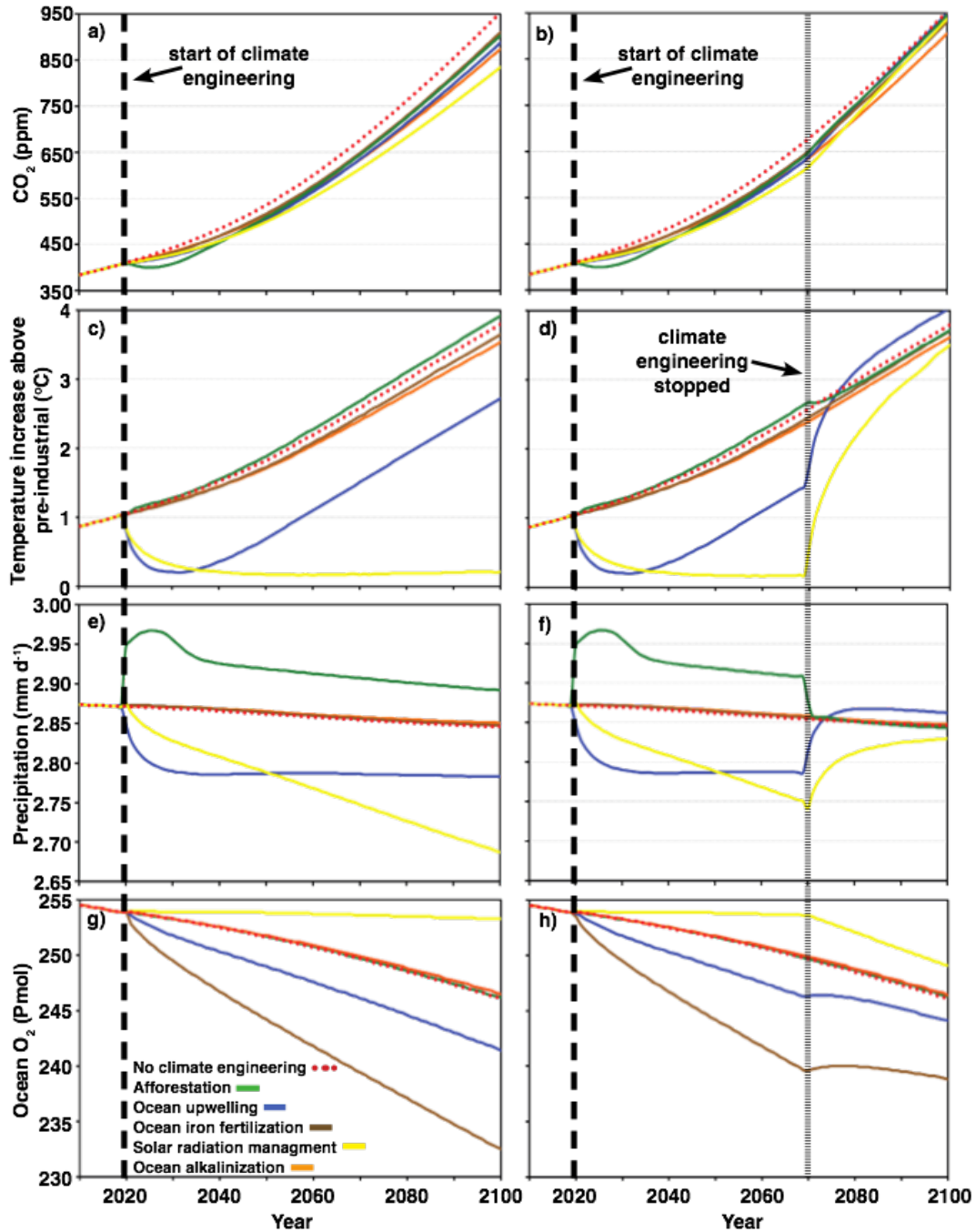
Figure 6-2. Simulated changes in globally averaged annual atmospheric CO₂ and surface air temperature (relative to a pre-industrial temperature of 13.05° C) and the total amount of annual global precipitation and ocean oxygen for model runs where climate engineering was continuously deployed (a, c, e, and g) and runs where it was discontinued after 50 years (b, d, f, and h). The control run, with no climate engineering, is also shown.

124

Table 6-1. Climate engineering (CE) annual average surface air temperature (SAT) and carbon inventory differences. The simulation that combines afforestation (AF), ocean alkalinization (OA), and ocean iron fertilization (OIF) does not show linear, additive effects because of method specific side effects and climate feedbacks (see main text).

	Year	No CE Control	Afforestation	Ocean Upwelling	Ocean Iron Fertilization	Ocean Alkalinization	Solar Radiation Management	AF, OA, OIF Combined
		(°C)	SAT Difference [CE Simulation – Control Simulation] (°C)					
SAT	2030	14.32	0.01	-1.06	-0.05	-0.04	-0.96	-0.05
	2100	16.85	0.12	-1.08	-0.15	-0.26	-3.59	-0.06
Reservoir		(Gt C)	Carbon inventory difference [CE Simulation – Control Simulation] (Gt C)					
Atmosphere	2030	939	-74	-36	-23	-17	-32	-108
	2100	2022	-105	-138	-90	-166	-251	-276
Terrestrial	2030	1997	88	29	-4	-3	34	86
	2100	2247	131	75	-8	-15	249	113
Ocean	2030	37426	-14	7	27	20	-2	22
	2100	37766	-26	63	98	181	2	164

Table 6-2. Climate engineering (CE) induced changes in key Earth system properties (annual global values)

Property	Year	No CE control value	Afforestation	Artificial Upwelling	Ocean Iron Fertilization	Ocean Alkalinization	Solar Radiation Management
			Simulation				
			Difference (CE Simulation – Control Simulation)				
Land surface albedo	2030	0.271	-0.006	0.002	0	0	0.002
	2100	0.260	-0.007	0.002	0.001	0.001	0.010
Ocean surface albedo*	2030	0.132	0	0.001	0	0	0.001
	2100	0.127	0	0.001	0	0.001	0.006
Sea ice area (1010 km2)	2030	2.03	0.01	0.10	0.01	0.01	0.16
	2100	1.35	-0.01	0.15	0.04	0.07	0.83
Ocean pH	2030	8.007	0.025	0.018	0.013	0.021	0.013
	2100	7.714	0.021	0.030	0.016	0.059	0.094
Ocean Ω Calcite	2030	4.087	0.200	0.022	0.082	0.238	0.004
	2100	2.463	0.119	0.068	0.083	0.475	0.251
Ocean Ω Aragonite	2030	2.672	0.130	0.006	0.052	0.156	-0.004
	2100	1.619	0.081	0.038	0.052	0.311	0.151
Precipitation (mm yr-1)	2030	2.87	32.85	-29.20	0	0	-14.60
	2100	2.85	18.25	-25.55	0	0	-58.40
Soil resp. (Pg C yr-1)	2030	70.8	8.9	-2.5	-0.5	-0.3	-2.6
	2100	96.5	9.8	0.4	-1.3	-2.4	-2.3
Land NPP (Pg C yr-1)	2030	74.3	11.4	-0.3	-0.9	-0.7	0.5
	2100	98.5	12.0	1.1	-1.0	-2.1	1.7
Ocean NPP (Pg C yr-1)	2030	49.6	-0.3	28.9	10.6	0	-1.2
	2100	48.1	-1.4	37.5	1.8	0	1.1

*the change in ocean surface albedo is entirely due to changes in sea-ice

6.2.3. Climate Engineering Termination

If SRM is discontinued at any time then extremely rapid warming occurs (up to 0.36° C yr⁻¹), along with an increased rate of atmospheric CO_2 accumulation (Figure 6-2, E10). For temperature, this termination effect is well known and has been consistently reproduced in SRM studies (Matthews and Caldeira 2007, Broken *et al.* 2009, Jones *et al.* 2013, Llanelli *et al.* 2010, Ross and Matthews 2009). However, there

is much less certainty concerning the response of the carbon cycle to SRM discontinuation (Jones *et al.* 2013). Here, we show that there is a substantial termination effect on the carbon cycle since the reduction in atmospheric CO_2, which for the simulated SRM deployment is even larger than that of the CDR methods (Table 6-1, Figure 6-2(a)), quickly reverses with atmospheric CO_2 levels reaching those of the control run within a few decades (Figure 6-2(b)). For OU, rapid warming (up to $0.33°$ C yr^{-1}) also occurs when it is discontinued with surface air temperature ultimately becoming $0.24°$ C higher, due to the method's impacts on the planetary energy budget, than if the method had not been deployed at all. Atmospheric CO_2 concentrations also rise again with the discontinuation of OU until they are at essentially the same level as if no climate engineering had occurred. If the other methods are discontinued less dramatic changes occur. When OIF and OA are discontinued then the ocean stops taking up CO_2 at a higher rate (Figure 6-2(b), E10). However, essentially all of the CO_2 that was taken up (Figure 6-3) remains in the ocean through the duration of the simulation and atmospheric CO_2 concentrations are 21 (OIF) and 48 (OA) ppm lower in the year 2100 than if the methods had not been deployed at all. Because of this, surface air temperatures in the OIF and OA simulations always remain slightly lower, by 0.09 and 0.18 °C by the year 2100, respectively, than in the control run (Figure 6-2, E10). For OIF, this result is consistent with an earlier study (Oschlies *et al.* 2010).

When AF is discontinued by stopping irrigation, the afforested desert regions eventually return to a desert state and the carbon that was stored in the plant biomass and soil (Figure 6-3) is slowly returned to atmosphere through decay and

127

respiration. As in studies of deforestation (Bala *et al.* 2007), surface air temperature then drops from slightly higher (0.1 °C) than the control run to slightly lower (0.08 °C) than it once the vegetation-related albedo change ends (Table 6-2). The temperature becomes slightly lower than in the control run because atmospheric CO_2 is lower since not all of the stored carbon has returned to the atmosphere by the year 2100 and because during desertification the deserts expand (~1 to 3 model grid cells; not shown) beyond their former range (e.g., the desert areas in the control simulation). Since more desert area increases the land surface albedo this contributes to the slight decrease in surface air temperature. The expansion of the deserts occurs because during simulated afforestation the vegetation in the grid cells next to the irrigated regions receive more water due to runoff and additional precipitation (see text below) and thus the vegetation changes from grass land (C3 and C4 types), as in the control simulation, to a shrub type. When simulated irrigation stops, the vegetation is unable to revert from a shrub type to grass types in our model world that has undergone climate change and instead becomes desert. Similar shifts in vegetation have been observed in other simulations in response to perturbations (Dekker *et al.* 2010).
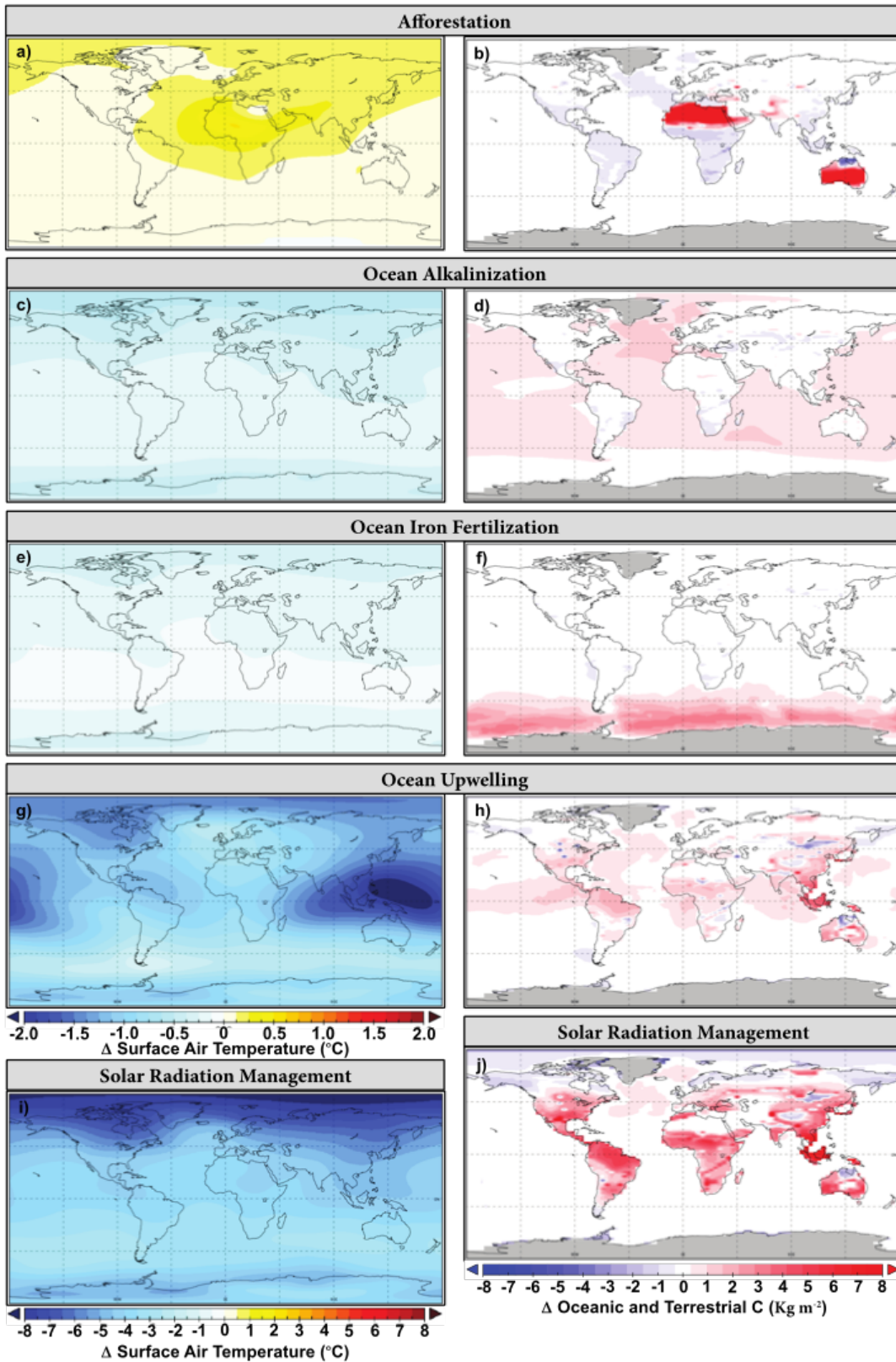
Figure 6-3. The simulated year 2100 mean annual differences between the climate engineering runs and the control run (climate engineering run minus the control run) for surface air temperature (left panels) and terrestrial and oceanic carbon inventories (right panels). Note the difference in the surface air temperature scale for solar radiation management.

129

6.2.4. Climate Engineering Efficacy

Although most of the CDR methods appear to gradually affect atmospheric CO_2 and the surface air temperature (Figure 6-2), their CDR efficacy is actually quite non-linear with time (Figure 6-4) and there is often a backflux of carbon from non-targeted areas as they adjust to the change in atmospheric CO_2 (for example the ocean in the case of AF; backfluxes may also occur within the reservoirs). Indeed, even with SRM, whose purpose is to gradually reduce incoming solar radiation (Figure 6-4) to regulate the surface air temperature, the effectiveness-amplifying (in terms of surface air temperature reductions) CDR side effects (mainly on terrestrial productivity and soil respiration; see text below) are substantial (Figure 6-4). Some CDR methods, like AF, OIF, and OU are quite effective on short time scales (peak C removal occurs in the first 5 years), but less so on longer ones, a result that has been previously shown for OIF and OU (Aumont and Bopp 2006, Oschlies and Koeve *et al.* 2010, Oschlies and Pahlow *et al.* 2010). In contrast, CDR for OA increases in effectiveness over time (Figure 6-4) because the ocean buffering capacity (Egleston *et al.* 2010) remains high, unlike in the other simulations, even as atmospheric CO_2 increases, thus allowing the ocean to take up more CO_2. For SRM, CDR per change in insolation is highest during the first few years, then declines, and then gradually increases in intensity again (Figure E11). The change in surface air temperature per change in insolation for SRM occurs mostly during the first decade of deployment (Figure E11). These results highlight the non-linear relationship between changes in temperature and CO_2, illustrated in Figure 6-4, that occur because of other, often

method specific, feedbacks involving, among others, the hydrological cycle, vegetation, and ocean chemistry (see text below).
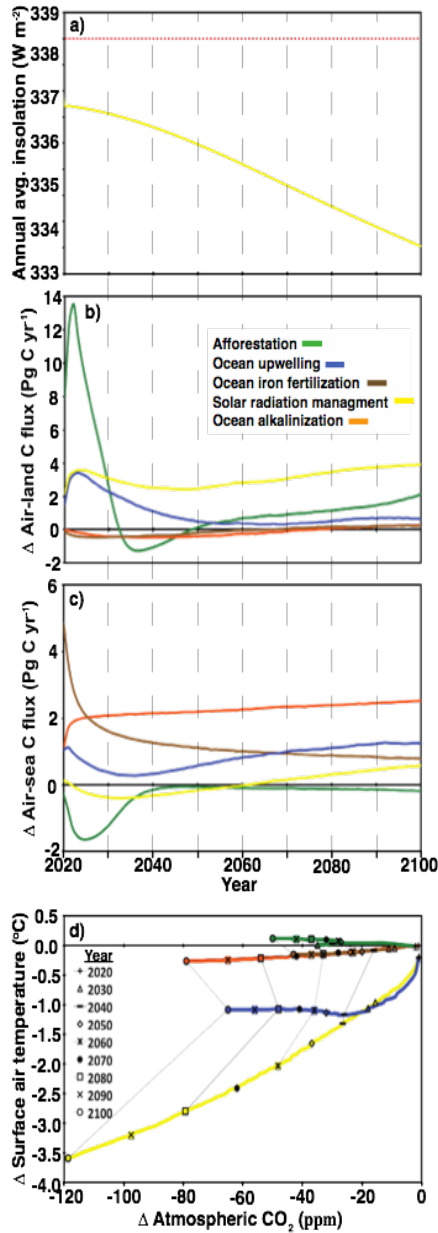
Figure 6-4. (a) Insolation at the top of the atmosphere for the solar radiation management (SRM) model run and all other simulations. The climate engineering model run differences (relative to the no climate engineering model run) in the annually averaged fluxes of carbon from the atmosphere to the (b) land and (c) ocean. Comparison (d) of surface air temperature versus atmospheric CO_2 differences (relative to the no climate engineering model run) for the climate engineering simulations.

131

6.2.5. The Side Effects of Climate Engineering

All of the methods have unintended side effects. Here we mainly focus on physical and biogeochemical side effects that can be diagnosed with the current model (Tables 6-2 and 6-3), but we will also mention some other commonly discussed ones. When possible, we have tried to indicate if a system or cycle will be perturbed by a side effect, but in most cases we are unable to make robust inferences on specific responses to a perturbation (e.g., how species or small-scale regions may be affected).

The side effects of AF tend to be regional, with the large-scale regions defined here as N. Africa, Australia, and the surrounding few hundred kilometers. However, although regional changes would certainly be expected, caution must be taken when interpreting the robustness of these results since the model has fixed atmospheric circulation patterns that essentially do not change (see Methods) in response to afforestation. Regional precipitation and terrestrial productivity both increase (Table 6-2), which could be beneficial for some species and, presumably, humans as long as the increase in precipitation does not cause severe storms or flooding. However, these changes would have a large and perturbing impact on local ecosystems and any societies that depend on them. Productivity increases because in addition to the direct effects of having more water from irrigation, which allows plants to grow in a former desert, there is the fertilizing effect of increasing CO_2 on growth (Keenan *et al.* 2013). Increasing CO_2 during the simulations has a further effect on vegetation and the hydrological cycle because vegetation water-use efficiency increases with increasing atmospheric CO_2 concentrations (Fyfe *et al.* 2013, Keenan *et al.* 2013, Betts

et al. 2007). Although the increase in precipitation is regional it increases the total amount of global precipitation (Figure 6-2(e)) because more water is added to the hydrological cycle. The higher soil moisture and precipitation, which also results in more terrestrial runoff into the ocean, thereby decreases coastal salinity (Figure E7) and raises the global-mean sea level by ~13 cm in the year 2100, unless the water used for irrigation is desalinated seawater. As a result of this change in salinity regional ocean circulation patterns (Figure E8) and ecosystems would likely be affected as well. Increasing the amount of soil moisture also results in evaporative cooling (Figure E8). However, this cooling is countered by a decrease in the regional surface albedo (Figure E6) when the more reflective desert is replaced by darker vegetation. As a result the air temperature in the region increases (Figure 6-3) because of a sensible heat gain. Present-day afforestation simulations in boreal areas have produced similar albedo-related increases in temperature (Betts 2000). Another interesting, but not simulated, potential side effect of AF is that there would likely be less dust blown off of these desert regions if afforested (i.e., both wind patterns and sources of dust may change). Since this dust contains iron and other nutrients that are known to fertilize the ocean (Galbraith *et al.* 2010) and distant forests such as the Amazon, it is possible that productivity in these regions could decrease (Ornstein and Rind 2009, Ridgwell *et al.* 2002). Thus, an increase in productivity and carbon uptake in the afforested areas could result in a decrease in other areas, making this method potentially less effective as a carbon sink (Ridgwell *et al.* 2002).

Table 6-3. Side effects

Method	Side Effects		
Afforestation	Alters terrestrial productivity and carbon storage Increases regional precipitation Increases local evaporative cooling	Decreases the local surface albedo Increases adjacent regional surface air temperatures	Increases regional freshwater ocean input thereby reducing coastal salinity and altering currents and stratification
Ocean Upwelling	Increases marine productivity, except in some equatorial upwelling regions Alters terrestrial productivity Alters ocean circulation, salinity, and stratification Reduces soil temperatures	Cools surface atmosphere Increases surface ocean pCO_2 and acidification in equatorial upwelling regions Reduces precipitation Enhances terrestrial carbon storage	Reduces sea-ice melting Increases ocean deoxygenation and the volume of oxygen minimum zones Imbalances the global heat budget Rapid climate change occurs when stopped
Ocean Alkalinization	Reduces the rate of ocean acidification in the alkalized region	Reduces the rate at which the saturation states of aragonite and calcite decrease	
Ocean Iron Fertilization	Increases marine productivity south of 40° S Reduces marine productivity north of 40° S	Increases surface ocean pCO_2 and acidification in some of the fertilized region	Increases ocean deoxygenation, but decreases the volume of oxygen minimum zones
Solar Radiation Management	Alters terrestrial productivity and respiration Decreases surface ocean pCO_2 and the rate of ocean acidification	Alters precipitation patterns Reduces total precipitation Alters the carbon cycle	Reduces ocean deoxygenation Atmospheric CO_2 continues to accumulate and rapid climate change occurs if the method is stopped

Both OU and OIF increase local marine productivity (Table 6-2, Figure E6), which may be beneficial for some species and fisheries (Oschlies and Pahlow *et al.* 2010). However, the ecosystems of these fertilized regions (throughout the water column) would be disrupted by these changes (Oschlies and Koeve *et al.* 2010,

Oschlies and Pahlow *et al.* 2010). Indeed, because of all the carbon that is locally

sequestered and then respired during OIF, pCO2 increases and the pH decreases

more rapidly near Antarctica than in the control run (Figure E13). Other OIF studies

(Oschlies and Koeve *et al.* 2010) have reported a similar result with regional declines

in pH of up to 0.15 units (relative to a control run). A similar effect (pCO$_2$ increase,

pH decrease) occurs during OU when sequestered carbon is upwelled, e.g. in the

tropical upwelling regions (Figure E13). These methods also decrease productivity

in some unfertilized regions because more nutrients are utilized before being

transported out of the fertilized region (Aumont and Bopp 2006, Oschlies and Koeve

et al. 2010). Thus, non-local ecosystems and fisheries could also be affected.

As has previously been shown for OIF (Oschlies and Koeve *et al.* 2010), it and

OU increase ocean deoxygenation (Figure 6-2, E9), due to the respiration (data not

shown) of fertilization-induced organic matter in deeper waters. As a result the size

of suboxic (O$_2$ < 10 μM) regions changes (Figure E9), impacting marine ecosystems

and biogeochemical cycles (Oschlies and Koeve *et al.* 2010, Oschlies and Pahlow *et al.*

2010). The simulated 265 % increase in the size of the suboxic zones caused by OU

may be particularly important because it could have climatic feedbacks due to the

production of methane and N$_2$O, which are potent greenhouse gases, in low-oxygen

waters (Oschlies and Pahlow *et al.* 2010, Zamora *et al.* 2012). Although the overall

percent fraction that is suboxic with OIF decreases by 43 % because of less

productivity, export, and respiration outside of the fertilized area (Oschlies and

Koeve *et al.* 2010), oxygen declines in the Southern Ocean in our model (Figure E9)

with some regions becoming suboxic by the year 2125. This OIF-induced oxygen

decline is much stronger than in an earlier OIF modeling study (Oschlies and Koeve

et al. 2010) that found only minor decreases in oxygen (60 mmol m^{-3}) in the Southern

Ocean by the year 2110. Since most of the oxygen is consumed in deeper waters that

will not be at the surface, where air-sea gas exchange can occur, for tens to hundreds

or thousands of years, discontinuing OIF and OU does not restore oxygen to the state

that it is in the control simulation (Figure 6-2).

For OU there are also a number of simulated side effects related to the cooling

of the Earth's surface. Terrestrial productivity is perturbed and in most places there

is less soil respiration (Table 6-2, Figure E6 and E9), which together results in more

terrestrial C storage (Figure 6-3, Table 6-1). However, unlike in an earlier OU study

(Oschlies and Pahlow *et al.* 2010) where 80% of sequestered C was stored in the

terrestrial system by the year 2100, only 54% was in our study, which can be

explained by the consideration of iron limitation and iron upwelling in our study

(see Methods). Precipitation patterns are also altered (Figure E12), with a decrease in

total precipitation (Figure 6-3, Table 6-2) because of decreases in evaporation and

evapotranspiration (Matthews and Caldeira 2007). In addition, as in an earlier study

(Oschlies and Pahlow *et al.* 2010), OU decreases sea-ice loss and perturbs ocean

temperature, salinity, stratification, and circulation (Figure E7 and E8). Together

these side effects alter the planet's heat-budget and cause the Earth to take up

additional heat and store it in the ocean's low-latitude subsurface waters (Figure E14).

As a result this method cannot be stopped without causing rapid warming that

ultimately exceeds that of the control run (Oschlies and Pahlow *et al.* 2010) (Figure 6-

2).

Ocean alkalinization has few side effects that can be diagnosed with our model. The ones that we can diagnose reduce the rate of ocean acidification (Figure E13) and keep the saturation states of aragonite and calcite higher than with most other methods (Table 6-2), despite higher oceanic carbon uptake (Figure 6-3, Table 6-1). However, other studies have noted that there are likely to be other side effects that impact marine ecosystems (Köhler at al 2013, Harvey 2008) and shown that certain species physiology would be altered by OA (Cripps *et al.* 2013). Furthermore, this method is also likely to have a substantial impact on terrestrial systems due to the mining and production process associated with the alkalizing agent (Köhler *et al.* 2013, Harvey 2008).

For SRM there are a number of side effects related to the cooling of the Earth's surface. Terrestrial and marine productivity are perturbed and there is less soil respiration (Table 6-2, Figure E6 and E9), which ultimately results in more terrestrial C storage (Table 6-1). For global terrestrial NPP, which is 1.7 Pg C yr^{-1} higher in the year 2100 than in the control run, this increase is consistent with other SRM studies (for example in the GeoMIP G1 experiments the models mean change in NPP between the SRM runs and the quadrupled CO_2 control runs was 1.8 Pg C yr^{-1}) (Kravitz *et al.* 2013a, Naik *et al.* 2003) Interestingly, this accumulation of C on land decreases surface ocean pCO_2 and reduces the rate of ocean acidification (Table 6-2 and Figure E13). Precipitation patterns are also altered, with a decrease in total precipitation (Figure 6-3, Table 6-2 and Figure E12), because of less evapotranspiration (Matthews and Caldeira 2007) and evaporation (Fyfe *et al.* 2013, Feichter and Leisner 2009). Other studies (Fyfe *et al.* 2013, Matthews and Caldeira

2007, Kravitz *et al.* 2013b, Bala *et al.* 2008) have found a similar decrease in precipitation when SRM is implemented. However, since evapotranspiration in our model is more sensitive to CO_2 increases than in other models and precipitation is simulated with a simple energy moisture balance model, we performed the GeoMIP G1 experiment (Kravitz *et al.* 2011) to gain a better understanding of how this particular result compares with other SRM experiments. This experiment (G1) involves instantaneously quadrupling the CO_2 concentration (from pre-industrial levels) while simultaneously reducing the solar constant to counteract this forcing (50 year simulation). In this experiment we found that global precipitation decreased by 0.26 mm d^{-1} (a 9% reduction), which is more than the mean 0.1 (range: 0.1 to 0.2) mm d^{-1} decrease (a mean reduction of 4.5%) found with the GeoMIP models (Kravitz *et al.* 2013a). While this appears to be a substantial difference, when we spatially compare the results of last 10 years of our G1 simulation with the results from one of the GeoMIP models (MPI-ESM-LR), which has itself been comparatively assessed (Kravitz *et al.* 2013a), we are able to discern that the regional changes are higher in the MPI-ESM-LR even though the global-mean effect is smaller (Figure E15). Thus, these GeoMIP model results actually indicate that larger, more extreme SRM-induced changes in regional tropical precipitation are possible, even if the global-mean change is less than in our simulations. These differences likely reflect the differences in the atmospheric model components (e.g., UVic's simple atmosphere versus the more complex, higher resolution one in the MPI-ESM-LR).

Another important side effect is that CO_2 continues to accumulate and therefore SRM cannot be discontinued without causing rapid global change

(Matthews and Caldeira 2007, Broken *et al.* 2009, Jones *et al.* 2013) (Figure 6-2). The C stored mostly in the soils during the deployment of SRM is released rapidly once temperatures increase. Finally, there are also likely to be other side effects beyond what we can diagnose, as other studies have indicated that if SRM is aerosol-based it will potentially affect atmospheric chemistry by depleting the ozone layer (Heckendorn *et al.* 2009) and altering the optical properties of the sky (i.e., color, whiteness) (Crutzen *et al.* 2006). Furthermore, chemical-aerosol altering interactions may occur and reduce the methods effectiveness (Heckendorn *et al.* 2009). As discussed in other studies (Vaughan and Lenton 2011, Lenton and Vaughan 2009, Matthews and Caldeira 2007, Feichter and Leisner 2009, Heckendorn *et al.* 2009), these side effects, especially in the case that SRM is discontinued could severely disrupt ecosystems and human societies.

6.3. Discussion

While the effectiveness and the consequences of discontinuing the methods have, for some methods, been studied before (Vaughan and Lenton 2011, Jones *et al.* 2013) and evaluated and ranked in comparative frameworks (Vaughan and Lenton 2011, Boyd 2008, Lenton and Vaughan 2009), this study for the first time uses an Earth system model for a comparative evaluation of the effectiveness of the different schemes. Unlike in previous studies, we thereby have been able to compare many of the side effects associated with the methods (Table 6-3) in a quantitative manner (Table 6-2). However, our study does have its limits. Foremost, our experiments were conducted with a single model for a limited number of idealized methods. Since every model has its own particular deficiencies and is only as good as its

assumptions, further research with other models and scenarios is required. Model intercomparison projects such as GeoMIP (Kravitz *et al.* 2011) and model uncertainty analyses, both individual and multi-model, will also be necessary to achieve a high level of confidence in the results. More methods may also need to be included in these evaluations, along with possible combinations of methods (e.g., SRM and OA) and mitigation efforts (e.g., SRM and carbon capture and storage). Another aspect that needs to be considered is that while we do discuss large-scale regional effects, these results are likely to be less robust than the global-scale ones due to the coarse resolution of our model. Therefore, future climate engineering studies should also be conducted with less heavily parameterized, higher resolution models to investigate regional effects. Furthermore, since these experiments were designed to evaluate what we deemed near-maximum effects, they did not consider any practical realities of deployment, which would have to be taken into account as the research becomes more focused.

Whether or not the magnitude (effectiveness) of the methods can be more than what we decided was optimistically feasible must also be considered in future research. To further increase AF efficacy the forests could be better managed (i.e., the careful husbandry of selected optimal species or even of genetically engineered species with the vegetation periodically harvested and the C biomass permanently removed from the active C cycle). More large-scale forests could also be planted, although this would likely bring AF into competition with existing areas of food production. For OIF, there is likely little that can be done to increase efficacy as a previous study (Aumont and Bopp 2006) found that fertilizing the areas outside of

the Southern Ocean results in a negligible amount of carbon sequestration. For OU, the pipe location selection criteria could be modified to include iron and nitrate limitation or non-Redfield nutrient uptake. This would mostly result in the placement of pipes in the Southern Ocean, which is the major area where pipes currently aren't placed. Since nutrients are already plentiful here the increase in efficacy would be similar to that of OIF, but with the additional side effects of OU. For OA, the CDR efficacy could theoretically be increased if production and transport logistics, which we used to constrain this method, allow more of the alkalizing agent to be added to the ocean. However, any increase would take time since shipping and production capacity would need to be built up. Given the limited effectiveness of the CDR methods in our study, even with our optimistically large deployments, a very substantial increase in the magnitude (efficacy) mentioned above would be needed to make much of a difference. However, for SRM, insolation could have been reduced more rapidly with our idealized methodology (i.e., as in other SRM experiments when it is deployed later in the 21st century to counter higher temperatures (Matthews and Caldeira 2007, Schmidt *et al.* 2012)), although there would be no reason to do so unless temperatures below pre-industrial levels were desired. Moreover, from a practical standpoint there are some legitimate concerns that have been discussed in other studies (Vaughan and Lenton 2011, Heckendorn *et al.* 2009) about the practical logistics of aerosol deployment or other SRM methods.

In summary, our study suggests that even if continuously deployed on a massive scale, the evaluated CDR-based methods are able to only sequester an amount of atmospheric CO_2 that is small compared to cumulative anthropogenic

emissions in the RCP 8.5 scenario and are thus, unable to prevent the mean surface temperature from increasing to well above 2° C by the year 2100. This is a result that holds true even if the methods that can be safely stopped (AF, OIF, OA). SRM is the method that has the largest potential for preventing warming and even for sequestering carbon, which is an effectiveness-amplifying side effect. However, SRM also has some of the largest side effects and cannot be discontinued without causing rapid climate change. Together these results suggest that if CO_2 emissions remain high, the climate engineering methods discussed here should not be solely counted on to prevent warming or large-scale changes to the Earth system. Indeed, given the limited effectiveness of most of the evaluated methods, our results suggest, in agreement with other studies (Vaughan and Lenton 2011), that CO_2 emission mitigation seems the most effective way to prevent climate change. Climate engineering does not appear to be an alternative option, although it could possibly be used to compliment mitigation (Vaughan and Lenton 2011). However, if climate engineering is seriously considered as a one of the means of preventing climate change, care must be taken when evaluating whether the potential reductions in atmospheric carbon and temperature of a particular method are worth the risks and costs of its side effects.

6.4. Methods

6.4.1. Model Description

The model (UVic version 2.9) we use consists of three dynamically coupled components: a three-dimensional general circulation model of the ocean that includes a dynamic-thermodynamic sea ice model, a terrestrial model, and a simple

one-layer atmospheric energy-moisture balance model. All components have a common horizontal resolution of 3.6° longitude x 1.8° latitude. The oceanic component has nineteen levels in the vertical with thicknesses ranging from 50 m near the surface to 500 m in the deep ocean. The terrestrial model of vegetation and carbon cycles (Meissner *et al.* 2003) is based on the Hadley Center model TRIFFID. The atmospheric energy-moisture balance model interactively calculates heat and water fluxes to the ocean, land, and sea ice. Wind velocities, which are used to calculate the momentum transfer to the ocean and sea ice model, surface heat and water fluxes, and the advection of water vapor in the atmosphere, are determined by adding wind and wind stress anomalies (as determined from surface pressure anomalies that are calculated from deviations in pre-industrial surface air temperature) to prescribed NCAR/NCEP monthly climatological wind data (Weaver *et al.* 2001). The model has been extensively used in climate change studies and is also well validated under pre-industrial to present day conditions (Eby *et al.* 2009, Keller *et al.* 2012, Eby *et al.* 2013, Zickfeld *et al.* 2013, Zickfeld *et al.* 2011).

6.4.2. Experimental Design

The model was spun up for 10,000 years under pre-industrial atmospheric and astronomical boundary conditions and then run from 1765 to 2000 using historical fossil-fuel and land-use carbon emissions. From the year 2000 to 2100 the model was forced with CO_2 emissions following the Representative Concentration Pathway (RCP) 8.5 scenario, which is a "business-as-usual" high CO emission scenario (Meinshausen *et al.* 2011). Continental ice sheets, volcanic forcing, and astronomical boundary conditions were held constant to facilitate the experimental

143

setup and analyses (i.e., prevent confounding feedback effects). Appendix Figure E2 and E3 show the "control" run results, which are, with the exception of precipitation and evaporation over land, very close to or within the range of other RCP 8.5 scenario simulations, e.g., global-mean warming of 2.8 °C relative to a 1986 – 2005 reference period, which is within the ranges of an EMIC intercomparison (1.6 – 4.1 °C) (Zickfeld *et al.* 2013) and the CMIP5 models (2.5 – 5.0 °C) (Knutti and Sedlacek 2013). Simulated climate engineering starts in year 2020 and is either applied continuously until the year 2100 or stopped after one, ten, and fifty years, with the runs continuing thereafter until year 2100 (Figure 6-1). All methods, except for SRM and OU, are instantaneously deployed and stopped at full scale.

6.4.3. Simulated Afforestation

The simulated afforestation of North Africa (the Sahara desert) and the Australian Outback is based on a previous study (Ornstein *et al.* 2009), which we have chosen to replicate because this avoids conflicts with current food production, even though it requires expensive large-scale irrigation measures. Irrigation is simulated by forcing the soil moisture to have a constant value of 360 kg m^{-3} (Figure E17), which then allows vegetation to grow and remove CO_2 from the atmosphere. The irrigated regions were chosen to replicate the previous experiment (Ornstein *et al.* 2009) and we refer readers to this article for justification of the chosen locations. In our simulations only the direct effects of afforestation on carbon uptake, surface albedo, and the energy moisture balance are considered. The frictional effect on winds is not investigated, nor is the potential limitation of vegetative growth by

nutrients other than carbon. The possible reduction of desert dust transport and deposition are not considered here either and will be further investigated elsewhere.

6.4.4. Simulated Artificial Ocean Upwelling

Simulated artificial ocean upwelling was based on a previous study with the UVic model (Oschlies *et al.* 2010). This method places "pipes" that pump water from the specified lower end of the pipe (up to 1000 meters deep) to the ocean surface, in areas where upwelling has been calculated to reduce surface-ocean pCO$_2$ (Figure E14). The simulated upwelling works by transferring water adiabatically from the grid box at the lower end of the pipe to the surface grid box at a rate of 1 cm d^{-1}. A compensating downwelling velocity at all intermediate levels insures volume conservation. The modeled pipes operate at any water column at any time for which a pipe-induced local reduction in surface pCO$_2$ can be expected (included in this calculation is the assumption that surface phosphate concentrations are lower than 0.4 mmol m^{-3}, e.g. so that a fertilization effect occurs). In contrast to the previous study (Oschlies *et al.* 2010), the ecosystem model now includes phytoplankton iron limitation (Keller *et al.* 2012) and the method was modified so that iron is not limiting in the grid cells where the pipes are located. This implementation relies on the assumption that either there is bioavailable iron at the depths from which the pipes draw water or that particle bound iron is desorbed and becomes bioavailable when it is pumped to the surface. Observations (Moore and Broacher 2008) indicate that in ocean regions where dust deposition is low, dissolved iron concentrations are higher at depth than at the surface, suggesting that artificially upwelling these waters will increase surface iron concentrations. Since bioavailable iron is quickly utilized or

abiotically scavenged (Galbraith *et al.* 2010, Moore and Braucher 2008) it was also assumed that upwelled dissolved iron is removed before it can be exported to adjacent grid cells.

6.4.5. Simulated Ocean Alkalinization

Ocean alkalinization by $Ca(OH)_2$ addition was simulated by evenly increasing the total alkalinity of surface waters between 70° N and 60° S (i.e., in ice free waters accessible throughout the year) (Figure E18). The premise behind this method is that the addition and dissolution of $Ca(OH)_2$ in seawater increases the total alkalinity and thereby removes CO_2 from seawater in the following reaction:

$$Ca(OH)_2 + 2CO_2 \rightarrow Ca^{2+} + 2HCO_3^- \qquad (6\text{-}1)$$
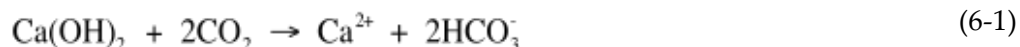
As a result of (6-1) the ocean takes up more CO_2 due to the conversion of CO_2 to HCO_3^- at a molar ratio of 2 moles per added mole of $Ca(OH)_2$. Equation (6-1) also implies that for every mole of $Ca(OH)_2$ added total alkalinity increases by 2 moles. Since limestone, from which $Ca(OH)_2$ is derived, is readily abundant the major limits are either those of production or the capacity to deliver it. The amount we added, 10 Pg yr^{-1}, is based on another study (Köhler *et al.* 2013), which estimated that the total transport capacity of all large cargo ships and tankers is ~10Pg yr^{-1}. Our simulation of OA may thus be viewed as of maximum intensity based on current transport capacity.

6.4.6. Simulated Ocean Iron Fertilization

To simulate the maximum potential of ocean iron fertilization we followed previous studies (Oschlies *et al.* 2010, Sarmiento *et al.* 2010) and focused on the Southern Ocean as the region with the largest carbon sequestration potential by OIF

146

because it has the largest inventory of unused surface macronutrients, has been identified as being iron limited (Boyd *et al.* 2012, Martin 1992), and is a site of large water-mass transformations (Judicone *et al.* 2011, Judicone *et al.* 2008), which help to keep regionally exported carbon in the ocean's interior. Furthermore, Southern Ocean surface pCO$_2$ drawdown and deep carbon export has been observed during iron fertilization experiments (Smetacek *et al.* 2012, Boyd *et al.* 2007) and simulated by modeling studies (Aumont and Bopp 2006, Oschlies *et al.* 2010). Our simulated Southern Ocean iron fertilization works in an idealized manner by simply releasing phytoplankton from iron limitation everywhere south of 40°.

6.4.7. Simulated Solar Radiation Management

There is, so far, little information about the maximum possible intensity of SRM. In this study we set the intensity of SRM such that SRM restores and maintains near pre-industrial atmospheric temperatures. The methodology is based on previous SRM simulations with the UVic model (Matthews and Caldeira 2007) and works by reducing the radiative forcing in the model to mimic what would happen if hypothetical SRM techniques, such as the stratospheric injection of reflective aerosols or space-based sunshades (Vaughan and Lenton 2011), were successfully deployed. As in a previous study (Matthews and Caldeira 2007) SRM is represented by applying a factor, K_g, during each time step to incoming solar radiation (e.g. the solar constant), S_c^0, before the incoming shortwave radiation at the top of the atmosphere, S_c is calculated for each grid cell so that

$$S_c = S_c^0 \cdot (1 - K_g) \tag{6-2}$$

and

$$K_g = \frac{F \cdot ln(\frac{CO_2}{\chi_{CO_2}})}{\frac{S_C^0}{4} \alpha_p} \qquad (6\text{-}3)$$

In Equation (6-3) F is the atmospheric CO_2 radiative forcing term (Weaver *et al.* 2001) and has a constant value of 5.35 W m^{-2}, CO_2 is the simulated atmospheric CO_2 concentration, and χ_{CO_2}, which equals 280 ppm, is the atmospheric CO_2 concentration that corresponds to the target radiative forcing, and α_p equals 0.7, which is approximately one minus the globally averaged planetary albedo.

Acknowledgements

7. Outlook

Research #1 has provided a new angle to perceive AOA technologies, from which AOA can be used at regional scale for coral reef conservation, i.e., as a climate adaptation measure, other than mitigating climate change. Albeit implementing AOA to protect coral reef habitat costs enormously and the ocean acidification threat might not be so urgent compared with bleaching threat for coral reefs, this research can potentially reframe people's visions on AOA as well as other CE technologies from both natural and social science perspectives, and subsequently offers new drives for climate engineering research. To better understand the detailed hydrological and biogeochemical interactions, a following AOA study can be conducted with a higher resolution regional model coupled with biogeochemical cycles.

Research #2 is the first study using 3-D climate model to simulate and evaluate olivine-based COA in environmental science angle. The results demonstrated some considerable climate mitigation potential via olivine-based COA when the local aragonite thresholds are applied to prevent excessive alkalinization. In addition, the analysis on olivine grain size shows that smaller olivine is more effective than bigger ones in CO_2 sequestration potential. Considering the limitations of UVic model, this research can be followed by some evaluations using more complex regional models to better understand the hydrodynamics and biogeochemistry in refined temporal and spatial dimensions. Also, some investigations for understanding how the sequestrated CO_2 via COA is transported into the deep ocean are also meaningful.

149

According to Research #3, if ECS is predicted higher, CE induced the global-mean atmospheric temperature reduction in year 2099 from respective control run will get larger for the same CE intensity. Meanwhile CE engineering input designed to meet 1.5 °C global warming target, will also increase when ECS is set higher. Accordingly, a trade-off has to be made regarding the potential loss from climate change and intensive engineering costs from implementing CE. The study also presents a significant contribution from climate feedbacks to CE global cooling effects. Therefore there could be a big doubt over the results that were produced by models without some important feedbacks, e.g. the climate-carbon feedback. For models with dynamical feedbacks between different cycles, some intercomparison studies on feedback perturbations induced by CE are strongly needed. The new diagnostic metric in this study is based on the idea using fewer parameters to present the uncertainties in complex processes via their generated affects. Likely this approach can also be employed in the future for analyzing model intercomparisons and perturbed physical ensembles (PPE).

Research #4 is an attempt using a climate system model for interdisciplinary study. The combined SRM/AOA schemes are new CE implementation scenarios and need more study over it according to its advances in reducing engineering costs compared to AOA sole implementations. But the interactions generated from combining AOA and SRM together, can lead to increased marginal costs, which is a downside of this approach. In this research, combined SRM/AOA is implemented following prescribed CE intensities. In the future, varied SRM/AOA input at each time step might be employed to simulate more realistic implementation scenarios.

Research #5 is a comprehensive study on multiple CE technologies. Under idealized implementation scenarios, those CE technologies cannot offer considerable climate mitigation potential and minimal environmental side effects concurrently. So far this conclusion is well accepted by the majority of CE researchers.

It has to be clarified that the results and conclusions from Research #1~5 are based on particularly designed CE implementation intensities and manners. The climatic impacts from SRM on marine carbon cycle is little in Research #4 (presented in surface aragonite saturation level), but significant in Research #3 and #5 (presented in sea surface pH and pCO_2). For conducting a CE experiment using numeric models, following existed CE implementation scenarios is advised.

For modeling studies, it is very important to consider the compatibility between chosen model and research questions. If UVic is used for future CE studies, the research questions should be chosen carefully judging upon UVic's own advances and weaknesses:

UVic has only energy-moisture function dominated atmosphere, which makes it inappropriate in most cases to study complex dynamical and chemical processes within atmosphere. In some early studies about SRM, UVic model was employed for testing some CE proposals conceptually, which was well accepted before. However in the past ten years, there has been a huge improvement on understanding SRM technologies. The questions that remain unsolved in this field often require either a complex circulation model, or modeling intercomparisons from various simulations. Therefore, using UVic model alone to study SRM associated topics in the future should take some cautions.

Inspired by the progresses in ocean science and the urgency to protect the ocean, I predict the marine-based CE research will continue growing. Since most marine-based CE technologies operate through biogeochemical cycles, UVic model, with coupled carbon cycle and biology, is one of the very few EMIC models that are frequently employed for studying marine-based CE technologies. Still, there are some constrains, e.g. the coarse spatial resolution and absence of sub-grid processes, which might limit UVic's involvement in small scaled CE studies.

As an EMIC model, UVic has advances in computation efficiency. Therefore it can be very useful to generate CE simulation ensembles. Through statistical analysis and comparisons, those ensembles may provide particular usages that other complex climate models cannot offer. UVic model has also been used frequently in paleo-climate studies. For CE research, some simulations from for paleo-climate period might be taken as analogues to CE modified future climate.

Appendix A

Here we briefly evaluate the UVic model's ability to simulate the ocean chemistry and physical dynamics that are relevant for this study. We first evaluate the model's capacity to simulate present-day ocean total alkalinity and oceanic dissolved inorganic carbon by making comparisons to GLODAP observational data (Key *et al.* 2004). However, since the observations are very limited in the regions where we implement our AOA experiments (Figure A1 and Figure A2), validating the model with only this data is difficult. In the portion of the Great Barrier Reef region that is available for comparison we find that the difference in surface alkalinity and dissolved inorganic carbon between the model and the observations are both around 11 mol/m^3. For regions where no AOA is simulated, the surface total alkalinity and dissolved inorganic carbon are higher than the GLODAP data in the Southern Ocean and the North Pacific. Underestimations exist in the east and west equatorial regions for both total alkalinity and dissolved inorganic carbon.

Since GLODAP data was limited in the areas where we simulated AOA we next compare the simulated oceanic pCO_2 global distribution with Surface Ocean CO_2 Atlas average data from year 1998 through 2011 (SOCAT) (Bakker *et al.* 2014, Landschützer *et al.* 2014), since this variable also provides some information on how well the model simulates ocean carbonate chemistry. Specifically, we compare (Figure A3) with a global annual climatology (1°×1°) of sea surface pCO_2 derived from SOCAT data by (Landschützer *et al.* 2014) using a neural network-based method. Note that the number of observations in the SOCAT database is also limited in our study regions (Bakker *et al.* (2014), their Figure 2 and Figure 8). The

153

comparisons of surface ocean pCO$_2$ between the UVic model and the climatological data generally show that the models performance is reasonable. On a regional scale, we find that UVic overestimates surface seawater pCO$_2$ by 27.34$\pm$2.5 µatm (GB), 17.83 $\pm$5.4 µatm (CS) and 33.28$\pm$11.0 µatm (SC) in the GB, CS and SC regions, respectively. Larger disagreement is found at high latitudes and in the equatorial East Pacific with the model overestimating surface pCO$_2$ by up to 100 µatm at specific grid points. This could either be due to UVic's relatively weak simulation of equatorial upwelling or the lack of a dynamic atmosphere. This disagreement could be due to residuals between data and the neural network-based climatology itself in those areas (Figure 2 of Landschützer *et al.* (2014)). We exemplarily refer to MPI-ESM for checking how well our model does versus such more complex Earth system models. The UVic model did not do any worse than the broadly used MPI-ECM (Ilyina *et al.* (2013b), their Figure 2 and Figure 3), in which HAMOCC model's surface pCO$_2$ has a variance of 40 µatm spatially and a general overestimation globally with 50~150 umol/kg (equivalent to 0.050 ~ 0.150 mol/m3).

Sea Surface Temperature (SST) is commonly used as an important indicator to evaluate modelled ocean circulation and thermodynamics (Wang *et al.* 2014). SST simulated by UVic is validated against World Ocean Atlas (WOA) 2013 climatology (Locarnini *et al.* 2013). This simulated SST distribution agrees well with the WOA (Figure A4) except for a warm bias in the subpolar North Pacific, eastern Equatorial Pacific and smaller regions in the Southern Ocean. Simulated SST is also too low in Atlantic Ocean, especially at higher latitudes. In some specific regions such as Northwest Pacific, the model-data difference can be as large as 6 °C at some grid

points. We find the magnitude of local/regional differences to be similar to what is observed in CMIP5 models. Such biases are common in all global models as shown in an analysis by Wang *et al.* (2014), who found that CMIP5 models on average appear to have a stronger and more widespread warm bias in the Southern Ocean, a stronger cold bias in the subtropical ocean and North Pacific/Atlantic Oceans. In contrast to most CMIP5 models that have a moderate cold bias in the North Pacific, UVic displays a large warm bias in this region. One reason for this difference is the lack of a dynamic atmosphere in the UVic model. Importantly, however, regions to which we apply AOA in our study are not characterized by particularly large model-data SST misfits. For the regions where AOA is implemented, UVic's RMS model-data SST misfit is less than 0.8 °C.

We also estimated the potential impacts of model biases in simulated carbonate chemistry on our AOA model results. A rigorous bias-correction process would require observational DIC and TA data from our AOA regions, which is unfortunately not available based on published data sets such as GLODAP. However, in our AOA regions, observational pCO_2 and SST are accessible. Variations in the oceanic buffer factor depend mainly on changes in oceanic pCO_2 and the ratio of DIC to TA. A bias in pCO_2 can thus induce a bias in the ocean buffer factor and the sea surface aragonite Ω change per unit alkalinity addition. To estimate this possible bias, we first use model-generated values of pCO_2, TA, SST and sea surface salinity (SSS) to calculate a model based sea surface aragonite Ω through CO2sys (Lewis and Wallace 1998, van Heuven *et al.* 2009). Assuming TA and SSS are unbiased, we use observational pCO_2 and SST data to estimate a bias-corrected sea surface aragonite Ω

155

through CO2sys, too (Table A1). This estimated bias-corrected sea surface aragonite Ω from GB and SC is 6% and 5% higher than the model based aragonite Ω. Without (with) bias corrected values of pCO_2 and SST, the aragonite Ω increments per unit alkalinity addition (computed from the model results of the first year of AOA, see Table A1) amount to 4.15 (4.29) m^3/mol in GB, 3.37 (3.11) m^3/mol in CS and 3.39 (3.526) m^3/mol in SC. The estimated biases in omega translate into an uncertainty of required lime additions of roughly 3% more (GB), 7% less (CS) and 4% more (SC).
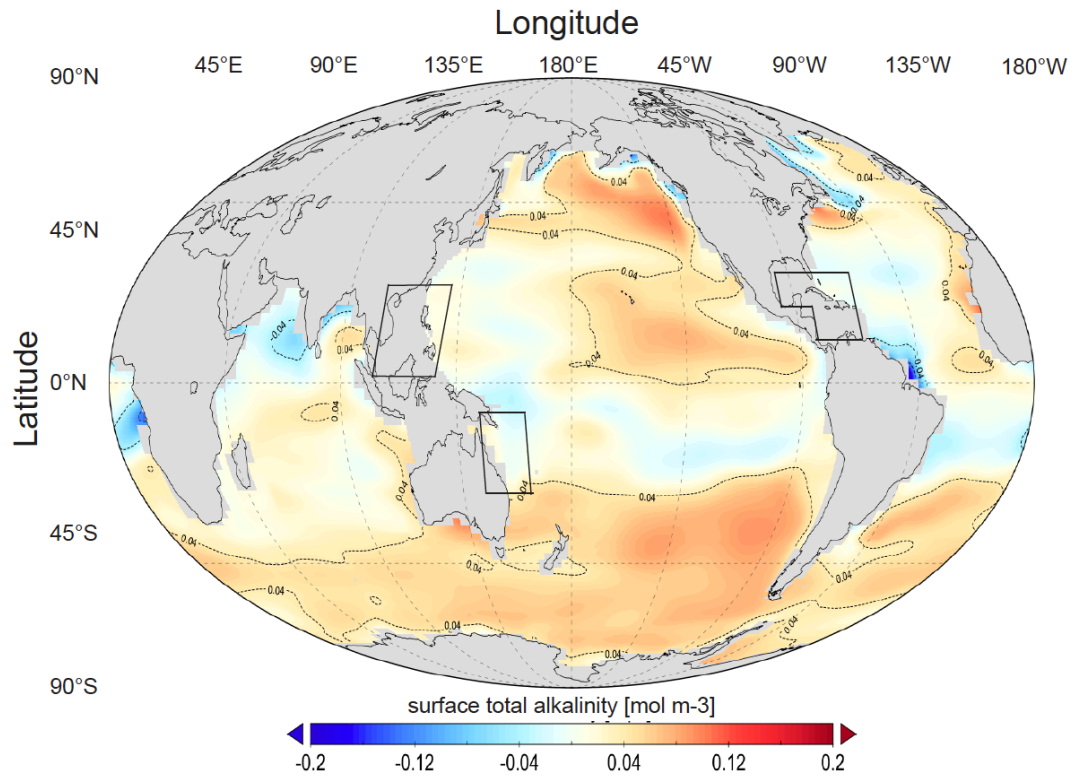
Figure A1. The sea surface total alkalinity difference between the UVic model (year 2020) and GLODAP v1 data (Key *et al.* 2004). UVic's data is regrided to fit GLODAP's 1°×1° spatial resolution. GLODAP vertical total alkalinity data was averaged over the first 50 meters to be comparable with the UVic surface grid box height of 50m.
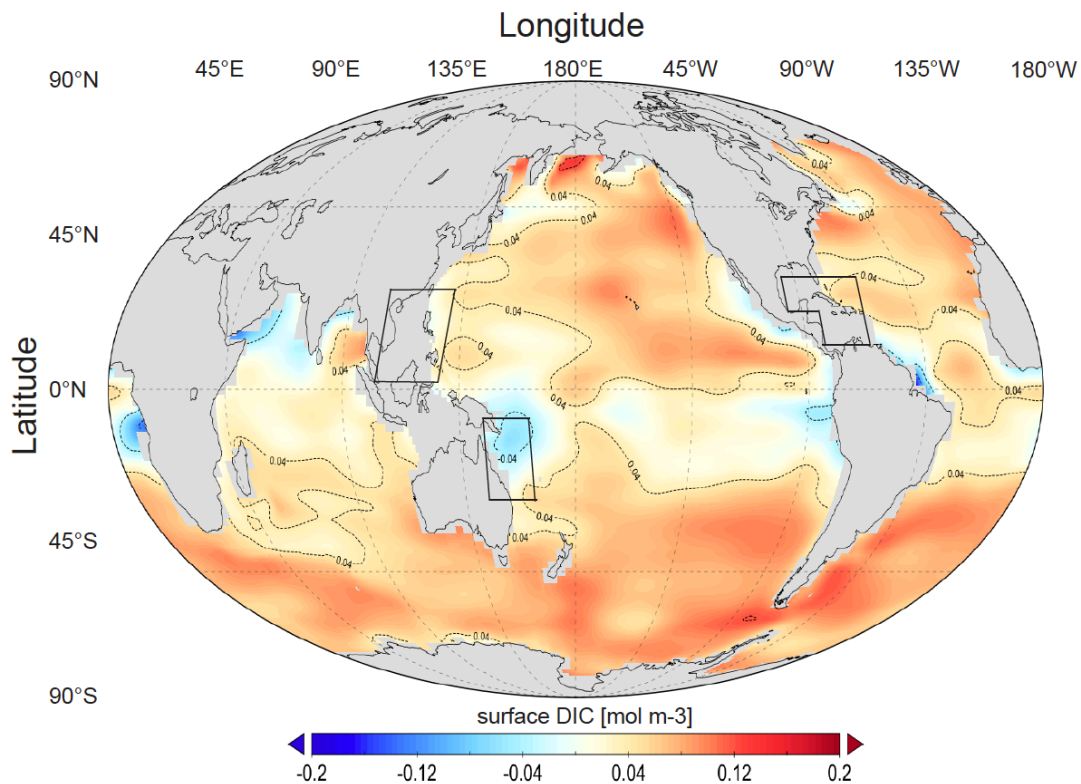
Figure A2. The sea surface dissolved inorganic carbon (DIC) difference between the UVic model (year 2020) and GLODAP v1 data (Key *et al.* 2004). UVic's data is regrided to fit GLODAP's 1° ×1° spatial resolution. GLODAP vertical DIC data was averaged over the first 50 meters to be comparable with the UVic surface grid box height of 50m.
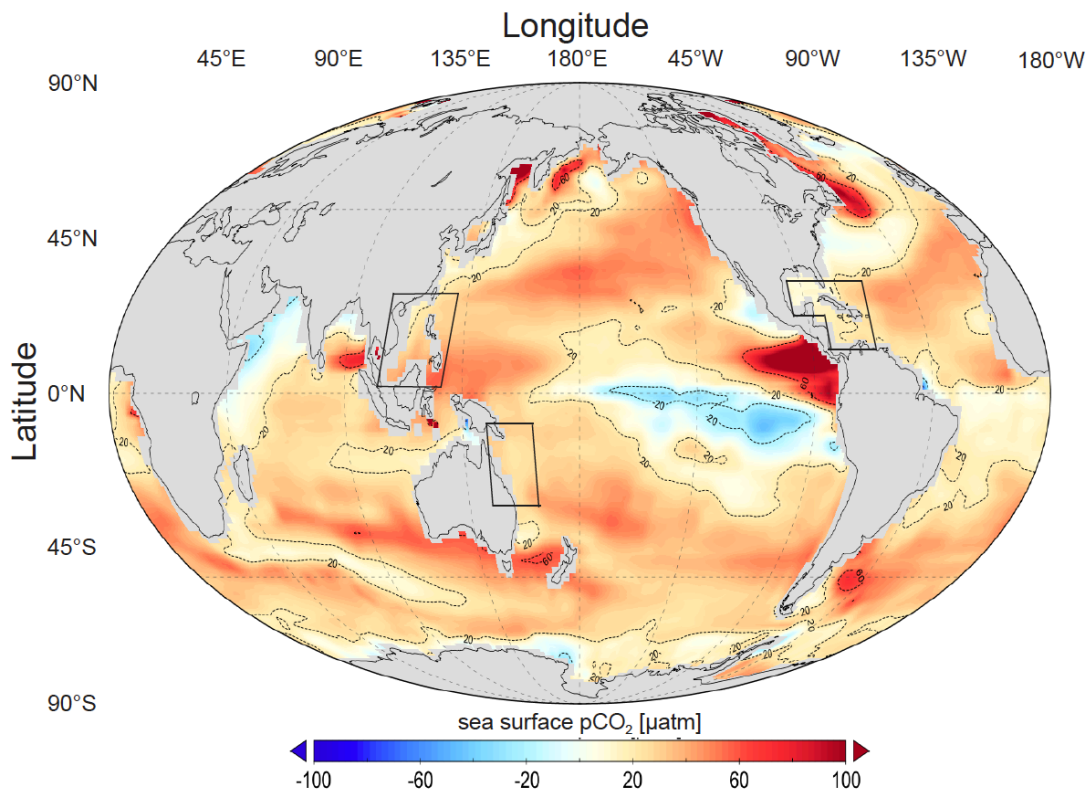
Figure A3. Global distribution for sea surface pCO₂ difference between UVic model (year 2020) and a SOCAT data based climatology (Landschützer *et al.* 2014). UVic's data is regrided to fit SOCAT's 1° ×1° spatial resolution. SOCAT vertical pCO₂ data was averaged over the first 50 meters to be comparable with the UVic surface grid box height of 50m.
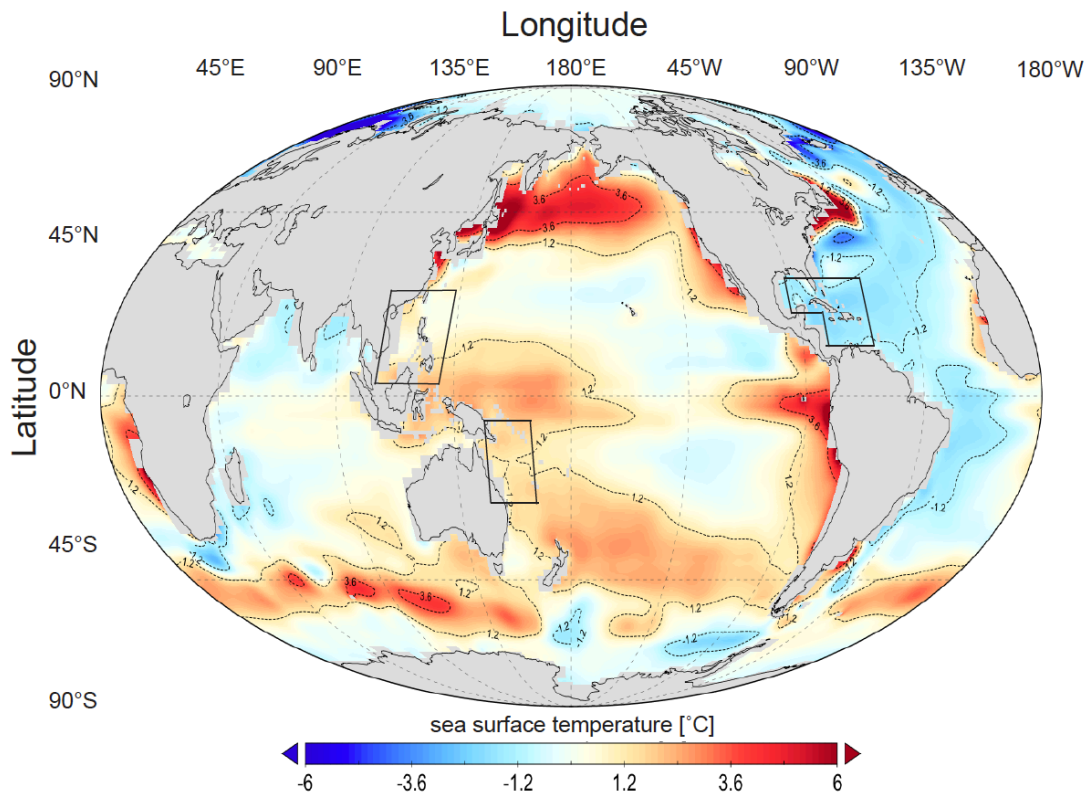
Figure A4. Global distribution for sea surface temperature (SST) difference between UVic model (year 2020) and World Ocean Altas (WOA) 2013 climatology data (Locarnini *et al.* 2013). UVic's data is regrided to fit WOA's 1°×1°spatial resolution. WOA vertical temperature data was averaged over the first 50 meters to be comparable with the UVic surface grid box height of 50m.

Table A1. Carbonate chemistry variables for model year 2020 (and 2021, the first year of AOA). Variables are regionally averaged from Great Barrier Reef (GB), Caribbean Sea (CS) and South China Sea (SC). Inputs from model runs and corresponded output are gathered in "non-bias-correction" rows, while the same for observations are gathered in "bias-correction" rows (non-bias-corrected variables in those rows are left blank).

	Sea surface pCO_2 [μatm]	Sea surface TA [mol/m³]	SST [°C]	SSS [‰]	ΔTA [mol/m³]	Ω_{2020}	Ω_{2021}	ΔΩ/ΔTA
GB (non-bias-correction)	179.3	2.643	27.75	34.84	0.20	7.065	7.894	4.15
GB (bias correction)	151.9		26.62			7.401	8.259	4.29
CS (non-bias-correction)	251.0	2.563	25.30	35.31	0.127	3.89	4.318	3.37
CS (bias-correction)	251.0		26.67			3.884	4.279	3.11
SC (non-bias-correction)	272.6	2.386	28.67	33.79	0.095	4.984	5.306	3.39
SC (bias-correction)	238.5		27.47			5.241	5.576	3.53

Abbreviation notes: TA (total alkalinity); SST (sea surface temperature); SSS (sea surface salinity); ΔTA (regional mean sea surface alkalinity change due to AOA from year 2020 to year 2021); Ω_{2020} (regional mean sea surface aragonite Ω in year 2020); Ω_{2021} (regional mean sea surface aragonite Ω in year 2021); ΔΩ/ΔTA (sea surface aragonite Ω change per unit total alkalinity change)

We calculate the global-mean surface aragonite Ω and pCO$_2$ levels to investigate if the optimal AOA scheme will significantly perturb the global carbon cycle as illustrated for global-mean surface aragonite Ω and pCO$_2$ in Figure A5.
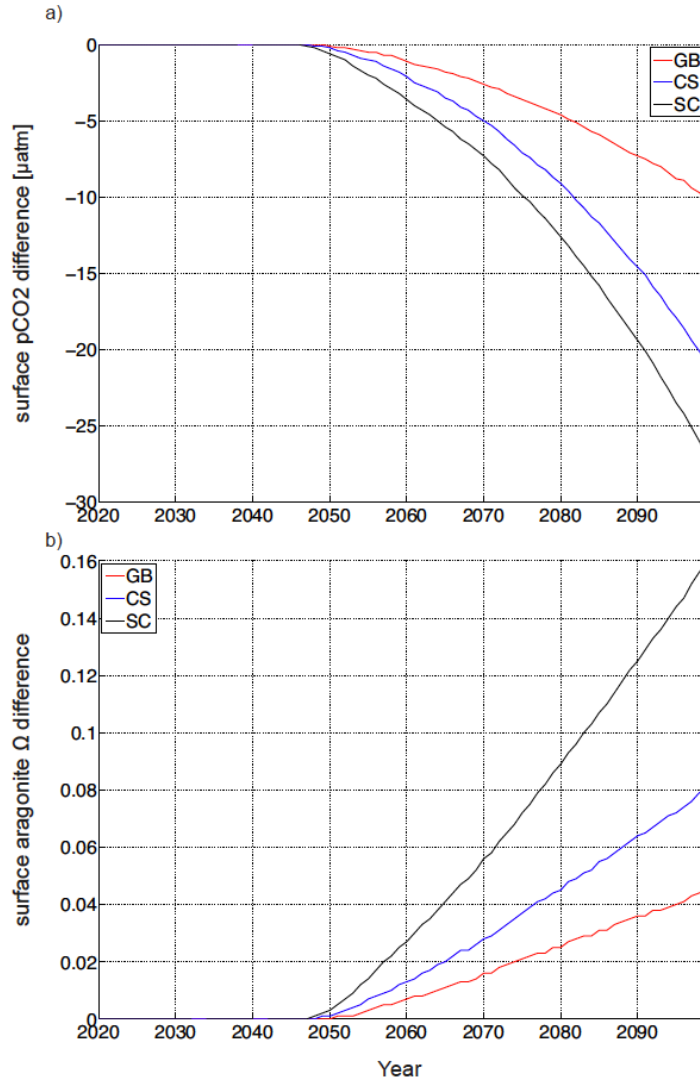
Figure A5. Time series of the simulated global annual-mean surface pCO₂ level (a) and surface aragonite Ω level difference (b) between the optimal runs from Ensemble C and the control run.

Adding calcium hydroxide would perturb the local marine dissolved inorganic carbon (DIC) system. Considering three different theoretical scenarios (invasion of anthropogenic CO₂, AOA-closed system and AOA open system), we calculated the changes of CO₂ (aq), carbonate and bicarbonate concentrations using

the Matlab®-version of CO2SYS (Lewis and Wallace 1998, van Heuven *et al.* 2009) and present results in Bjerrum plots (Wolf-Gladrow *et al.* 2007) as a part of the perturbation protocol. Here CO_2 (aq) represents the sum of carbonate acid (H_2CO_3) and soluble CO_2 (Pilson 2013). Considering ocean acidification without AOA, CO_2 (aq) and bicarbonate ions will increase while carbonate ions decrease, which then causes the aragonite saturation state to decline (Figure A6(a)) and the pH to become lower. If we consider a closed system (no air-sea gas exchange) of a water sample under continuous AOA, CO_2 (aq) and bicarbonate will both decline, while carbonate ions increase (Figure A6(b)) along with pH. This demonstrates the chemistry behind using AOA to prevent ocean acidification and enhance the local aragonite saturation state. This situation can also serve as an analogue for either an abrupt AOA addition for a short time period or a very large AOA scheme where CO_2 invasion can be neglected. However, local AOA, like in our study, has a very limited impact on the pCO_2 of the well-mixed atmosphere. Hence, finally, we consider the case of an open system, where AOA is optimized to keep seawater pCO_2 approximating to a fixed value of 500 µatm but still allow for CO_2 invasion. For this case we find that there is a tendency for both carbonate and bicarbonate to increase together with a slight increase of pH (Figure A6(c), A6(d)).
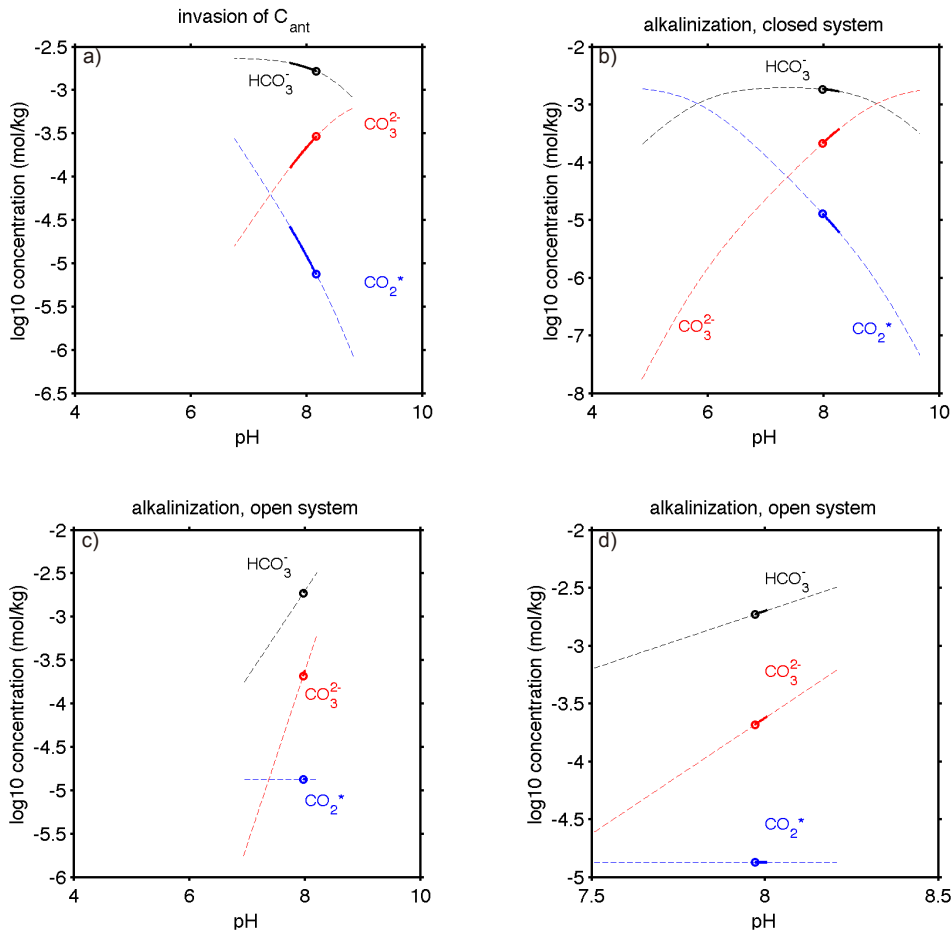
Figure A6. The marine dissolved inorganic carbon system under ocean acidification and AOA. (a) is for a case without alkalinization but with the invasion of anthropogenic CO₂. (b) is for a hypothetical closed system case (no air-sea gas exchange) with alkalinization of a water sample initially equilibrated with an atmospheric pCO₂ of 500 μatm. (c) is for an open system case optimized to fix the oceanic pCO₂ to 500 μatm. (d) is the same as (c) but with a zoomed-in scale to show more detail.

In our AOA experiments we change alkalinity assuming the addition of Ca(OH)₂ , which has an Alkalinity: Calcium (Ca) stoichiometric ratio of 2. We estimate the change in Ca concentration over time by computing the alkalinity difference (AOA-control) and dividing by 2. Results for Ensemble C's optimal simulations are shown in Figure A7 as an example. The maximum calcium elevation happens in year 2099, where the GB (Great Barrier Reef) reaches a value of 0.16

mmol/kg, the CS (Caribbean Sea) of 0.26 mmol/kg and the SC (South China Sea) of 0.34 mmol/kg. These increases are small compared to the background Ca concentration of 10.27 mmol/kg (Pilson 2013).
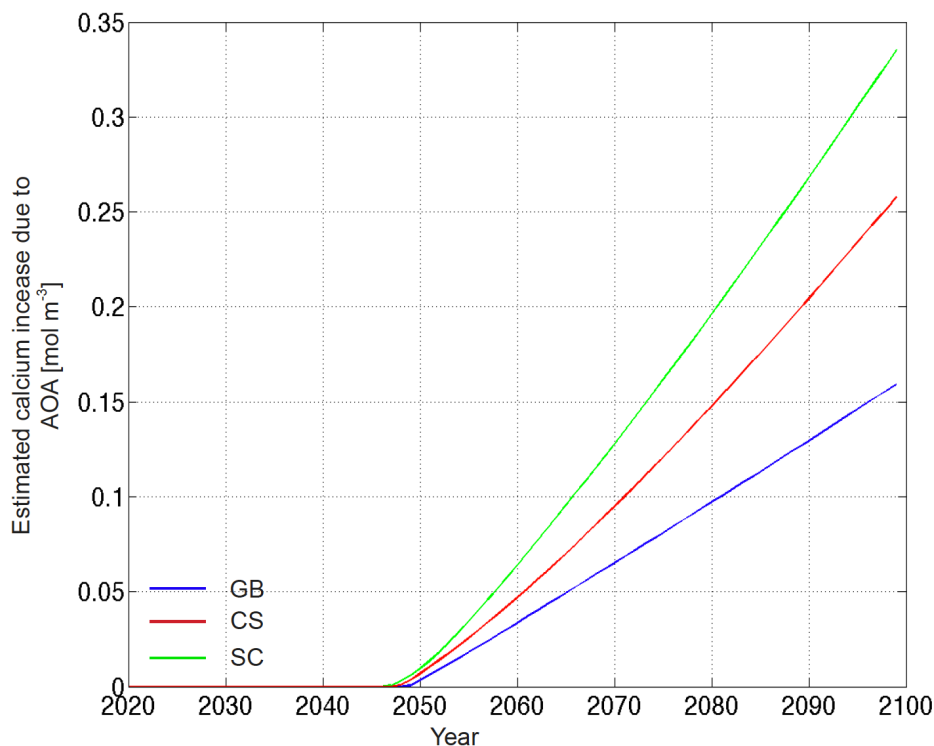
Figure A7. Estimated annual-mean calcium increase in the respective regions for the Ensemble C's optimal simulations. SC represents the "South China Sea", CS the "Caribbean Sea" and "GB" the Great Barrier Reef region.

Changes in alkalinity in sub-surface waters as a result of surface AOA in our regions of interests are investigated here (Figure A8, Figure A9). We first look into the zonally averaged vertical alkalinity change between the optimal runs and control run in year 2099 in the AOA regions (Figure A8). The next figure (Figure A9) shows the total alkalinity change on horizontally averaged chemistry within AOA implemented regions of the optimal runs. The longitude dimension only covers the AOA implemented regions for both figures.

165
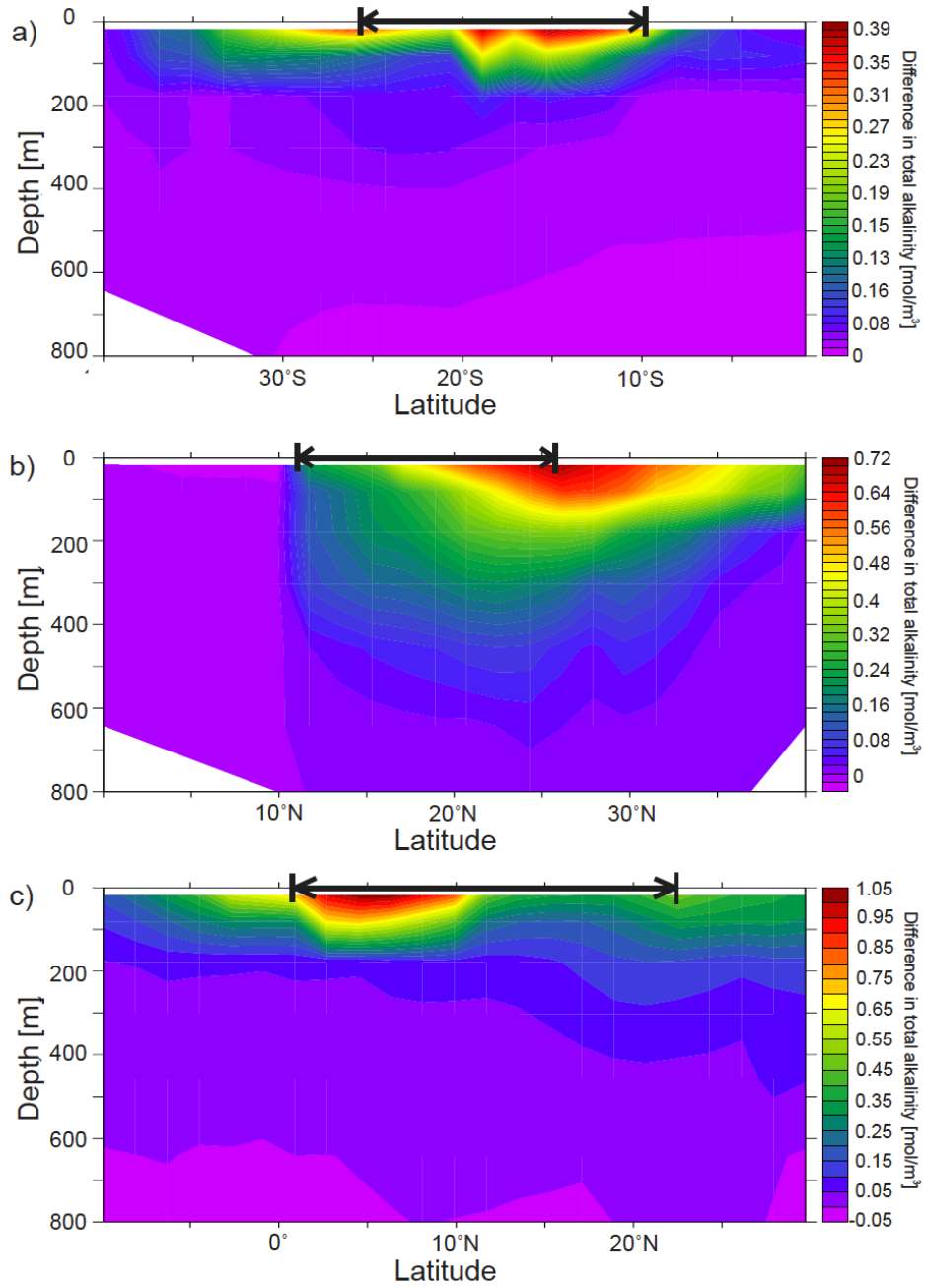
Figure A8. Annual meridional oceanic total alkalinity differences between the optimal AOA runs and the control run in the year 2099. Regions where AOA are implemented: a) Great Barrier Reef, b) Caribbean Sea, and c) South China Sea, are marked within the arrows on the top of each subplot.
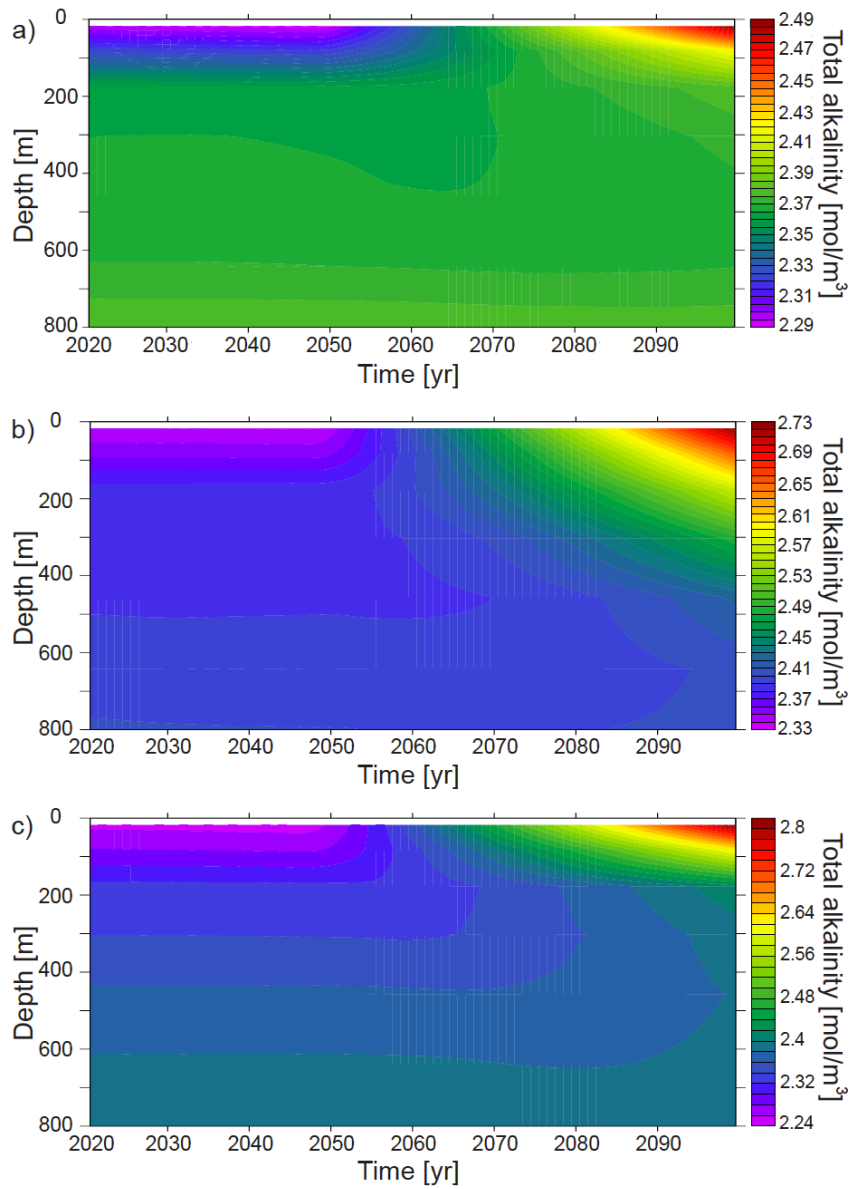
Figure A9. Simulated total alkalinity changes in regional average for AOA implemented regions: a) Great Barrier Reef, b) Caribbean Sea, and c) South China Sea, from year 2020 to 2099 for optimal runs.
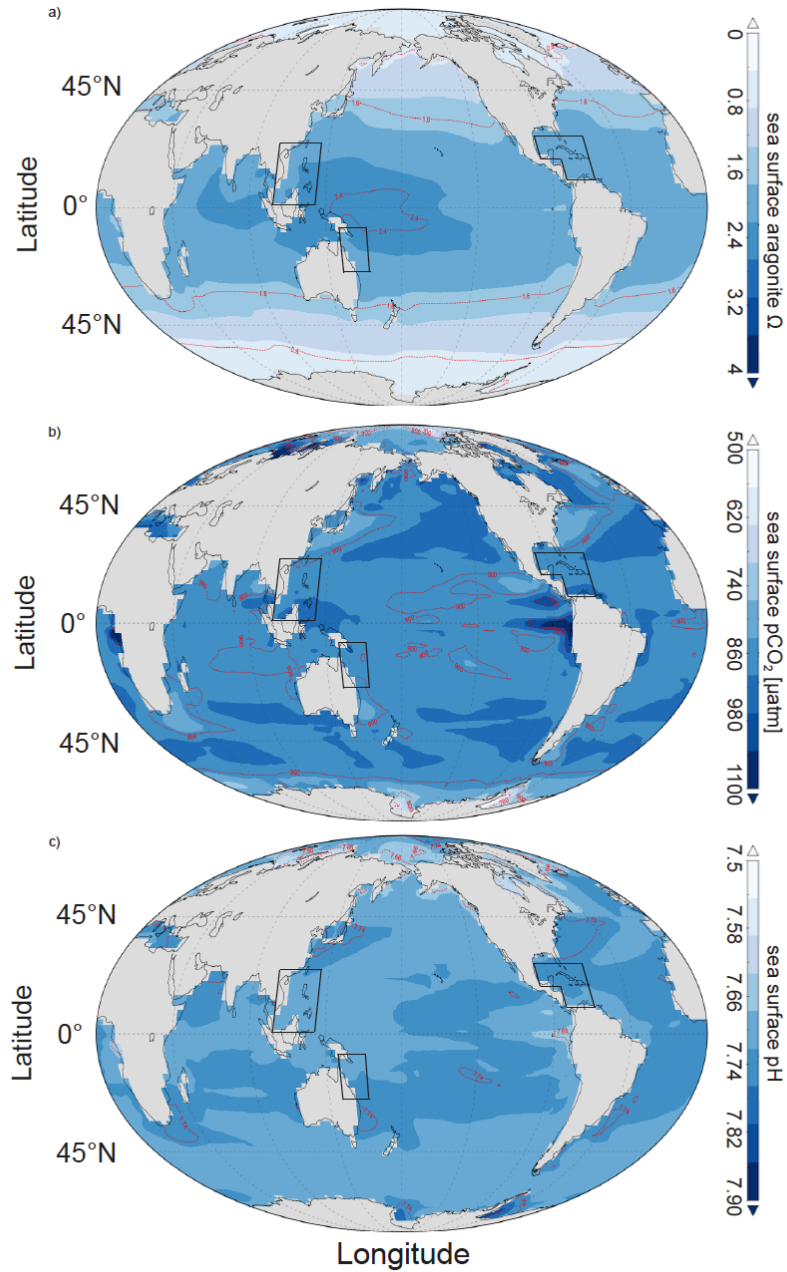
Figure A10. Annual global control run distributions of (a) surface aragonite Ω in the year 2099, (b) surface pCO₂ in the year 2099, (c) surface pH in the year 2099. Regions where AOA is implemented in the experimental runs are marked with boxes.
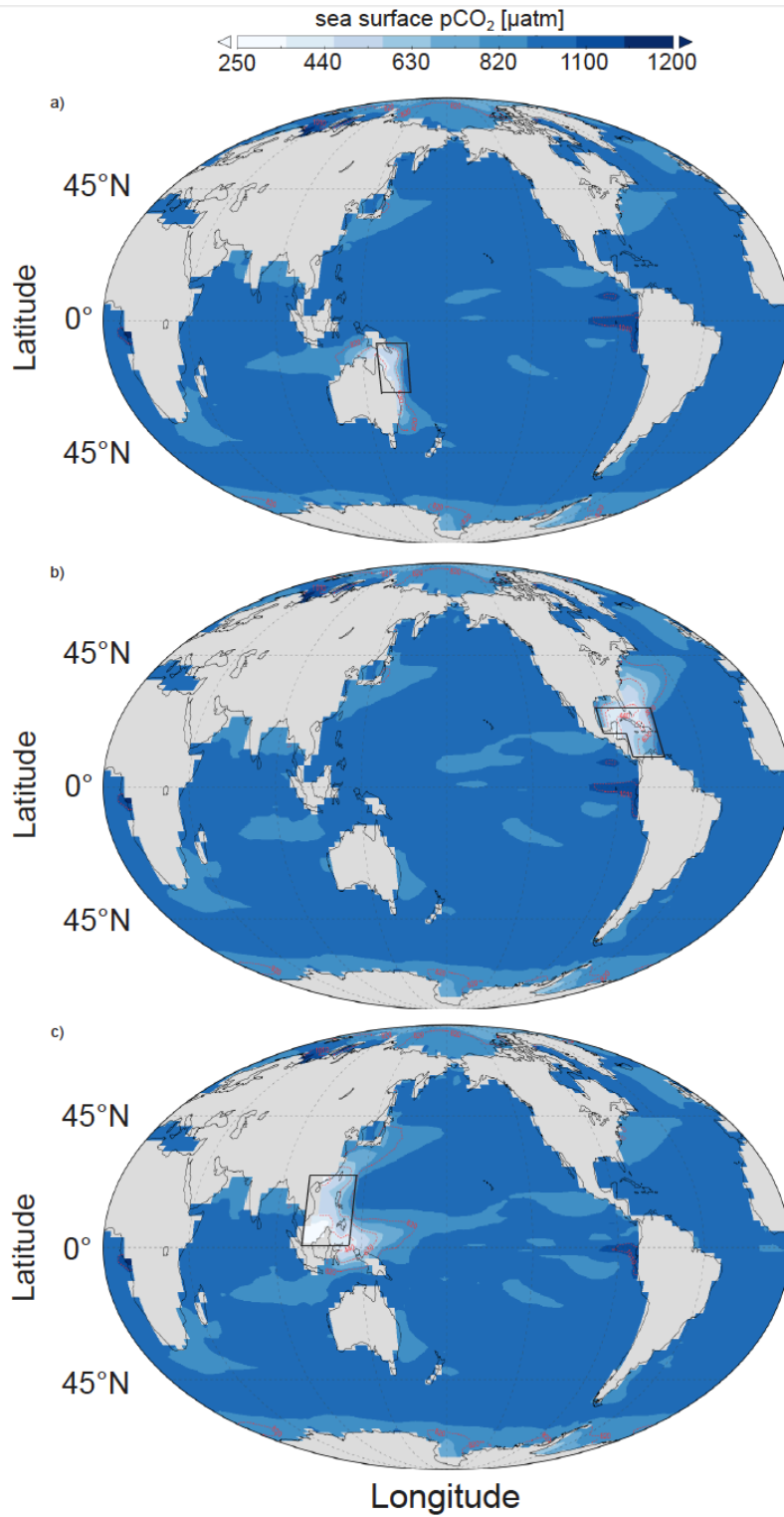
Figure A11. Global annual optimal AOA run distributions of ocean surface pCO₂ in the year 2099 in (a) Great Barrier Reef, (b) Caribbean Sea, (c) South China Sea. Regions where AOA is implemented are marked with boxes.
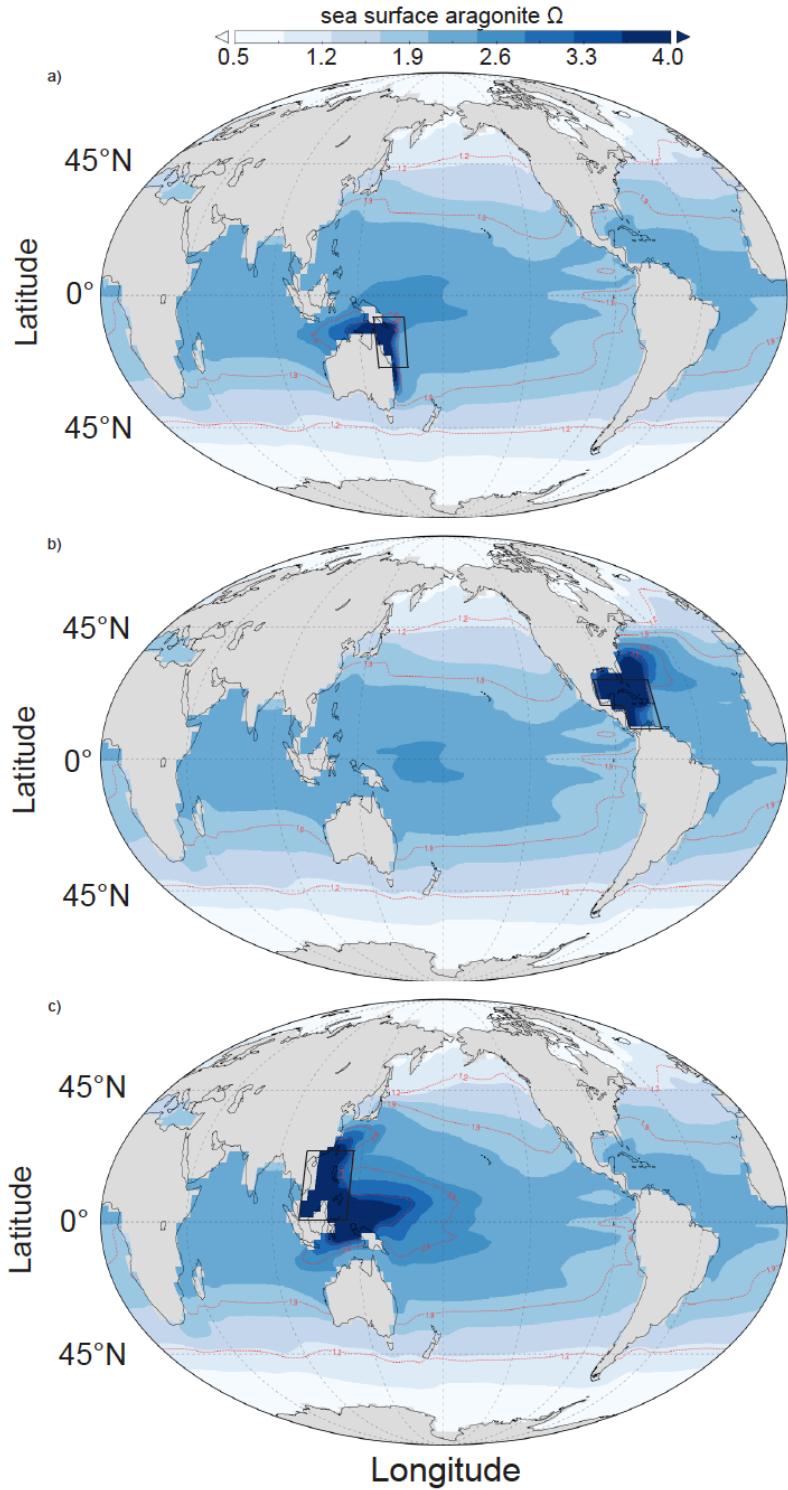
Figure A12. Global annual optimal run distributions of the ocean surface aragonite saturation level in the year 2099 for (a) Great Barrier Reef, (b) Caribbean Sea, (c) South China Sea. Regions where AOA is implemented are marked with boxes.

Here we show close-up figures of the AOA regions for the optimal runs in the year 2099 (Figure A13). About 36% grid boxes in the GB, 40% in the CS and 58% in the SC have passed the pCO$_2$=500 regional mean thresholds.
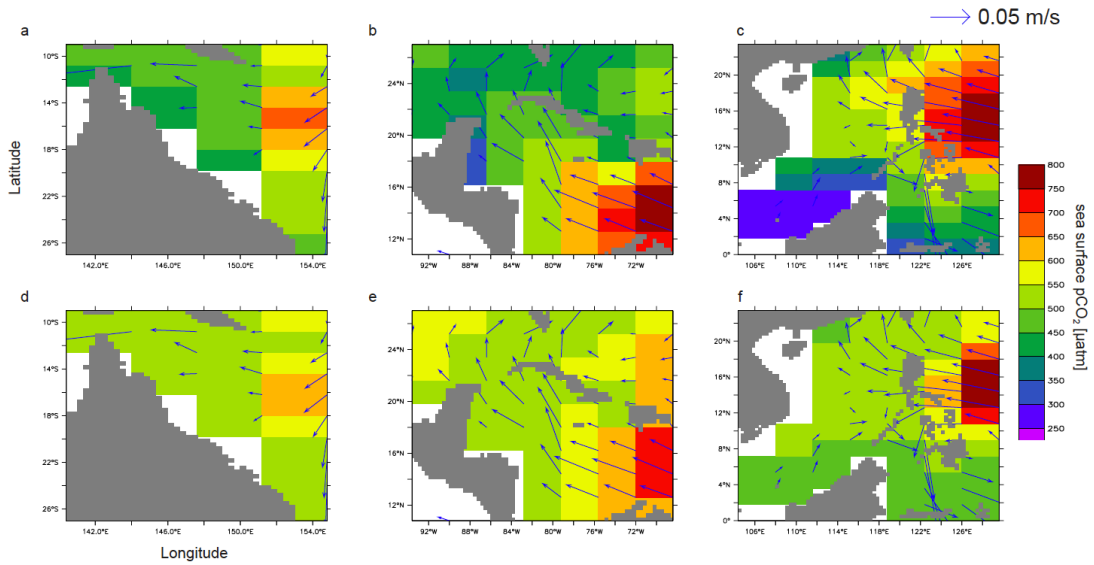
Figure A13. Sea surface annual-mean pCO$_2$ values in year 2099 for AOA regions in our original optimal runs; GB(a), CS(b) and SC(c), with the pCO$_2$ = 500 μatm applied as a regional mean threshold. Another three runs with same configurations as optimal runs, but applying a pCO$_2$ = 500 μatm threshold in every grid box are shown for the GB(d), CS(e), and SC(f). These three runs are not discussed in the main text. Sea surface current velocities are shown in arrows.

Annually averaged SST (*NOAA_OI_SST_V2 data provided by the NOAA/OAR/ESRL PSD, Boulder, Colorado, USA, from their Web site at http://www.esrl.noaa.gov/psd/*) (Reynolds *et al.* 2002) and surface delta-pCO_2 data (Surface Ocean CO_2 Atlas, positive values indicate CO_2 flux from ocean to atmosphere) (Landschützer *et al.* 2014) are used to illustrate the pattern changes of strong El-Niño year (1988) and strong La-Niña year (2011), referenced to climatology data averaged from 1980 to 2011 (Figure A14 and A15).

We found the regional averaged SST from our studied regions increases around 0.25 °C (Great Barrier Reef region, i.e. GB), 0.15 °C (Caribbean Sea, i.e. CS) and 0.34 °C (South China Sea, i.e. SC) in El-Niño year, and 0.14 °C (GB), 0.1 °C (CS) and 0.05 °C (SC) in La-Niña year. The regional averaged surface delta-pCO2 has anomaly of +5 μatm (GB), 2 μatm (CS) and 9 μatm (SC) in El-Niño year, -5 μatm (GB), 3 μatm (CS), -1 μatm (SC) in La-Niña year.
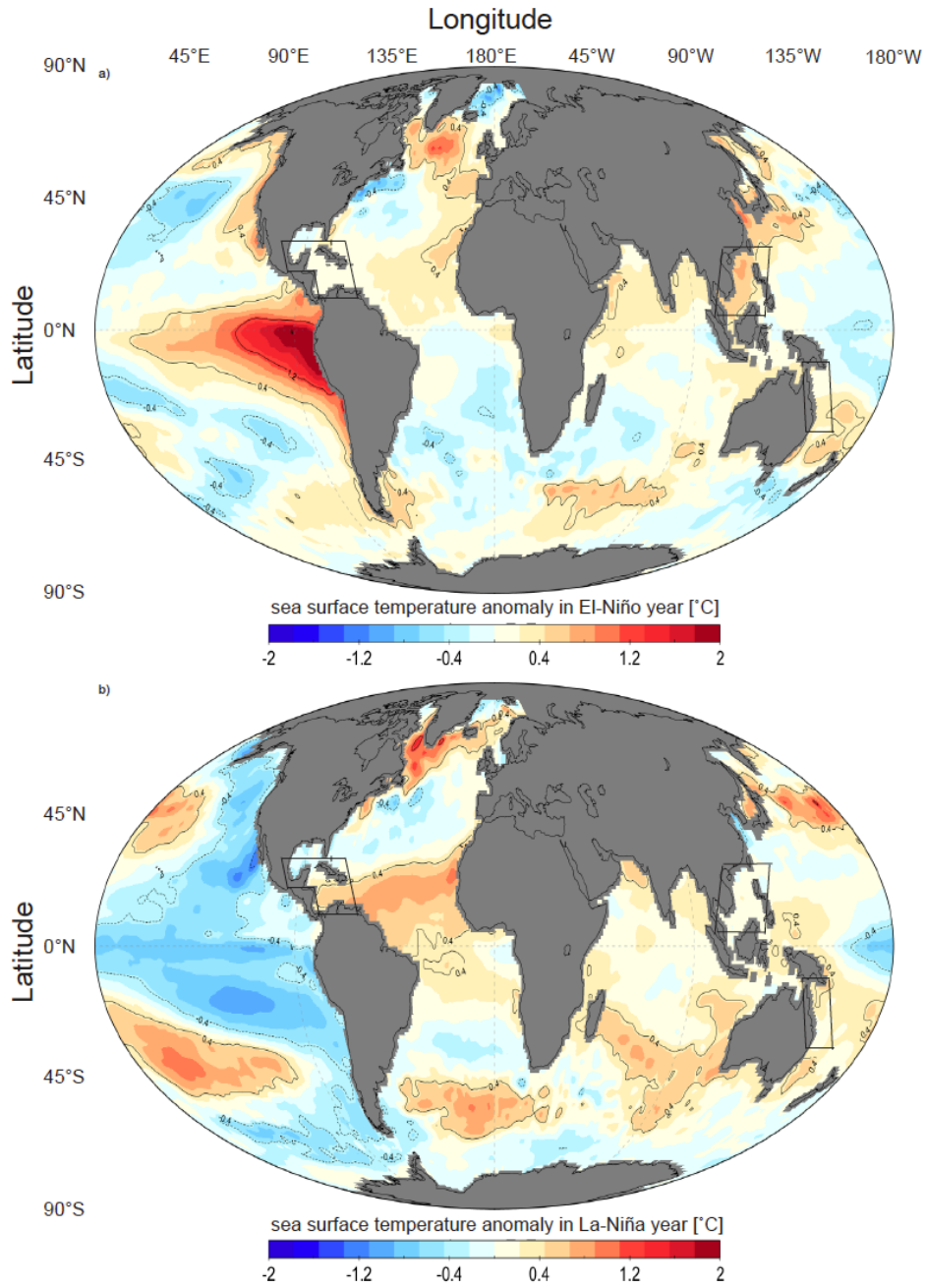
Figure A14. Global annual-mean SST anomalies of a) El-Niño year (1998) and b) La-Niña year (2011) referenced to climatology average from year 1981 to year 2011. Data provided by the NOAA/OAR/ESRL PSD, Boulder, Colorado, USA, from their Web site at http://www.esrl.noaa.gov/psd/ (Reynolds *et al.* 2002)

173
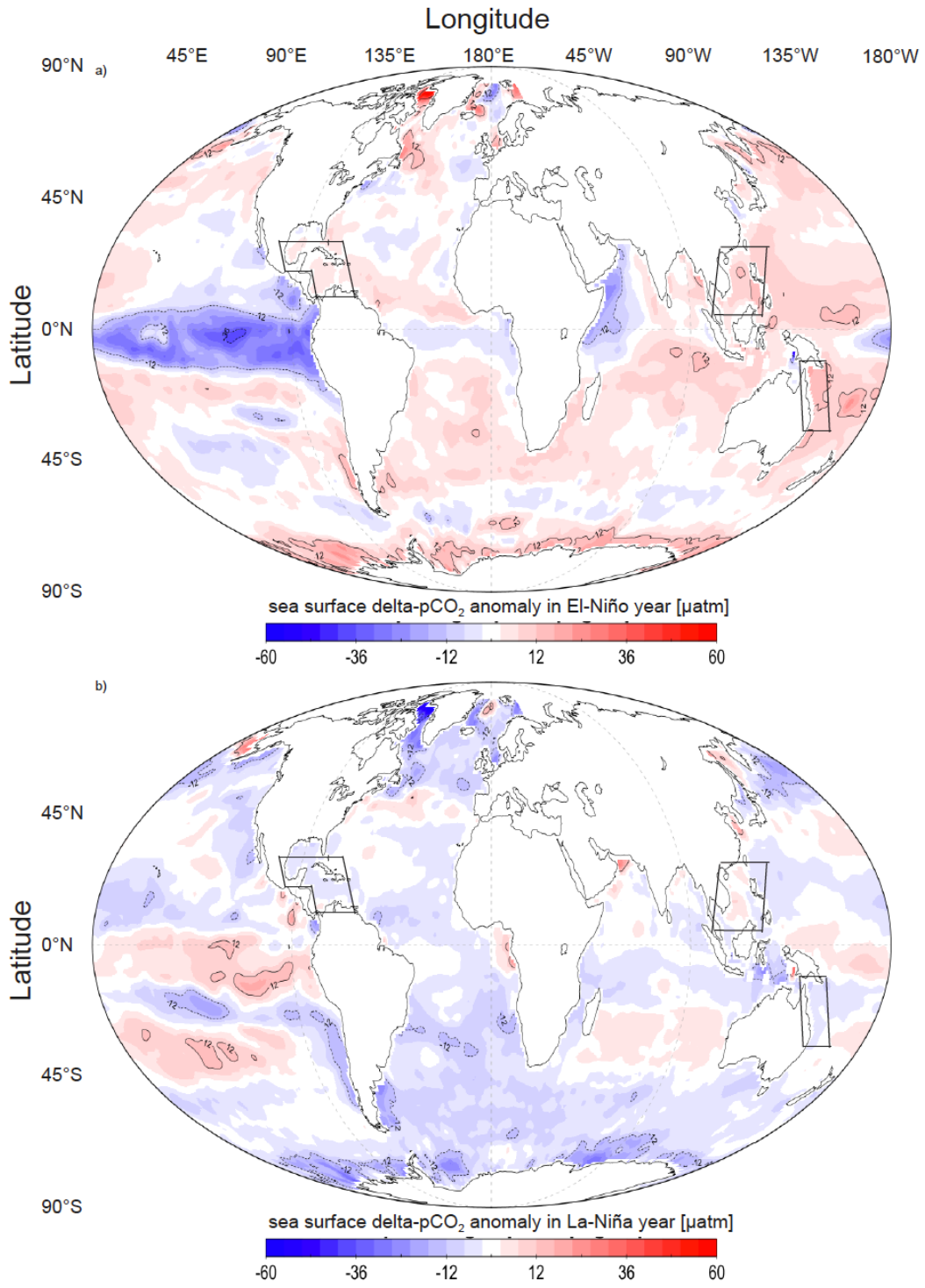
Figure A15. Global annual-mean delta-pCO₂ anomalies of a) El-Niño year (1998) and b) La-Niña year (2011) referenced to climatology average from year 1998 to year 2011 Surface delta-pCO₂ data is provided by Surface Ocean CO₂ Atlas (positive values indicate CO₂ flux from ocean to atmosphere) (Landschützer *et al.* 2014)

Appendix B

We conducted three model runs with similar set-ups to *Oliv100_con*, but excluding the dissolution dependencies on seawater temperature (*Oliv_nosst*), pH (*Oliv_nopH*) and both temperature and pH (*Oliv_no*). The results are shown below in Table B1 and Figure B1.

Table B1. Experimental design and model results for *Oliv_no*, *Oliv_nopH* and *Oliv_nosst*. Output is compared with *Oliv100_con*.

Model run	CO_2 drawdown (ppm) [*]	Coastal aragonite Ω [†]	Cumulative olivine dissolution (Pmol Alk yr^{-1}) [§]
Oliv_no	-72	2.79	19.7
Oliv_nopH	-68	2.82	18.8
Oliv_nosst	-71	2.78	19.5
Oliv100_con	-68	2.81	19

[*] **Annual-mean atmospheric CO_2 differences relative to the control run *RCP8.5* in year 2099 (944.4 ppm).**

[†] **Annual-mean sea surface aragonite Ω in year 2099 of coastal grid boxes where COA has been implemented. This value from the control run *RCP8.5* is 1.80.**

[§] **Integrations are undertaken from year 2020 to year 2099. The olivine molar mass is assumed to be 153.31 g mol^{-1}.**
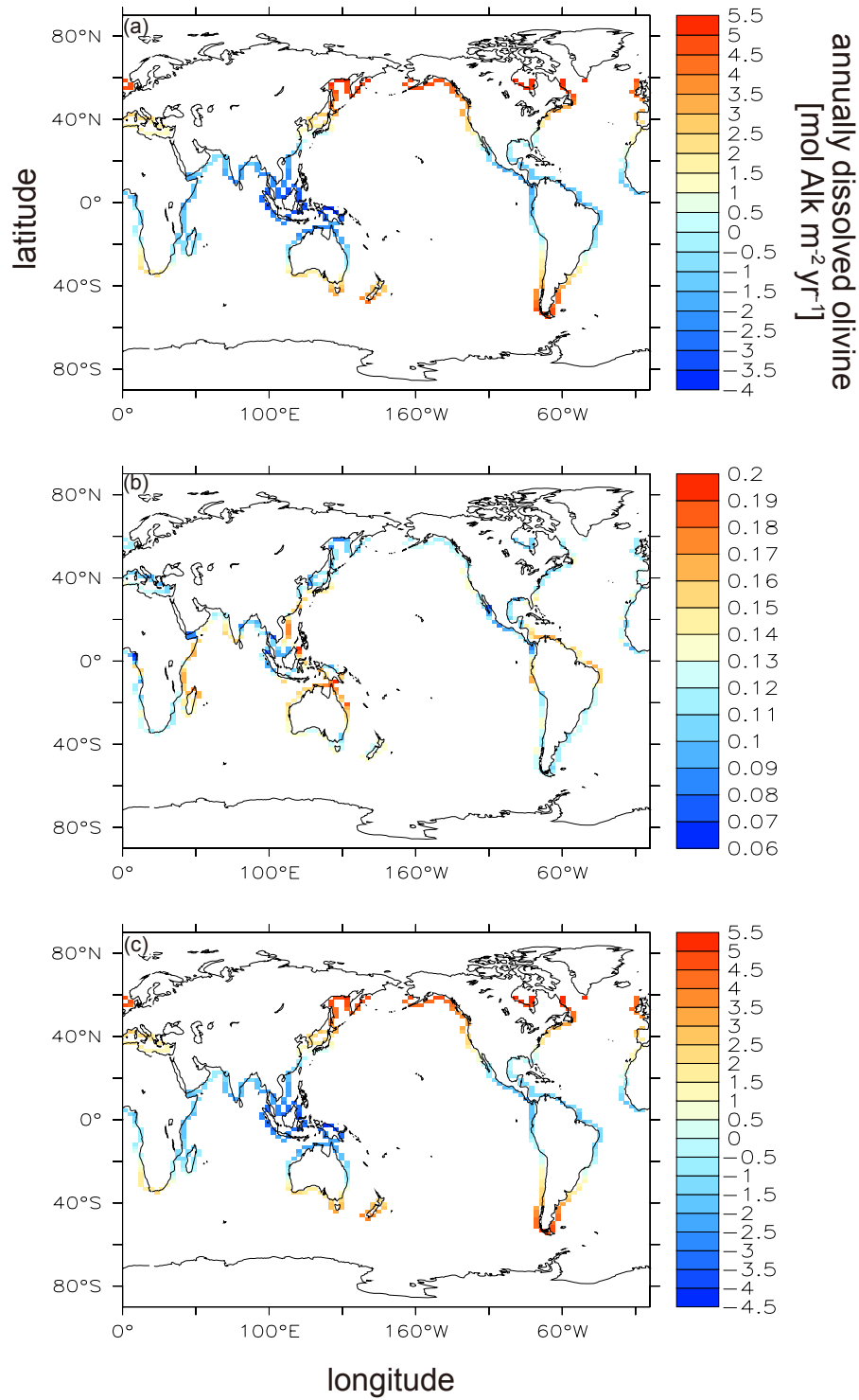
Figure B1. Year 2099 global distribution difference in annually dissolved olivine between the *Oliv100_con* run and *Oliv_nosst* (a), *Oliv_noph* (b), and *Oliv_no* (c).
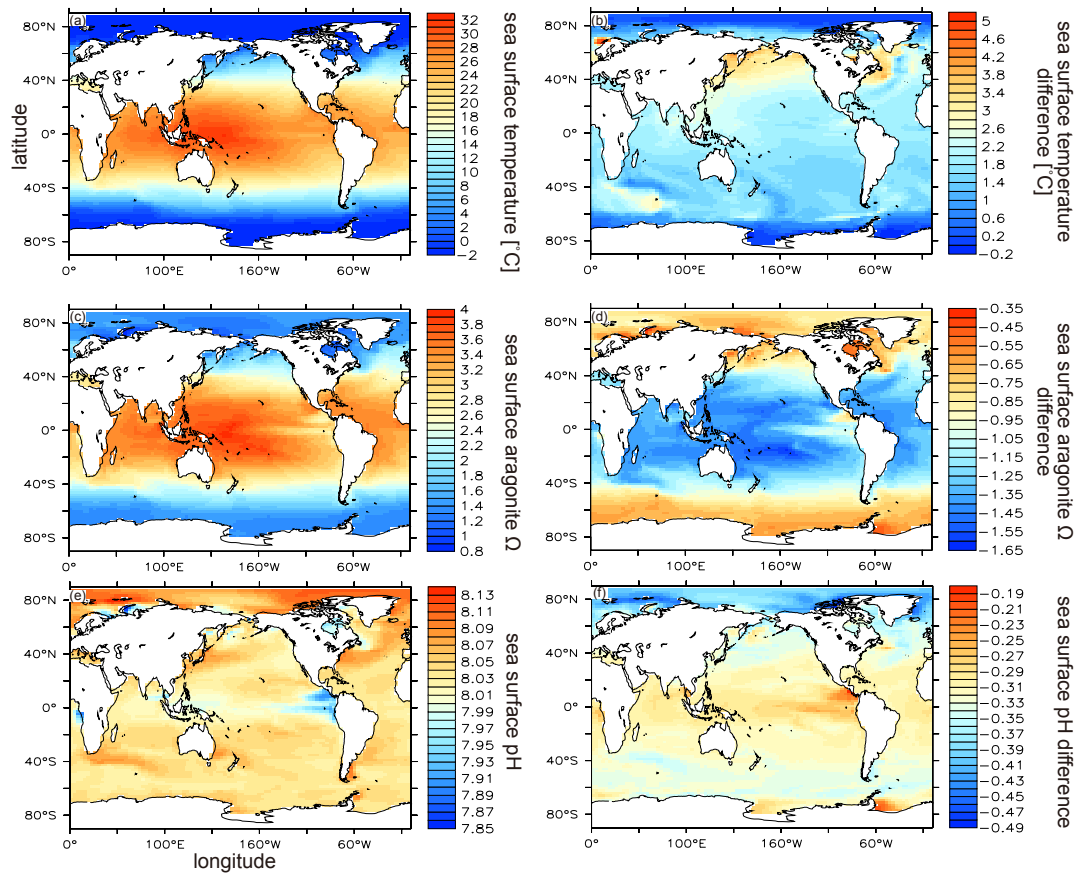
Figure B2. Global distribution in year 2099 for sea surface temperature (a) and its difference referenced to the condition in year 2020 (b); sea surface aragonite Ω (c) and its difference to the condition in year 2020 (d); sea surface pH (e) and its difference to the condition in year 2020 (f)
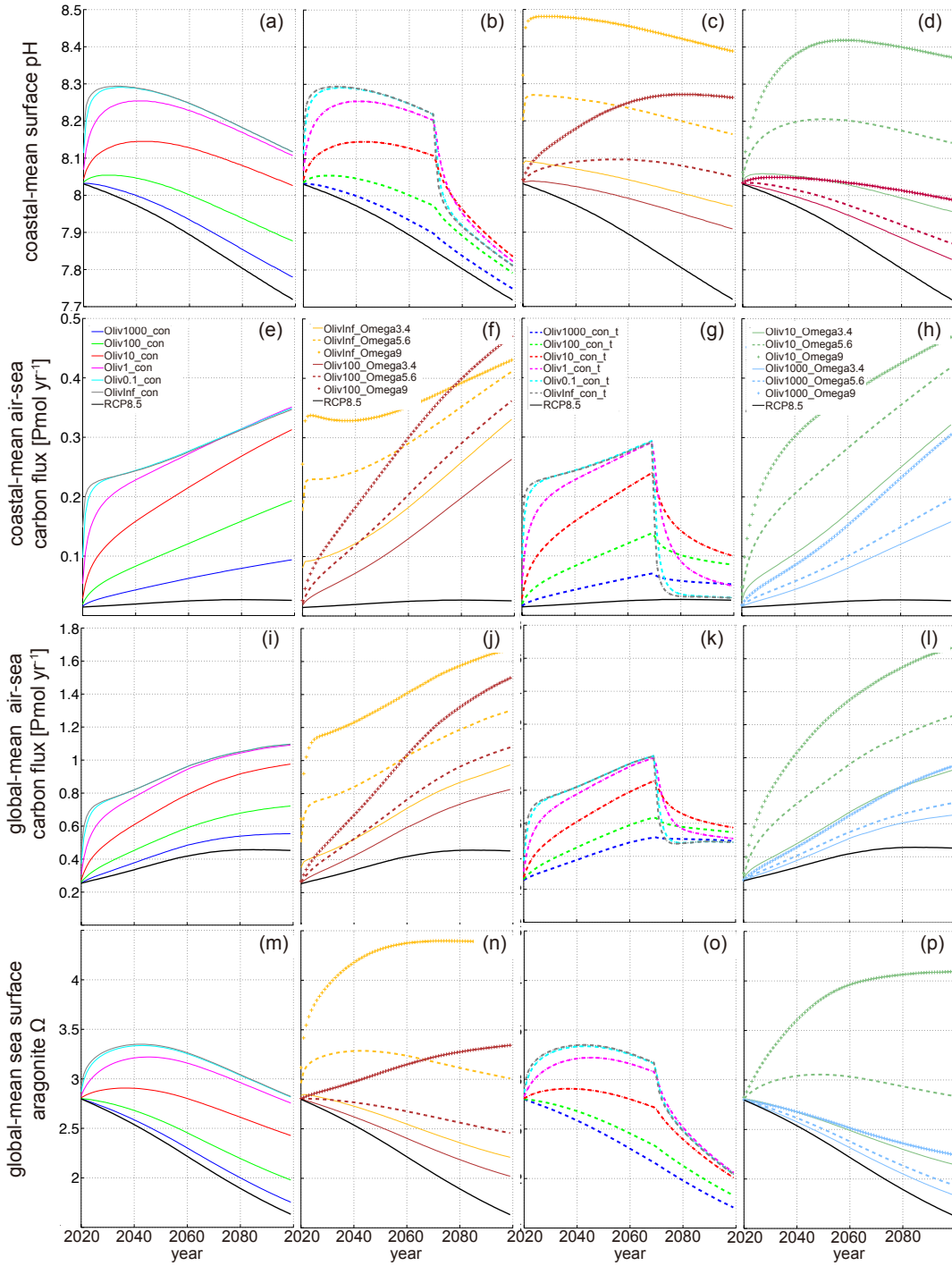
Figure B3. Time series of coastal-mean pH, coastal (global)-mean air-sea carbon flux and global-mean sea surface aragonite Ω are shown in (a)(b)(c)(d), (e)(f)(g)(h), (i)(g)(k)(l) and (m)(n)(o)(p).
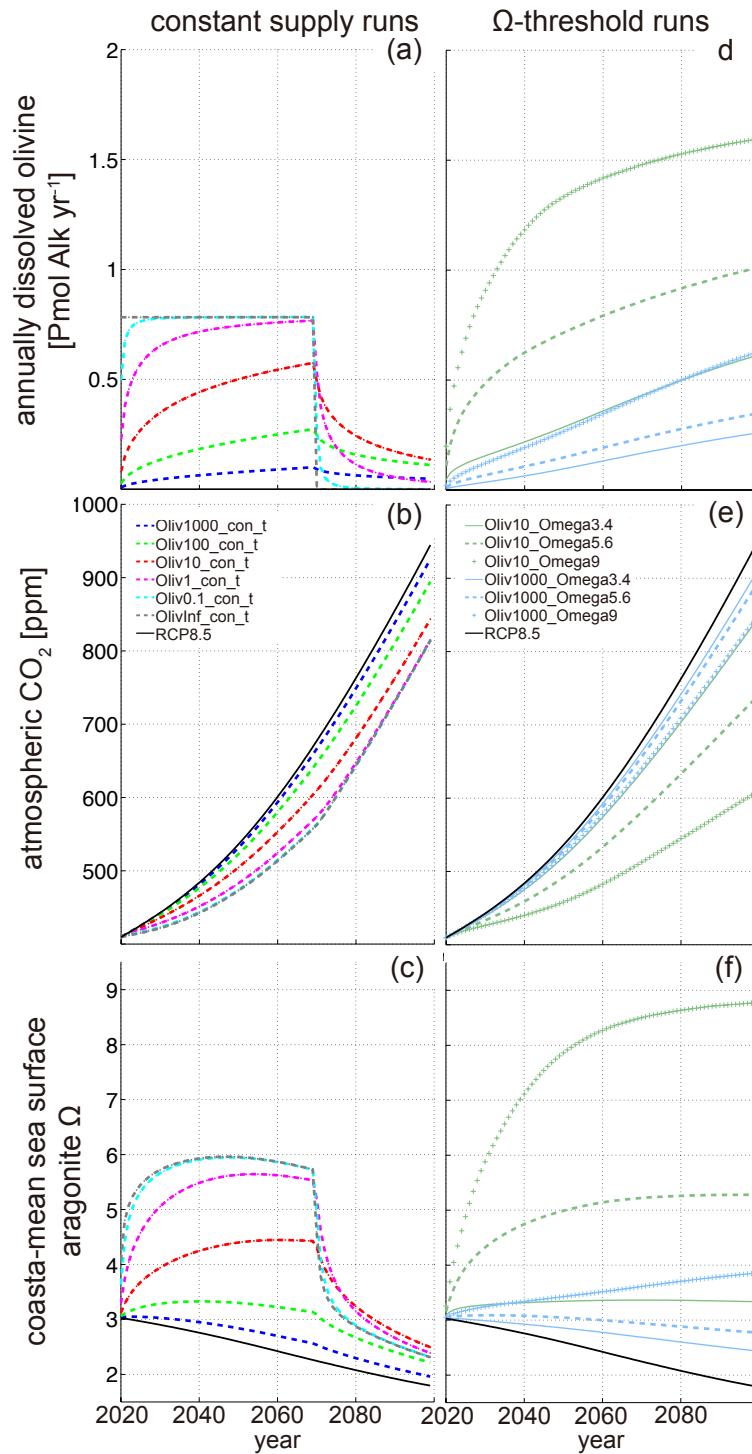
Figure B4. Time series of annually dissolved olivine (a, d), global-mean atmospheric CO_2 concentration (b, e), and coastal-mean sea surface aragonite Ω in COA regions (c, f). Runs from discontinuous constant supply subgroup as well as Ω threshold runs for 10 and 1000 μm olivine grains are shown in the leftside (rightside) column with respective legends. *RCP8.5* is RCP 8.5 scenario control run without COA.

179
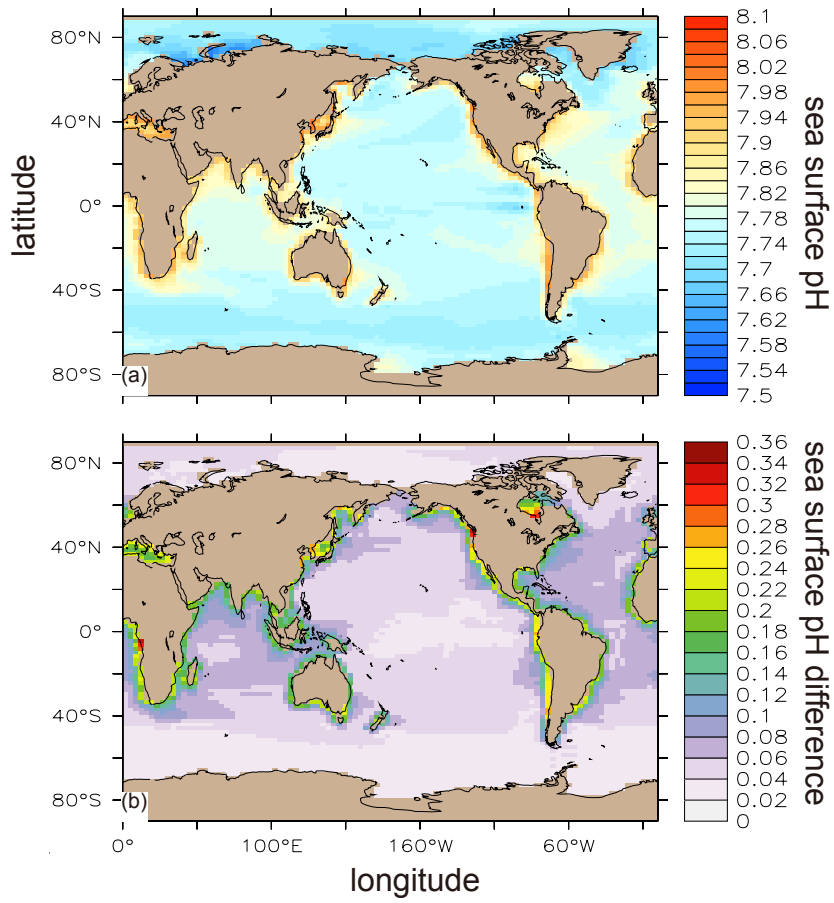
Figure B5. Year 2099 annually averaged sea surface pH (a) and its difference relative to the control run (b).

To study the overshoots in more detail, we carried out two 8-year model runs, with higher temporal resolution output in one grid box (2°N~3°N, 105°E~106°E) (location is marked in Figure B6(a)), following the general model set-up for *Oliv100_Omega3.4* and starting in year 2020. The model results are averaged and written out every 5 days for 8 years. The first run (termed *Oliv100_test0.8*) has the same COA intensity as *Oliv100_Omega3.4* (molar ratio 0.8 to CO_2 emissions), while the other one (termed *Oliv100_test0.6*) with more moderated (molar ratio 0.6 to CO_2 emissions) intensity is set to test whether the amount added plays a role in the overshoot.

During most of the year for both model runs, aragonite Ω in this particular grid box is above the Ω threshold 3.4. However, during a short period in spring in which Ω is below the threshold, olivine is added, causing the annual-mean aragonite Ω to exceed the threshold. In addition, added but undissolved olivine from previous time steps will continue to dissolve regardless whether new olivine is added. Accordingly dissolved olivine is easily exceeding the requested amount to perfectly avoid Ω threshold overshoots. In Figure B6 *Oliv100_test*0.8 run with higher COA engineering intensity has a higher aragonite Ω. Therefore, the "oversized" olivine addition in each time step can increase the annual-mean Ω overshoots. Moreover, the grid box we investigate, is semi-enclosed by landmasses and the water exchange nearby oceanic grid boxes is slow. This characteristic makes these waters with high alkalinity difficult to dilute, and maintains a high aragonite Ω level thereafter.

181
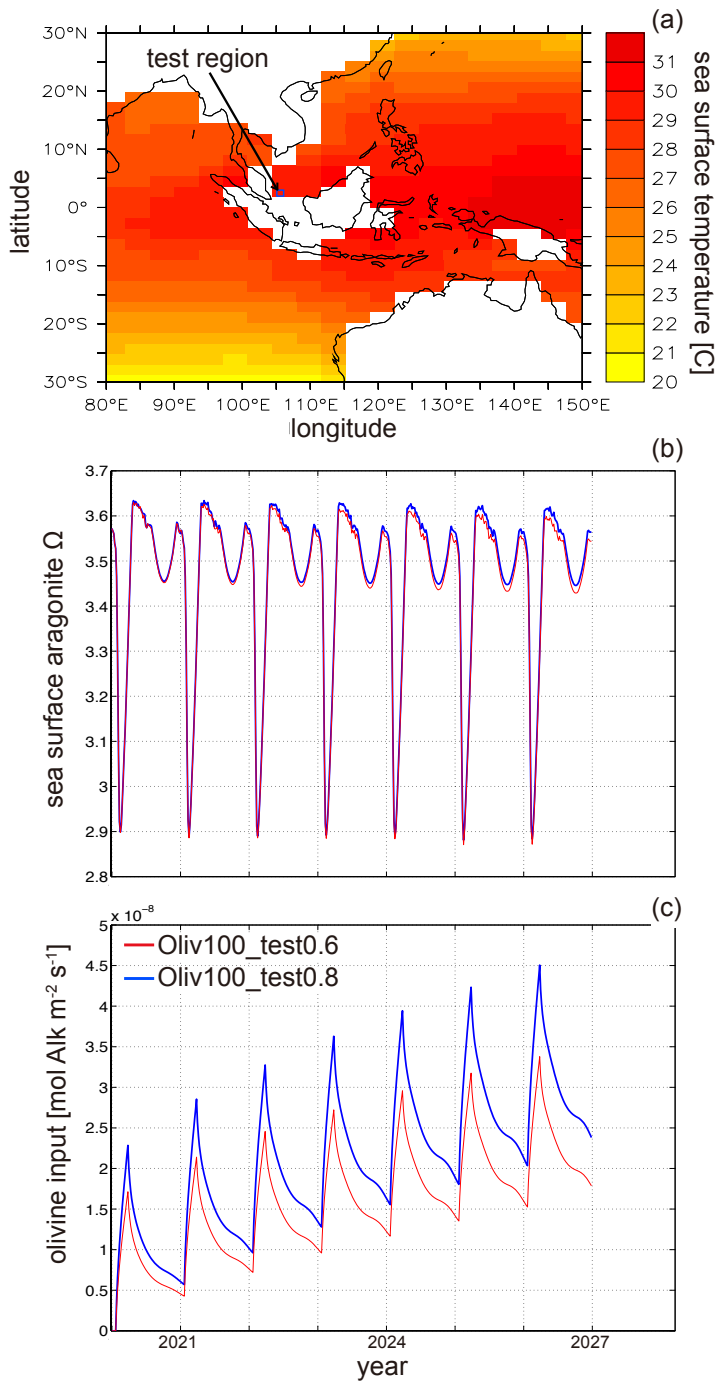
Figure B6. Location for testing COA induced sea surface aragonite Ω overshoot is illustrated (a). Time series of local sea surface aragonite Ω (b) and olivine addition (c) for grid box (2°~3°N, 105°~106°E) from year 2020 to 2028 with output written in every 5 days. For both model runs the local sea surface aragonite Ω threshold is set at 3.4.

To compare large-scale spatial differences in these runs, we divide the ocean into three zonal bands (20°S-60°S, 20°S-20°N, and 20°N-60°N), and calculate the zonally averaged cumulative percentage contribution of olivine dissolution within each band relative to total global olivine dissolution by the end of year 2099 (Figure B7). For runs from "constant supply group", the largest fraction of dissolution (>45%) occurs at low latitudes ("20°S~20°N" band), with a larger fraction for larger grain sizes. This is because olivine dissolves faster in warm low latitude waters (Figure B1). For larger olivine grain sizes, not all olivine dissolves before the end of the model simulation. The fraction that dissolves is, however, larger in warmer tropical waters. This phenomenon also occurs in the "Ω threshold group" runs with the same aragonite Ω thresholds, but different olivine grain sizes (Figure B7). Additionally, in the "Ω threshold group" runs when the aragonite Ω threshold increases from 3.4 to 9, the contribution to global dissolution from low latitudes increases (Figure B7). Coastal grid boxes at low latitude generally have aragonite Ω higher than 3.4 even in year 2099, but very few grid boxes have local aragonite Ω exceeding 5.6, and no grid boxes have aragonite Ω as high as 9 (Figure B2). Therefore, more grid boxes become "available" at low latitude for olivine to be added to as the aragonite Ω threshold increases, which contributes to this higher geographical percentage.
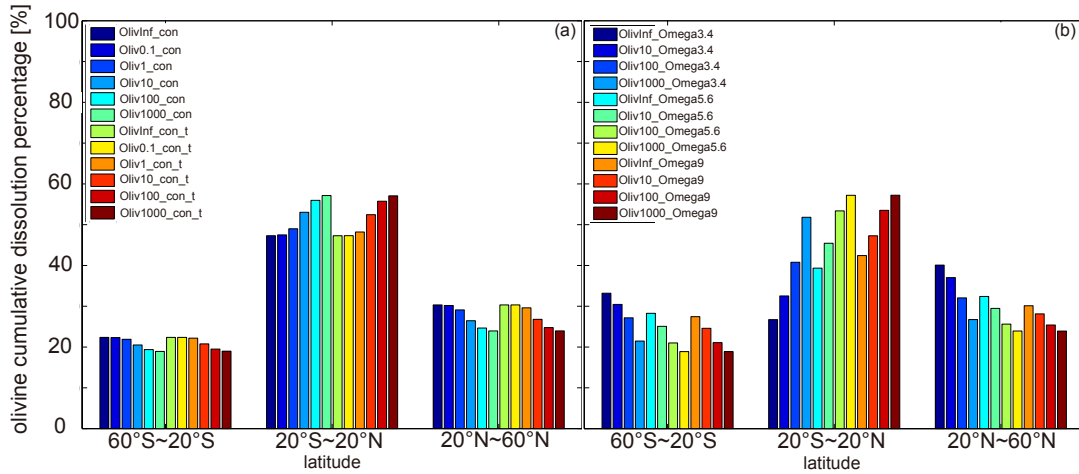
Figure B7. Zonally-averaged cumulative percentage contributions of olivine dissolution within selected bands relative to total global olivine dissolution by the end of year 2099

Appendix C
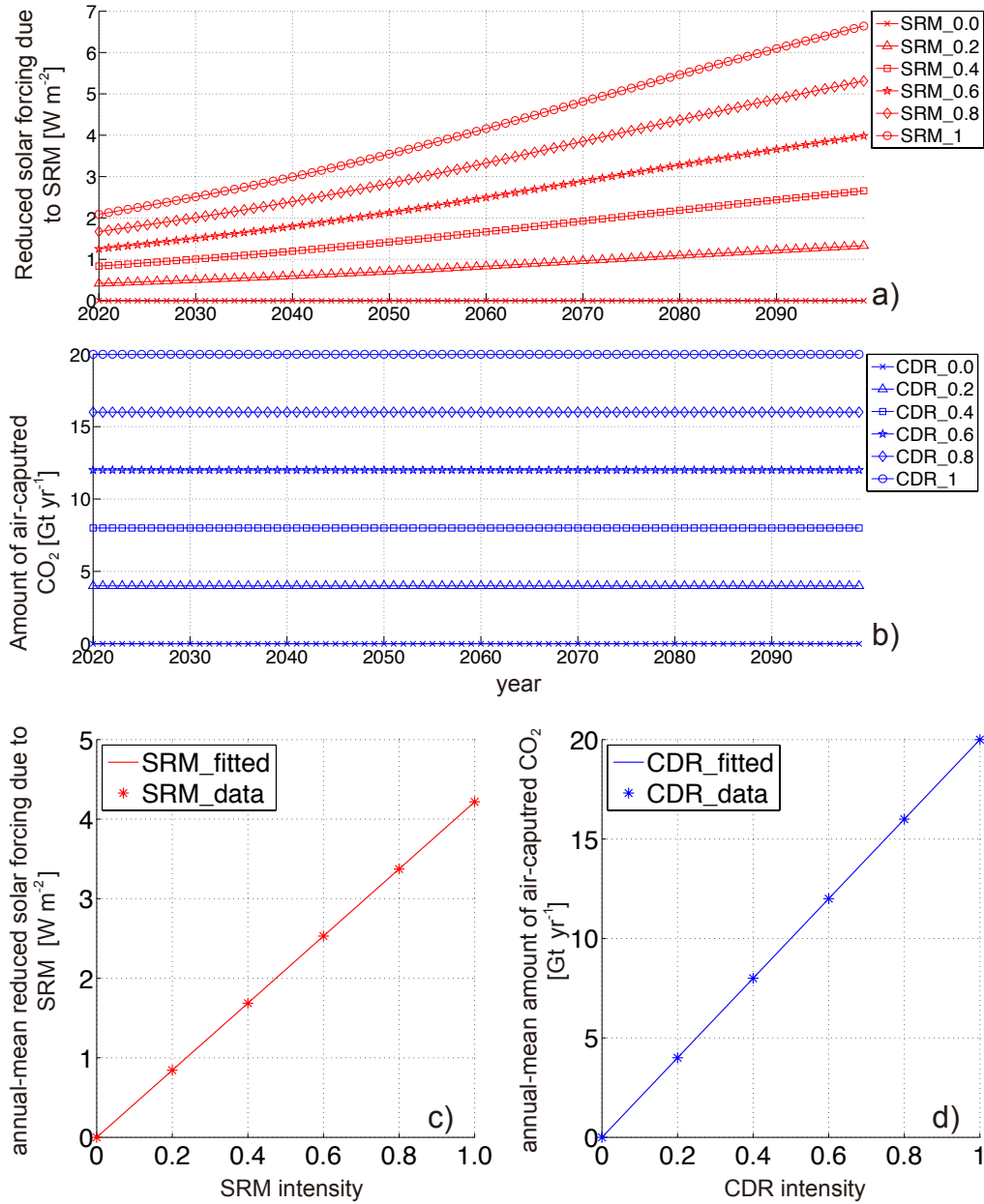
Figure C1. Climate engineering (CE) intensity time series for model experiments shown in Panel (a) and (b). The linear regressions between CE intensity and corresponded annual-mean solar insolation reduction and prescribed CO₂ sequestration shown in Panel (c) and (d).

We took the examples of previous studies (Ross *et al.* 2012, Zickfeld *et al.* 2009) as references and introduced an ensemble of 11 model runs to determine the relationships between outgoing longwave radiation and ECS. We first set "*p*" in each model version with 11 different values ranging from "-0.625 to 2.5". Through this process we've set 11 model runs in parallel with 11 different ECSs. Then we run the 11 models forced by instantaneously doubled atmospheric CO_2 concentration (~560 ppmv) from year 1800 for around 500 years. The global-mean surface atmospheric temperature difference referenced to the preindustrial are plotted for each model run in Figure C2, and the temporal mean values are achieved from year 2200 to 2500 as ECSs. We in following used polynomial fitting tool to get the relationships between ECSs and preset "*p*" values in Figure C3.
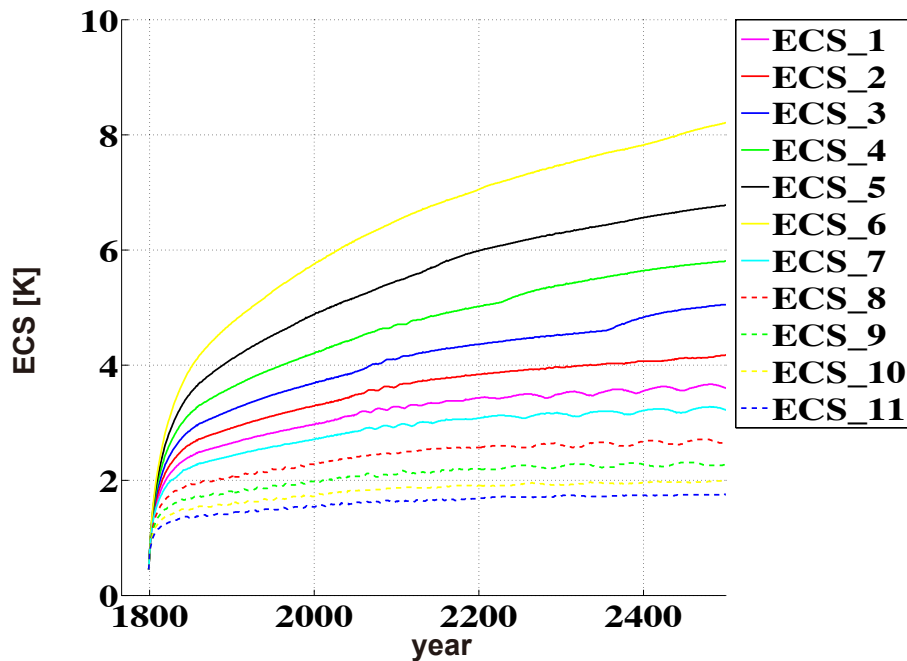
Figure C2. Global-mean surface atmospheric temperature difference to the preindustrial from year 1800 to 2450 from 11 model runs with different "*p*" values.
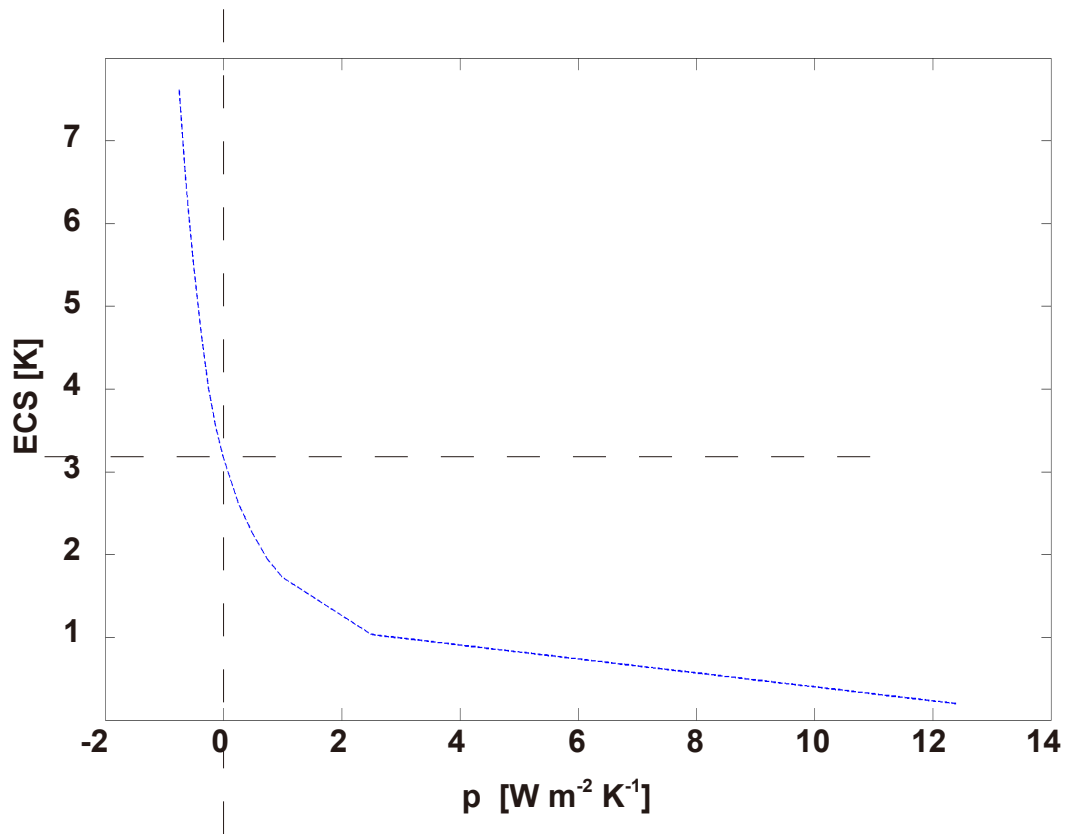
Figure C3. Polynomial fitted relationship between "*p*" values and ECSs. ECS reaches 3.2 K when "*p*" is set 0 W m^{-2} K^{-1}.
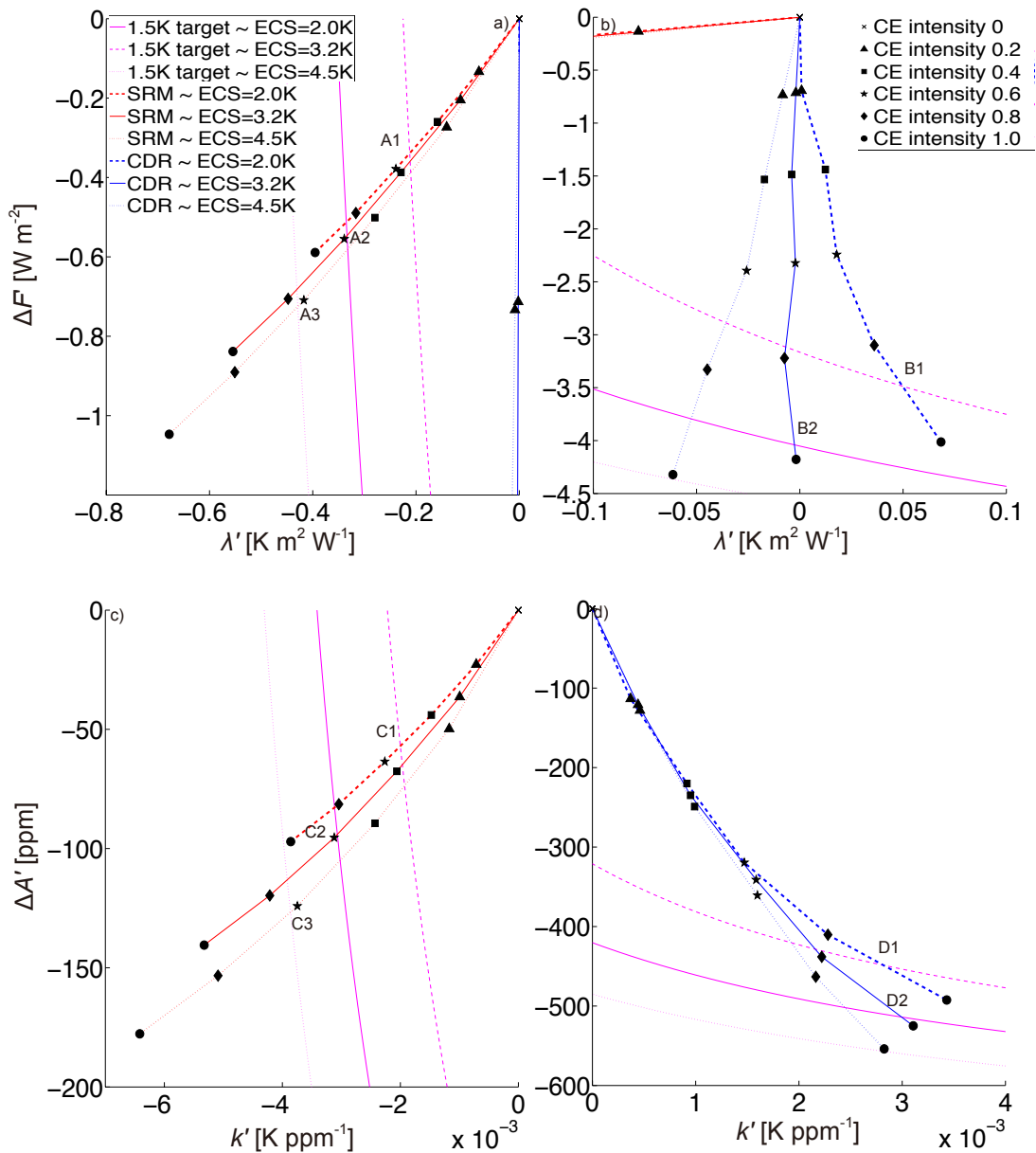
Figure C4. In year 2099, CE perturbation plotted as the CE induced climate sensitivity to CO₂ forcing change anomaly versus the CE induced longwave radiative forcing anomaly (a) and the CE induced climate sensitivity to CO₂ concentration anomaly versus the CE induced atmospheric CO₂ anomaly (b). This is a zoomed-in view of Figure 4-2(a)(b). Global-mean 1.5 °C warming from preindustrial level is highlighted in pink isoclines. Plots with ECS of 2.0, 3.2 and 4.5 K are showed in solid, bold dashed and light dashed curves. Crossing points (e.g. A1, A2, A3, etc.) are marked when CE curves have crossed with the 1.5 °C mitigation target isoclines under the same ECSs.

Appendix D
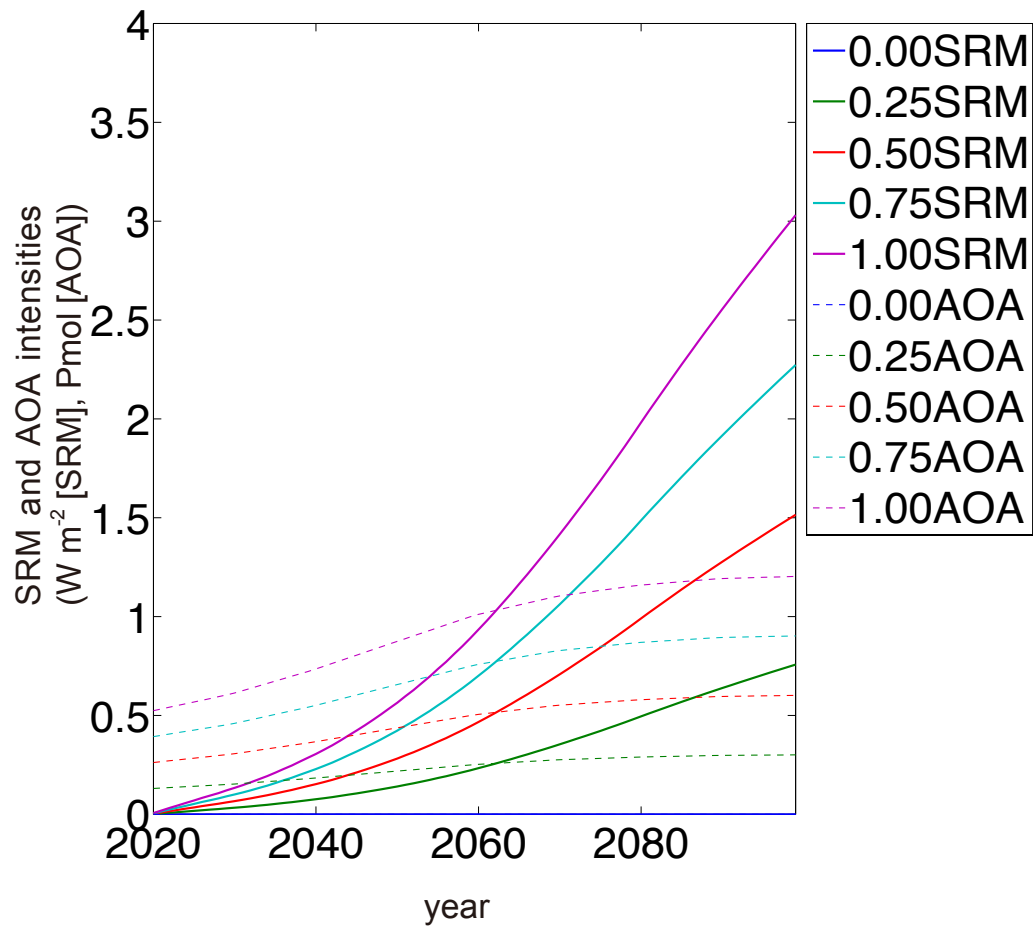
Figuer D1. Time series of SRM and AOA intensities applied in model simulations.
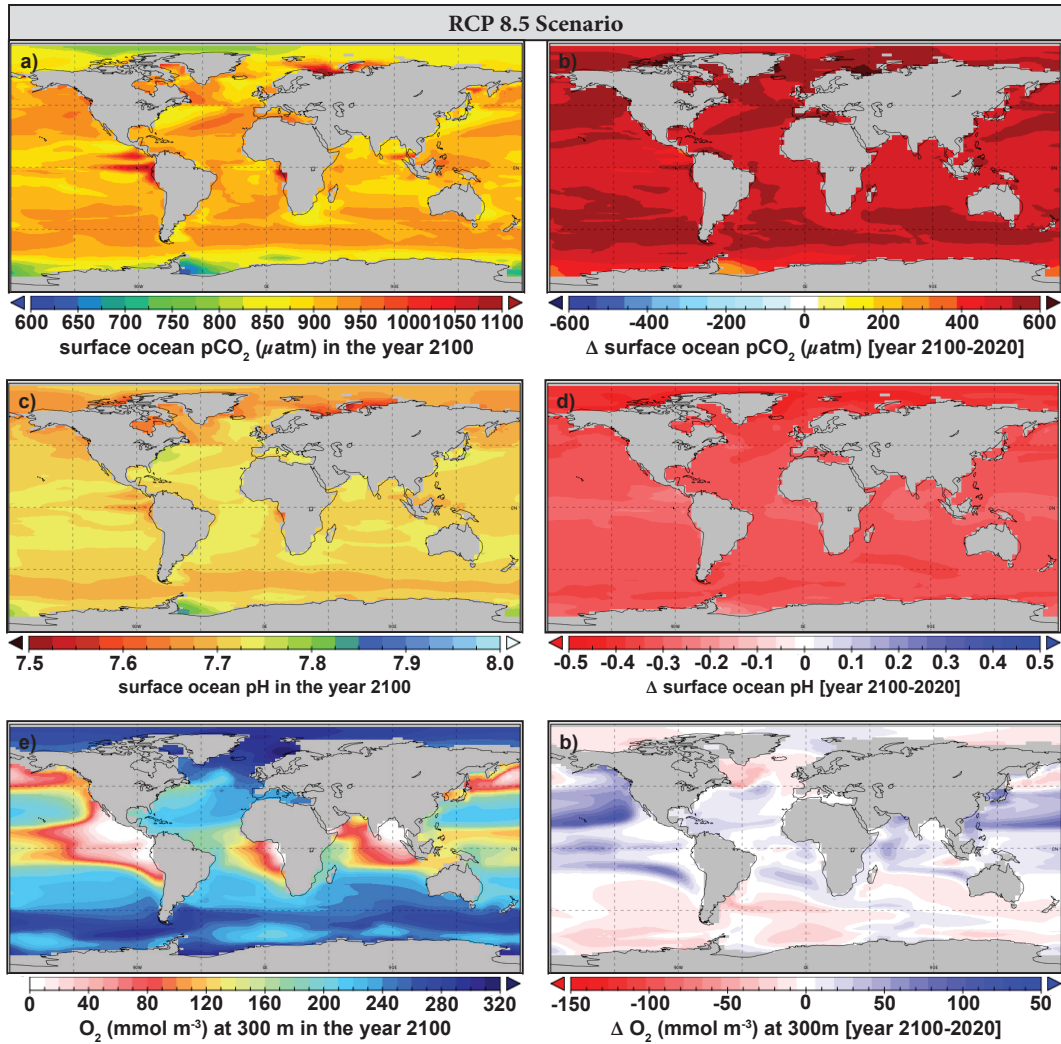
Appendix E
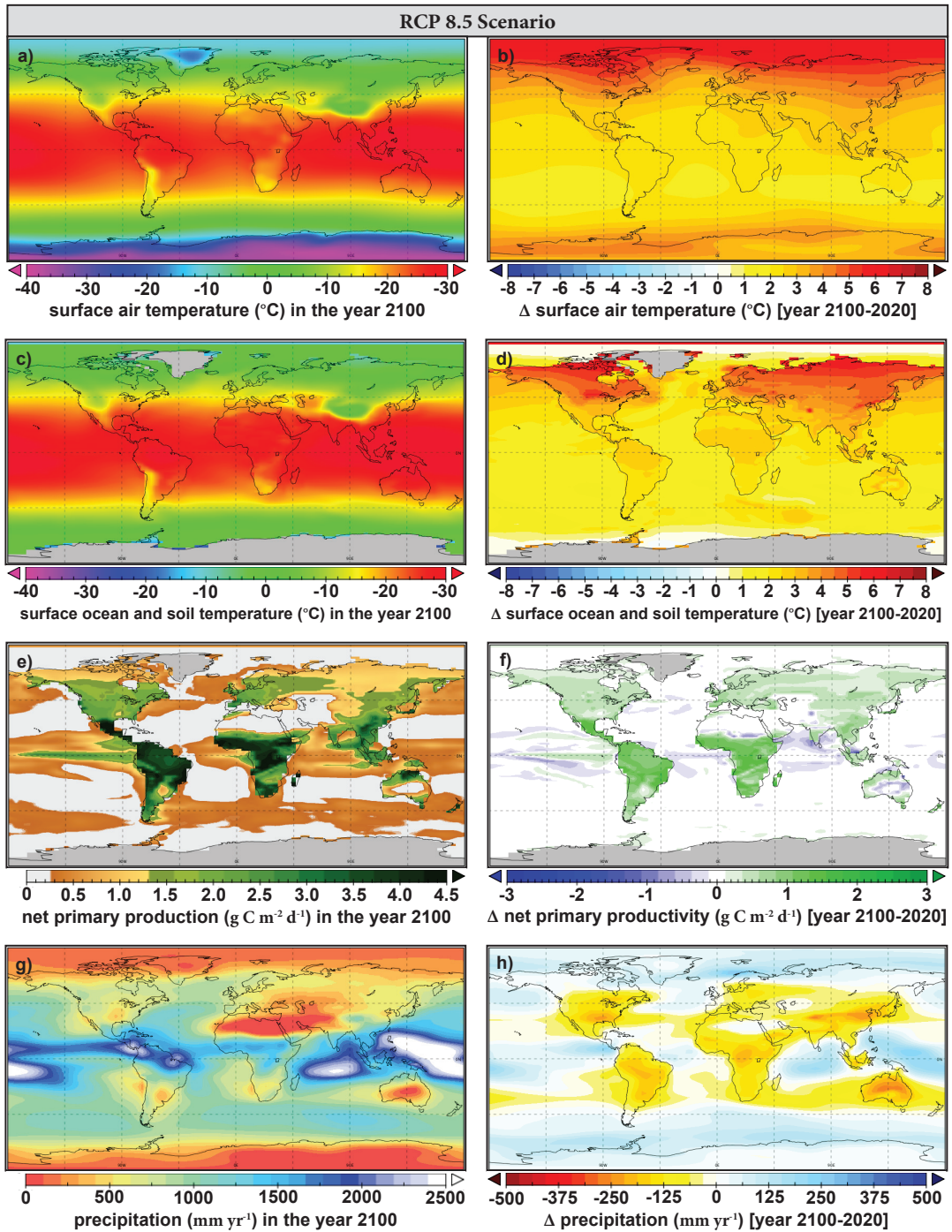
Figure E1. RCP 8.5 control run simulation year 2100 properties and the change from year 2020. The simulated control run (RCP 8.5 scenario) year 2100 mean annual surface air temperature (a), surface ocean and soil temperature (c), marine and terrestrial net primary productivity (e), and precipitation (g) and the change in each property (b, d, f, h) from the year 2020 to 2100.
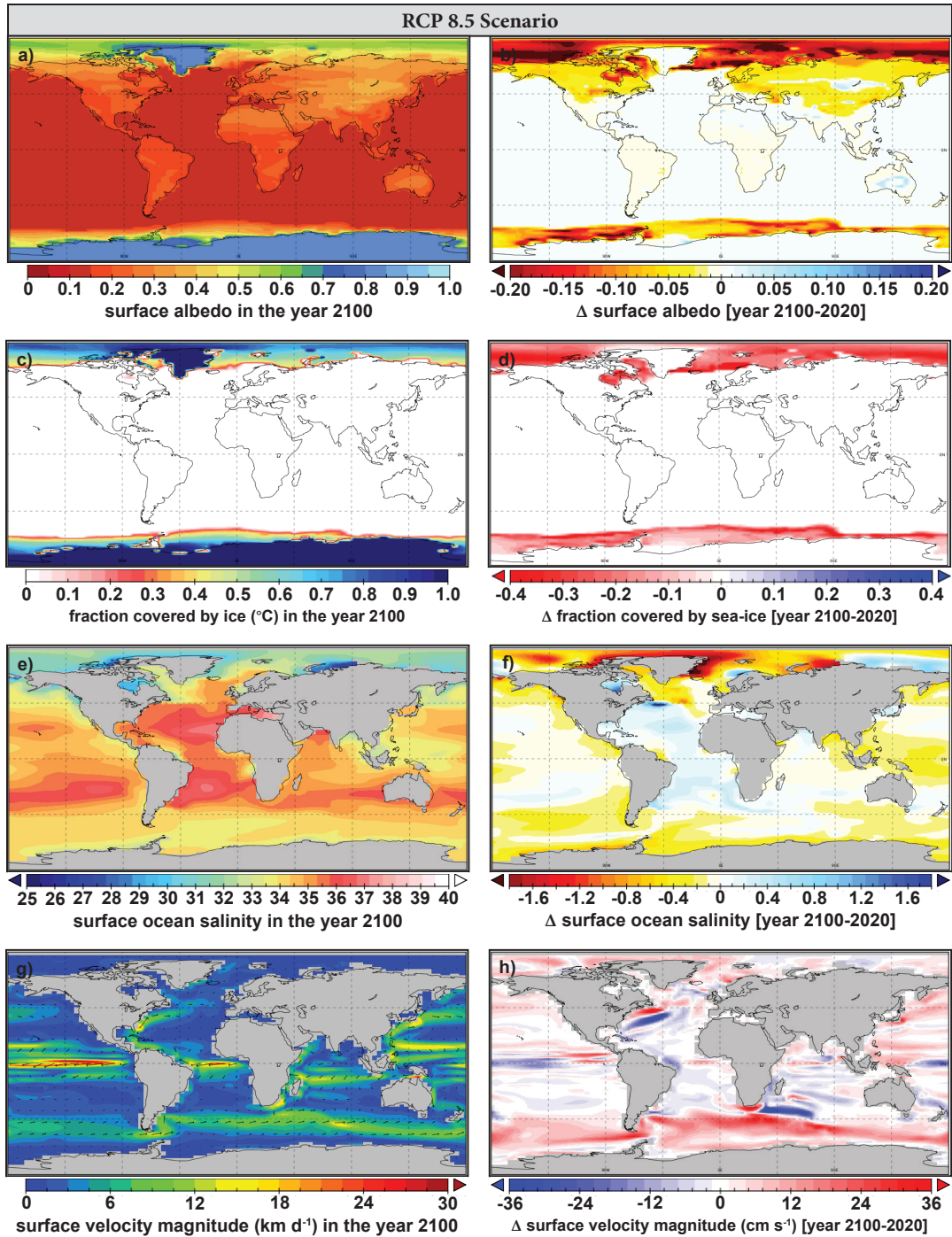
Figure E2. RCP 8.5 control run simulation year 2100 properties and the change from year 2020. The simulated control run (RCP 8.5 scenario) year 2100 mean annual surface albedo (a), fraction of each grid cell covered by sea-ice (c), surface ocean salinity (e), and surface velocity magnitude (g) and the change in each property (b, d, f, h) from the year 2020 to 2100.

Figure E3. RCP 8.5 control run simulation year 2100 properties and the change from year 2020. The simulated control run (RCP 8.5 scenario) year 2100 mean annual surface ocean pCO₂ (a), surface ocean pH (c), and sub-surface ocean oxygen (e) and the change in each property (b, d, f) from the year 2020 to 2100.
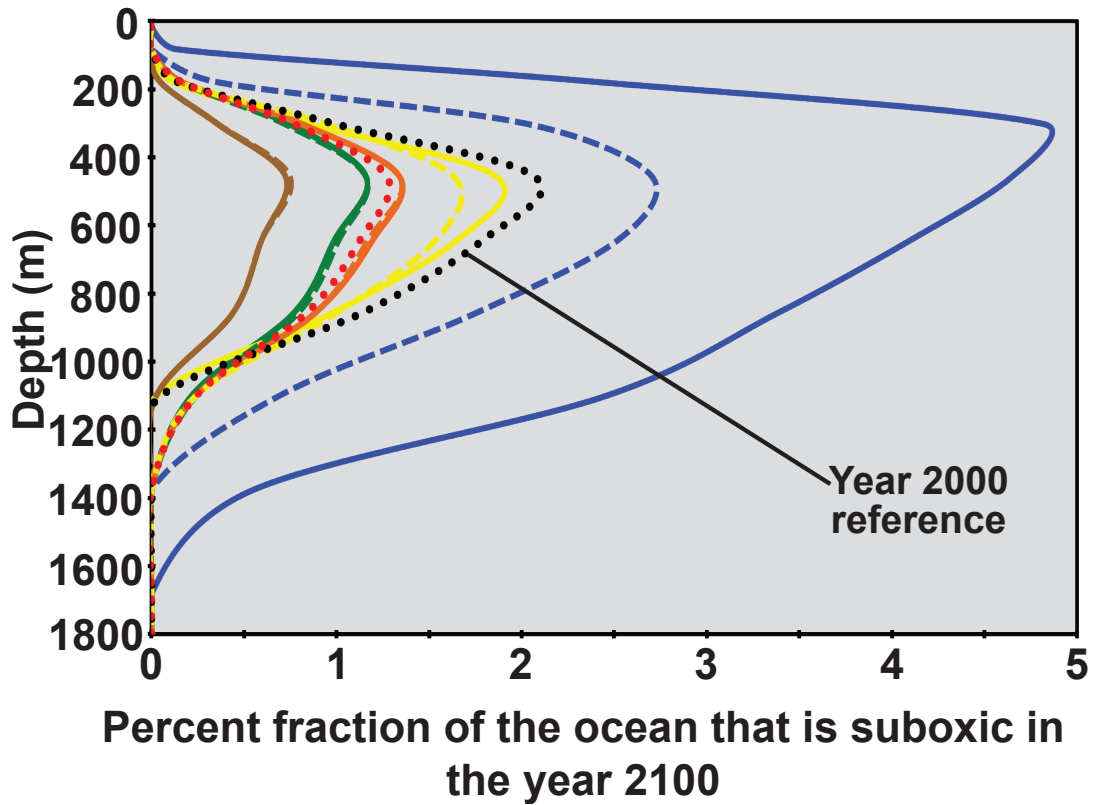
Figure E4. Comparison of simulated ocean suboxic volumes. Simulated percent fraction of the ocean that is suboxic in the year 2100 for model runs where climate engineering is continuously deployed (solid lines) and runs where it was discontinued after 50 years (dashed lines). The control run, with no climate engineering, is also shown.
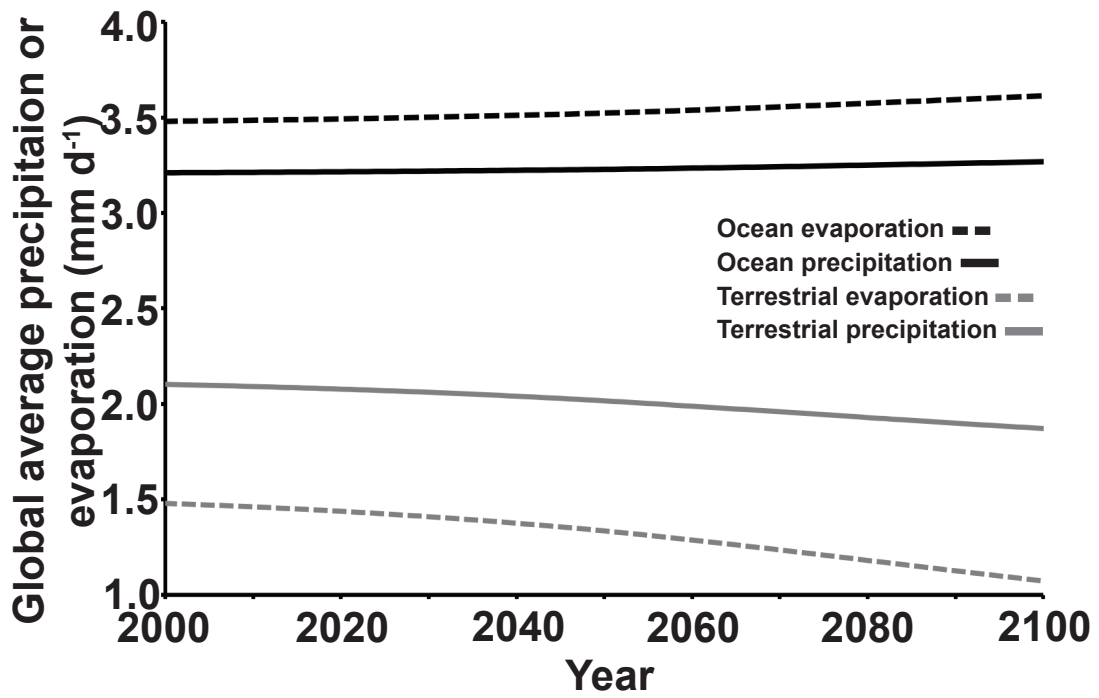
Figure E5. Mean annual evaporation and precipitation in the RCP 8.5 control run. Simulated global annual-mean evaporation and precipitation over the ocean and land during the RCP 8.5 control model run.
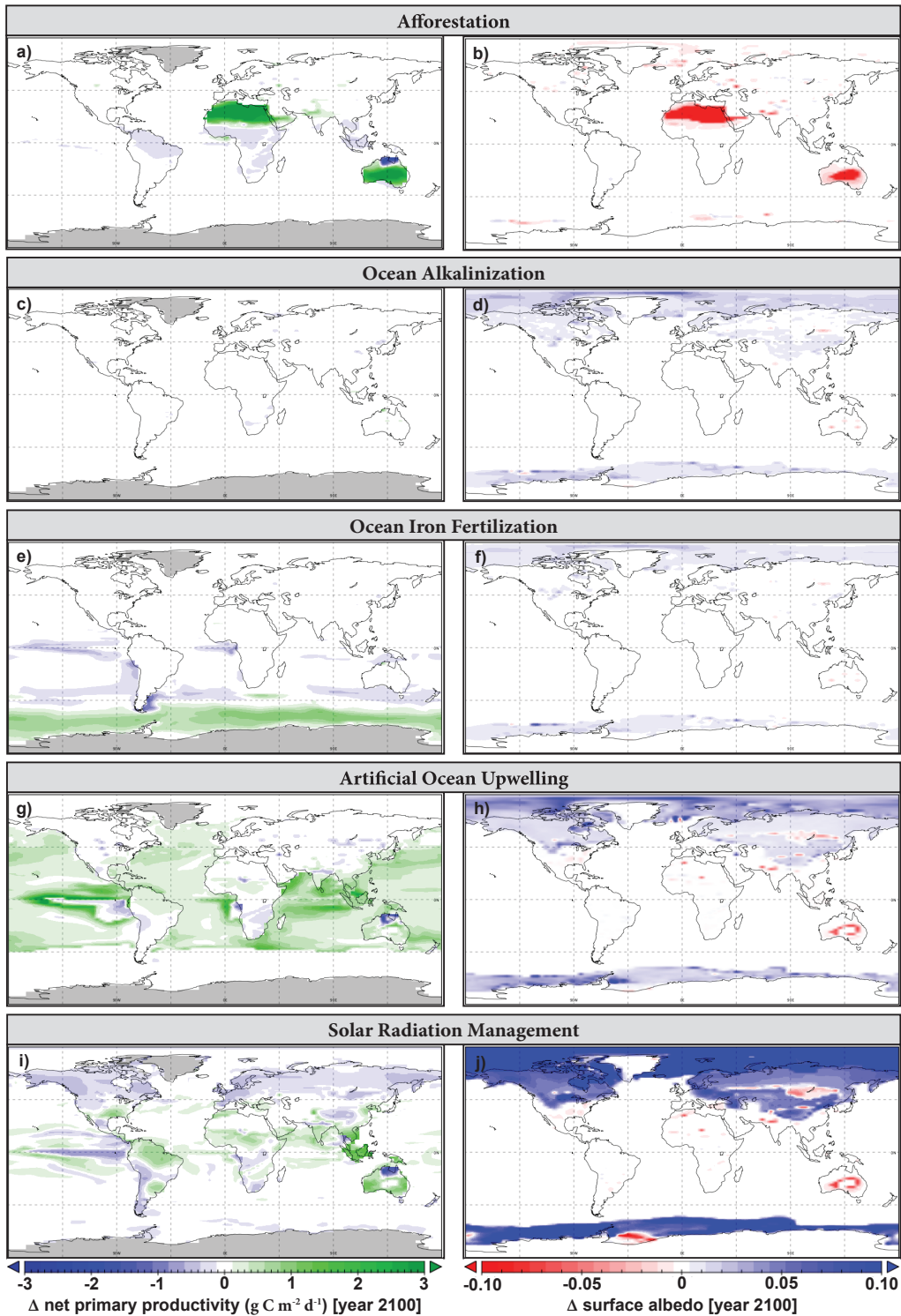
Figure E6. Climate engineering method effects on primary productivity and albedo.
The simulated year 2100 mean annual differences between the climate engineering
runs and the control run (climate engineering run minus the control run) for
marine and terrestrial primary productivity (a, c, e, g, i) and the land and ocean
surface albedo (b, d, f, h, j).

195
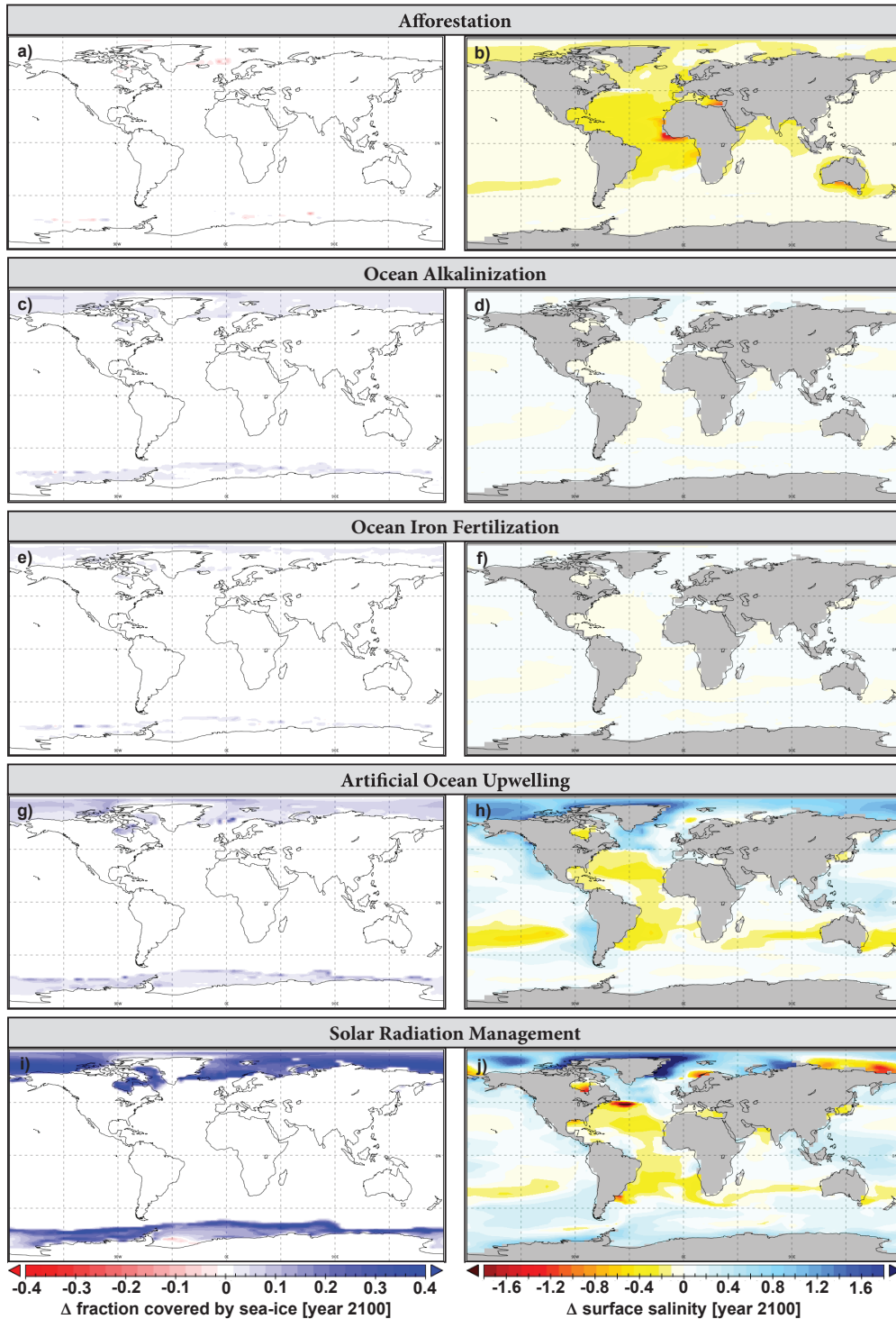
Figure E7. Climate engineering method effects on sea-ice coverage and surface ocean salinity. The simulated year 2100 mean annual differences between the climate engineering runs and the control run (climate engineering run minus the control run) for the fraction of each grid cell covered by sea-ice (a, c, e, g, i) and surface ocean salinity (b, d, f, h, j).
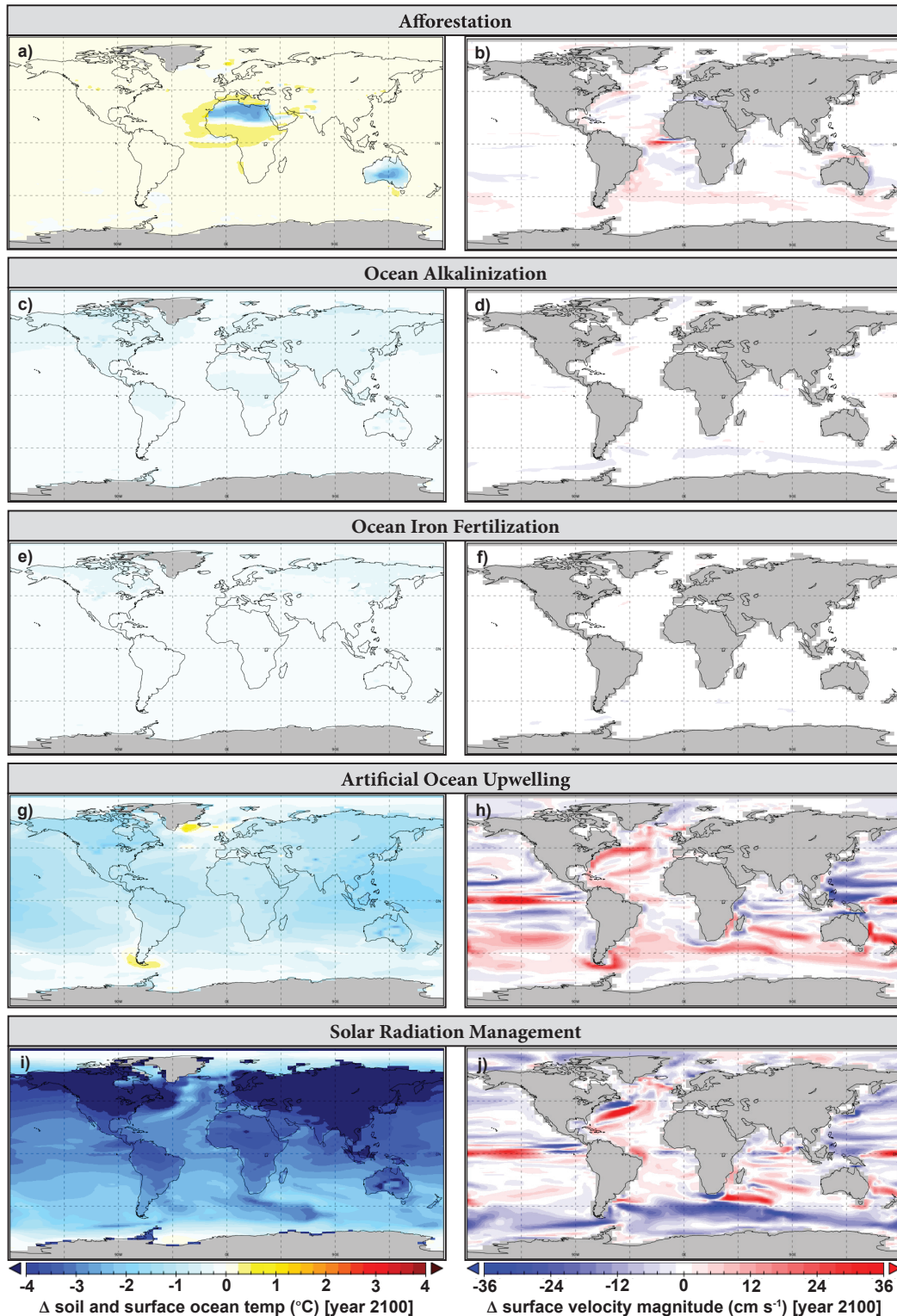
Figure E8. Climate engineering method effects on surface skin temperature and ocean surface current velocities. The simulated year 2100 mean annual differences between the climate engineering runs and the control run (climate engineering run minus the control run) for surface ocean and soil temperatures (left panels) and the magnitude of surface ocean velocity (right panels).
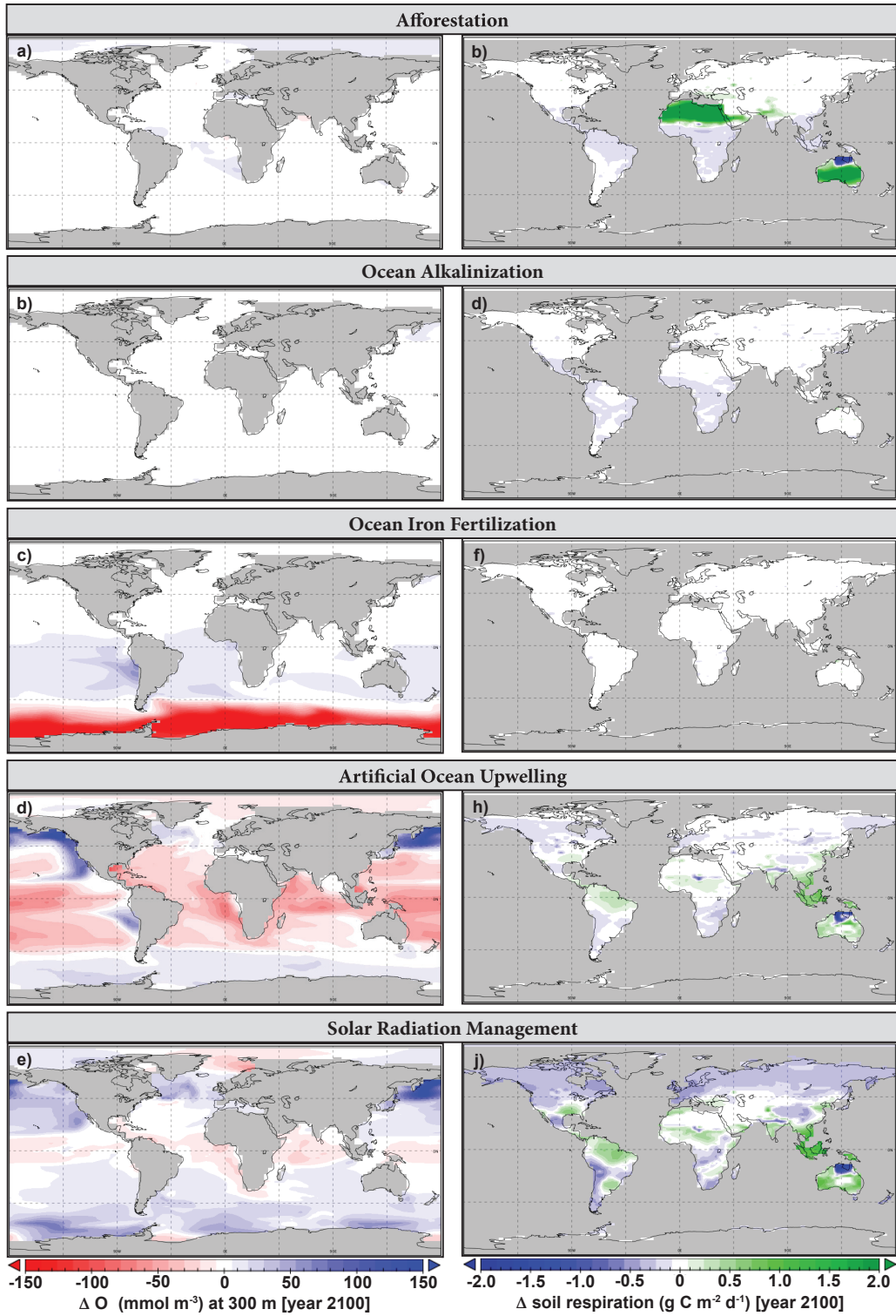
197

Figure E9. Climate engineering method effects on sub-surface ocean oxygen and soil respiration. The simulated year 2100 mean annual differences between the climate engineering runs and the control run (climate engineering run minus the control run) for sub-surface ocean oxygen (a, c, e, g, i) and soil respiration (b, d, f, h, j).
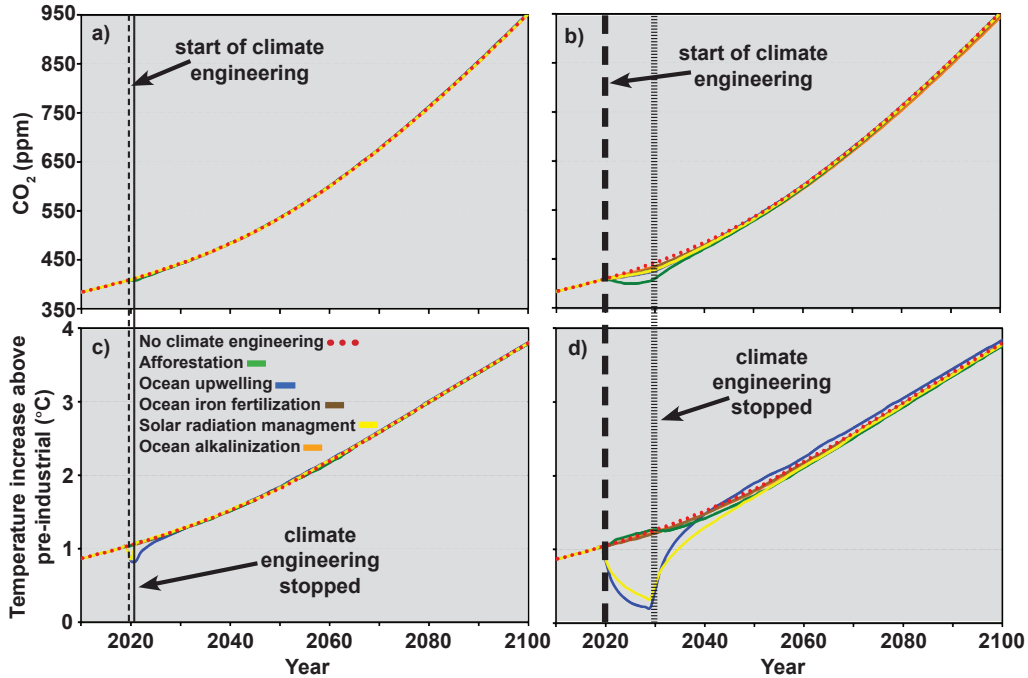
Figure E10. Comparison of climate engineering method effects on temperature and CO₂. Simulated changes in globally averaged annual atmospheric CO₂ and surface air temperature (relative to a pre-industrial temperature of 13.05° C) for limited duration (1 and 10 year) climate engineering simulations. The control run, with no climate engineering, is also shown.
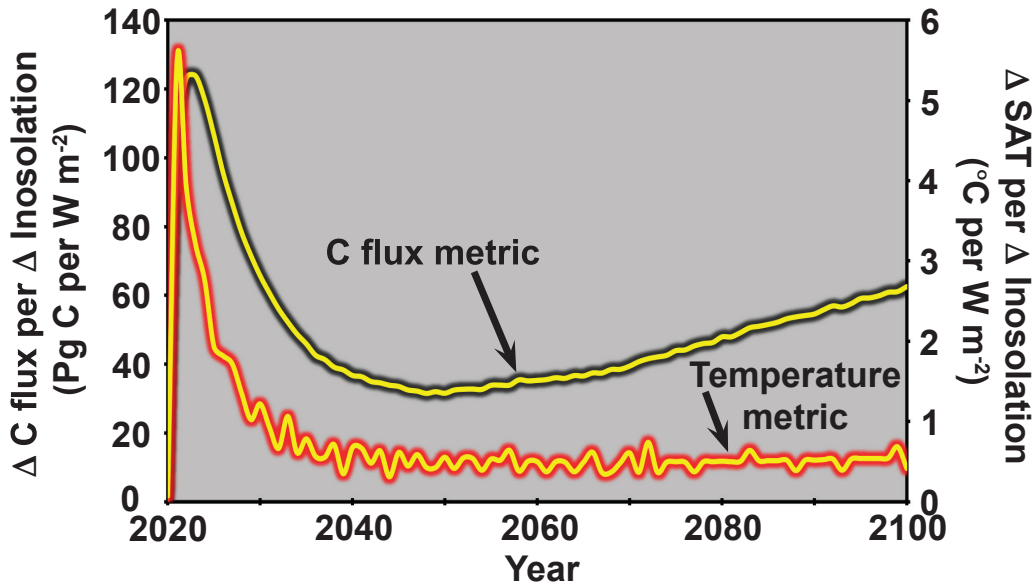

Figure E11. Simulated solar radiation management efficacy. Simulated solar radiation management (SRM) annual change in the flux of carbon from the atmosphere to the ocean or land per change in insolation and the rate of surface air temperature change (reduction) per change in insolation.
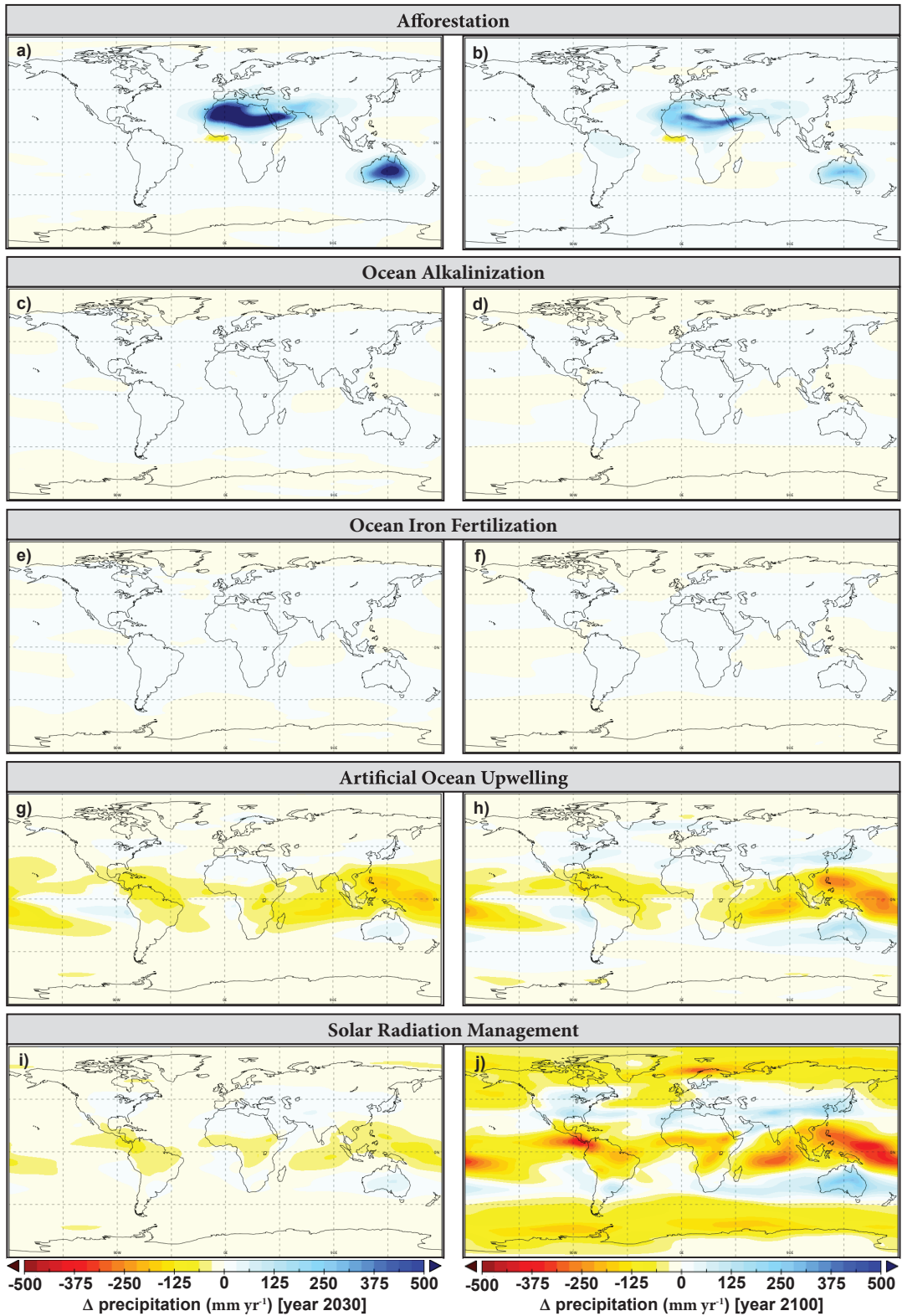
Figure E12. Climate engineering method effects on precipitation. The simulated year 2030 (a, c, e, g, i) and 2100 (b, d, f, h, j) mean annual differences between the climate engineering runs and the control run (climate engineering run minus the control run) for precipitation.
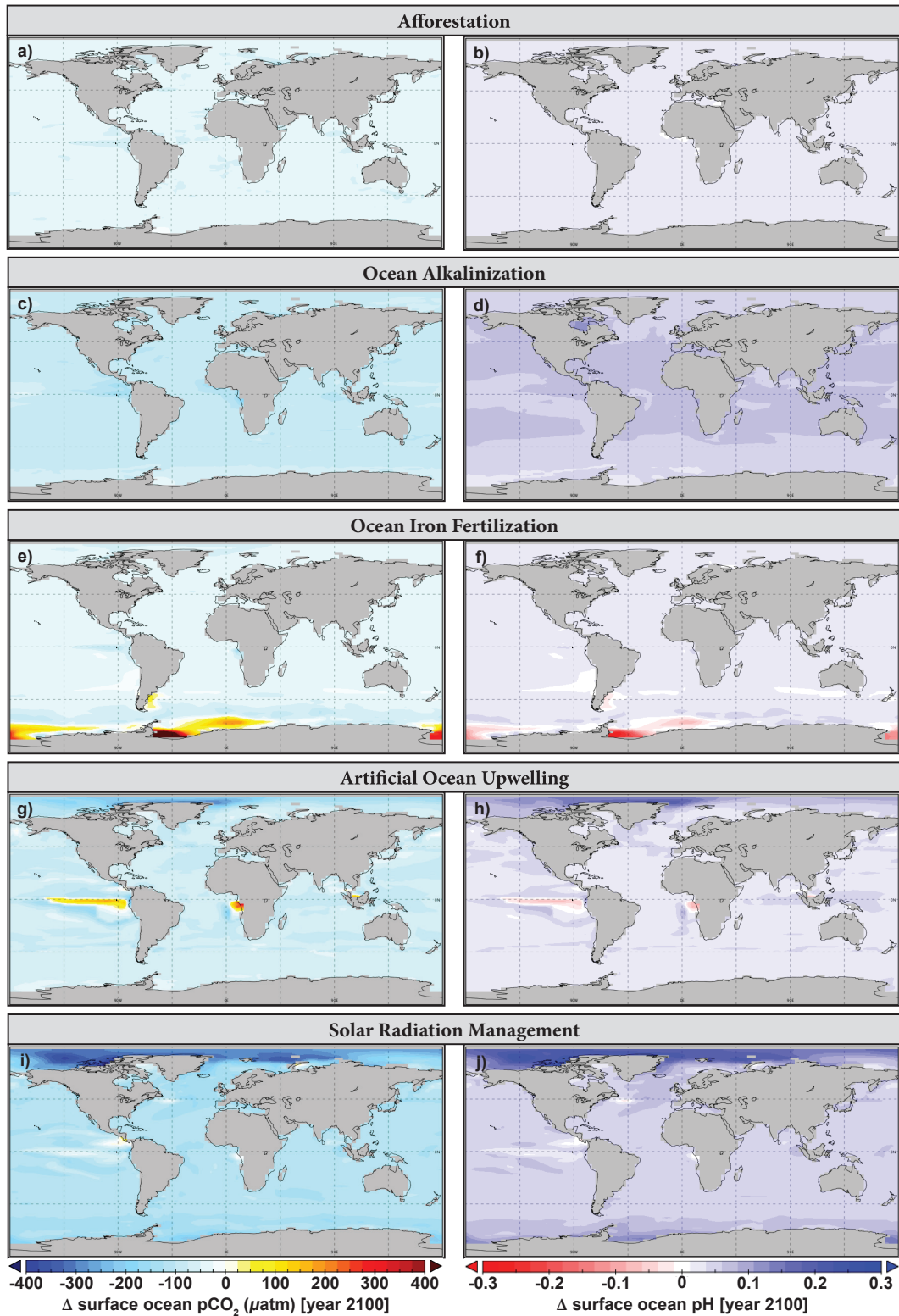
Figure E13. Climate engineering method effects on surface ocean pCO₂ and pH.
The simulated year 2100 mean annual differences between the climate engineering
runs and the control run (climate engineering run minus the control run) for
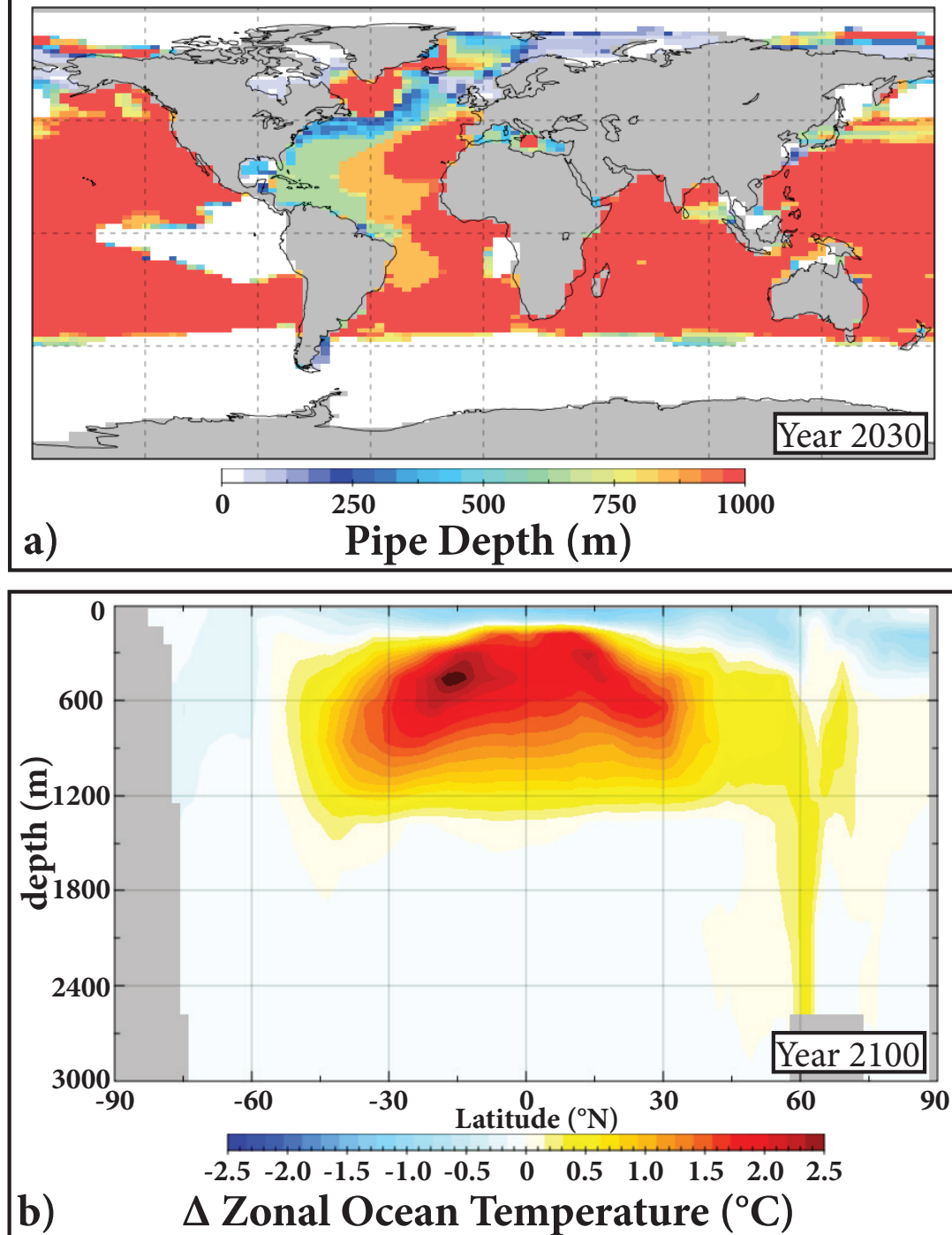**surface ocean pCO₂ (a, c, e, g, i) and pH (b, d, f, h, j).**

Figure E14. Simulated artificial ocean upwelling pipe placement and the effects on ocean temperature. Simulated artificial ocean upwelling pipe locations and depths (a) and the simulated year 2100 mean annual zonal ocean temperature difference (b) between the climate engineering run and the control run (climate engineering run minus the control run).
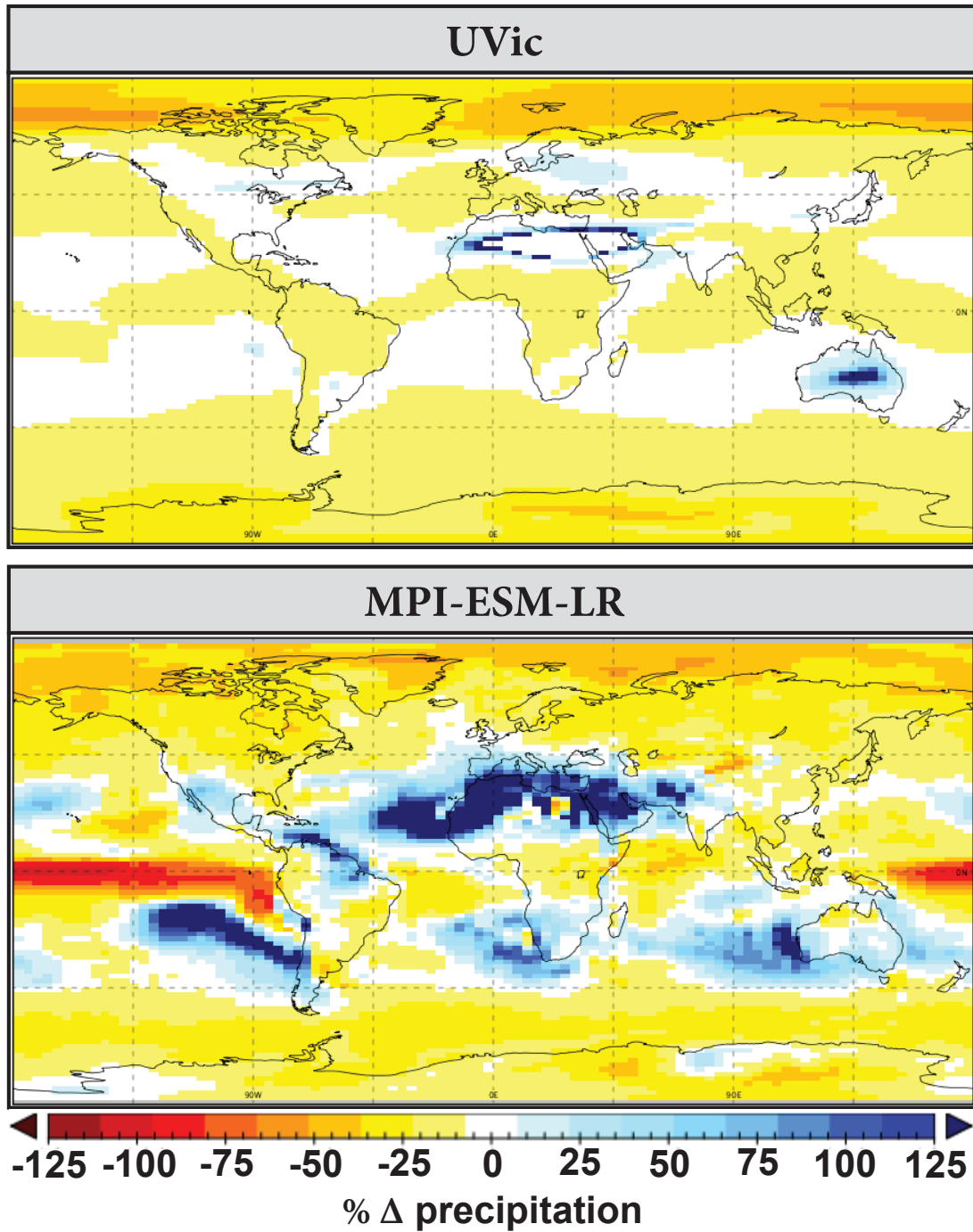
UVic

MPI-ESM-LR

% Δ precipitation

Figure E15. Comparison of the change in precipitation with the UVic and MPI-ESM-LR models during GeoMIP G1 simulations. GeoMIP G1 experiment simulated percent changes in precipitation ((G1_SRM_run –Control_run)/ Control_run), averaged over years 40-50 of the simulations. This experiment (G1_SRM_run) is conducted by instantaneously quadrupling the CO_2 concentration (from pre-industrial levels) while simultaneously reducing the solar constant to counteract this forcing (50 year simulation). The Control_run here for both the UVic and the MPI-ESM-LR simulations is an abrupt 4 x CO_2 run (from pre-industrial levels) with no SRM.
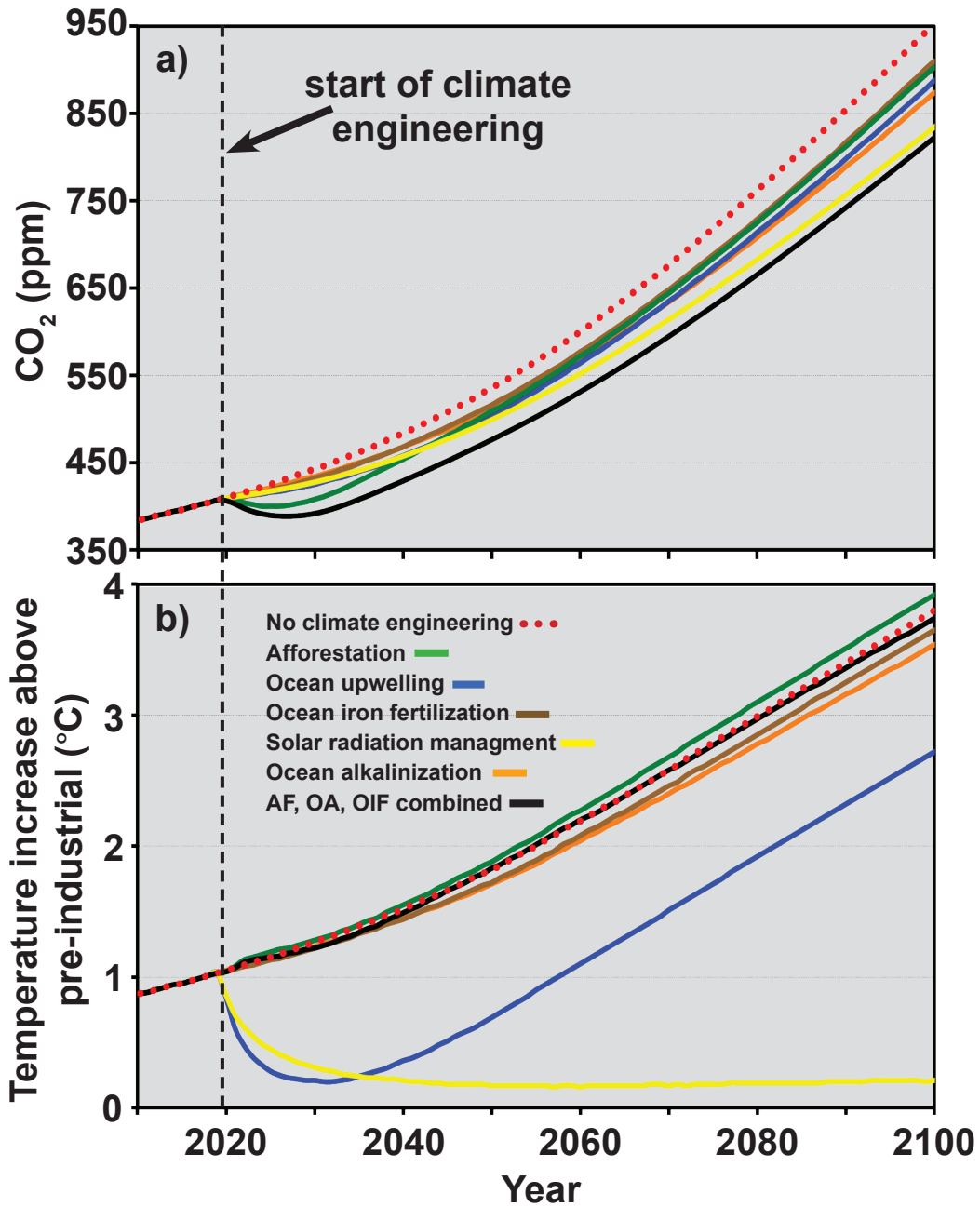
Figure E16. Comparison of climate engineering method effects on temperature and CO₂. Simulated changes in globally averaged annual atmospheric CO₂ and surface air temperature (relative to a pre-industrial temperature of 13.05° C) for the climate engineering simulations. The control run, with no climate engineering, is also shown.

Afforestation

Irrigated Region

Supplementary Figure 17 | Simulated irrigated region for the afforestation method.
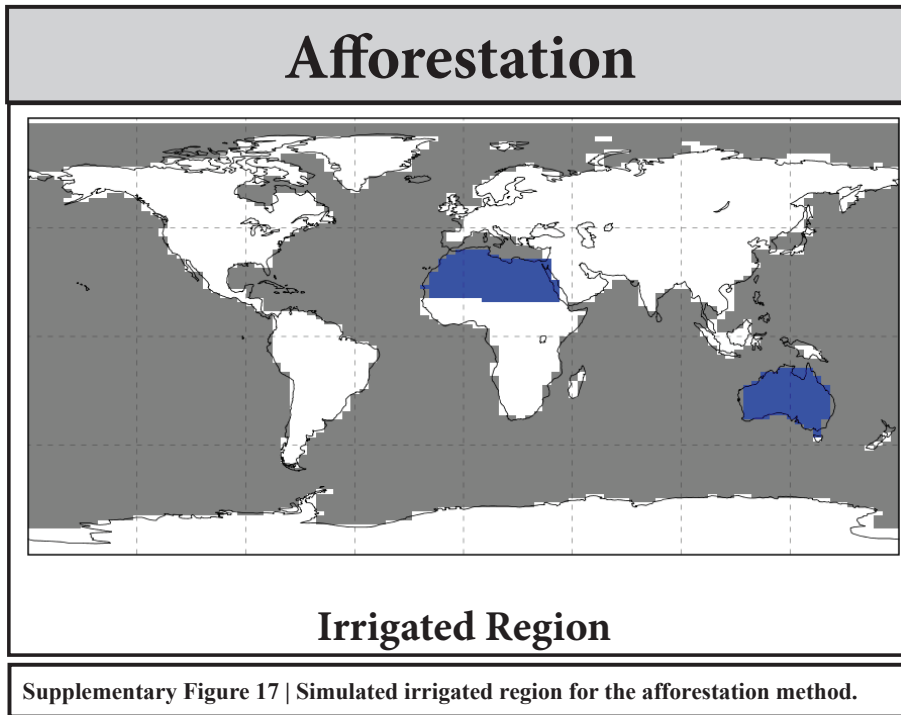
Figure E17. Simulated irrigated region for the afforestation method

Ocean Alkalinization

Year 2100

-160 -80 0 80 160

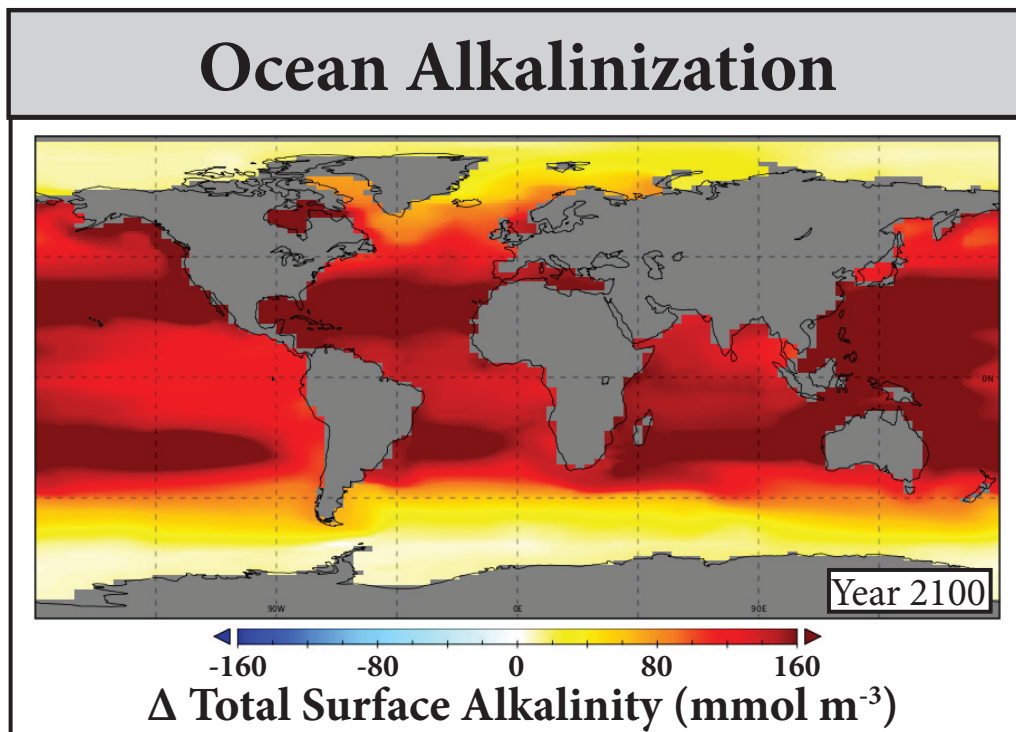**Δ Total Surface Alkalinity (mmol m^{-3})**

Figure E18. The effects of simulated ocean alkalinization on surface ocean alkalinity. The simulated year 2100 difference between the ocean alkalinization run and the control run for total surface ocean alkalinity.

References

Ahlström A, Schurgers G, Arneth A and Smith B 2012 Robustness and uncertainty in terrestrial ecosystem carbon response to CMIP5 climate change projections. *Environ. Res. Lett.* 7 044008

Allan R P *et al.* 2014 Physically consistent responses of the global atmospheric hydrological cycle in models and bbservations *Surveys in Geophysics* 35 533-52

Allen J T *et al.* 2005 Diatom carbon export enhanced by silicate upwelling in the northeast Atlantic *Nature* 437 728-32

Alterskjær K, Kristjánsson J E and Seland O 2012 Sensitivity to deliberate sea salt seeding of marine clouds - observations and model simulations *Atmos. Chem. Phys.* 12 2795–807

Aronson R B, Precht W F, Toscano M A and Koltes K H 2002 The 1998 bleaching event and its aftermath on a coral reef in Belize *Mar. Biol.* 141 435–47

Aumont O and Bopp L 2006 Globalizing results from ocean in situ iron fertilization studies *Global Biogeochem. Cycles* 20 GB2017

Bakker D C E *et al.* 2014 An update to the surface ocean CO2 atlas (SOCAT version 2) *Earth Syst. Sci. Data* 6 69–90

Bala G, Caldeira K and Duffy P B 2003 Geoengineering Earth's radiation balance to mitigate climate change from a quadrupling of CO2 *Glob. Planet. Change* 37 157–68

Bala G *et al.* 2007 Combined climate and carbon-cycle effects of large-scale deforestation. *Proc. Natl. Acad. Sci. U. S. A.* 104, 6550-55,

Bala G, Duffy P B and Taylor K E 2008 Impact of geoengineering schemes on the global hydrological cycle. *Proc. Natl. Acad. Sci. U. S. A.* 105, 7664-9,

Baldwin M, Kirooka T, O'Neill A and Yoden S 2003 Major stratospheric warming in the southern hemisphere in 2002: dynamical aspects of the ozone hole split 20 24–6

Barrett S 2008 The incredible economics of geoengineering *Environ. Resour. Econ.* 39 45–54

Bates N R 2007 Interannual variability of the oceanic CO2 sink in the subtropical gyre of the North Atlantic Ocean over the last 2 decades *J. Geophys. Res.* 112 C09013

Bathiany S *et al.* 2010 Combined biogeophysical and biogeochemical effects of large-scale forest cover changes in the MPI earth system model. *Biogeosciences* 7:1383–1399

Bernier P Y *et al.* 2011 Boreal lichen woodlands: a possible negative feedback to climate change in eastern North America. *Agric. for. Meteorol.* 151:521–528

Betts R A *et al.* 2007 Projected increase in continental runoff due to plant responses to increasing carbon dioxide *Nature* 448, 1037-1041

Betts R A 2000 Offset of the potential carbon sink from boreal forestation by decreases in surface albedo *Nature* 409, 187-190

Berner R A 1975 The role of magnesium in the crystal growth of calcite and aragonite from sea water *Geochim. Cosmochim. Acta* 39

Bide T P, Styles M T and Naden J 2014 An assessment of global resources of rocks as suitable raw minterals for carbon capture and storage by mineralization *Applied Earth Sci* 123 179-95

Birch F 2013 Density and composition of the upper mantle: first approximation as an olivine layer *the Earth's crust and upper mantle* (American Geophysical Union) pp 18–36

Bischoff J L 1968 Kinetics of calcite nucleation: magnesium ion inhibition and ionic strength catalysis *J. Geophys. Res.* 73 3315–22

Bitz C M and Liscomb W H 1999 An energy-conserving thermodynamic model of sea ice *J. Geophys. Res.* 104 15669

Blain S *et al.* 2007 Effect of natural iron fertilization on carbon sequestration in the Southern Ocean. *Nature* 446 1070–4

Blok K, Turkenburg W C, Hendriks C A and Steinberg M 1992 Proceedings of the first international conference on carbon doxide removal *energy convers. Manag.* 5-8 283–826

Boyd P W 2008 Ranking geo-engineering schemes. *Nature Geoscience* 1, 722 - 724, doi:10.1038/ngeo348

Boyd P W *et al.* 2007 Mesoscale iron enrichment experiments 1993-2005: Synthesis and Future Directions *Science* 315, 612-7

Boyd P W, Arrigo K R, Strzepek R, and van Dijken G L 2012 Mapping phytoplankton iron utilization: Insights into Southern Ocean supply mechanisms *J. Geophys. Res.* 117 C06009

Boysen L R *et al.* 2014 Global and regional effects of land-use change on climate in 21st century simulations with interactive carbon cycle *Earth Syst Dyn* 5 309–319

Brander L M, Rehdanz K, Tol R S J and Van P J H 2009 Working Paper No . 282 The economic impact of ocean acidification on coral reefs

Broecker W S and Takahashi T 1966 Calcium carbonate precipitation on the Bahama Banks *J. Geophys. Res.* 71 1575

Brovkin V *et al.* 2009 Geoengineering climate by stratospheric sulfur injections: Earth system vulnerability to technological failure. *Climatic Change* 92 243 – 259

Caldeira K and Wood L 2008 Global and Arctic climate engineering: numerical model studies. *Philos. Trans. R. Soc. A Math. Phys. Eng. Sci.* 366 4039–56

Caldeira K and Rau G H 2000 Acceleratibecause carbonate dissolution to sequester carbon dioxide in the ocea: geochemical implications *Geophys. Res. Lett.* 27 225-8.

Caldeira K and Wickett M E 2003 Anthropogenic carbon and ocean pH *Nature* 425 365

Caldeira K 2013 Coral Bleaching: Coral "refugia" amid heating seas *Nat. Clim. Chang.* 3 444–5

Cao L and Caldeira K 2008 Atmospheric CO2 stabilization and ocean acidification *Geophys. Res. Lett.* 35 L19609

Cao L and Caldeira K 2010 Atmospheric carbon dioxide removal : long-term consequences and commitment 024011

Cao L, Gao C C and Zhao L Y 2015 Geoengineering: basic science and ongoing research efforts in China *Adv. Clim. Chang. Res.* 6 188–96

Comeau S, Carpenter R C and Edmunds P J 2012 Coral reef calcifiers buffer their response to ocean acidification using both bicarbonate and carbonate *Proc. Biol. Sci.* 280:20122374

Collins M, Soon-Il A, Cai W, Ganachaud A, Guilyardi E, Fei-Fei J, Jochum M, Lengaigne M, Power S, Timmermann A, Vecchi G, Wittenberg A 2010 The impact of global warming on the tropical pacific ocean and El Nino *Nature Geosci* 3:391-7

Couce E, Ridgwell A and Hendy E J 2013 Future habitat suitability for coral reef ecosystem under global warming and ocean acidification *Glob. Change Biol* gcb12335

Cox P M, Betts R A, Jones C D, Spall S A and Totterdell I J 2000 Acceleration of global warming due to carbon-cycle feedbacks in a coupled climate model. *Nature* 408 184–7

Cripps G, Widdicombe S, Spicer J I and Findlay H S 2013 Biological impacts of enhanced alkalinity in Carcinus maenas. *Mar. Pollut. Bull.* 71 190–8

Cooper T F, De'Ath G, Fabricius K E, and Lough J M 2008 Declining coral calcification in massivePorties in two nearshore regions of the northern Great Barrier Reef *Glob. Change Biol* 14, 529-38

Crook E D, Potts D, Rebolledo-Vieyra M, Hernandez L and Paytan a. 2011 Calcifying coral abundance near low-pH springs: implications for future ocean acidification *Coral Reefs* 31 239–45

Crutzen P J 2006 Albedo Enhancement by Stratospheric Sulfur Injections: A Contribution to Resolve a Policy Dilemma? *Clim. Change* 77 211–20

Curry C L *et al.* 2014 A multi-model examination of climate extremes in an idealized geoengineering experiment *J. Geophys. Res. Atmos.* 119 3900–23

De'ath G, Fabricius K E, Sweatman H and Puotinen M The 27-year decline of coral cover on the Great Barrier Reef and its causes *Proc. Natl. Acad. Sci. U. S. A.* 109, 44 17995-9

de Boer H J, Lammertsma E I, Wagner-Cremer F, Dilcher D L, Wassen M J and Dekker S C 2011 Climate forcing due to optimization of maximal leaf conductance in subtropical vegetation under rising CO2 *Proc. Natl. Acad. Sci. U. S. A.* 108 4041–6

Dekker, S. C. *et al.* 2010 Biogeophysical feedbacks trigger shifts in the modelled vegetation-atmosphere system at multiple scales *Biogeosciences* 7, 1237-1245

De Rooij J F, Heughebaert J C and Nancollas G H 1984 A pH study of calcium phosphate seeded precipitation *J. Colloid Interface Sci.* 100 350

Dirmeyer P A, Jin Y, Singh B and Yan X 2013 Trends in land-atmosphere interactions from CMIP5 simulations *J. Hydrometeorol.* 14 829-849

Donner S D 2009 Coping with commitment: projected thermal stress on coral reefs under different future scenarios. *PLoS One* 4 e5712

Dufault A M, Cumbo V R, Fan T Y and Edmunds P J 2012 Effects of diurnally oscillating pCO2 on the calcification and survival of coral recruits *Proc. Biol. Sci.* 279 2951–8

Dupont S, Orteg-Martínez O and Thorndyke M 2010 Impact of near-future ocean acidification on echinoderms *Ecotoxicology* 19 449–62

Duteil O and Oschlies A 2011 Sensitivity of simulated extent and future evolution of marine suboxia to mixing intensity *Geophys. Res. Lett.* 38 L06607

Dykema J A, Keith D W, Anderson J G and Weisenstein D 2014 Stratospheric controlled perturbation experiment: a small-scale experiment to improve understanding of the risks of solar geoengineering *Philos. Trans. R. Soc. A Math. Phys. Eng. Sci.* 372 20140059

Eakin C M *et al.* 2010 Caribbean corals in crisis: record thermal stress, bleaching, and mortality in 2005 *PLoS One* 5(11) e13969

Eby M *et al.* 2013 Historical and idealized climate model experiments: an intercomparison of Earth system models of intermediate complexity *Clim. Past* 9 1111–40

Eby M *et al. 2009* Lifetime of anthropogenic climate change: millennial time scales of potential CO2 and surface temperature perturbations. *J. Clim.* 22, 2501-2511,

Edenhofer O *et al.* 2011 *IPCC Expert Meeting on Geoengineering. Lima, Peru 20-22 June 2011*

Egleston E S, Sabine C, and Morel F M M 2010 Revelle revisited: buffer factors that quantify the response of ocean chemistry to changes in DIC and alkalinity. *Global Biogeochemical Cycles* 24, GB1002

English J M, Toon O B and Mills M J 2012 Microphysical simulations of sulfur burdens from stratospheric sulfur geoengineering *Atmos. Chem. Phys.* 12 4775–93

Fanning A F and Weaver A J 1996 An atmospheric energy-moisture balance model: climatology, interpentadal climate change, and coupling to an ocean general circulation model *J. Geophys. Res.* 101 15111

Feely R A, Sabine C L, Lee K, Berelson W, Kleypas J, Fabry V J and Millero F J 2004 Impact of anthropogenic CO2 on the CaCO3 system in the oceans. *Science* 305 362–6

Feng E Y, Keller D P, Koeve W and Oschlies A 2016 Could artificial ocean alkalinization protect tropical coral ecosystems from ocean acidification? *Environ. Res. Lett.* 11 074008

Feichter J and Leisner T 2009 Climate engineering: a critical review of approaches to modify the global energy balance *Eur. Phys. J. Spec. Top.* 176, 81-92

Fortey N J 2000 *Environmental Mineralogy* ed D J Vaughan and R A Wogelius (Budapest: Eötvös University Press)

Friedlingstein P *et al.* 2006 Climate – carbon cycle feedback analysis : results from the C MIP Model Intercomparison *J. Clim.* 19 3337

Frommel A Y, Maneja R, Lowe D, Malzahn A M, Geffen A J, Folkvord A, Piatkowski U, Reusch T B H and Clemmesen C 2011 Severe tissue damage in atlantic cod larvae under increasing ocean acidification *Nat. Clim. Chang.* 2 42–6

Frieler K, Meinshausen M, Golly A, Mengel M, Lebek K, Donner S D and Hoegh-Guldberg O 2012 Limiting global warming to 2 °C is unlikely to save most coral reefs *Nat. Clim. Chang.* 3 165–70

Fyfe J C, Cole J N S, Arora V K and Scinocca J F 2013 Biogeochemical carbon coupling influences global precipitation in geoengineering experiments *Geophysical Research Letters* 40 651-655

Galbraith E D, Gnanadesikan A, Dunne J P and Hiscock M R 2010 Regional impacts of iron-light colimitation in a global biogeochemical model *Biogeosciences* 7, 1043-1064

Gattuso J-P, Frankignoulle M, Bourge I, Romaine S and Buddemeier R W 1998 Effect of calcium carbonate saturation of seawater on coral calcification *Glob. Planet. Change* 18 37–46

Gazeau F, Quiblier C, Jansen J M, Gattuso J-P, Middelburg J J and Heip C H R 2007 Impact of elevated CO2 on shellfish calcification *Geophys. Res. Lett.* 34 L07603

Great Barrier Reef Marine Park Authority (GBRMPA) 2013 *Access Economics 2013, economic contribution of Great Barrier Reef*

Goes M, Tuana N and Keller K 2011 The economics (or lack thereof) of aerosol geoengineering *Clim. Change* 109 719–44

Goreau T J and Hayes R L 1994 Coral Bleaching and Ocean "Hot Spots" *Ambio* 23 176–80

Golubev S V, Pokrovsky O S and Schott J 2005 Experimental determination of the effect of dissolved CO2 on the dissolution kinetics of Mg and Ca silicates at 25 °C *Chem. Geol.* 217 227–38

Greiner J T, McGlathery K J, Gunnell J, McKee B A 2013 Seagrass restoration enhances "Blue Carbon" sequestration in coastal waters *PLoS One* 8:1–8.

Guilyardi E, Wittenberg A, Fedorov A, Collins M, Wang C, Capotondi A, von Oldenborgh G, and Stockdale T 2009 Understanding El-Nino in ocean-atmosphere general circulation models, progress and challenges. *Bull Am Meteorol Soc* 90:325-40

Guinotte J M, Buddemeier R W and Kleypas J 2003 Future coral reef habitat marginality: temporal and spatial effects of climate change in the Pacific basin *Coral Reefs* 22 551–8

Hangx S J Tand Spiers J C 2009 Coastal spreading of olivine to control atmospheric CO2 concentrations: A critical analysis of viability *Int. J. Greenh. Gas Control* 3 757–67

Harris N R P, Ancellet G, Bishop L, Hofmann D J, Kerr J B, McPeters R D, Prendez M, Randel W J, Staehelin J, Subbaraya B H, Volz-Thomas A, Zawodny J and Zerefos C S 1997 Trends in stratospheric and free tropospheric ozone *J. Geophys. Res. Atmos.* 102 1571–90

Hartmann J, West A J, Renforth P, Köhler P, De La Rocha C L, Wolf-gladrow D A, Dürr H H and Scheffran J 2013 Enhanced chemical weathering as a geoengineering strategy to reduce atmospheric carbon dioxide, supply nutirents, and mitigate ocean acidification *Rev. Geophys.* 51 20004

Harvey L D D 2008 Mitigating the atmospheric CO2 increase and ocean acidification by adding limestone powder to upwelling regions *J. Geophys. Res.* 113 C04028

Hauck J, Köhler P, Wolf-Gladrow D and Völker C 2016 Iron fertilisation and century-scale effects of open ocean dissolution of olivine in a simulated CO2 removal experiment *Environ. Res. Lett.* 11 024007

Hansen P J, Lundholm N and Rost B 2007 Growth limitation in marine red-tide dinoflagellates: effect of pH versus inorganic carbo availability *Marine Ecology Progress Series* 334 63-71

Heckendorn P, Weisenstein D, Fueglistaler S, Luo B P, Rozanov E, Schraner M, Thomason L W and Peter T 2011 The impact of geoengineering aerosols on stratospheric temperature and ozone *Environ. Res. Lett.* 4 045108

Hoegh-Guldberg O 1999 Climate change, coral bleaching and the future of the world's coral reefs *Mar. Freshw. Res.* 50 839–66

Hoegh-Guldberg O *et al.* 2007 Coral reefs under rapid climate change and ocean acidification *Science* 318 1737–42

House K Z, Baclig A C, Ranjan M, van Nierop E A, Wilcox J and Herzog H J 2011 Economic and energetic analysis of capturing CO2 from ambient air *Proc. Natl. Acad. Sci. U. S. A.* 108 20428–33

House K Z, House C H, Schrag D P and Aziz M J 2007 Electrochemical accelerationa of chemical weathering as an energetically feasible approach to mitigating anthropogenic climate change *Environ. Sci. Technol.* 41 8464–70

Ilyina T, Wolf-Gladrow D, Munhoven G and Heinze C 2013a Assessing the potential of calcium-based artificial ocean alkalinization to mitigate rising atmospheric CO2 and ocean acidification *Geophys. Res. Lett.* 40 5909-14

Ilyina T, Six K D, Segschneider J Maier-Reimer E, Li H and Ismael N-R 2013b Global ocean biogeochemistry model HAMOCC : Model architecture and performance as component of the MPI-Earth system model in different CMIP5 experimental realizations *J. Advances in Modeling Earth Systems* 5 287–315

IPCC 2014 *Climate Change 2014: Synthesis Report. Contribution of Working Groups I, II and III to the Fifth Assessment Report of the Intergovernmental Panel on Climate Change* (Geneva, Switzerland)

IPCC-WG1 2013 *Climate Change 2013: The Physical Science Basis. Contribution of Working Group I to the Fifth Assessment Report of the Intergovernmental Panel on Climate Change* (Cambridge, United Kingdom and New York, USA)

IPCC-WG2 2014 *Climate Change 2014: Impacts, Adaptation, and Vulnerability. Contribution of Working Group II to the Fifth Assessment Report of the*

Intergovernmental Panel on Climate Change (Cambridge, United Kingdom and New York, USA)

Iudicone D, Speich S, Madec G and Blanke B 2008 The Global conveyor belt from a southern ocean perspective *J. Phys. Ocean.* 38 1401-25

Iudicone D *et al.* 2011 Water masses as a unifying framework for understanding the Southern Ocean Carbon Cycle. *Biogeosciences* 8, 1031-1052

Izrael Y A *et al.* 2009 Field studies of a geo-engineering method of maintaining a modern climate with aerosol particles *Russ. Meteorol. Hydrol.* 34 635–8

Jones A, Haywood J and Boucher O 2009 Climate impacts of geoengineering marine stratocumulus clouds *J. Geophys. Res. Atmos.* 114 D10106

Jones A, Haywood J, Boucher O, Kravitz B and Robock A 2010 Geoengineering by stratospheric SO2 injection: results from the Met Office HadGEM2 climate model and comparison with the Goddard Institute for Space Studies ModelE *Atmos. Chem. Phys.* 10 5999–6006

Jones A *et al.* 2013 The impact of abrupt suspension of solar radiation management (termination effect) in experiment G2 of the Geoengineering Model Intercomparison Project (GeoMIP) *J. Geophys. Res. Atmos.* 118 9743–52

Jones I S F 1996 Enhanced carbon dioxide uptake by the world's oceans *Energy Convers. Manag.* 37 1049–52

Jungclaus J H, Fischer N, Haak H, Lohmann K, Marotzke J, Matei D, Mikolajewicz U, Notz D and von Storch J S 2013 Characteristics of the ocean simulations in the Max Planck Institute Ocean Model (MPIOM) the ocean component of the MPI-Earth system model *J. Adv. Model. Earth Syst.* 5 422–46

Keenan T F *et al.* 2013 Increase in forest water-use efficiency as atmospheric carbon dioxide concentrations rise *Nature* 499 324-7

Keith D W 2000 Geoengineering the climate: History and prospect *Annu. Rev. Energy Env.* 25 245–84

Keith D W 2010 Photophoretic levitation of engineered aerosols for geoengineering. *Proc. Natl. Acad. Sci. U. S. A.* 107 16428–31

Keith D W, Duren R and MacMartin D G 2014 Field experiments on solar geoengineering: report of a workshop exploring a representative research portfolio *Philos. Trans. R. Soc. A Math. Phys. Eng. Sci.* 372 20140175–20140175

Keith D W and MacMartin D G 2015 A temporary, moderate and responsive scenario for solar geoengineering *Nat. Clim. Chang.* 5 201–6

Keith D W, Ha-Duong M and Stolaroff J K 2006 Climate strategy with CO2 capture from the air *Clim. Change* 74 17–45

Keller D P, Feng E Y and Oschlies A 2014 Potential climate engineering effectiveness and side effects during a high carbon dioxide-emission scenario *Nat. Commun.* 5 3304

Keller D P, Oschlies A and Eby M 2012 A new marine ecosystem model for the University of Victoria Earth System Climate Model *Geosci. Model Dev.* 5 1195–220

Key R M *et al.* 2004 A global ocean carbon climatology: results from global data analysis project (GLODAP) *Global Biogeochem. Cycles* 18 GB4031

Kleidon A, Kravitz B and Renner M 2015 The hydrological sensitivity to global warming and solar geoengineering derived from thermodynamic constraints *Geophys. Res. Lett.* 42 138–44

Klepper G and Rickels W 2012 The real economics of climate engineering *Econ. Res. Int.* 2012 1–20

Kleypas J A, Buddemeier R W, Archer D, Gattuso J-P, Langdon C and Opdyke B N 1999a Geochemical consequences of increased atmospheric carbon dioxide on coral reefs *Science* 284 118–20

Kleypas J A, McManus J W and Menet L A B. 1999b Environmental limits to coral reef development : where do we draw the line? *Amer. Zool.* 39 146–59

Knutti R and Sedlacek J 2013 Robustness and uncertainties in the new CMIP5 climate model projections *Nature Clim. Change* 3, 369-373

Köhler P, Hartmann J and Wolf-Gladrow D A 2010 Geoengineering potential of artificially enhanced silicate weathering of olivine. *Proc. Natl. Acad. Sci. U. S. A.* 107 20228–33

Köhler P, Abrams J F, Völker C, Hauck J and Wolf-Gladrow D A 2013 Geoengineering impact of open ocean dissolution of olivine on atmospheric CO2 , surface ocean pH and marine biology *Environ. Res. Lett.* 8 014009

Kravitz B, Robock A, Boucher O, Schmidt H, Taylor K E, Stenchikov G and Schulz M 2011 The geoengineering model intercomparison project (GeoMIP) *Atmos. Sci. Lett.* 12 162–7

Kravitz B *et al.* 2013a Climate model response from the geoengineering model intercomparison project (GeoMIP). *J. Geophys. Res. Atmos.*118, 8320-8332

Kravitz B *et al.* 2013b An energetic perspective on hydrological cycle changes in the geoengineering model intercomparison project *J. Geophys. Res. Atmos.* 118 13087–102

Kravitz B *et al.* 2013c Sea spray geoengineering experiments in the geoengineering model intercomparison project (GeoMIP): experimental design and preliminary results *J. Geophys. Res. Atmos.* 118 11175–86

Kump L R, Brantley S L and Arthur M A 2000 Chemical weathering, atmospheric CO2, and climate *Annu. Rev. Earth Planet. Sci.* 28 611–67

Lammertsma E I, de Boer H J, Dekker S C, Dilcher D L, Lotter A F and Wagner-Cremer F 2011 Global CO2 rise leads to reduced maximum stomatal conductance in Florida vegetation. *Proc. Natl. Acad. Sci. U. S. A.* 108 4035–40

Landschützer P, Gruber N, Bakker D C E and Schuster U 2014 Recent variability of the global ocean carbon sink *Global Biogeochem. Cycles* 927–49

Langdon C and Atkinson M J 2005 Effect of elevated pCO2 on photosynthesis and calcification of corals and interactions with seasonal change in temperature/ irradiance and nutrient enrichment *J. Geophys. Res. C Ocean.* 110 C9

Latham J 2002 Amelioration of global warming by controlled enhancement of the albedo and longevity of low-level maritime clouds *Atmos. Sci. Lett.* 3 52–8

Latham J, Parkes B, Gadian A and Salter S 2012 Weakening of hurricanes via marine cloud brightening (MCB) *Atmos. Sci. Lett.* 13 231–7

Latham J, Kleypas J, Hauser R, Parkes B and Gadian A 2013 Can marine cloud brightening reduce coral bleaching? *Atmos. Sci. Lett.* 14 214–9

Lenton T M and Vaughan N E 2009 The radiative forcing potential of different climate geoengineering options *Atmos. Chem. Phys. Discuss.* 9 2559–608

Lewis E and Wallace D W R 1988 Program developed for CO2 system calculations, carbon dixoide information analysis center, report ORNL/CDIAC-105 (Oak Ridge, USA)

Liu C and Allan R P 2013 Observed and simulated precipitation responses in wet and dry regions 1850-2100 *Environ. Res. Lett.* 8 034002

Liu C C K and Jin Q 1995 Artificial upwelling in regular and random waves *Ocean Eng.* 22 337–50

Llanillo P, Jones P D and von Glasow R 2010 The influence of stratospheric sulphate aerosol deployment on the surface air temperature and the risk of an abrupt global warming *Atmosphere* 1 62-84

Locarnini R A, Mishonov A V, Antonov J I, Boyer T P, Garcia H E, Baranova O K, Zweng M M, Paver C R, Reagan J R, Johnson D R, Hamilton M and Seidov D 2013 *NOAA Atlas NESDIS 62 WORLD OCEAN ATLAS 2013 Volume 1 : Temperature* vol 1

Loh T-L, McMurray S E, Henkel T P, Vicente J and Pawlik J R 2015 Indirect effects of overfishing on Caribbean reefs: sponges overgrow reef-building corals *PeerJ* 3 e901

Lovelock J E and Rapley C G 2007 Ocean pipes could help the Earth to cure itself *Nature* 449 403

MacMartin D G, Caldeira K and Keith D W 2014 Solar geoengineering to limit the rate of temperature change *Philos. Trans. R. Soc. A Math. Phys. Eng. Sci.* 372 20140134

MacMartin D G, Keith D W, Kravitz B and Caldeira K 2012 Management of trade-offs in geoengineering through optimal choice of non-uniform radiative forcing *Nat. Clim. Chang.* 3 365–8

Marion G M, Millero F J and Feistel R 2009 Precipitation of solid phase calcium carbonates and their effect on application of seawater S-A-T-P models *Ocean Sci.* 5 285–91

Manzello D P 2015 Is there a CO2 tipping point for coral reefs ? *Ocean Carbon and Biogeochemi. News* 8 2012–3

Marshall P A and Baird A H 2000 Bleaching of corals on the Great Barrier Reef: differential susceptibilities among taxa *Coral Reefs* 19 155-63

Matthews H D and Caldeira K 2007 Transient climate – carbon simulations of planetary geoengineering *Proc. Natl. Acad. Sci. U. S. A.* 104 9949-54

Mathesius S, Hofmann M, Caldeira K and Schellnhuber H J 2015 Long-term response of oceans to CO2 removal from the atmosphere *Nat. Clim. Chang.* 5 1107-13

McClellan J *et al.* 2010 *Geoengineering cost analysis, final report prepared under contract to the University of Calgary, AR10-108* (Cambridge, USA)

McClimans T A, Handa A, Fredheim A, Lien E and Reitan K I 2010 Controlled artificial upwelling in a fjord to stimulate non-toxic algae *Aquac. Eng.* 42 140–7

McCormick M P, Thomason L W and Trepte C R 1995 Atmospheric effects of the Mt Pinatubo eruption *Nature* 373 399–404

Mccoy S J and Ragazzola F 2014 Skeletal trade-offs in coralline algae in response to ocean acidification *Nat. Clim. Chang.* 4 719–23

McCusker K E, Battisti D S, Bitz C M, Battisti D S, Bitz C M 2015 Inability of stratospheric sulfate aerosol injections to preserve the West Antarctic Ice Sheet *Geophys. Res. Lett.* 42 4989–97

Meinshausen M *et al.* 2011 The RCP greenhouse gas concentrations and their extensions from 1765 to 2300 *Clim. Change* 109 213–41

Meissner K J, Weaver A J, Matthews H D and Cox P M 2003 The role of land surface dynamics in glacial inception : a study with the UVic Earth System Model *Clim. Dyn.* 21 515–37

Meissner K J, Lippmann T and Sen Gupta A. 2012a Large-scale stress factors affecting coral reefs: open ocean sea surface temperature and surface seawater aragonite saturation over the next 400 years *Coral Reefs* 31 309–19

Meissner K J, McNeil B I, Eby M and Wiebe E C 2012b The importance of the terrestrial weathering feedback for multimillennial coral reef habitat recovery *Global Biogeochem. Cycles* 26 GB3017

Mekmene O, Quillard S, Rouillon T, Bouler J-M, Piot M and Gaucheron F 2009 Effects of pH and Ca/P molar ratio on the quantity and crystalline structure of calcium phosphates obtained from aqueous solutions *Dairy Sci. Technol.* 89 301–16

Melzner F *et al.* 2012 Future ocean acidification will be amplified by hypoxia in coastal habitats *Mar. Biol.* 160 1875-88

Mercado L M, Bellouin N, Sitch S, Boucher O, Huntingford C, Wild M and Cox P M 2009 Impact of changes in diffuse radiation on the global land carbon sink *Nature* 458 1014–7

Mizumukai K, Sato T, Tabeta S and Kitazawa D 2008 Numerical studies on ecological effects of artificial mixing of surface and bottom waters in density stratification in semi-enclosed bay and open sea *Ecol. Modell.* 214 251–70

Moore J K, Lindsay K, Doney S, Long M C and Misumi K 2013 Marine ecosystem dynamics and biogeochemical cycling in the Community Earth System Model

(CESM1 (BGC)): Comparison of the 1990s with the 2090s under the RCP 4.5 and RCP 8.5 Scenarios *J. Clim.* 30

Moosdorf N, Renforth P and Hartmann J 2014 Carbon dioxide efficiency of terrestrial enhanced weathering *Environ. Sci. Technol.* 48 4809–16

Moore J K and Braucher O 2008 Sedimentary and mineral dust sources of dissolved iron to the world ocean *Biogeosciences* 5 631-656

Munday P L, Cheal A J, Dixson D L, Rummer J L and Fabricius K E 2014 Behavioural impairment in reef fishes caused by ocean acidification at CO2 seeps *Nature* 4 487–92

Myhre G, Highwood E J, Shine K P and Stordal F 1998 New estimates of radiative forcing due to well mixed greenhouse gases *Geophys. Res. Lett.* 25 2715

NAS (National Research Council of the National Acadamies) 2015 *Climate Intervention: Carbon Dioxide Removal and Reliable Sequestration* (Washington D.C., USA)

Nielsen L T, Lundholm N and Hansen P J 2007 Does irradiance influence the tolerance of marine phytoplankton to high pH *Marine Biology* 3:6 446-53

Naik V, Wuebbles D J, Delucia E H and Foley J A Influence of geoengineered climate on the terrestrial biosphere. *Environ. Manag* 32, 373-381

Ohde S and Hossain M M M 2004 Effect of CaCO3 (aragonite) saturation state of seawater on calcification of Porites coral *Geochem. J.* 38 613–21

Ornstein L, Aleinov I and Rind D 2009 Irrigated afforestation of the Sahara and Australian Outback to end global warming. *Climatic Change* 97, 409-437

Orr J C Najjar R, Sabine C L and Joos F 1999 *Abiotic-HOWTO. Internal OCMIP Report*, LSCE/CEA Saclay, Gif-surYvette, France, 25pp

Oschlies A, Koeve W, Rickels W and Rehdanz K 2010 Side effects and accounting aspects of hypothetical large-scale Southern Ocean iron fertilization. *Biogeosciences* 7 4017-35

Oschlies A, Pahlow M, Yool A and Matear R J 2010 Climate engineering by artificial ocean upwelling: channelling the sorcerer's apprentice *Geophys. Res. Lett.* 37 L04701

Oschlies A, Schulz K G, Riebesell U and Schmittner A 2008 Simulated 21st century's increase in oceanic suboxia by CO_2-enhanced biotic carbon export *Global Biogeochem. Cycles* 22 doi:10.1029/2007GB003147

Pacanowski R C 1996 MOM2: Documentation, user's guide and reference manual *GFDL Ocean Tech. Rep.* 3.2 329pp

Pan Y *et al.* 2015 Research progress in artificial upwelling and its potential environmental effects *Sci China Earth Sci* 59 2

Partanen A-I, Kokkola H, Romakkaniemi S, Kerminen V-M, Lehtinen K E J, Bergman T, Arola A and Korhonen H 2012 Direct and indirect effects of sea spray geoengineering and the role of injected particle size *J. Geophys. Res.* 117 D02203

Pearson P N and Palmer M R 2000 Atmospheric carbon dioxide concentrations over the past 60 million years *Nature* 406 695–9

Peters G P *et al.* 2013 The challenge to keep global warming below 2 [deg]C. *Nat. Clim. Chang.* 3 4-6

Pidgeon N, Parkhill K, Corner A and Vaughan N 2013 Deliberating stratospheric aerosols for climate geoengineering and the SPICE project *Nat. Clim. Chang.* 3 451–7

Pilson M E Q 2013 Major constituents of seawater *an introduction to the chemistry of the sea* (Cambridge university press) p 67

Pokrovsky O S and Schott J 2000 Kinetics and mechanism of forsterite dissolution at 25°C and pH from 1 to 12 *Geochim. Cosmochim. Acta* 64 3313–25

Pollard R T *et al.* 2009 Southern Ocean deep-water carbon export enhanced by natural iron fertilization *Nature* 457 577–80

Pope F D, Braesicke P, Grainger R G, Kalberer M, Watson I M, Davidson P J and Cox R A 2012 Stratospheric aerosol particles and solar-radiation management *Nat. Clim. Chang.* 2 713–9

Pope K O, D'hondt S L and Marshall C R 1998 Meteorite impact and the mass extinction of species at the Cretaceous / Tertiary boundary *Proc. Natl. Acad. Sci. U. S. A.* 95 11028–9

Zhang Q, L X and W Y 2015 A simulation of air-lift artificial upwelling in vertical pipe *Int. Conf. Intell. Syst. Res. Mechatronics Eng. (ISRME 2015)* 1347–51

Rasch P J *et al.* 2008 An overview of geoengineering of climate using stratospheric sulphate aerosols *Philos. Trans. R. Soc. A Math. Phys. Eng. Sci.* 366 4007–37

Rau G H 2008 Electrochemical splitting of calcium carbonate to increase solution alkalinity: implications for mitigation of carbon dioxide and ocean acidity *Environ. Sci. Technol.* 42 8935–40

Rau G H and Caldeira K 1999 Enhanced carbonate dissolution : a means of sequestering waste CO2 as ocean bicarbonate *Energy Convers. Manag.* 40 1803–13

Rau G H, Caldeira K, Knauss K G, Downs B and Sarv H 2001 Enhanced carbonate dissolution as a means of capturing and sequestering carbon dioxide *First National Conference on Carbon Sequestration* vol 2 pp 1–7

Reddy M M and Wang K K 1980 Crystallization of calcium carbonate in the presence of metal ions: I. Inhibition by magnesium ion at pH 8.8 and 25°C *J. Cryst. Growth* 50 470–80

Renforth P, Jenkins B G and Kruger T 2013 Engineering challenges of ocean liming *Energy* 60 442

Reynold R W, Rayner N A, Smith T M, Stokes D C and Wang W 2002 An improved in situ and satellite SST analysis for climate *J. Clim.* 15 1609 25

Ricke K L, Rowlands D J, Ingram W J, Keith D W and Granger M M 2011 Effectiveness of stratospheric solar-radiation management as a function of climate sensitivity *Nat. Clim. Chang.* 2 92–6

Ricke K L, Orr J C, Schneider K and Caldeira K 2013 Risks to coral reefs from ocean carbonate chemistry changes in recent earth system model projections *Environ. Res. Lett.* 8 034003

Rickels W *et al.* 2011 *Large-Scale Intentional Interventions into the Climate System ?Assessing climate enginering Debate* (Kiel, Germany)

Ridgwell A, Maslin M A and Watson A J 2002 Reduced effectiveness of terrestrial carbon sequestration due to an antagonistic response of ocean productivity. *Geophys. Res. Lett.* 29

Riebesell U, Körtzinger A and Oschlies A 2009 Sensitivities of marine carbon fluxes to ocean change *Proc. Natl. Acad. Sci. U. S. A.* 106 20602–9

Robock A, Oman L and Stenchikov G L 2008 Regional climate responses to geoengineering with tropical and Arctic SO2 injections *J. Geophys. Res. D Atmos.* 113

Robock A 1984 Snow and ice feedbacks prolong effects of nuclear winter *Nature* 310 667–70

Robock A and Toon O B 2012a Artificial upwelling in regular and random waves *Bull. atmoic Sci.* 68 66–74

Rochelle G T 2009 Amine scrubbing for CO2 capture *Science* 325 1652–4

Rockström J *et al.* 2009 Planetary boundaries : exploring the safe operating space for humanity *Ecol. Soc* 14 32

Rogelj J, Luderer G, Pitzcker R C, Kriegler E, Schaeffer M, Krey V and Riahi K 2016 Energy system transformations for limiting end-of-century warming to below 1.5 degree C *Nat. Clim. Chang.* 5 520–38

Rosa R and Seibel B A 2008 Synergistic effects of climate-related variables suggest future physiological impairment in a top oceanic predator *Proc. Natl. Acad. Sci. U. S. A.*105 20776–80

Roy K J and Smith S V. 1971 Sedimentation and coral reef development turbid water: fanning lagoon *Pacific Sci.* 234–48

Ross A and Matthews H D 2009 Climate engineering and the risk of rapid climate change *Environ. Res. Lett.* 4 4

Ross A, Matthews H D, Schmittner A and Zavareh K 2012 Assessing the effects of ocean diffusivity and climate sensitivity on the rate of global climate change *Tellus B* 64 17733

Royal Society 2009 *geoengineering the climate: science, governance and uncertainty* (London, UK)

Sarmiento J, Slater R D, Dunne J, Gnanadesikan A and Hiscock M R 2010 Efficiency of small scale carbon mitigation by patch iron fertilization *Biogeoscience* 7, 3593 - 624

Salter S, Sortino G and Latham J 2008 Sea-going hardware for the cloud albedo method of reversing global warming *Philos. Trans. R. Soc. A Math. Phys. Eng. Sci.* 366 3989–4006

Schmidt H *et al.* 2012 Solar irradiance reduction to counteract radiative forcing from a quadrupling of CO2: climate responses simulated by four earth system models *Earth Syst. Dynam.* 3 63-78

Shaw T A and Shepherd T G 2008 Atmospheric science: raising the roof *Nat. Geosci.* 1 12–3

Schäfer S, Lawrence M G, Stelzer H, Wanda B and Sean L 2015 *The european transdisciplinary assessment of climate engineering (EuTRACE): removing greenhouse gases from the atmosphere and reflecting sunlight away from Earth* (Potsdam: Institute for Advanced Sustainability Studies Potsdam (IASS) e. V.)

Schuiling R D and Krijgsman P 2006 Enhanced weathering: an effective and cheap tool to sequester CO2 *Clim. Change* 74 349–54

Schuiling R D and de Boer P L 2011 Rolling stones: fast weathering of olivine in shallow seas for cost-effective CO_2 capture and mitigation of global warming and ocean acidification *Earth Syst. Dyn. Discuss.* 2 551–68

Smetacek V *et al.* 2012 Deep carbon export from a southern ocean iron-fertilized diatom bloom *Nature* 487 313–9

Song Y, Hahn H H and Hoffmann E 2002 The effect of carbonate on the precipitation of calcium phosphate. *Environ. Technol.* 23 207–15

Stramma L, Johnson G C, Sprintall J. and Mohrholz V 2008 Expanding oxygen minimum zones in the tropical oceans *Science* 230 655-658

Taylor L L, Quirk J, Thorley R M S, Kharecha P A, Hansen J, Ridgwell A, Lomas M R, Banwart S A and Beerling D J 2015 Enhanced weathering strategies for stabilizing climate and averting ocean acidification *Nat. Clim. Chang.* 6 402–6

Teneva L, Karnauskas M, Logan C A, Bianucci L, Currie J C and Kleypas J A. 2012 Predicting coral bleaching hotspots: The role of regional variability in thermal stress and potential adaptation rates *Coral Reefs* 31 1–12

Tilmes S *et al.* 2013 The hydrological impact of geoengineering in the Geoengineering Model Intercomparison Project (GeoMIP) *J. Geophys. Res. Atmos.* 118 11036–58

Tilmes S, Müller R and Salawitch R 2008 The sensitivity of polar ozone depletion to proposed geoengineering schemes *Science.* 320 1201–4

Tilmes S, Kinnison D E, Garcia R R, Salawitch R, Canty T, Lee-Taylor J, Madronich S and Chance K 2012 Impact of very short-lived halogens on stratospheric ozone abundance and UV radiation in a geo-engineered atmosphere *Atmos. Chem. Phys.* 12 10945–55

Trenberth K E and Dai A 2007 Effects of Mount Pinatubo volcanic eruption on the hydrological cycle as an analog of geoengineering *Geophys. Res. Lett.* 34 L15702

van Heuven S, Pierrot D, Lewis E and Wallace D W R 2009 Matlab program developed for CO2 system calculations, ORNL/CDIAC-105b, carbon dioxide information analysis center (Oak Ridge, USA)

Vaughan N E and Lenton T M 2011 A review of climate geoengineering proposals *Climatic Change* 109, 745-790, doi:10.1007/s10584-011-0027-7.

Waheed Z, Benzoni F, van der Meij S E T, Terraneo T I and Hoeksema B W 2015 Scleractinian corals (Fungiidae, Agariciidae and Euphylliidae) of Pulau Layang-Layang, Spratly Islands, with a note on Pavona maldivensis (Gardiner, 1905) *Zookeys* 2015 1–37

Wang C, Zhang L, Lee S-K, Wu L and Mechoso C R 2014 A global perspective on CMIP5 climate model biases *Nat. Clim. Chang.* 4 201–5

Watson A J, Bakker D C, Ridgwell A J, Boyd P W and Law C S 2000 Effect of iron supply on Southern Ocean CO2 uptake and implications for glacial atmospheric CO2 *Nature* 407 730–3

Weaver A J *et al.* 2001 The UVic earth system climate model: model description, climatology, and applications to past, present and future climates *Atmosphere-Ocean* 39 361–428

Weaver A J *et al.* 2012 Stability of the Atlantic meridional overturning circulation: A model intercomparison *Geophys. Res. Lett.* 39 L20709

Weisenstein D K, Keith D W and Dykema J A 2015 Solar geoengineering using solid aerosol in the stratosphere *Atmos. Chem. Phys.* 15 11835–59

Wentz F J, Ricciardulli L, Hilburn K and Mears C 2007 How much more rain will global warming bring? *Science* 317

Whiteley N M 2011 Physiological and ecological responses of crustaceans to ocean acidification *Mar. Ecol. Prog. Ser.* 430 257–71

Wigley T M L 2006 A combined mitigation/geoengineering approach to climate stabilization *Science* 314 452–4

Williamson P and Turley C 2012 Ocean acidification in a geoengineering context. *Philos. Trans. R. Soc. A Math. Phys. Eng. Sci.* 370 4317–42

Wittmann A C and Pörtner H-O 2013 Sensitivies of extant animal taxa to ocean acidification *Nat. Clim. Chang.* 3 995–1001

Wogelius R A and Walther J V 1991 Olivine dissolution at 25°C: Effects of pH, CO2, and organic acids *Geochim. Cosmochim. Acta* 55 943–54

Wolf-Gladrow D A, Zeebe R E, Klaas C, Koertzinger A and Dickson A G 2007 Total alkalinity: the explicit conservative expression and its application to biogeochemical processes *Mar. Chem.* 106 287-300

Xia L, Robock A, Tilmes S and Neely III R R 2016 Strtospheric sulfate geoengineering could enhance the terriestrial photosynthesis rate *Atmos. Chem. Phys.* 16 1479-89

Yool A, Shepherd J G, Bryden H L and Oschlies A 2009 Low efficiency of nutrient translocation for enhancing oceanic uptake of carbon dioxide *J. Geophys. Res. Ocean.* 114 1–13

Yu X, Moore J C, Cui X, Rinke A, Ji D, Kravitz B and Yoon J-H 2015 Impacts, effectiveness and regional inequalities of the GeoMIP G1 to G4 solar radiation management scenarios *Glob. Planet. Change* 129

Zickfeld K *et al.* 2013 Long-term climate change commitment and reversibility: an EMIC intercomparison *J. Clim.* 26 5782–809

Zickfeld K, Eby M, Matthews H. D, Schmittner A and Weaver A J 2011 Nonlinearity of carbon cycle feedbacks *J. Clim.* 24 4255-4275

Zamora L M *et al. 2012* Nitrous oxide dynamics in low oxygen regions of the Pacific: insights from the MEMENTO database *Biogeosciences* 9 5007-22

Zhang J P, Shen C De, Ren H, Wang J and Han W D 2012 Estimating change in sedimentary organic carbon content during mangrove restoration in southern china using carbon isotopic measurements *Pedosphere* 22 58–66

Acknowledgements

想和未来。还要感谢曾经一起同舟共济创办"旅德海洋大气学者联合会"的校友们，让我看到了中国学子们团结起来的振奋力量。感谢陶艺越和常昊，与我为邻居的岁月里度过在德国的一个个日日夜夜。最终，作为一个儿子，我要感谢对我有生养和教育之恩的父母，在过去的一段时间我没能多与你们联络，深感愧疚。我会在未来的生活中更好地管理时间，处理好感情和事业的关系。

Biography

(Ellias) Yuming Feng, born in Shandong, China, April 7, 1988. Enrolled at Ocean University of China in year 2006 to study Marine Science, and graduated ahead of regular curriculum with degree Bachelor of Science in year 2009. In the same year, began the master program subjecting in physical oceanography at Ocean University of China supervised of Prof. Dr. Changlong Guan. Graduated in year 2012 with degree Master of Science. The notable academic fellowships earned are listed in following:

- National Fellowship for Master Students Lv1 (2010 and 2011)
- Humboldt Researcher Alumni Travel funds (2014)
- Chunhui Researcher Exchange funds (2015)

Publications (peer reviewed)

1. Parameterization of air-sea inorganic salt flux induced by wavebreak, *Yuming Feng (Ellias Y. Feng), Changlong Guan, Jian Huang,* 2012, *Journal of Ocean University of China*

2. Potential climate engineering effectiveness and side effects during a high carbon dioxide emission scenario, *David P. Keller, Ellias Y. Feng, Andreas Oschlies*, 2014, *Nature Communication* **5** 3304

3. Can artificial ocean alkalinization protect tropical coral habitats from ocean acidification? (Highlighted), *Ellias Y. Feng, David P. Keller, Wolfgang Koeve and Andreas Oschlies,* 2016 *Environmental Research Letters* **11** 7

4. Modelbased assessment of the potential of coastal ocean alkalinization (to be submitted), *Ellias Y. Feng, Wolfgang Koeve, David P. Keller, Andreas Oschlies*

5. Cooling effects from climate feedbacks in climate engineering implementations (prepared manuscript), *Ellias Y. Feng, David P. Keller and Andreas Oschlies*

6. Modeling assessment for combined SRM and AOA implementation schemes (in prepared manuscript), *Ellias Y. Feng*

Eidesstattliche Erklärung

Hiermit erkläre ich, dass die vorliegende Dissertation mit dem Titel

„ Modeling Assessments of Climate Engineering"

selbstständig von mir angefertigt wurde. Die Dissertation-abgesehen von der Beratung durch die Betreuerin oder den Betreuer-ist nach Form und Inhalt meine eigene Arbeit und es wurden keine anderen als die angegebenen Quellen und Hilfsmittel verwendet. Die vorliegende Arbeit ist unter Einhaltung der Regeln guter wissenschaftlicher Praxis der Deutschen Forschungsgemeinschaft entstanden und wurde weder ganz noch zum Teil an anderer Stelle im Rahmen eines Prüfungsverfahrens vorgelegt oder veröffentlicht. Weiterhin erkläre ich mich einverstanden, dass diese Dissertation an die Bibliothek des GEOMAR und die Universitätsbibliothek der CAU weitergeleitet wird.

_____